

Identification and functional characterization of cytoskeletal proteins in cyanobacteria

Dissertation

Submitted in fulfilment of the requirements for the degree

Doktor der Naturwissenschaften (Dr. rer. Nat.)

in the Faculty of Mathematics and Natural Sciences

of the Christian-Albrechts University Kiel

Submitted by

Benjamin Lennart Springstein

Kiel

2018

Data Sheet

Title of thesis: Identification and functional characterization of cytoskeletal proteins in cyanobacteria

Institute: Institute of General Microbiology

Group: Genomic Microbiology

Name, Given Name: Springstein, Benjamin Lennart

Address: Muhliusstraße 30, 24103 Kiel, Germany

Phone: 0152 - 22706169

E-Mail: benjamin.springstein@hamburg.de or bspringstein@ifam.uni-kiel.de

First Evaluator and Supervisor: Prof. Dr. Tal Dagan

Second Supervisor: Dr. Karina Stucken

Second Evaluator: Prof. Dr. Axel Scheidig

Third Evaluator: Prof. Dr. Ruth Schmitz-Streit

Head of Committee: Prof. Dr. Matthias Leippe

Date of Delivery: May 4th, 2018

Date of Disputation: July 6th, 2018

Contributions to conferences:

In the course of this thesis the following contributions to conferences were made in accordance with the supervisors:

Benjamin Springstein

Presentation: "Haben Bakterien Muskeln?"

Kieler Woche 2017, Kiel, Germany

Benjamin Springstein, Christian Wöhle, Tal Dagan, Karina Stucken

Poster: Function and evolution of cytoskeletal proteins in cyanobacteria

Studierendentagung zu den Life Sciences in Kiel 2016, Kiel, Germany

Benjamin Springstein

Presentation: Function and evolution of cytoskeletal proteins in cyanobacteria

First Young Investigator Symposium on Cyanobacteria (2016), Rostock, Germany

Benjamin Springstein, Christian Wöhle, Tal Dagan, Karina Stucken

Poster: Function and evolution of cytoskeletal proteins in cyanobacteria

Gordon Research Conference (2016), Proctor Academy in Andover NH, United States of America

Benjamin Springstein

Presentation: Function and evolution of cytoskeletal proteins in cyanobacteria

Studierendentagung zu den Life Sciences in Kiel 2015, Kiel, Germany

Benjamin Springstein, Christian Wöhle, Tal Dagan, Karina Stucken

Poster: Function and evolution of cytoskeletal proteins in cyanobacteria

Annual Conference of the German Genetics Society (2015), Kiel, Germany

Benjamin Springstein, Christian Wöhle, Tal Dagan, Karina Stucken

Poster: Function and evolution of cytoskeletal proteins in cyanobacteria

15th international Symposium on Phototropic Prokaryotes (2015), Tübingen, Germany

I hereby assure that I have compiled the present thesis entitled "Identification and functional characterization of cytoskeletal proteins in cyanobacteria" independently and have used no other appliances than indicated. Parts gathered from other works I have indicated in every single case by the declaration of the respective source. This thesis, or parts of it, have not been previously submitted to any other institution. Furthermore, I hereby state that I have produced my work in compliance to the principles of good scientific practice in accordance with the guidelines of the Deutsche Forschungsgemeinschaft.

Kiel, May 4th, 2018

Benjamin Springstein

Dedicated to Traute Springstein

Table of contents

1	Abstract.....	1
2	Abbreviations	3
3	General introduction	4
3.1	The eukaryotic cytoskeleton	4
3.1.1	Intermediate filaments.....	5
3.1.2	Cytolinker proteins	6
3.2	The bacterial cytoskeleton.....	7
3.2.1	Tubulin-like proteins in prokaryotes.....	8
3.2.2	Actin-like proteins in prokaryotes	10
3.2.3	Intermediate filament-like proteins in prokaryotes	12
3.2.4	Prokaryotic-specific cytoskeletal proteins.....	15
3.3	Evolution of cytoskeletal proteins from enzymes – the enzyme theory	16
3.4	Origin of the cytoskeleton	17
3.5	Cyanobacteria	19
3.5.1	Characteristics of cyanobacteria	21
3.5.2	Cyanobacterial motility.....	22
3.5.3	Cell to cell communication in cyanobacteria.....	23
4	Thesis motivation	25
5	Outline of the thesis.....	27
6	Material and methods.....	29
6.1	Bioinformatic analysis.....	33
6.1.1	Predictions of coiled-coil rich proteins	33
6.1.2	Multiple sequence alignments and phylogenetic trees	33
6.2	Molecular biology methods.....	34
6.2.1	Generation of chemically competent <i>E. coli</i>	34
6.2.2	Transformation of chemically competent <i>E. coli</i>	34
6.2.3	Isolation of genomic DNA	34
6.2.4	RNA isolation.....	35
6.2.5	Polymerase chain reaction.....	36
6.2.6	Agarose gel electrophoresis.....	36
6.2.7	Enzymatic digestion of nucleic acids and ligation of DNA fragments.....	37
6.2.8	Gibson assembly	37
6.2.9	Plasmid isolation.....	37
6.2.10	Spectrometric measurement of nucleic acid concentration	38
6.2.11	Colony PCR	38
6.2.12	Reverse transcription PCR.....	38
6.2.13	DNA sequencing – Verification of cloning constructs.....	38
6.2.14	Cryoconservation	38
6.2.15	Construction of mutant strains.....	39

6.2.16	Verification of gene replacements	39
6.3	Cell biology methods	40
6.3.1	Bacterial strains and growth conditions	40
6.3.2	Cell viability tests	41
6.3.3	Influence of osmotic factors on cell growth.....	42
6.3.4	Motility test.....	42
6.3.5	Transformation of cyanobacteria.....	42
6.3.6	Microscopic procedures	44
6.3.7	Fluorescence recovery after photobleaching (FRAP).....	45
6.3.8	Determination and calculation of cell morphological features	45
6.4	Protein and biochemical methods.....	46
6.4.1	Discontinuous SDS polyacrylamide gel electrophoresis.....	46
6.4.2	Immunological detection of immobilized proteins	46
6.4.3	Evaluation of protein-protein interactions	47
6.4.3.1	Bacterial two hybrid assay	47
6.4.3.2	Identification of protein-protein interactions using GFP-reassembly.....	48
6.4.3.3	Protein purification and <i>in vitro</i> filamentation assay.....	49
6.4.3.4	Protein concentration measurement	50
6.4.3.5	Co-immunoprecipitation	51
6.4.3.6	Mass spectrometry analysis.....	52
6.4.4	<i>In vivo</i> immunodetection of protein candidates	53
6.4.4.1	Immunofluorescence of <i>Anabaena</i>	53
6.4.4.2	Immunofluorescence of <i>Synechococcus</i>	54
7	Chapter I: Identification and characterization of coiled-coil rich cytoskeletal proteins from cyanobacteria.....	55
7.1	Abstract.....	55
7.2	Introduction	55
7.3	Results	57
7.4	Discussion.....	83
8	Chapter II: Evolutionary diversification of cytoskeletal networks in cyanobacteria.....	91
8.1	Abstract.....	91
8.2	Introduction	91
8.3	Results	93
8.4	Discussion.....	109
9	Chapter III: A cytoskeletal network stabilizes cell-cell connections in the multicellular cyanobacterium <i>Anabaena</i>	115
9.1	Abstract.....	115
9.2	Introduction	115
9.3	Results	117
9.4	Discussion.....	132

10	General Discussion	138
11	Outlook.....	140
12	References.....	142
13	Supplementary figures Chapter I	157
14	Supplementary figures Chapter II	169
15	Supplementary figures Chapter III	177
16	Supplementary tables – Oligonucleotides, plasmids and strains.....	191
17	Acknowledgements	221

Figures

Fig. 1: Eukaryotic cytoskeletal networks	5
Fig. 2: Structural model of a cytoplasmic human vimentin dimer	6
Fig. 3: Bacterial tubulin homologs.....	10
Fig. 4: Bacterial actin homologs.....	12
Fig. 5: IF-like cytoskeletal proteins CreS and FilP.....	15
Fig. 6: Cyanobacterial morphological diversity.....	22
Fig. 7: Schematic representation of a double homologous recombination-based gene replacement	40
Fig. 8: Principle of the bacterial adenylate cyclase two hybrid system	48
Fig. 9: Domain architecture of IF-like protein candidates	59
Fig. 10: <i>In vitro</i> polymerization of protein candidates into diverse filamentous structures.....	65
Fig. 11: Interaction of IF-like proteins in a beta-galactosidase assay	66
Fig. 12: <i>In vivo</i> localization of protein candidates heterologously expressed in <i>E. coli</i>	67
Fig. 13: Fm7001 and CreS form filaments in cyanobacteria.....	70
Fig. 14: Identification of proteins interacting with YFP-Fm7001	72
Fig. 15: <i>In vivo</i> localization of Slr7083	73
Fig. 16: Impact of $\Delta slr7083$ on motile and non-motile <i>Synechocystis</i> substrains.....	75
Fig. 17: All4981 forms species-independent cell-traversing filaments in cyanobacteria	76
Fig. 18: Identification of proteins interacting with YFP-All4981	77
Fig. 19: Synpcc7942_2039 forms filamentous polymers <i>in vivo</i>	79
Fig. 20: Impact of $\Delta synpcc7492_2039$ on <i>Synechococcus</i> viability	81
Fig. 21: Alr3364 localized to the Z-ring in <i>Anabaena</i>	82
Fig. 22: Conserved sequence motifs of homologous proteins.....	94
Fig. 23: <i>In vitro</i> polymerization of homologous proteins	95
Fig. 24: Interactions of IF-like homologous proteins in a beta-galactosidase assay	95
Fig. 25: <i>In vivo</i> localization of homologous proteins in <i>E. coli</i>	96
Fig. 26: <i>In vivo</i> localization of homologous proteins in <i>Synechocystis</i>	98
Fig. 27: <i>In vivo</i> localization of homologous proteins in <i>Synechococcus</i>	99
Fig. 28: <i>In vivo</i> localization of homologous proteins in <i>Anabaena</i>	101
Fig. 29: Homologous proteins interact with each other and other CCRPs.....	103
Fig. 30: Phenotypic effects of $\Delta alr0931$ in <i>Anabaena</i>	105
Fig. 31: $\Delta slr1301$ impairs cell motility in the PCC-M substrain	106
Fig. 32: Non-segregated $\Delta synpcc7942_1139$ displays decreased culture viability.....	108
Fig. 33: <i>In vitro</i> filamentation of Alr4504 and Alr4505	119
Fig. 34: Alr4504-NGFP and Alr4505-CGFP form filamentous structures in co expressing <i>E. coli</i>	121

Fig. 35: Localization of Alr4504 and Alr4505 in <i>Synechocystis</i> substrains	122
Fig. 36: Co-expressed Alr4504-eCFP and Alr4505-GFP polymerize into heteropolymers in <i>Anabaena</i>	124
Fig. 37: $\Delta alr4504\Delta alr4505$ affects perpendicular growth of <i>Anabaena</i> trichomes.....	125
Fig. 38: Expression of Alr0931-His induces morphological defects	126
Fig. 39: Heterologous expression of All2460-GFP affects <i>Anabaena</i> morphology	127
Fig. 40: $\Delta all2460$ leads to cell fragmentation	129
Fig. 41: Identification of proteins interacting with All2460-GFP and Alr4504-GFP.....	131
Fig. 42: Interconnected cytoskeletal network stabilizing cell-cell connections.....	132

Supplementary figures

Fig. S1: Phylogenetic tree of Fm7001 and its homologous proteins.....	157
Fig. S2: Genomic environment of <i>fm7001</i>	157
Fig. S3: Genomic environment of <i>all4981</i>	158
Fig. S4: <i>In vitro</i> polymerization of Fm7001 into filamentous sheets.....	158
Fig. S5: CreS forms aggregate-like filaments without monovalent ions.....	159
Fig. S6: Heterologously expressed MBP-Fm7001-His induces a filamentous phenotype in <i>E. coli</i>	159
Fig. S7: <i>fm7001</i> is expressed in early growth stages.....	160
Fig. S8: <i>slr7083</i> expression occurs at later growth stages	160
Fig. S9: Tag-orientation dependency of Slr7083 in <i>Anabaena</i>	161
Fig. S10: Verification of $\Delta slr7083$	162
Fig. S11: Slr7083 affects cell viability and colony formation.....	163
Fig. S12: All4981 interacts with MreB and SepJ in a bacterial two-hybrid assay.....	163
Fig. S13: All4981-GFP forms extracellular filaments upon cell lysis.....	164
Fig. S14: <i>synpcc7942_2039</i> is expressed in stationary phase cultures	164
Fig. S15: Verification of $\Delta synpcc7942_2039$	165
Fig. S16: $\Delta synpcc7942_2039$ does not affect cell viability	165
Fig. S17: $\Delta synpcc7942_2039$ does not affect FtsZ localization	166
Fig. S18: Alr3364 interacts with SepJ in a bacterial two-hybrid assay.....	166
Fig. S19: Western blot analysis of anti-GFP co-IP from Alr3364-GFP expressing <i>Anabaena</i> cells.....	167
Fig. S20: Western blot analysis of FtsZ-His degradation assay	167
Fig. S21: Western blot analysis of indirect co-IP of Alr3364-His with <i>Anabaena</i> extract.....	168
Fig. S22: Alr0931 assembles into a filamentous network.....	169
Fig. S23: Slr1301-YFP forms filaments in the motile PCC-M substrain.....	170

Fig. S24: Displacement of thylakoid membranes by Alr0931-GFP and Slr1301-GFP in <i>Synechococcus</i>	170
Fig. S25: Diffuse localization of Alr0931-GFP in <i>Anabaena</i>	171
Fig. S26: Verification of $\Delta alr0931$	171
Fig. S27: Verification of $\Delta slr1301$	172
Fig. S28: Colony PCRs of non-segregated $\Delta synpcc7942_1139$	172
Fig. S29: Interactor proteins of Slr1301-YFP and Alr0931-GFP	173
Fig. S30: Viability tests of $\Delta slr1301$ GT-Kazusa and $\Delta slr1301$ PCC-M.....	173
Fig. S31: Non-segregated $\Delta synpcc7942_1139$ alters <i>Synechococcus</i> colony morphology.	174
Fig. S32: Cell length of non-segregated $\Delta synpcc7942_1139$ is increased	174
Fig. S33: Non-segregated $\Delta synpcc7942_1139$ has no effect on FtsZ localization	175
Fig. S34: Non-segregated $\Delta synpcc7942_1139$ displays decreased viability in a spot assay	176
Fig. S35: <i>alr4504</i> and <i>alr4505</i> share no common transcript.....	177
Fig. S36: Genomic region of <i>alr4504</i> and <i>alr4505</i> in <i>Anabaena</i> genome	177
Fig. S37: Prediction of All2460 transmembrane domains	178
Fig. S38: <i>In vitro</i> filamentation of Alr4505	178
Fig. S39: Alr4504-GFP and Alr4505-GFP show motile properties upon ectopic expression in <i>Anabaena</i>	179
Fig. S40: Verification of $\Delta alr4504\Delta alr4505$	179
Fig. S41: Growth of <i>Anabaena</i> deletion strains in liquid media with osmotic stress factors.	180
Fig. S42: Overexpression of Alr0931-His alters cell shape and chlorophyll distribution in <i>Anabaena</i>	180
Fig. S43: Growth of <i>Anabaena</i> strains expressing fluorescently tagged CCRPs.....	181
Fig. S44: Verification of $\Delta all2460$	181
Fig. S45: Immunolocalization of FtsZ in <i>Anabaena</i> deletion strains	182
Fig. S46: DAPI-staining of <i>Anabaena</i> gene mutant strains	183
Fig. S47: Alcian blue staining of <i>Anabaena</i> deletion strains.....	184
Fig. S48: Spot assay of <i>Anabaena</i> deletion strains.....	185
Fig. S49: Fluorescence recovery of bleached cells from <i>Anabaena</i> mutant strains.....	186
Fig. S50: Fluorescence recovery for representative bleached cells	187
Fig. S51: Network-forming CCRPs self-interact and cross-interact.....	188
Fig. S52: Network-forming CCRPs interact with the MreB cytoskeleton	189
Fig. S53: Interactions of network-forming CCRPs with SepJ and Alr3364	190

Tables

Table 1: <i>E. coli</i> strains	30
Table 2: Growth media and buffer for cellbiological procedures.....	30
Table 3: Buffer and solutions for protein biochemical methods:	31
Table 4: Protein polymerization buffers	32
Table 5: Buffer and solution for nucleic acid procedures.....	32
Table 6: Antibodies.....	32
Table 7: Characteristics of protein candidates	62
Table 8: <i>Anabaena</i> mutant strains reveal defects in calcein exchange rates between cells in a trichome	130
Table 9: Chapter I oligonucleotides	191
Table 10: Chapter I bacterial strains and plasmids	197
Table 11: Chapter II oligonucleotides	202
Table 12: Chapter II bacterial strains and plasmids	206
Table 13: Chapter III oligonucleotides	210
Table 14: Chapter III bacterial strains and plasmids	216

1 Abstract

Cytoskeletal proteins have been long thought to be eukaryote-specific, however, studies of the past 30 years have demonstrated that they exist also in prokaryotes where they regulate essential cellular processes. Intermediate filament (IF)-like coiled-coil rich proteins (CCRPs) were identified in several bacterial species and were shown to regulate cell shape in *Caulobacter crescentus* and mechanical resistance in *Streptomyces coelicolor*. The Cyanobacteria phylum is renowned for its enormous morphological diversity, ranging from unicellular to cell-differentiating and multicellular species. The prokaryotic microtubule homolog FtsZ and the actin-like protein MreB have been studied in cyanobacteria as determinants of cell-shape. Nonetheless, information on IF proteins in the phylum is still lacking. Here we show that IF-like coiled-coil rich cytoskeletal proteins are widespread in cyanobacteria and that they regulate cell shape, motility and trichome integrity in a collaborative manner. Employing the COILS algorithm, we found several thousand CCRPs in cyanobacteria. Of these, we experimentally characterized 21 IF-like protein candidates. This revealed ten novel IF-like cytoskeletal proteins. CCRPs polymerized into a multitude of different structures *in vitro* and had the tendency to assemble into multiplanar sheet-like structures. The taxonomic distribution of the identified IF-like proteins ranges from species-specific to universal proteins within the phylum. Though, several of the proteins studied show a high level of sequence conservation, our results suggest that their function may vary between cyanobacterial species. CCRPs were shown to form interconnected networks with other CCRPs, jointly performing their cellular tasks. Furthermore, a sophisticated cytoskeletal network was identified in *Anabaena sp.* PCC 7120, including at least four CCRPs – Alr0931, Alr4504, Alr4505 and All2460. Together with the MreB cytoskeletal system, they provide scaffolding and stabilizing properties, which link neighboring cells through intercellular pore complexes (i.e., the septosomes). Notably, the polymerization of Alr4504 and Alr4505 is interdependent as they are assembled into heteropolymers only upon co-expression. Our study reveals multiple novel IF-like cytoskeletal proteins in cyanobacteria. We provide insights into the involvement of those in essential cellular processes, often through the formation of interconnected cytoskeletal networks within and between cells. Our results expand the set of known IF-like proteins in prokaryotes and demonstrate that IF-like cytoskeletal proteins are prevalent in prokaryotes. Taken together, this constitutes a profound starting point for further research on cytoskeletal proteins in prokaryotes.

Zusammenfassung

Zytoskelettproteine gelten seit langem als Eukaryoten-spezifisch, jedoch haben Studien der letzten 30 Jahre gezeigt, dass sie auch in Prokaryoten existieren, wo sie essenzielle zelluläre Prozesse regulieren. Intermediärfilament (IF)-ähnliche coiled-coil-reiche Proteine (CCRPs) wurden in verschiedenen Bakterienarten identifiziert und es wurde gezeigt, dass sie die Zellform in *Caulobacter crescentus* und die mechanische Resistenz in *Streptomyces coelicolor* regulieren. Das Phylum der Cyanobakterien ist für seine enorme morphologische Diversität bekannt, welche von einzelligen bis hin zu zellendifferenzierenden und multizellulären Spezies reicht. Das prokaryotische Mikrotubuli-Homolog FtsZ und das Aktin-ähnliche Protein MreB wurden in Cyanobakterien als Determinanten der Zellform untersucht. Nichtsdestotrotz fehlen bis heute Informationen über IF-Proteine in diesem Phylum. Hier demonstrieren wir, dass IF-ähnliche coiled-coil-reiche Zytoskelettproteine in Cyanobakterien weit verbreitet sind und dass diese die Zellform, Motilität und Trichomintegrität kollaborativ regulieren. Unter Verwendung des COILS-Algorithmus identifizierten wir mehrere tausend CCRPs in Cyanobakterien. Von diesen haben wir 21 IF-ähnliche Proteinkandidaten experimentell charakterisiert. Diese Untersuchung ergab zehn neue IF-ähnliche Zytoskelettproteine. CCRPs polymerisierten *in vitro* zu einer Vielzahl von unterschiedlichen Strukturen und hatten die Tendenz, sich zu multiplanaren Strukturen zu assemblieren. Die taxonomische Verteilung der identifizierten IF-ähnlichen Proteine reicht von Spezies-spezifischen bis zu universellen Proteinen innerhalb des Phylums. Obwohl einige der untersuchten Proteine ein hohes Maß an Sequenzkonservierung zeigen, legen unsere Ergebnisse nahe, dass ihre Funktion zwischen verschiedenen Cyanobakterienarten variiert. Wir fanden heraus, dass CCRPs untereinander verbundene Netzwerke mit anderen CCRPs bilden, und so kooperativ ihre zellulären Aufgaben ausführen. Darüber hinaus identifizierten wir ein ausgeklügeltes Zytoskelett-Netzwerk in *Anabaena sp.* PCC 7120, das mindestens vier CCRPs umfasst (Alr0931, Alr4504, Alr4505 und All2460). Zusammen mit dem MreB-Zytoskelettsystem verleihen sie dem Cyanobakterium Gerüst- und Stabilisierungseigenschaften, welche benachbarte Zellen durch interzelluläre Porenkomplexe (sogenannte Septosomen) miteinander verbinden. Bemerkenswerterweise ist die Polymerisation von Alr4504 und Alr4505 voneinander abhängig, da sie nur bei der Co-Expression zu Heteropolymeren assemblieren können. Unsere Studie identifiziert mehrere neue IF-ähnliche Zytoskelettproteine in Cyanobakterien. Wir geben Einblicke über die Funktionen dieser Proteine in essenziellen zellulären Prozessen, welche sich oft durch die Bildung von miteinander verbundenen Zytoskelett-Netzwerken innerhalb und zwischen Zellen manifestieren. Unsere Ergebnisse erweitern das Maß bekannter IF-ähnlicher Proteine in Prokaryoten und zeigen, dass IF-ähnliche Zytoskelettproteine in Prokaryonten weit verbreitet sind. Zusammengefasst bildet diese Arbeit einen umfassenden Ausgangspunkt für die weitere Erforschung von Zytoskelettproteinen in Prokaryoten.

2 Abbreviations

Amp	Ampicillin (100 µg ml ⁻¹)
<i>Anabaena</i>	<i>Anabaena</i> sp. PCC 7120
BACTH	Bacterial adenylate cyclase two hybrid
bp	Base pair
cAMP	Cyclic adenosine monophosphate
cDNA	Complementary DNA
<i>Chlorogloeopsis</i>	<i>Chlorogloeopsis fritschii</i> PCC 6912
Cm	Chloramphenicol (25 µg ml ⁻¹)
cPCR	Colony PCR
CreS	Crescentin
CTAB	Cetrimonium bromide
DAPI	4',6-Diamidin-2-phenylindol
DMSO	Dimethyl sulfoxide
DTT	Dithiothreitol
EDTA	Ethylenediaminetetraacetic acid
<i>Fischerella</i>	<i>Fischerella muscicola</i> PCC 7414
gDNA	Genomic DNA
gRNA	Guide RNA
HEPES	2-[4-(2-hydroxyethyl)piperazin-1-yl]ethanesulfonic acid
HGT	Horizontal gene transfer
IF	Intermediate filament
ImF	Immunofluorescence
IPGT	Isopropyl β-D-1-thiogalactopyranoside
kDa	Kilo Dalton
Km	Kanamycin (50 µg ml ⁻¹)
Nm	Neomycin (30 µg ml ⁻¹)
ORF	Open reading frame
PCC	Pasteur Culture Collection of Cyanobacteria
PIPES	1,4-Piperazinediethanesulfonic acid
RT	Room temperature
RT-PCR	Reverse transcriptase PCR
SDS	Sodium dodecyl sulfate
Sm	Streptomycin (2.5 µg ml ⁻¹)
Sp	Spectinomycin (2.5 µg ml ⁻¹)
<i>Synechococcus</i>	<i>Synechococcus elongatus</i> PCC 7942
<i>Synechocystis</i>	<i>Synechocystis</i> sp. PCC 6803
TSS	Transcriptional start site
WB	Western blot
wt	Wild type
X-gal	5-bromo-4-chloro-3-indolyl-β-D-galactopyranoside

3 General introduction

Unless otherwise stated, information below are adapted from Alberts *et al.* (2014).

3.1 The eukaryotic cytoskeleton

Cellular organization is a prerequisite for proper cellular functions. Cells have to erect and sustain a certain shape in order to properly interact with themselves and with their environment and they have to provide an organized internal structure for an efficient mode of operation. During different life cycles, internal components must dynamically adapt in order to allow proper cell growth, cell division and cellular movements depending on the current requirements of the cell. These manifold tasks are complied by the so-called cytoskeleton. The (eukaryotic) cytoskeleton is a crosslinked network of numerous proteinaceous polymers that assemble into filaments or tubules and which is involved in almost every cellular process. It can be divided into three main filament systems common to most eukaryotic cells: microfilaments (also called actin filaments), microtubules and intermediate filaments. Each of those filament systems is characterized by specific structures, dynamics and cellular and intercellular biological functions. Only the collective collaboration allows them to efficiently coordinate and organize their numerous assigned cellular tasks (Fig. 1A). But there is one thing they all have in common: they are able to form linear polymers within cells (*in vivo*) and in a cell-free environment (*in vitro*) (Moseley, 2013). Cytoskeletal filaments, or biopolymers, easily span the whole diameter of a cell, thereby crossing up to a few hundred micrometers (Fig. 1A). Unlike other biopolymers, including DNA, RNA, subunits of cytoskeletal filaments are not covalently linked to each other and are only connected by comparably weak non-covalent interactions. Accordingly, protein filaments exhibit a stable structure by the sum of their comparable weak interactions. Those interactions can also easily be dissolved providing them with the ability to dynamically adapt. Cytoskeletal proteins can also function as scaffolds for other proteins, commonly employed by nucleotide-dependent motor-proteins (such as kinesin, myosin or dynein) that use the filaments as highway-like transportation routes to guide cargos through the cells in a directed manner. The properties of the different cytoskeletal filament systems are also largely dependent on numerous accessory proteins that physically interact with them. They regulate their function and shape or link them to cellular compartments, highlighting the importance of a tightly regulated cytoskeletal network. A cross-talk of cytoskeletal networks is provided by so-called cytolinker proteins that link different cytoskeletal filament system to one another, thereby coupling the individual functions of the different polymers (Fig 1B; Köster *et al.*, 2015).

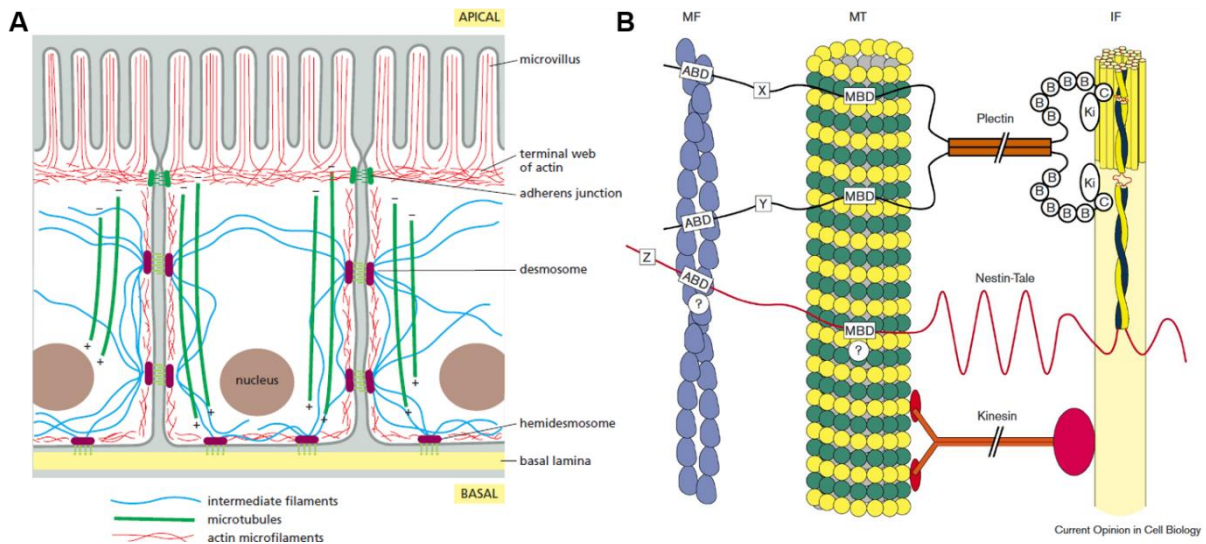


Fig. 1: Eukaryotic cytoskeletal networks

(A) Collaboration of all cytoskeletal systems is essential to shape and organize specialized cells. A two-dimensional network of actin microfilaments (red) lies underneath the plasma membrane and protrudes into the microvilli. Intermediate filaments (blue) provide structural support for the cell and attach to cell-cell connections. Microtubules (green) provide the cell with a polar system and enable directed transport of organelles or other components. (B) Representation of the three interconnected cytoskeletal systems - (MF) microfilaments, (MT) microtubules and (IF) intermediate filaments – linked by the cytolinker protein plectin or directly linked by the type VI IF protein nestin. Kinesin may also connect IF proteins to MTs. Figures taken from (A) Alberts *et al.*, 2014 and (B) Herrmann and Aebi, 2000.

3.1.1 Intermediate filaments

Intermediate filaments (IF) are rope-like cytoskeletal biopolymers that exhibit an intermediate filaments size with a diameter of about 10 nm. They produce the most flexible filaments, fibers and networks among the cytoskeletal systems and are composed of a heterogenous group of IF proteins. Unlike actin and tubulin isoforms that are encoded by only a few genes, whose function are relatively similar, eukaryotic IF protein families are encoded by at least 70 different genes encoding proteins with distinct and cell type-specific functional properties. Among these are prominent IF classes such as vimentin, keratin, desmin and neurofilaments which evolved from duplication of the genes encoding for nuclear lamins (Erber *et al.*, 1999; Alberts *et al.*, 2014; Hering *et al.*, 2016). A distinct feature of IF proteins, compared to the other two cytoskeletal systems, is their ability to spontaneously polymerize in a nucleotide-independent manner without any other mandatory co-factors. They often span the cytoplasm and adhere to cell-cell or cell-matrix junctions like desmosomes or hemidesmosomes, respectively, in epithelial cells (Fig. 1A). IF proteins show only low levels of sequence conservations and even among IF proteins of the same class only about 30% of the amino acid sequence is shared (Hanukoglu and Fuchs, 1983). As a result of their sequence divergence and despite their similar domain organization, different IF proteins yield distinct filamentous structures (Köster *et al.*, 2015). Vimentin and desmin form meshwork-like networks while keratin IF proteins mainly form filamentous bundles which are only sparsely connected (Köster *et al.*, 2015).

Despite their poor sequence conservation and different *in vivo* and *in vitro* characteristics, IF proteins share a common structural tripartite building plan, consisting of a central α -helical rod-domain of conserved size, which is N- and C-terminally flanked by highly variable head and tail domains (Fig. 2) (Herrmann and Aebi, 2004). The rod-domain largely consists of regular heptad repeats (a repetitive 7 amino acid residue pattern) forming three coiled-coil segments (coil 1A, coil 1B and coil 2), separated by two linkers (L1, L12) with a discontinuity of the heptad repeat pattern – named stutter – in the third coiled coil segment (Fig. 2) (Herrmann and Aebi, 2004; Köster *et al.*, 2015). The heptad repeats in the α -helical segments of the rod-domain are a repeated pattern - hxxhcxc – of (c) charged and (h) hydrophobic amino acids (x being a variable for any amino acid) that mediate the arrangement of the α -helices into unstaggered parallel coiled-coils (Ausmees, Kuhn and Jacobs-Wagner, 2003; Köster *et al.*, 2015). The extended coiled-coil structures of two IF proteins assemble in a non-polar fashion into dumbbell-shaped parallel dimers. These dimers further associate in a staggered antiparallel tetramer that forms oligomers and subsequently polymers with other tetramers by lateral association. Due to their tight subunit association, IF proteins are extremely stable and insoluble under physiological conditions, a feature that, up until now, prevented any crystallization-based structural studies (Cabeen and Jacobs-Wagner, 2010). In order to employ them for *in vitro* studies, IF proteins have to be solubilized using chaotropic agents (6-8 M urea or 6 M guanidine-HCl) (Herrmann and Aebi, 2004). IF proteins subjected to subsequent dialysis form dimers and oligomers in high molar urea containing buffers (Köster *et al.*, 2015). For example, vimentin is present as a monomer in 6 M urea and assembles into tetramers in 5 M urea (Köster *et al.*, 2015). Intriguingly, different IF protein types do not co-polymerize and have thus been divided into three different assembly groups (Herrmann and Aebi, 2000).

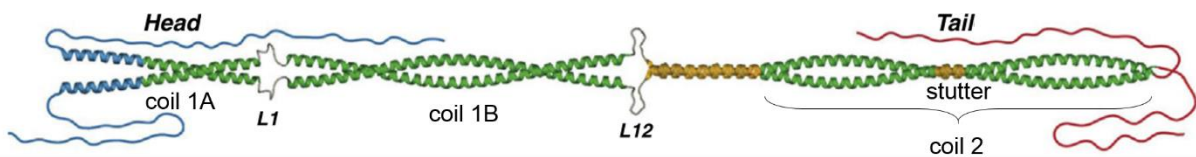


Fig. 2: Structural model of a cytoplasmic human vimentin dimer

Human vimentin dimer shows a central α -helical rod-domain that is divided into three coiled-coil segments (1A, 1B, 2). Non-coiled-coil linker sequences (L1, L12) connect the individual coiled-coil segments. Right-handed α -helices are shown in green, nearly parallel α -helices and the stutter are depicted in yellow. Variable N- and C-terminal domains are indicated in blue and red, respectively. Figure modified from Herrmann *et al.*, 2007.

3.1.2 Cytolinker proteins

Plectin belongs to the plakin superfamily of large globular cytolinkers that connect the three main cytoskeletal systems (MFs, MTs; IFs) and link them to organelles like the nucleus, adhesive structures such as desmosomes or hemidesmosomes at the plasma membrane or

to motor proteins (Fig. 1B) (Wiche, Osmanagic-Myers and Castañón, 2015). Thus, plakins play an essential role for the intracellular orchestration, cellular polarity and maintaining of tissue integrity by regulating cell-cell and cell-matrix junctions (Leung, Green and Liem, 2002; Bouameur, Favre and Borradori, 2014). **Catenins** directly bind to the cytosolic actin cytoskeleton and the cadherin adhesion proteins in adherence junctions, linking the actin cytoskeleton of two neighboring cells. The cell-cell connecting function of cadherins is relying on adapter proteins such as β -catenin and p120-catenin as well as the not directly associated α -catenin. This network of adapter proteins jointly forms dense attachment plaques that hold the cadherin clusters of adherence junctions together. α -catenin and β -catenin are also involved in Wnt signaling pathway, a process ultimately leading to contact inhibition, preventing unusual tissue growth pattern. Catenin function, like plakin function, is therefore an essential contributor to cellular and tissue development and maintenance.

3.2 The bacterial cytoskeleton

On average, a prokaryotic cell is between 0.2-5 μm long, this is less than a tenth of a eukaryotic cell, whose cell size ranges from 10-100 μm (Reece *et al.*, 2013). Prokaryotes lack any form of discernable internal compartmentalization into membrane-enclosed organelles such as the nucleus (Reece *et al.*, 2013). There is no boundary between the nucleoid and the cytosol in prokaryotes with no DNA-packaging structures like histones (Reece *et al.*, 2013). Unlike eukaryotes, prokaryotes are usually surrounded by a distinct and chemically complex cell wall that protects them from external influences, which seemingly would relieve them from the need to evolve a cell-stabilizing cytoskeleton like in eukaryotes (Reece *et al.*, 2013). As a consequence, it was long thought that prokaryotes do not require a distinct cytoskeletal network and that intracellular contents are just randomly placed within the cells by diffusion (Löwe and Amos, 2017). However, this dogma was rapidly overturned by the discovery of the cell-division protein FtsZ, a bacterial tubulin homolog (Bi and Lutkenhaus, 1991; de Boer, Crossley and Rothfield, 1992). Shortly afterwards, MreB, the first bacterial actin homolog was discovered and found to be involved in cell-shape determination (Bork, Sander and Valencia, 1992; Ent, Amos and Löwe, 2001). Since then, many other prokaryotic homologs to actin and tubulin were discovered and the ongoing research also led to the identification of bacterial intermediate filament-like proteins, such as Crescentin (CreS), and even entirely new bacterial cytoskeletal classes (Ausmees, Kuhn and Jacobs-Wagner, 2003; Ramamurthi and Losick, 2008; Kühn *et al.*, 2010). These discoveries revealed that even simple organisms like bacteria depend on a sophisticated cytoplasmic filamentous cytoskeleton which mediates numerous cellular activities, including replication, cell wall synthesis or cell-shape manifestation (Löwe and Amos, 2017). The three cytoskeletal systems (MFs, MTs and IFs) and their intracellular abundance show a remarkable conservation among all kingdoms of life. This evidences the

evolutionary preservation of cytoskeletal networks in a group of microorganisms whose genomes have been under a strong evolutionary pressure compared to eukaryotes (Koonin, 2015; Wagstaff and Löwe, 2018). Thus, phyla-independent conservation of long scaffolding structures illustrates the importance and the usefulness of these filaments for the orchestration of cellular processes, which is why cytoskeletal proteins were preserved over time (Löwe and Amos, 2017; Wagstaff and Löwe, 2018). In an evolutionary context, the study of related cytoskeletal proteins provides a distinct advantage over studying enzymes (Löwe and Amos, 2017). Enzymes often catalyze reactions of small common molecules and thus can easily be exchanged between different species, whereas a sophisticated interconnected and interdependent filamentous network is rather unlikely to be replaced by gene transfer (Koonin, 2015). Despite conservation of major cytomotive and cytoskeletal systems, the great variety of function, composition and structure of prokaryotic and eukaryotic cytoskeleton reveals that certain evolutionary relationships may be indistinct (Wickstead and Gull, 2011).

3.2.1 Tubulin-like proteins in prokaryotes

Tubulin homologs are broadly distributed and can be found in bacteria as well as in archaea where they orchestrate distinct cellular functions (Wagstaff and Löwe, 2018). Some proteins are present in all species of a respective family while others have so far only been identified in a single species (Wagstaff and Löwe, 2018). Tubulin homologs are usually encoded on the chromosome but have also been identified on plasmids or prophages as in the case of TubZ and PhuZ, respectively (Larsen *et al.*, 2007; Kraemer *et al.*, 2012).

FtsZ - the ancestor of the eukaryotic tubulin - is an essential and highly conserved cell-division gene present in almost all bacteria, Euryarchaeota as well as in chloroplasts of photosynthetic eukaryotes and it has also been identified in some other archaea or even in mitochondria (Osteryoung and Nunnari, 2003; Miyagishima *et al.*, 2004; Yoshida *et al.*, 2016; Wagstaff and Löwe, 2018). FtsZ exhibits a very low level of sequence conservation to eukaryotic tubulins (< 10%) but reveals a striking resemblance in the tertiary structure (Löwe and Amos, 1998; Nogales *et al.*, 1998). Archaeal species from the Crenarchaeota phylum and a few parasitic bacteria such as *Mycoplasma mobile* and *Chlamydia trachomatis* that exhibit a highly reduced genome lack FtsZ and undergo cell division by a so far unknown mechanism (Miyagishima *et al.*, 2014). Like in many parasitic bacteria, FtsZ is also absent in a broad spectrum of bacterial endosymbionts that have lost their peptidoglycan (PG) synthesis machinery, indicating a likely link between the loss of a PG cell wall and a loss of FtsZ (Miyagishima *et al.*, 2014). FtsZ polymerization is GTP-dependent and resembles the treadmilling pattern of eukaryotic tubulin, providing dynamic properties to the protofilament (Wagstaff and Löwe, 2018). *In vitro* and *in vivo*, FtsZ polymerizes into straight or ring-shaped filaments that can assemble into superstructures of bundles or sheets upon application of

crowding agents or multivalent cations (González *et al.*, 2003; Wagstaff and Löwe, 2018). Despite its different polymerization pattern, microtubule-like structures were never identified for FtsZ so far (Mukherjee and Lutkenhaus, 1994; Lu, Reedy and Erickson, 2000; González *et al.*, 2003). In eukaryotes, the formation of the cytokinetic ring is an actin-mediated process, while in prokaryotes, the comparable task is performed by the tubulin homolog FtsZ (Celler *et al.*, 2013). After completed chromosome segregation, FtsZ assembles to form the contractile cytokinetic Z-ring at the future division site (Cabeen and Jacobs-Wagner, 2010; Celler *et al.*, 2013). The subsequent process of cell-wall remodeling, cytokinesis and cell division is relying on the so-called divisome that is recruited by the Z-ring (which usually arrives first at the septum site), thereby functioning as a scaffolding structure (Lutkenhaus, Pichoff and Du, 2012). Based on the discovery that FtsZ polymers play an essential role already in early cell division stages, and further studies that revealed a constrictive force of purified FtsZ in liposomes, it was long assumed that the Z-ring, and thus FtsZ, is the main constricting force during cytokinesis (Szwedziak *et al.*, 2014). However, using higher-resolution microscopy of the peptidoglycan synthesis process, a new model was proposed that points to the idea that the cell wall synthetic machinery operates as the main constriction force during septum formation (Daley, Skoglund and Söderström, 2016; Xiao and Goley, 2016; Wagstaff and Löwe, 2018). In the unicellular rod-shaped cyanobacterium *Synechococcus elongatus* PCC 7942 (hereafter *Synechococcus*), the circadian clock has been linked to the FtsZ-driven cell division apparatus (Mori and Johnson, 2001). In the coccoid cyanobacterium *Synechocystis* sp. PCC 6803 (hereafter *Synechocystis*) and in the nitrogen-fixing, cell-differentiating and multicellular cyanobacterium *Anabaena* sp. PCC 7120 (hereafter *Anabaena*), FtsZ is an essential cellular component and its cellular concentration is tightly controlled by a so far undescribed protease in *Anabaena* (Zhang *et al.*, 1995; Lopes Pinto *et al.*, 2011). Apart from its impact on cell division, the FtsZ-driven divisome also mediates the localization of SepJ, a cyanobacterial cell junction protein, highlighting its impact on the cyanobacterial multicellular phenotype (Ramos-León *et al.*, 2015).

Apart from the most extensively studied tubulin homolog – FtsZ - other members of the tubulin superfamily comprise FtsZm, CetZ, TubZ, BtubAB, FtsZI and Artubulin (Wagstaff and Löwe, 2018). Not all of them were yet assigned to a specific cellular function and CetZ and Artubulin seem to be archaea-specific proteins (Wagstaff and Löwe, 2018). Despite their different cellular functions tubulin homologs all share dynamic properties, often being used to move particles through the cell (Ingerson-Mahar and Gitai, 2012). Tubulin homologs reveal a conserved monomeric structure with a distinct bipartite globular domain containing an essential GTPase domain but assemble into diverse filamentous structures *in vivo* and *in vitro* (Fig. 3) (Nogales *et al.*, 1998). FtsZ consists of only one protofilament whereas BtubAB and TubZ form narrow microtubules of 4 associated protofilaments, thereby more closely resembling the

eukaryotic microtubules, which are composed of 13 parallel protofilaments (Deng *et al.*, 2017; Wagstaff and Löwe, 2018).

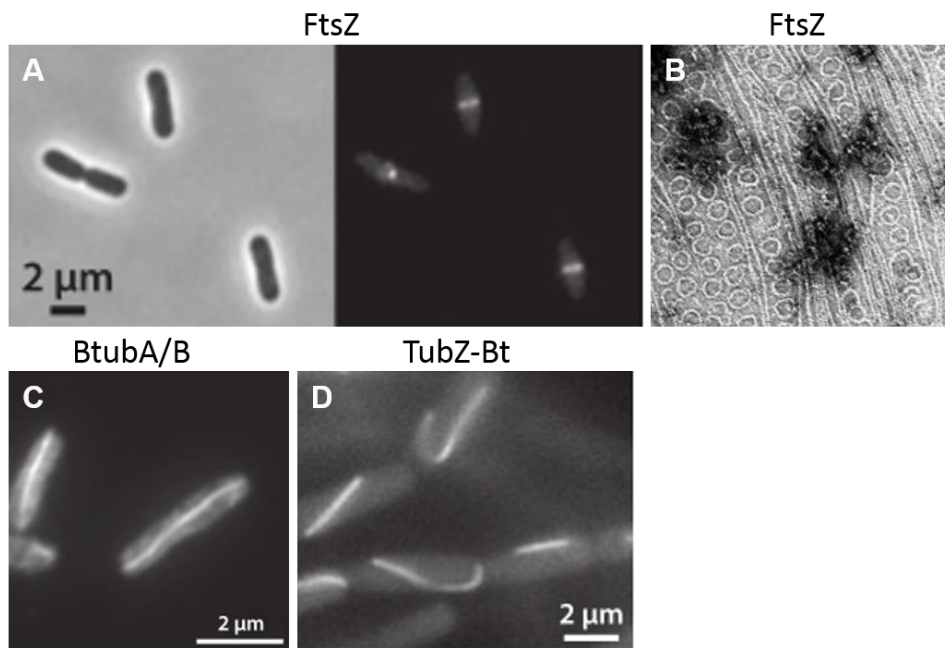


Fig. 3: Bacterial tubulin homologs

Epifluorescence and transmission electron microscope (TEM) micrographs of bacterial tubulin homologs (A,B) FtsZ, (C) BtubA/B and (D) TubZ-Bt. (A) FtsZ-GFP localizes as Z-rings at sites of cell division in *E. coli*. (B) Negatively stained *E. coli* FtsZ forming straight or curved protofilaments in the presence of GTP. (C) Immunofluorescence of long and straight BtubA/B filaments in *E. coli*. (D) Curved and straight TubZ-GFP filaments in *Bacillus thuringiensis*. Figures modified from (A,C,D) Cabeen and Jacobs-Wagner (2010) and (B) Erickson and Osawa (2017).

3.2.2 Actin-like proteins in prokaryotes

The actin superfamily is an ancient and highly divergent group of proteins that are widely distributed among different domains of life (Bork, Sander and Valencia, 1992). All these proteins share the presence of an ATP-binding site and an ATP hydrolyzing capability preserved in an actin-like fold (Bork, Sander and Valencia, 1992; Kabsch and Holmes, 1995; Carballido-Lopez, 2006). Prominent members of the superfamily comprise eukaryotic sugar kinases, hexokinases and actin, while MreB, ParM and FtsA are of prokaryotic origin (Bork, Sander and Valencia, 1992; Carballido-Lopez, 2006). Phylogenetic analysis revealed more than 20 subgroups of actin homologs, some being encoded on the chromosome while others, like ParM, are encoded on plasmids (Derman *et al.*, 2009). Proteins of the actin superfamily display only very low levels of sequence similarity (~15%) and only limited shared functional properties to each other and it is believed that they all descended from a common ATP-hydrolyzing ancestor (Bork, Sander and Valencia, 1992). It is assumed that filament-forming actins belong to a monophyletic group of proteins that diverged early during the evolution of actin-like proteins, implying that actin-like polymerization only evolved once (Wagstaff and Löwe, 2018). Members of the filament-forming clade have sequentially evolved to form an

enormous diversity of different filamentous structures but with a prevailed head-to-tail assembly of protein monomers (van den Ent *et al.*, 2014; Wagstaff and Löwe, 2018). Two of them, MreB and ParM, are functional homologous of actin and they further share similar functional features (Wagstaff and Löwe, 2018). For example, both proteins are not only dependent on ATP but can also bind GTP and employ both nucleotides for polymerization (Popp, Narita, *et al.*, 2010).

MreB is a chromosomally encoded cell shape-determining protein that is conserved in almost all cell-wall-engulfed and elongated bacteria and in some archaea (Jones, Carballido-López and Errington, 2001). It is essential for cell wall synthesis in almost all elongated, helical and filamentous prokaryotes and is absent from most coccoid-shaped bacteria, suggesting a major role in non-spherical cell shape determination (Ent, Amos and Löwe, 2001; Jones, Carballido-López and Errington, 2001). Some Gram-positive species, like the rod-shaped *Bacillus subtilis* encode even multiple *mreB* copies (*mbl* and *mreBH*), a feature not present in Gram-negative bacteria (Carballido-López *et al.*, 2006). MreB polymers form linear antiparallel and non-polar protofilament pairs (*in vitro* crystal structures and *in vivo*) that tightly associate with the plasma membrane (Fig. 4A,B) (van den Ent *et al.*, 2014; Wagstaff and Löwe, 2018). The latter feature, which is provided by an amphipathic helix and the fact that MreB filaments can only bend in one direction, distinguishes MreB from actin. (van den Ent *et al.*, 2014; Wagstaff and Löwe, 2018). Furthermore, MreB assembly into duplets is essential for its cell shape-determining function (van den Ent *et al.*, 2014). Together with the so-called elongasome - a multi-enzyme cell wall synthesis machinery – short discontinuous MreB filaments locally organize cell wall synthesis in a patchy pattern moving around the cell in a circumferential pattern (Garner *et al.*, 2011; Swulius and Jensen, 2012). Albeit, in contrast to FtsZ, MreB is directed by the motor activity of the elongasome while FtsZ treadmilling motion moves the divisome (Ingerson-Mahar and Gitai, 2012; Wagstaff and Löwe, 2018). This elongasome, in part, is composed of many cell wall-associated proteins such as MreC, MreD, MurG, Pbp2 and RodA (Shaevitz and Gitai, 2010). MreB is essential in a variety of organisms, including *B. subtilis*, *Caulobacter crescentus* and *E. coli* (Kruse, Bork-Jensen and Gerdes, 2005; Carballido-Lopez, 2006). MreB is not essential for the vegetative state of *Streptomyces coelicolor* but is indispensable for spore formation, possibly through misguided cell wall assembly (Mazza *et al.*, 2006). MreB is essential in the rod-shaped cyanobacterium *Synechococcus*, and partially segregated mutants reveal a coccoid phenotype (Jain, Vijayan and O'Shea, 2012). In the filamentous cyanobacteria *Anabaena*, MreB is not essential but it is involved in cell shape determination, which is in agreement with the morphogenic observations of MreB in the filamentous cyanobacterium *Fremyella diplosiphon* (Hu *et al.*, 2007; Singh and Montgomery, 2014).

ParM belongs to the large number of plasmid-encoded actin-like protein and is encoded on the R1 plasmid in *E. coli* and only exhibits about 20% sequence identity to MreB (Gerdes, Larsen and Molin, 1985; Wickstead and Gull, 2011). Unlike actin, purified ParM filaments form left-handed instead of right handed helices (Orlova *et al.*, 2007). The ParM system, with homologs restricted to the Enterobacteriaceae, mediates stable inheritance of low-copy plasmids and its function reveals a simple and yet effective mode of DNA segregation (Shih and Rothfield, 2006; Popp, Xu, *et al.*, 2010). ParM polymerizes between the two dividing plasmids providing the mechanical force for plasmid-segregation (Fig. 4C) (Carballido-Lopez, 2006). The bipolar ParM spindles consist of an bundle of four protofilaments which are extended from the ParRC-bound ends (Van den Ent *et al.*, 2002; Gayathri *et al.*, 2012). Fluorescence resonance energy transfer experiments further revealed that ParM undergoes dynamic instability (i.e. catastrophe as present in tubulin), a process essential for plasmid segregation (Garner, Campbell and Dyce Mullins, 2004).

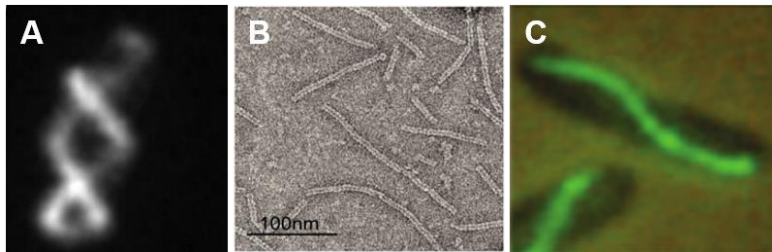


Fig. 4: Bacterial actin homologs

Epifluorescence and TEM micrographs of MreB and ParM. (A) Helical localization of YFP-MreB in *E. coli*. (B) Negatively stained MreB filaments. (C) Immunofluorescence of spindle-like bundles of ParM in *E. coli*. Figures modified from (A) Vats and Rothfield (2007), (B) van den Ent *et al.* (2014) and (C) Carballido-Lopez (2006).

3.2.3 Intermediate filament-like proteins in prokaryotes

The first intermediate filament (IF)-like protein – CreS from the stalked Gram-negative species *C. crescentus* - was discovered shortly after the first bacterial actin and tubulin homologs were described (Ausmees, Kuhn and Jacobs-Wagner, 2003). IF-like proteins, like their eukaryotic homologs, are mainly characterized by extended structural coiled-coil domains that form parallel or antiparallel helices with each other (Wagstaff and Löwe, 2018). This domain motif has also been successfully employed in order to predict novel prokaryotic IF-like proteins using an algorithm that specifically detects coiled-coil rich regions within a given protein sequence – the so-called COILS algorithm (Lupas, Van Dyke and Stock, 1991). Using this algorithm, Bagchi *et al.* (2008) identified several IF-like proteins from *S. coelicolor* (SCO5396, later termed FilP), *Mycobacterium bovis* (MB1709) and *Janibacter sp.* (JNB03975), confirming its predictive power. Unlike actin and tubulin homologs, IF homologs hardly share any sequence similarities and appear to be relatively variable in size and coiled-coil domain order (Bagchi *et al.*, 2008; Lin and Thanbichler, 2013). The few existing similarities are mainly accounted by the

coiled-coil motif with its conserved heptad-repeat pattern (Cabeen and Jacobs-Wagner, 2010). Instead, the versatile group of IF proteins rather shares common functional and structural properties, forming non-dynamic rigid and stable structure-providing scaffolds within the cells, many of which only being present in a very limited subset of species (Lin and Thanbichler, 2013).

CreS is currently the best studied member of the bacterial IF-like protein family and was the first bacterial IF-like protein ever to be identified in *C. crescentus*, where it provides the cell with its typical curved morphology (Ausmees, Kuhn and Jacobs-Wagner, 2003). Like eukaryotic IF proteins, CreS is able to spontaneously polymerize into filaments in a nucleotide-independent manner *in vitro*, forming straight filaments (Fig. 5B, lower panel; 10 nm in width) that can assemble into bundles by lateral association (Ausmees, Kuhn and Jacobs-Wagner, 2003). CreS's domain organization is reminiscent to eukaryotic IF protein domain composition including the spacer region in the last coiled-coil domain (Fig. 5A) (Ausmees, Kuhn and Jacobs-Wagner, 2003). In the cells, CreS filaments line the inner curvature of *C. crescentus* (Fig. 5B, upper panel) and it is assumed that CreS attaches to the cell membrane where it exudes local mechanical force. This force regulates the rate of PG synthesis, ultimately leading to a curved morphotype (Cabeen *et al.*, 2009; Lin and Thanbichler, 2013). Heterologous expression of CreS in *E. coli* results in a likewise curved phenotype, suggesting that species-conserved interacting partners – like MreB - link CreS to the cell membrane (Lin and Thanbichler, 2013). Intracellular CreS filaments are extremely stable without any apparent dynamic turnover as indicated by FRAP (Fluorescence Recovery After Photobleaching) experiments and newly synthesized CreS is incorporated into the CreS filament along the whole structure, indicating a lack of polarity (Charbon, Cabeen and Jacobs-Wagner, 2009; Lin and Thanbichler, 2013). CreS polymerization is halted at the tip of the cell by a so far unknown mechanism, thereby preventing the formation of a U-shaped cell (Cabeen *et al.*, 2009; Charbon, Cabeen and Jacobs-Wagner, 2009). The cytoskeletal metabolic enzyme CtpS (discussed in more detail below) co-localizes and interacts with CreS and additionally acts as a negative regulator of CreS assembly, thereby preventing excessive bending of the cell (Ingerson-Mahar *et al.*, 2010). Point mutations that disrupt CtpS's metabolic function don't alter its morphogenic capacity and *C. crescentus* cells lacking CtpS becomes overly curved, indicating that CreS polymerization might be kept in check by CtpS (Ingerson-Mahar *et al.*, 2010). During cell division, membrane-attached CreS filaments are disassembled in a putative divisome-dependent manner and distributed to the daughter cells with subsequent re-assembly (Lin and Thanbichler, 2013). Crescentin is often considered a prokaryotic homologue to eukaryotic IF proteins like laminin or vimentin, however, given its restricted distribution to so far only one identified organism, it is currently disputed whether CreS is a real homolog to

eukaryotic IF proteins or whether it was rather acquired in *C. crescentus* by horizontal gene transfer (Erickson, 2007; Wickstead and Gull, 2011).

Employing the COILS algorithm from Lupas et al. (1991), Bagchi and colleagues (2008) identified several coiled-coil rich, central rod-domain-containing proteins from a diverse set of species, indicating that rod-domain proteins are broadly distributed among bacteria and are frequently used to perform morphological functions. Among those proteins, **FilP** from *S. coelicolor*, was identified and further characterized as another prokaryotic cytoskeletal protein fulfilling IF-like properties (Bagchi *et al.*, 2008). Like CreS, FilP forms an extended network of filaments in a nucleotide-independent manner *in vitro* (Fig. 5C, lower panel). Within *S. coelicolor*, FilP polymerizes into filamentous structures that underline the cell membrane with a pronounced localization to the tip of a hyphae (Fig. 5C, upper panel). FilP is important for proper cell growth and germination of *S. coelicolor*, possibly through an interaction with the polar cell wall synthesis machinery as cells lacking FilP show defects in mechanical resistance (Bagchi *et al.*, 2008). Thus, FilP, like eukaryotic IF proteins, is important for the cellular resistance to deformations (Cabeen and Jacobs-Wagner, 2010).

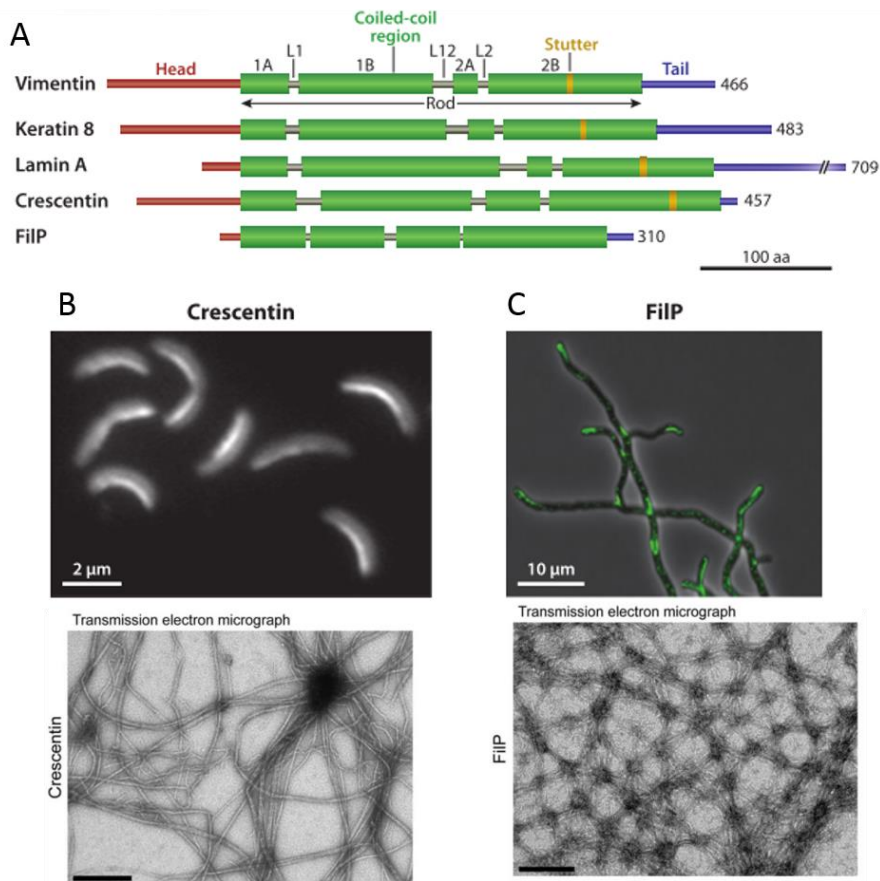


Fig. 5: IF-like cytoskeletal proteins CreS and FilP

(A) Depiction of coiled-coil domain architecture of eukaryotic Vimentin, Keratin 8 and Lamin A compared to prokaryotic CreS and FilP. (B) Top panel: Fluorescence micrographs of FIAH-stained CreS-TC expressed in *C. crescentus*. Lower panel: Transmission electron micrographs of negatively stained CreS. (C) Top panel: Fluorescence micrograph of FilP-GFP filaments in *S. coelicolor*. Lower panel: Transmission electron micrograph of negatively stained FilP. Figure modified from Cabeen and Jacobs-Wagner (2009) and Lin and Thanbichler (2013).

3.2.4 Prokaryotic-specific cytoskeletal proteins

The long evolutionary history of prokaryotes, coupled with the relatively strong evolutionary pressure to which they are exposed, not only gave rise to altered homologous counterparts to the eukaryotic cytoskeleton but eventually also produced a variety of prokaryotic-specific cytoskeletal proteins (Koonin, 2015; Löwe and Amos, 2017). Many of which are still only poorly characterized or not even yet identified (Dobro *et al.*, 2017). Electron cryotomography micrographs revealed several filamentous structures of unknown origin that putatively comprise novel prokaryotic cytoskeletal proteins (Dobro *et al.*, 2017). Nevertheless, the great diversity of filamentous (cytoskeletal) proteins is another indication for the efficiency and suitability of polymeric structures to orchestrate cellular functions (Wagstaff and Löwe, 2018).

Members of the **bactofilin** family mark one of those prokaryotic-specific and yet highly conserved and widely distributed cytoskeletal classes (Cabeen and Jacobs-Wagner, 2010). Bactofilins are rather small proteins (~18 kDa) that exhibit a central, yet uncharacterized

domain (DUF583) (Kühn *et al.*, 2010). Their function and polymerization dynamics are still only poorly understood but they were shown to be involved in the cell-wall remodeling system by direct interaction with PbpC in *C. crescentus* (Penicillin-binding protein) (Kühn *et al.*, 2010). In *C. crescentus*, two paralogs, BacA and BacB, exist and usually co-localize to one cell pole (Kühn *et al.*, 2010). They physically interact with each other and reveal a CreS-independent impact on the cell curvature (Kühn *et al.*, 2010). Like other cytoskeletal proteins, BacA, BacB and homologous proteins form filaments *in vitro* but exhibit quite diverse functional properties in their species of origin (Kühn *et al.*, 2010). For example, bactofilin homologs in *Myxococcus xanthus* form cell-traversing filaments which are involved in social motility (Kühn *et al.*, 2010; Koch, McHugh and Hoiczky, 2011).

The ParA/MinD family encompass another prokaryotic-specific group of cytoskeletal proteins with no existing members of eukaryotic origin, which is characterized by the presence of a Walker A-motif ATPase domain (Cabeen and Jacobs-Wagner, 2010). Although bacterial ParA and MinD function relies on ATP hydrolysis they belong to the P-loop GTPase superfamily with homologous proteins being identified in archaea and in plant or green algae plastids (Ingerson-Mahar and Gitai, 2012; Lutkenhaus, 2012). ParA and MinD mediate the proper localization of large cellular components like chromosomes and plasmids or the Z-ring (Cabeen and Jacobs-Wagner, 2010). ParA-driven plasmid and chromosome segregation is based on a similar albeit different mechanism to plasmid segregation driven by ParM (Cabeen and Jacobs-Wagner, 2010). ParA polymerizes *in vitro* in an ATP-dependent manner, a property that has not yet been described to full satisfaction for MinD (Hu, Gogol and Lutkenhaus, 2002; Suefuji, Valluzzi and RayChaudhuri, 2002; Ebersbach *et al.*, 2006). In *E. coli*, MinD together with MinC and MinE (in the MinCDE system) regulate accurate placement of the cytokinetic Z-ring in an ATP-dependent, cell-rotating oscillatory fashion with a decreasing gradient towards the cell center (Lutkenhaus, 2012). ATP-binding induces MinD dimer formation and a subsequent association with the cell membrane followed by binding to MinE and MinC (Lutkenhaus, 2012). Thereby, MinC gets activated and then acts as an FtsZ capping protein, preventing Z-ring formation at sites of high MinCD concentration (Lutkenhaus, 2012). MinE regulates the MinCD complex, preventing its formation at the cell center (Lutkenhaus, 2012).

3.3 Evolution of cytoskeletal proteins from enzymes – the enzyme theory

Apart from the classical cytoskeletal proteins (MF, MT, IF), prokaryotes possess several other unique cytoskeletal proteins as indicated above. Those proteins have been identified and characterized to different degrees and functions and polymerization properties were assigned. A common theme for all those proteins, in varying degrees, is the involvement in structural or cellular organizational processes often providing mechanical resistance to external influences.

However, recent research has identified another, so far only scarcely described class of novel cytoskeletal proteins that, apart from their filamentous and structural properties, also implement metabolic functions in the cells (Ingerson-Mahar and Gitai, 2012). GFP-localization studies by Werner *et al.* (2009) showed that CtpS, the enzyme that catalyzes the synthesis of CTP from UTP, ATP and glutamine forms filaments *in vivo*. The CtpS enzyme is an ubiquitous enzyme conserved in all organisms and has a morphogenic impact on *C. crescentus* where it localizes as a filamentous structure at the site of cell curvature (Ingerson-Mahar *et al.*, 2010). CtpS filamentation can be stimulated by CTP, which is a common property that was also described for CtpS in yeast, flies, rats and in *E. coli* (Ingerson-Mahar *et al.*, 2010; Liu, 2010; Noree *et al.*, 2010). The polymerization capability and cell shape maintenance properties are independent of CtpS's metabolic function (Ingerson-Mahar *et al.*, 2010). In *C. crescentus*, CtpS associates with CreS and gene deletion mutants exhibit a more pronounced cell curvature compared to the wildtype (Ingerson-Mahar *et al.*, 2010). However, metabolic and cell shape maintenance functions can be rescued by *E. coli* CtpS, suggesting that the cytoskeletal role of CtpS in *C. crescentus* evolved after its polymerization capacity (Ingerson-Mahar and Gitai, 2012). Developing filamentous properties to perform enzymatic functions was also shown for other metabolic enzymes such as the acetyl-CoA carboxylase, the glutamate synthase or even the crystallin proteins in the eye, although their cytoskeletal tasks are yet to be described (Gregolin *et al.*, 1966; Zigler and Rao, 1991; Noree *et al.*, 2010; Ingerson-Mahar and Gitai, 2012). As described above, even actin and MreB are related to sugar kinases, suggesting that the scaffolding and local restriction of catalytic reactions is advantageous compared to random cellular distribution and it is therefore conceivable that filamentous properties were only later co-opted for cytoskeletal properties and originally evolved for a purely metabolic purpose (Ingerson-Mahar and Gitai, 2012). As all cells perform enzymatic reactions, this would also explain the ubiquitary conservation of filamentous cytoskeletal elements throughout all domains of life (Ingerson-Mahar and Gitai, 2012). From an evolutionary and practical point of view it also seems advantageous to exploit already existing structures to the hilt instead of evolving entirely new ones (Ingerson-Mahar and Gitai, 2012).

3.4 Origin of the cytoskeleton

The difference between the large, compartmentalized and highly structured eukaryotic cells and the rather small and undefined prokaryotic cells is so evident that it can be difficult to even try to assign proper statements about their respective relationships, especially when taking into considerations that no intermediate has been found that could close this tremendous gap (Koonin, 2015). This is even more apparent considering that all specialized attributes of the eukaryotic cell – termed the eukaryome, consisting of a distinct cytoskeleton, the ubiquitin system and a cell division and membrane remodeling system (including phagocytosis

properties) - were already part of the last eukaryotic common ancestor (LECA) (Koonin, 2015). Thus, these clear differences led to the development of a tree of life with three main domains, which is present in most biology textbooks in which the eukaryotic domain (Eukarya) exists next to two prokaryotic domains (Bacteria and Archaea), sharing a common ancestor with the Archaea (Reece *et al.*, 2013; Spang *et al.*, 2015). However, currently there arises more and more substantial evidence for a two-domains-based tree in which the Eukarya domain originates from within the Archaea domain, indicating that eukaryotes are direct descendants of archaea (Reece *et al.*, 2013; Koonin, 2015). The three-domains tree was mainly supported by early phylogenetic analyses that gave rise to the idea of a primary amitochondrial eukaryote that subsequently engulfed the proto-mitochondrial endosymbiont and because the prerequisite for symbiosis, the capacity to perform phagocytosis, is absent in archaea (Koonin, 2015). The identification of mitochondria-like structures in these organisms by comparative genomics, however, has left that theory without substantial support (Koonin, 2015). Instead, recent data support the theory of symbiogenetic eukaryogenesis, which states that eukaryotes arose from the symbiosis of an archaeon, possibly from the TACK superphylum (formerly consisting of Thaumarchaeota, Aigarchaeota, Crenarchaeota and Korarchaeota), with a Gram-negative α -proteobacterium that eventually gave rise to the mitochondria (Koonin, 2015). A prerequisite for this theory is a last common ancestor that, at least to a certain degree, exhibits the above stated attributes of the eukaryome (Koonin, 2015). The symbiogenetic idea is supported by the presence of many eukaryotic genes of archaeal and bacterial origin in the eukaryotic genome and by recent phylogenetic analyses of universal proteins placing the origin of eukaryotic proteins deep within the TACK superphylum (Koonin, 2010; Wickstead and Gull, 2011). In further support for this theory, phylogenetic studies revealed a scattered eukaryome in various archaeal species of the TACK clade, including key components of the actin (named crenactins; putative mediators of phagocytosis) and tubulin cytoskeleton, an FtsZ and/or ESCRT-III-based cell division system, a ubiquitin central signaling and regulatory system and a RNA interference system (Koonin, 2015). Thus, a common ancestor having possessed all of these attributes at once is conceivable, especially considering that those attributes prevailed in extant archaea even though this domain is characterized by a gradual gene loss (Wolf and Koonin, 2013; Koonin, 2015). These genetic features could have provided the archaeal ancestor with the necessary means to engulf another prokaryote (Koonin, 2015). In conformity with this theory, the recently identified Lokiarchaeota exhibit such eukaryotic signatures in their genome (Spang *et al.*, 2015). Consequently, the origin of the cytoskeleton is inevitably linked to the origin of Eukarya as both, cell division and cellular orchestration, including phagocytosis, are of essential importance for this process (Koonin, 2015; Spang *et al.*, 2015).

Conserved cytomotive and cytoskeletal structures show a higher degree of variation in bacteria and archaea than in eukaryotes, likely reflecting the longer evolutionary history as well as a

more pronounced pressure on their genomes (Löwe and Amos, 2017). This led to a diverged set of prokaryotic cytoskeletal proteins from the core cytoskeleton (Wickstead and Gull, 2011). Even though the eukaryotic cytoskeleton is more complex in terms of interconnectivity, it is in fact based on a much smaller set of prevailed core genes than that of their prokaryotic counterparts (Wickstead and Gull, 2011). It is assumed that only one paralog of MreB and one FtsZ paralog formed the present actin and tubulin families in extant eukaryotes with subsequent gene specializations and duplications (Wickstead and Gull, 2011). All eukaryotic tubulin isoforms (α , β , γ , δ and ϵ) are more closely related to each other than to FtsZ, indicating that they arose from a common ancestor, which was present before the LECA (Wickstead and Gull, 2011). Further gene acquisition by horizontal gene transfer (HGT) from, for example, phages (ParM or TubZ) increases the given variety in prokaryotes (Löwe and Amos, 2017). So far, no prokaryotic motor proteins have been identified, indicating that prokaryotic accessory proteins are most likely the result of an independent evolution of similar features (convergent evolution) with no direct relationship to eukaryotic cytoskeleton-binding proteins (Wickstead and Gull, 2011; Löwe and Amos, 2017). Many coiled-coil rich IF-like prokaryotic cytoskeletal proteins have been identified in the past years but it has yet to be shown that these are factual homologous proteins to eukaryotic IF proteins or just functional analogs (Lin and Thanbichler, 2013). So far, there is only one example for the HGT of a cytoskeletal protein from eukaryotes to prokaryotes, namely BtubAB from *Prostheco bacter* (Schlieper *et al.*, 2005). It is not unprecedented that prokaryotic IF-like proteins could have evolved in a similar lateral fashion, given their often very limited distribution among other prokaryotes (Wickstead and Gull, 2011). However, direct homologs to eukaryotic IF proteins have most likely not been present in the LECA, thus impeding vertical inheritance of prokaryotic IF-like proteins and no apparent architectural parallels to lamins or other eukaryotic IF proteins are present, indicating that prokaryotic IF-like proteins could have originated independently of each other (Wickstead and Gull, 2011).

3.5 Cyanobacteria

Cyanobacteria are one of the largest group of Gram-negative bacteria and today's only known prokaryotes able to perform oxygenic photosynthesis (Rippka *et al.*, 1979). The ancient and remarkably diverse group of cyanobacteria emerged around 3 billion years ago and is accountable for the great oxidation event (GOE) about 2.45-2.32 billion years ago (Schirmermeister *et al.*, 2013). However, 3.3 – 3.5 billion year old Archaean microfossils exhibiting cyanobacterial-like morphologies were identified, possibly predating the origin of cyanobacteria even further (Schopf, William and Packer, 1987). Thus, cyanobacteria are considered to be the inventors of the oxygenic photosynthesis, which makes them one of the major contributors to the life on earth as we know it today, since it enabled the development of

aerobic life forms (Schirromeister *et al.*, 2013; Walter *et al.*, 2017). The morphological diversity of today's extant cyanobacteria was putatively triggered by an evolutionary advantage of the arising multicellular cyanobacteria to conquer novel niches (Schirromeister, Antonelli and Bagheri, 2011). As a result of this diversification, cyanobacteria were able to occupy nearly every terrestrial and aquatic habitat, including extreme environments like hot springs and polar regions, thereby becoming one of the most widely distributed organisms on the planet (Rippka *et al.*, 1979; Henson *et al.*, 2004). To date, the Pasteur Culture Collection of Cyanobacteria (PCC) has acquired, purified and characterized more than 750 cyanobacterial strains from a wide range of different habitats, and yet, several thousand non-cultivated cyanobacterial strains have been described, thereby only a proportion of cyanobacteria can be subjected to thorough research (<https://webext.pasteur.fr/cyanobacteria/>; Bryant and Frigaard, 2006). It is nowadays widely accepted that plastids - eukaryotic organelles and sites of photosynthesis - are of cyanobacterial origin and gene acquisition studies as well as phylogenetic reconstructions of core cyanobacterial and plastid genes places the plastid ancestor among multicellular nitrogen-fixing and heterocyst-forming cyanobacteria of subsection IV or V (Deusch *et al.*, 2008; Dagan *et al.*, 2013; Ochoa De Alda *et al.*, 2014). Phylogenetic analyses have revealed that extant cyanobacteria are descendants of a photoautotrophic unicellular organism, demonstrating that cell-specialization and trichome-formation are succeeding attributes of the cyanobacterial phylum (Sánchez-Baracaldo, Hayes and Blank, 2005). However, it has to be noted that phylogenetic reconstruction of prokaryotes, owed to HGT, can be misleading, especially in a phylum that is characterized by a rather high degree of HGT, such as the cyanobacterial phylum (Dagan *et al.*, 2013).

Besides their crucial role in the oxygenation of the Earth's atmosphere and their function as primary producers, diazotrophic cyanobacteria have been shown to play an important role in the nitrogen as well as the carbon cycles (Henson *et al.*, 2004; Tomitani *et al.*, 2006). Some of those species are found in a symbiotic relationship with many plant species, supplying them with reduced nitrogen (e.g. NH_3) (Henson *et al.*, 2004; Bryant and Frigaard, 2006). Other cyanobacteria can be free-living, toxic, predators or in a few cases even non-photosynthetic (Melainabacteria) (Walter *et al.*, 2017). Given their importance for the carbon and nitrogen cycle, *Synechocystis*, a unicellular cyanobacterium, was the third prokaryote whose genome was fully sequenced (Kaneko, 2001). As a result, genetic tools were rapidly developed for this organisms and it became the most widely studied cyanobacterial model system (Grigorieva and Shestakov, 1982; Hagemann and Hess, 2018). Moreover, with the recent increasing emphasis on renewable energy supply, cyanobacteria have gradually become more and more employed for different biotechnological applications like biofuels and biosolar cell factories (Savakis and Hellingwerf, 2015). The recent development of a CRISPR-based genome editing

tool for *Synechocystis* and a few other cyanobacterial species will soon enable even more sophisticated biotechnological applications (Ungerer and Pakrasi, 2016).

3.5.1 Characteristics of cyanobacteria

Although of monophyletic origin, cyanobacterial morphologies are extremely diverse, ranging from unicellular species to sophisticated cell-differentiating filamentous (multicellular) strains (Rippka *et al.*, 1979). Based on their different morphologies and division pattern Cyanobacteria have thus been classically divided into five subsections (Fig. 6) (Rippka *et al.*, 1979). Cyanobacteria of subsection I and II comprise unicellular coccoid forms and while subsection I cyanobacteria (Chroococcales) divide by binary fission or budding, those of subsection II (Pleurocapsales) are also able to undergo multiple fission giving rise to so-called baeocytes. Subsection III (Oscillatoriales) is composed of filamentous, non-differentiating cyanobacteria with trichomes (a chain of cells) only composed of vegetative cells. The filamentous and cell-differentiating cyanobacteria are grouped in subsection IV and V (Nostocales and Stigonematales). Under detrimental or unfavorable conditions some of these cells can develop spore-like akinetes and in the absence of combined nitrogen these strains form heterocysts (Rippka *et al.*, 1979). Heterocysts are specialized cells for nitrogen fixation and can be distinguished from vegetative cells by their thick exopolysaccharide sheath and relatively little pigmentation (Rippka *et al.*, 1979). The thick layer insulates the cells from environmental oxygen thereby providing submissive non-oxygen conditions for the activity of the nitrogenase enzyme, which catalyzes the reduction of nitrogen to ammonium (Rippka *et al.*, 1979). Subsection III, IV and V grow by intercalary cell division and reproduce by random trichome breakage or by formation of hormogonia (Rippka *et al.*, 1979). While cyanobacteria of subsection IV only divide in one plane, subsection V are able to divide in multiple planes, thereby forming multiserate filaments (Rippka *et al.*, 1979).

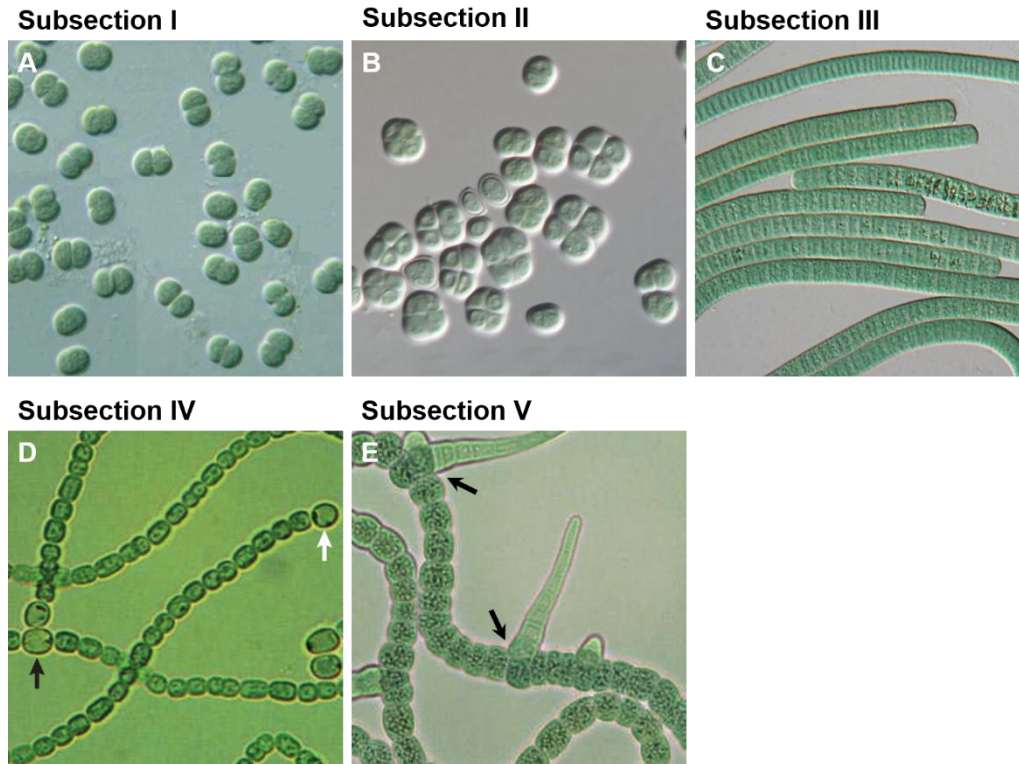


Fig. 6: Cyanobacterial morphological diversity

Bright field micrographs of representative members the five cyanobacterial subsections. (A) *Synechocystis*, (B) *Chroococcidiopsis* sp., (C) *Oscillatoria limosa*, (D), *Anabaena* and (E) *Fischerella muscicola* PCC 7414. Arrows point to (D) heterocysts or (E) branching points. Figures obtained from (A) the Protist Information Server (<http://protist.i.hosei.ac.jp/>), (B,C) the Culture Collection of Autotrophic Organisms (<http://ccala.butbn.cas.cz/en>) and (D,E) Flores and Herrero (2010).

3.5.2 Cyanobacterial motility

Unlike chemotactic bacteria that show a random but biased movement within a chemical gradient by switching from a running to a tumbling mode with constant reorientation into a different direction during the progress by alternating flagella rotations, cyanobacteria do not assemble flagella and thus use a different motility mechanism (Eisenbach, 2011; Schuergers, Mullineaux and Wilde, 2017). Instead, unicellular cyanobacteria, like *Synechocystis*, assemble type IV pili and move by a twitching movement on surfaces (Schuergers and Wilde, 2015). Type IV pili protein fibers consist of pilin subunits, which are driven by the ATPases PilB and PilT (Maier and Wong, 2015; Wilde and Mullineaux, 2017). Chemoattractants or chemorepellents are sensed by methyl-accepting chemotaxis proteins (MCP) (Maier and Wong, 2015; Wilde and Mullineaux, 2017). The exuded motility and directed movement of cyanobacteria, mainly of unicellular origin but also of some multicellular species, is partially driven by light-induced phototaxis using photoreceptors that sense the direction of the light (Schuergers *et al.*, 2016). In contrast to biased flagellar movement, phototaxis-driven movement can be specifically directed towards or away from a light source (Schuergers *et al.*, 2016; Schuergers, Mullineaux and Wilde, 2017). In order to sense the orientation of a light

source, *Synechocystis* employs its intrinsic micro-optic properties, in that way operating as a microscopic eyeball (Schuergers *et al.*, 2016). The movement of Subsection II cyanobacteria is directly linked to newly released baeocytes after cell division that initially form a cell wall consisting of peptidoglycan and outer membrane layers, which mediates gliding motility until the formation of a fibrous cell wall (Rippka *et al.*, 1979). Subsection III-V form small motile and reproductive elements, called hormogonia, which are released from the immotile mature trichome by trichome breakage (Rippka *et al.*, 1979). Hormogonia are structurally different from the vegetative filament as they do not possess a well-defined surrounding sheath and can be distinguished from the mature trichome by their gliding motility (Rippka *et al.*, 1979). The gliding motility of filamentous cyanobacteria is provided by a joint action of the two-dimensional proteinaceous array of S-layer (glycol-)proteins that covers the whole cell surface together with specific junctional pore complexes that, in cooperation, directionally excrete polysaccharide slime inducing a pushing of the cells into a certain direction (Hoiczky and Baumeister, 1998; Schuergers, Mullineaux and Wilde, 2017). However, recent studies have shown that the secreted hormogonium polysaccharides only provide a suitable basis for gliding motility and do not exude the directed force that is compulsory for movement (Khayatan, Meeks and Risser, 2015). Accordingly, *hps* (hormogonium polysaccharide) and *pil* (pilus) genes were identified in the junctional pore complexes in *Nostoc punctiforme*, suggesting that a type IV pilus-based motor - like in *Synechocystis* - is the driving force for motility in filamentous cyanobacteria (Khayatan, Meeks and Risser, 2015).

3.5.3 Cell-cell communication in cyanobacteria

An inevitable prerequisite for multicellularity of any given cell type or organism is the manifestation of cellular junctions at sites of cell-cell or cell-matrix contacts (Alberts *et al.*, 2002). A comparable amount of different junctional complexes has yet to be found in multicellular cyanobacteria. But it is imperative for these organisms to form alike structures in order to sustain trichome stability against external influences such as shearing stress (Corrales-Guerrero *et al.*, 2013; Flores *et al.*, 2016). The need for proper cell-cell communication is even more evident in cell-differentiating cyanobacterial strains (Flores *et al.*, 2016; Herrero, Stavans and Flores, 2016). The heterocyst-forming filamentous cyanobacterium *Anabaena* of subsection IV has become a model organism to study cyanobacterial multicellularity (Burnat, Schleiff and Flores, 2014; Ramos-León *et al.*, 2015; Flores *et al.*, 2016; Nieves-Morión, Mullineaux and Flores, 2017). *Anabaena* grows as long trichomes that easily can reach more than 100 cells in a row (Rippka *et al.*, 1979). Individual cells within an *Anabaena* filament possess their own plasma membrane and peptidoglycan layers but all cells are engulfed in a continuous outer membrane layer demonstrating that all cells are connected by a shared periplasm (Wilk *et al.*, 2011; Flores *et al.*, 2016). In the

absence of combined nitrogen, this cyanobacterium terminally differentiates a subpopulation of its vegetative cells into nitrogen-fixing heterocysts (Rippka *et al.*, 1979). Vegetative cells perform oxygenic photosynthesis while heterocysts carry out nitrogen fixation using the oxygen-sensitive nitrogenase enzyme (Rippka *et al.*, 1979; Kumar, Mella-Herrera and Golden, 2010). As a result of this cell specialization, a metabolic communication of heterocysts and vegetative cells is essential in order to exchange photosynthates like sucrose from the vegetative cells to the heterocysts and combined nitrogen sources, such as glutamine, from heterocysts to the vegetative cells (Wilk *et al.*, 2011; Nieves-Mori3n, Mullineaux and Flores, 2017). Diazotrophically grown *Anabaena* trichomes exhibit only about 5-10% heterocysts, indicating that also vegetative cells must possess communication-permissive cell-cell connections (Kumar, Mella-Herrera and Golden, 2010; Nieves-Mori3n, Mullineaux and Flores, 2017). For a time, it was debated whether this intercellular molecular communication is achieved by the continuous periplasm or by structures physically linking adjacent cells (Flores *et al.*, 2006, 2016). Studies using small fluorescent tracer molecules, including calcein and the sucrose analogue esculin, showed that a rapid intercellular communication takes place between two neighboring cells and the transfer shows diffusion properties (Flores *et al.*, 2016). Differentiated heterocysts directly inhibit cellular differentiation of neighboring cells, a process that involves the exchange of a small peptide morphogen, called PatS, showing that cell-cell connections are not only permissive for small fluorescent dyes but also larger proteinaceous structures (Yoon, 1998; Corrales-Guerrero *et al.*, 2013). Using electron microscopy, cell-joining structures were identified and termed septosomes in order to highlight their analogy to eukaryotic gap junctions (Wilk *et al.*, 2011). Septosomes traverse the septal peptidoglycan, forming so-called nanopores, which are dependent on the peptidoglycan amidase AmiC and the peptidoglycan-binding protein SjcF1 (Flores *et al.*, 2016). SepJ, FraC and FraD are putative proteinaceous components of the septosomes and gene deletion of any of the three encoded proteins was shown to abrogate intercellular transport of fluorescent markers (N3rnberg *et al.*, 2015). Like gap junctions that are made of two connexin hexamers, SepJ forms multimers and interacts with the peptidoglycan by means of its coiled-coil domains (Alberts *et al.*, 2002; Ramos-Le3n *et al.*, 2017). However, SepJ does not bear any structural homology to connexins, therefore, the exact buildup of septosomes is still largely obscure (Nieves-Mori3n, Mullineaux and Flores, 2017).

4 Thesis motivation

The discovery of the prokaryotic tubulin and actin homologs, FtsZ and MreB, respectively, has given the start signal for a stunning rally (Bi and Lutkenhaus, 1991; Bork, Sander and Valencia, 1992; Jinek *et al.*, 2012). Many prokaryotic cytoskeletal proteins of bacterial and/or archaeal origin have been discovered since, including a highly diverse intermediate filament (IF)-like cytoskeletal system (Wagstaff and Löwe, 2018). Despite performing similar cellular functions as their eukaryotic counterparts, bioinformatic prediction of homologous cytoskeletal proteins is often hampered by the low sequence conservation even among rather conserved prokaryotic cytoskeletal proteins (Møller-Jensen and Löwe, 2005; Shaevitz and Gitai, 2010). Thus, identification of prokaryotic cytoskeletal proteins was often based on three-dimensional structural similarities and/or *in vitro* and *in vivo* properties (Celler *et al.*, 2013). The COILS algorithm from Lupas, Van Dyke and Stock (1991) turned out to be a powerful tool to predict IF-like proteins from different prokaryotic strains based on coiled-coil content instead of sequence similarity (Bagchi *et al.*, 2008). The FilP IF-like protein identified by this means, was shown to have an impact on the cellular morphology of the multicellular and filamentous bacterium *S. coelicolor* (Bagchi *et al.*, 2008). Thus, employing this algorithm on other bacterial phyla could lead to the discovery of even more prokaryotic cytoskeletal proteins, possibly providing further insight into morphology-determining mechanisms of different bacterial species. Cyanobacterial morphology is extremely diverse, ranging from unicellular coccoid or rod-shaped bacteria of subsection I and II to multicellular species of subsection III, IV and V, with a cell-differentiating phenotype in subsection IV and V and a division pattern in more than one plane in subsection V (Rippka *et al.*, 1979). Even though, until today only little is known about the underlying principles for this morphological diversity and the apparent multicellular phenotype. Employing the COILS algorithm on this complex phylum could therefore provide us with further insight into the underlying mechanisms for multicellularity, cell differentiation and cell shape.

Cyanobacteria are often studied for their potential in biotechnology and as a model for the circadian cycle in prokaryotes (Cohen *et al.*, 2014; Jiang and Chen, 2016). Additionally, the discovery of a septosomal complex has accelerated the investigations of the multicellular trait of cyanobacteria, including research focusing on cell-cell communication (Ramos-León *et al.*, 2015, 2017; Herrero, Stavans and Flores, 2016). As a result, many genetic tools are available for these bacteria, providing an excellent basis for molecular biology research (Golden, Brusslan and Haselkorn, 1987; Wolk *et al.*, 1988).

Furthermore, cytoskeletal research in cyanobacteria was so far mainly limited to FtsZ and MreB, the two major cytoskeletal systems in bacteria. MreB was shown to be important for cell shape but dispensable for cell viability in *Anabaena* while FtsZ, like in most other bacteria, is

essential for strain survival (Zhang *et al.*, 1995; Hu *et al.*, 2007). There are indications that FtsZ is tightly regulated by proteolytic degradation in the multicellular cyanobacterium *Anabaena*, a process that seems to be associated with cell differentiation and heterocyst formation (Sakr, Jeanjean, *et al.*, 2006; Lopes Pinto *et al.*, 2011). In conclusion, none of those two cytoskeletal systems is sufficient to provide satisfactory explanations for the vast diversity of cyanobacterial morphotypes. It is therefore conceivable that additional cytoskeletal systems, possibly IF-like, are involved in their morphological diversity, also because IF proteins are known to be involved in cellular morphology even across taxa borders (Alberts *et al.*, 2014; Wagstaff and Löwe, 2018). The largely uncharacterized cyanobacterial morphology, established genetic tools and the link of the IF cytoskeleton to cell shape as well as the readily accessible prediction tool for IF-like proteins provided an excellent basis and the major motivation for structural research on cyanobacteria.

- Therefore, given the main role of cytoskeletal proteins in morphogenesis, **we hypothesize that cytoskeletal networks, specifically of IF-like proteins, exist in cyanobacteria and play an important role in their cellular morphology.**

Consistently, this doctoral thesis aims to identify and characterize novel cytoskeletal proteins in cyanobacteria and addresses several central questions that deal with the underlying principles of the cyanobacterial morphology:

- Are coiled-coil rich cytoskeletal proteins present in cyanobacteria and do they perform IF-like functions?
- Do cyanobacterial cytoskeletal systems, like in eukaryotes, form interconnected networks that jointly perform cellular tasks?
- And are cytoskeletal networks involved in the multicellular phenotype of *Anabaena*?

We approached these questions by several *in silico*-based bioinformatic predictions and performed genetic, biochemical and molecular biology techniques. For the purpose to obtain broadly-applicable results, we used several cyanobacterial model strains, including *Synechocystis*, *Synechococcus*, *Anabaena* and *Fischerella muscicola* PCC 7414 (hereafter *Fischerella*).

5 Outline of the thesis

The thesis at hand is organized into three chapters, which later shall lead to three individual publications with the doctoral candidate as the first author.

It was long assumed that prokaryotes, owed to their comparably small and simple cell shape, do not require and thus do not possess a distinct cytoskeletal network that orchestrates their internal components. However, the discovery of the first prokaryotic tubulin and actin homologs, FtsZ and MreB respectively, dramatically changed that view. The subsequent discovery of IF-like proteins in *C. crescentus* and *S. coelicolor* led to a real race of discovery ultimately leading to the identification of many more prokaryotic cytoskeletal proteins. In cyanobacteria, a phylum characterized by its high morphological diversity, however, cell shape-based research has been vaguely studied and limited to FtsZ and MreB. In **Chapter 1**, we describe the identification of candidate IF-like proteins. From a subset of those candidates, we validated the *in silico* predictions *in vitro* and characterized *in vivo* their functions in the cyanobacterium of origin and heterologous cyanobacteria. IF-like proteins were identified as those predicted to be rich in coiled-coil motifs by the COILS algorithm. *In vitro* and *in vivo* polymerizations were further confirmed by a bacterial two-hybrid system. Putative cellular functions of the respective proteins were explored by gene deletions and/or identification of interaction partners by mass spectrometry. The bioinformatic analysis was mainly provided by Christian Wöhle and Tal Dagan and the subsequent *in vitro* and *in vivo* experiments were performed by the doctoral candidate in consultation with Karina Stucken. Mass spectrometry-based identification of interactors were performed by Andreas Tholey (University Kiel) with his group (with a noteworthy contribution of Andreas Helbig) and in cooperation with Martin Thanbichler (University Marburg) and the proteomics core facility from Marburg University.

During the evolutionary timeline, prokaryotes have re-shaped and converted protein functions even of conserved proteins according to their respective needs, as it is the case of MreB. In **Chapter 2**, we characterize three homologous proteins from *Anabaena*, *Synechocystis* and *Synechococcus* predicted in **Chapter 1** as IF-like proteins. These species differ in morphology and morphological complexity. While *Synechocystis* is a unicellular cocci, and *Synechococcus* a unicellular rod, *Anabaena* is a multicellular, heterocyst-forming cyanobacterium. According to those entirely different species morphotype, we aimed to investigate putative functional and structural diversifications or adaptations of the three proteins that might have led to species-specific evolution. The respective properties were compared in the three different cyanobacterial species and in a heterologous *E. coli* system. In addition, the impacts of gene deletions were compared, and interaction partners were explored by bacterial two-hybrid assays and mass spectrometry in cooperation with the aforementioned collaborators.

Cytoskeletal networks in eukaryotes as well as in prokaryotes are tightly controlled and strongly interconnected. Thus, cell division, cell shape stability and other cellular organization properties are executed in a joint operation of different cytoskeletal systems. Many of those networks are linked to cell-cell junctions in order to mediate, for example, cell-cell communication or tissue maintenance. During the investigation of cyanobacterial IF-like protein candidates identified in **Chapter 1**, four proteins were early recognized as cytoskeletal proteins putatively being organized in a network-like fashion. **In Chapter 3**, these proteins were then investigated for interactions with themselves and with known cytoskeletal components as well as the recently identified septosomal complex. Co-localization studies and gene deletions were further employed to assess the impact of this cytoskeletal network in *Anabaena*. The contribution to the parts of this chapter are the same as in **Chapter 1**.

6 Material and methods

All chemicals, devices and other materials were obtained from the following companies:

Abcam, Cambridge, United Kingdom
AppliChem, Darmstadt, Germany
B. Braun, Melsungen, Germany
Bertin, Darmstadt, Germany
Binder, Tuttlingen, Germany
Bio-Rad Laboratories, Hercules, U.S.A. (hereafter Bio-Rad)
Bioline, Luckenwalde, Germany
Brand, Wertheim, Germany
Carl Zeiss, Jena, Germany
Eppendorf, Hamburg, Germany
Eurofins Scientific, Ebersberg, Germany
Euromedex, Souffelweyersheim, France
GE Healthcare, Buckinghamshire, UK
Greiner Bio-One, Frickenhausen, Germany
Invitrogen, Carlsbad, U.S.A.
Life Technologies, Darmstadt, Germany
Merck, Darmstadt, Germany
Miltenyl Biotec, Bergisch Gladbach, Germany
New England Biolabs, Massachusetts, U.S.A. (hereafter NEB)
Nippon Genetics Europe GmbH, Dueren, Germany
Nerbe plus GmbH, Winsen/Luhe, Germany
Promega, Fitchburg, U.S.A.
QIAGEN, Hilden, Germany
Roth, Karlsruhe, Germany
Sarstedt, Nümbrecht, Germany
Sartorius, Göttingen, Germany
SERVA Electrophoresis GmbH, Heidelberg, Germany
Sigma-Aldrich Chemie, Schnelldorf, Germany
Thermo Fischer Scientific, Bonn, Germany
Th. Geyer, Renningen, Germany
Zymo Research, Irvine, California, U.S.A.

Table 1: *E. coli* strains

Name	Genotype	Reference
XL1 blue	endA1 gyrA96(nal ^R) thi-1 recA1 relA1 lac glnV44 F' [::Tn10 proAB ⁺ lacI ^q Δ(lacZ)M15] hsdR17(r _K ⁻ m _K ⁺)	Stratagene
HB101	F ⁻ mcrB mrr hsdS20(r _B ⁻ m _B ⁻) recA13 leuB6 ara-14 proA2 lacY1 galK2 xyl-5 mtl-1 rpsL20(Sm ^R) glnV44 λ ⁻	Boyer and Roulland-Dessoix, 1969
Dh5α	F ⁻ Φ80lacZΔM15 Δ(lacZYA-argF) U169 recA1 endA1 hsdR17 (rK ⁻ , mK ⁺) phoA supE44 λ ⁻ thi-1 gyrA96 relA1	(Meselson and Yuan, 1968)
DH5αMCR	F ⁻ endA1 supE44 thi-1 λ ⁻ recA1 gyrA96 relA1 deoR Δ(lacZYA-argF)U169 Φ80dlacZΔM15 mcrA Δ(mrr hsdRMS mcrBC)	(Grant <i>et al.</i> , 1990)
BL21 (DE3)	<i>E. coli</i> str. F ⁻ ompT gal dcm lon hsdS _B (r _B ⁻ m _B ⁻) λ(DE3 [lacI lacUV5-T7p07 ind1 sam7 nin5]) [malB ⁺] _{K-12} (λ ^S)	(Studier and Moffatt, 1986)
BTH101	F ⁻ , cya-99, araD139, galE15, galK16, rpsL1 (Str _r), hsdR2, mcrA1, mcrB1	Euromedex

Table 2: Growth media and buffer for cellbiological procedures

Name	Composition
LB medium	1% Bacto-tryptone, 0.5% Bacto-yeast extract, 17 mM NaCl, pH 7.4
BG11 medium	17.65 NaNO ₃ , 0.3 mM MgSO ₄ , 0.25 mM CaCl ₂ , 0.03 mM citric acid, 0.003 Na ₂ EDTA, 0.19 mM Na ₂ CO ₃ , 0.18 mM K ₂ HPO ₄ , 5 mM TES, 0.03 mM ferric ammonium citrate supplemented with 1 ml L ⁻¹ trace metal mix
Trace metal mix	46.3 mM H ₃ BO ₃ , 9.15 mM MnCl ₂ , 0.77 mM ZnSO ₄ , 1.61 mM Na ₂ MoO ₄ , 0.32 mM CuSO ₄ , 0.17 mM Co(NO ₃) ₂
BG11-0	BG11 without NaNO ₃
BG11/BG11-0-Cu	BG11/BG11-0 without CuSO ₄
M9 medium	33.7 mM Na ₂ HPO ₄ , 22 mM KH ₂ PO ₄ , 8.55 mM NaCl, 9.35 mM NH ₄ Cl, 0.4% glucose, 1 mM MgSO ₄ , 0.3 mM CaCl ₂ , 1 μg L ⁻¹ biotin, 1 μg L ⁻¹ thiamin, 1x trace element solution
100x trace element solution	13.4 mM EDTA, 3.1 mM FeCl ₃ , 0.62 mM ZnCl ₂ , 76 μM CuCl ₂ , 42 μM CoCl ₂ , 162 μM H ₃ BO ₃ , 8.1 μM MnCl ₂
TB:	10 mM HEPES, 55 mM MnCl ₂ , 15 mM CaCl ₂ , 250 mM KCl, pH 6.8
SOB	2% Bacto-tryptone, 0.5% Bacto-yeast extract, 10 mM NaCl, 2.5 mM KCl, 10 mM MgCl ₂ , 10 mM MgSO ₄
SOC	SOB medium supplemented with 1/100 vol of sterilized 2 M glucose

Table 3: Buffer and solutions for protein biochemical methods:

Name	Composition
PBS	10 mM Na ₂ HPO ₄ , 140 mM NaCl, 2.7 mM KCl, 1.8 mM KH ₂ PO ₄ , pH 7.4
PBST	PBS supplemented with 0.05% Tween 20
Native Lysis Buffer (NLB)	50 mM NaH ₂ PO ₄ , 300 mM NaCl, 25 mM imidazole, pH 8.0
Native Elution Buffer (NEB)	NLB with 250 mM imidazole
Native Lysis Buffer with detergent (NLB-T)	50 mM NaH ₂ PO ₄ , 300 mM NaCl, 25 mM imidazole, 1% Triton X-100, pH 8.0
Native Elution Buffer with detergent (NEB-T)	NEB-T with 250 mM imidazole
Urea Lysis Buffer (ULB)	50 mM NaH ₂ PO ₄ , 300 mM NaCl, 25 mM imidazole, 6 M urea, pH 8.0
Urea Elution Buffer (UEB)	ULB with 250 mM imidazole
Cyanobacterial Lysis Buffer (CLB)	50 mM HEPES, 200 mM NaCl, 10 mM MgCl ₂ , 5% glycerol, 1% Triton X-100, pH 7.2 (supplemented with 1 mM DTT when appropriate)
PBS with detergent (PBS-N)	10 mM Na ₂ HPO ₄ , 140 mM NaCl, 2.7 mM KCl, 1.8 mM KH ₂ PO ₄ , pH 7.4, 1% NP-40
High Salt Lysis Buffer (HSLB)	50 mM Na ₂ HPO ₄ , 500 mM NaCl, 1% NP-40, pH 7.2
5x SDS-loading buffer	312 mM Tris-HCl, pH 6.8, 5 mM EDTA, 50 %glycerol, 10% SDS, 25% 2-Mercaptoethanol, 0.025% bromophenol blue
10x SDS running buffer	250 mM Tris-HCl, 14,3% glycine, 1% SDS
Blotting buffer	25 mM Tris base, 190 mM glycine, 0.1% SDS, 20% methanol
Tris-buffered saline with detergent (TBST)	50 mM Tris-HCl, 150 mM NaCl, pH 7.6, 0.1% Tween 20
Blocking buffer	5% dry skim milk in TBST

Table 4: Protein polymerization buffers

Name	Composition
HLB	25 mM HEPES, 150 mM NaCl, pH 7.4
PLB	50 mM PIPES, 100 mM KCl; pH 7.0

Table 5: Buffer and solution for nucleic acid procedures

Name	Composition
50x TAE	500 mM Tris pH 8.0, 20 mM acetic acid, 50 mM EDTA pH 8.0
6x DNA loading dye	10 mM Tris-HCl, pH 8.0, 60% glycerol, 60 mM EDTA pH 8.0, 0.03% bromophenol blue, 0.03% xylene cyanol FF

Table 6: Antibodies

Antigen	Species	Description	Source	Dilution
His6	Mouse	---	Thermo Fischer Scientific (#MA1-21315)	1:2000 (WB) or 1500 (ImF)
FtsZ	Rabbit	<i>Anabaena</i> FtsZ (Alr3858) expressed in <i>E. coli</i>	Agrisera	1:2000 (WB) or 1:150 (ImF)
Mouse IgG	Goat	Conjugated to Horseradish peroxidase (HRP)	Agrisera	1:10,000
Rabbit IgG	Goat	Conjugated to HRP	Agrisera	1:10,000
Rabbit IgG	Goat	Conjugated to Alexa Fluor 488	Thermo (#R37116)	7.5 $\mu\text{g ml}^{-1}$

6.1 Bioinformatic analysis

6.1.1 Predictions of coiled-coil rich proteins

The execution of the COILS algorithm was mainly performed by Christian Wöhle (University Kiel) and the candidate performed the subsequent filtering. COILS data are attached as Supplementary File 1.

Cytoskeletal proteins form filamentous structures based on polymerization of single monomeric units. Coiled-coil domains comprise one of many protein interaction motifs that facilitate protein-protein association that are suitable for oligomerization or polymerization. Unlike actin filaments and microtubules (or their prokaryotic homologs), IF proteins exhibit a high coiled-coil content within their secondary structures (section 3.1.1). Based on this, we employed the COILS algorithm from Lupas, Van Dyke and Stock (1991) to obtain a set of protein candidates with a high probability of folding into coiled-coils. The search considered all available 141 cyanobacterial genomes including *Synechocystis* plasmids pSYSM, pSYSA, pSYSG and pSYSX. The algorithm was run with a window width of 21 and the cut-off for amino acids in coiled-coil conformation was set to ≥ 80 amino acid residues as described by Bagchi *et al.* (2008). For functional characterization, protein candidates were limited to cyanobacterial strains available in our laboratory: *Fischerella*, non-motile *Synechocystis* GT-Kazusa substrain, motile *Synechocystis* PCC-M substrain (PCC-M), *Synechococcus*, *Thermosynechococcus elongatus* BP-1 (BP-1) and *Anabaena*. The resulting set of protein candidates was further manually examined with online available bioinformatic tools (NCBI Conserved Domain Search, NCBI BLAST, TMHMM Server, PSORTb, I-TASSER). Protein candidates exhibiting BLAST hits involved in cytoskeletal processes or similar domain architectures as known IF proteins like CreS, FilP, vimentin, desmin or keratin were selected, and proteins predicted to be involved in other cellular processes were excluded.

6.1.2 Multiple sequence alignments and phylogenetic trees

Multiple sequence alignments as well as phylogenetic trees employed in this study were generated by Prof. Dr. Tal Dagan (Kiel University) and protein families were obtained from Tria, Landan and Dagan (2017). Protein sequences were aligned using MAFFT (Kato and Standley 2013) and amino acid sequence similarities (in %) were calculated as the average pairwise sequence similarity with an in-house MatLab© script by Prof. Dr. Tal Dagan.

Identified homologs to protein candidates, including NCBI accession numbers and sequence similarity scores, are attached in Supplementary File 2.

6.2 Molecular biology methods

6.2.1 Generation of chemically competent *E. coli*

Chemically competent *E. coli* strains were obtained based on a protocol described by Inoue, Nojima and Okayama (1990). Cells were grown in 250 ml SOB medium in a 2 L Erlenmeyer flask at 18 °C and 250 rpm until an OD₆₀₀ of 0.6 was reached. The cells were kept on ice for 10 min, centrifuged at 3000 x *g* for 10 min at 4 °C and resuspended in 80 ml of ice-cold TB buffer. After an incubation for 10 min in an ice-water bath, the cells were centrifuged (3000 x *g*, 10 min, 4 °C) and resuspended in 20 ml of TB supplemented with DMSO (final concentration 7%). After another 10 min incubation in an ice-water bath, the cells were finally aliquoted into 1.5 ml reaction tubes, frozen in liquid nitrogen and stored at -80 °C.

6.2.2 Transformation of chemically competent *E. coli*

Unless otherwise stated, the following chemically competent *E. coli* strains were used in this study: BL21 (DE3), XL1 Blue, HB101, BTH101, DH5α or DH5αMCR. For each transformation, a 50 µl aliquot of competent cells was thawed on ice. The cells were mixed with plasmid DNA of various sources (5 µl ligation mixture, 5-15 µl NEBuilder assembly reaction mix or 1 µl of purified plasmid DNA) and incubated on ice for 30 min followed by a heat shock for 45 s at 42 °C. Subsequently, the transformation mixture was briefly incubated on ice and 900 µl pre-heated SOC medium was added to the cells. After an incubation for 1 h at 37 °C and 250 rpm, the cells were centrifuged (5 min, 4500 x *g*, RT), the supernatant was discarded, and the cells were resuspended in about 100 µl SOC medium. The resulting cell suspension was plated on LB plates containing the appropriate antibiotics. Plates were incubated at 37°C, 30 °C or RT until single colonies appeared and then stored at 4 °C until further use.

6.2.3 Isolation of genomic DNA

Genomic DNA (gDNA) from *Fischerella* and *Anabaena* was isolated using the CTAB method essentially as described by Sharma, Gill and Singh (2002). The method is designed to isolate genomic DNA from specimens containing large amounts of (exo)polysaccharides. For this method, about 10 ml cyanobacterial culture (OD₇₅₀ of 0.4-0.6) was pelleted by centrifugation, the supernatant was discarded, and cells were lysed by grinding in liquid nitrogen. The ground material was resuspended in Solution I (5 M NaCl, 2% sarcosyl) containing 1 mg ml⁻¹ Proteinase K and incubated for 30 min at 60 °C. Samples were centrifuged (6800 x *g*, 15 min, RT) and the resulting supernatant was transferred to a new tube and mixed by inversion with an equal volume of chloroform-isoamylalcohol (24:1). The solution was centrifuged (3200 x *g*, RT, 15 min) and the aqueous phase was transferred to a new tube and mixed by inversion with 2 volumes extraction buffer (100 mM Tris-HCl pH 8.0, 20 mM EDTA, 1.4 M NaCl, 2% CTAB). Samples were incubated at 60 °C for 35 min with mild agitation. Afterwards, an equal

volume of chloroform-isoamylalcohol (24:1) was added and the suspension was centrifuged at 3200 x g at RT for 15 min. A 1/30 volume of 3 M sodium acetate (pH 5.2) was added to the resulting supernatant and the DNA was precipitated by 0.6 volumes of isopropanol and then pelleted by centrifugation (3200 x g, RT, 10 min). The supernatant was discarded, and the DNA pellet was washed in 80% ethanol by centrifugation. After air-drying, the DNA was resuspended in TE buffer (10 mM Tris-HCl pH 8.0, 0.1 mM EDTA) and incubated at 37 °C for 30 min with 5 µl RNase A (10 mg ml⁻¹). After another protein extraction step with an equal volume of chloroform-isoamylalcohol (24:1), the aqueous phase was transferred to a new reaction tube and 2 volumes of cold 80% ethanol were added. The solution was centrifuged (3200 x g, RT, 10 min) and the pellet was washed with 80% ethanol. Finally, the pellet was air dried and dissolved in a suitable volume of nuclease-free water. DNA concentration was measured using the Multiskan GO spectrophotometer with a µDrop™ plate (Thermo Fischer Scientific). DNA integrity was evaluated by agarose gel electrophoresis using a 0.7% gel.

Besides the above described method, gDNA from *Anabaena*, *Synechocystis* and *Synechococcus* were isolated using the GeneJET Plant Genomic DNA Purification Kit (Thermo Fischer Scientific) and the DNeasy Plant Mini Kit (QIAGEN) according to the manufacturer's instructions from 10 ml of cyanobacterial cultures.

6.2.4 RNA isolation

Total RNA was isolated from 10 ml culture of indicated OD₇₅₀ using either the Direct-zol™ RNA MiniPrep Kit (Zymo Research; *Synechocystis*, and *Anabaena*) or the Plant RNA Reagent (Thermo Fischer Scientific; *Anabaena*, *Fischerella* and *Synechocystis*). For RNA isolation using the Plant RNA Reagent, a modified protocol was employed. To this aim, cells were pelleted by centrifugation (4800 x g, 10 min, 4 °C) and the supernatant was discarded. The pellet was resuspended in 0.5 ml of Plant RNA Reagent and lysed in a Precellys® 24 homogenizer (Bertin) with 3 strokes at 6500 rpm for 30 s in 2 ml soil grinding (SK38) or tough microorganism (VK05) lysis tubes (Bertin). To remove cellular debris, the solution was centrifuged at 21,000 x g for 2 min at RT. Afterwards, 0.1 ml of 5 M NaCl and 0.3 ml chloroform was added to the supernatant. Phase separation was accomplished by centrifugation at 12,000 x g for 10 min at 4 °C and the resulting aqueous nucleic acid-containing fraction was transferred to a new reaction tube. To precipitate the nucleic acids, an equal volume of isopropanol was added to the solution, mixed and incubated at RT for 10 min. The RNA was centrifuged at 12,000 x g for 3 min at 4 °C and the supernatant was discarded. The pellet was washed two times by centrifugation (12,000 x g, 2 min, RT) with 1 ml 75% ethanol, air dried and resuspended in 50 µl nuclease-free water.

Additionally, RNA from 10 ml cultures of indicated OD₇₅₀ from *Anabaena*, *Synechocystis* and *Synechococcus* cultures was isolated using the Direct-zol™ RNA MiniPrep Kit (Zymo Research) according to the manufacturer's instructions.

Isolated RNA was treated with DNA-free™ Kit (2 units rDNAs/reaction; Thermo Fischer Scientific) and 1 µg RNA was reverse transcribed using the Maxima™ H Minus cDNA Synthesis Master Mix (with dsDNase; Thermo Fischer Scientific). Integrity of isolated RNA was evaluated by agarose gel electrophoresis.

6.2.5 Polymerase chain reaction

The polymerase chain reaction (PCR) is an *in vitro* method for the enzymatic amplification of specific DNA sequences, initially described by Mullis and Faloona (1987) and Saiki *et al.* (1988). The method is based on heat-resistant DNA polymerases with an intrinsic 5' → 3' polymerase activity such as the *Taq* polymerase from the bacterium *Thermus aquaticus*, which allows for an automated procedure at high temperatures. Besides *Taq* polymerases, a broad spectrum of other polymerases have been developed in the past decades, which also exhibit 3'→5' exonuclease proofreading activity. The PCR reactions were performed according to Sambrook and Green (2012) using the Q5 or DreamTaq polymerase (NEB or Thermo Fischer Scientific, respectively) and oligonucleotide primers used in this study were obtained from Eurofins (Ebersberg, Germany). For some analytical procedures, the extension of the oligonucleotide primers by an antigenic tag, an enzymatic cleavage site or overlapping sequences to another DNA fragment was required. These sequences are not complementary to the template DNA sequence and were added to the 5' end of the oligonucleotides (Tables 9,11,13). The total reaction volume was either 50 µl or 10 µl and 100 ng gDNA or 10 ng Plasmid DNA served as template for the reaction. Amplified DNA products were then subjected to an agarose gel electrophoresis and, if applicable, purified by gel extraction (GeneJET Gel Extraction and DNA Cleanup Kit, Thermo Fischer Scientific) or were directly purified using the DNA Clean & Concentrator™-5 kit (Zymo Research).

6.2.6 Agarose gel electrophoresis

The agarose gel electrophoresis is used to separate DNA and RNA fragments in an electric field in which negatively-charged DNA and RNA molecules migrate through an agarose matrix towards the positively-charged anode in a size-dependent manner (Sambrook and Green, 2012). Nucleic acids were visualized in a ChemiDocMP® imaging system (Bio-Rad) using the DNA-binding dye Midori Green (Nippon Genetics Europe GmbH) directly added to the agarose gel according to the manufacturer's instructions. To estimate the size of specific DNA bands in the gel, a DNA Ladder (Hyperladder I or II; Bionline) with DNA fragments of known sizes was also loaded onto the gel. The separation was then performed in 1x TAE buffer by applying a

constant voltage of 130 V. In this study employed agarose gels contained 0.7, 1, or 2% agarose and amplified DNA samples were mixed with 6x loading dye (final concentration 1x).

6.2.7 Enzymatic digestion of nucleic acids and ligation of DNA fragments

Restriction-enzyme based cloning strategies require the digestion of plasmid DNA and insert DNA with the same set of restriction endonucleases. The different DNA fragments can then be joined together by DNA ligases. All restriction enzymes employed in this study were obtained from NEB or Thermo Fischer Scientific and reactions were performed according to the instructor's manual. Digested DNA fragments were either separated and purified by agarose gel electrophoresis using the GeneJet Gel Extraction Kit (Thermo Fischer Scientific) or directly purified from the enzymatic reaction using the Genomic DNA Clean & Concentrator kit (Zymo Research). Subsequently, purified DNA fragments and linearized vectors were ligated employing the Quick Ligation™ Kit (NEB) according to the manufacturer's instructions. The included T4 DNA ligase catalyzes the formation of phosphodiester bonds between the 3' hydroxyl group of one nucleotide with the 5'phosphate end of the following nucleotide.

6.2.8 Gibson assembly

Besides conventional restriction-based cloning techniques, the majority of constructs in this study were created by Gibson assembly using the NEBuilder® HiFi DNA Assembly Master Mix (NEB) following the manufacturer's instructions. This method provides the advantage that multiple fragments can be assembled simultaneously regardless of end compatibility. The only prerequisite is that the DNA fragments must contain short DNA overlaps to the previous and the following fragment to be assembled. In this work, overlapping DNA sequences of 15-25 bp were used. The method allows for simple integration of one, two or more DNA fragments into a linearized vector (linearized either by PCR or by restriction enzymes) or even the *de novo* assembly of whole plasmids. Gibson reactions contain three different enzymes: initially, an exonuclease digests the 5' ends of overlapping DNA fragments enabling the annealing of the complementary DNA fragments. Next, a high-fidelity polymerase fills in the gaps between the annealed fragments, which are then ligated by a DNA ligase. Using this method, we were able to assemble 6 to 8 different fragments within one reaction.

6.2.9 Plasmid isolation

Small scale plasmid isolation from *E. coli* was achieved using the GeneJET Plasmid Miniprep Kit (Thermo Fischer Scientific) according to the manufacturer's instructions. The kit relies on the principle of alkaline lysis initially described by Birnboim and Doly (1979) and employs silica-based spin columns to increase the yield and purity of isolated plasmid DNA. For medium scale plasmid isolation, the QIAGEN® Plasmid Midi Kit (QIAGEN) was employed.

6.2.10 Spectrometric measurement of nucleic acid concentration

The concentration of isolated plasmid DNA, gDNA, PCR-generated DNA fragments or linearized plasmid DNA was measured on a μ Drop plate (Thermo Fischer Scientific) in a Multiskan™ GO Microplate Spectrophotometer (Thermo Fischer Scientific) at 260 nm using the supplied SkanIt software.

6.2.11 Colony PCR

To validate the integrity of chromosomally inserted DNA fragments, gene deletions, gene replacements or transformed plasmids a colony PCR (cPCR) was performed. For this purpose, a standard PCR reaction mixture was prepared, however, instead of isolated DNA, bacterial cells served as a template for the PCR reaction. The cPCR had to be adjusted according to the requirements for each bacterial species. Therefore, bacterial cells were either picked from the plate, re-streaked on a new plate containing the same antibiotics and then resuspended in the PCR reaction mix (applied for *E. coli*, *Synechocystis* and *Synechococcus*) or picked and resuspended in a small volume of sterile H₂O (usually 10 μ l) from which 1 μ l was then transferred to the PCR reaction mix (*Anabaena* and in some cases *Synechocystis* and *Synechococcus*). The remaining cells were re-streaked on a new plate with suitable antibiotics. In case of cPCR from *Fischerella*, cells were picked, transferred to 20 μ l of H₂O and then boiled to release the DNA from the cells for 30 min at 95 °C. 2 μ l of the supernatant was added to the PCR reaction mix. PCR products were analyzed by agarose gel electrophoresis.

6.2.12 Reverse transcription PCR

To investigate gene expression pattern of gene candidates during different growth phases, total RNA was isolated from the respective organisms and reverse transcription PCR (RT-PCR) of reverse transcribed RNA (complementary DNA, cDNA) was carried out using the DreamTaq Green PCR Master Mix (50ng cDNA/reaction) with internal amplification primers that mediate the amplification of DNA sequences of about 300 bp length. Resulting DNA fragments were analyzed by agarose gel electrophoresis.

6.2.13 DNA sequencing – Verification of cloning constructs

All constructs created during this work were verified by Sanger sequencing (Eurofins) with respective sequencing primers and, if necessary, internal gene primers in order to span the whole sequence.

6.2.14 Cryoconservation

All plasmids generated in the course of this work were stored at -20 °C as pure plasmids. Additionally, *E. coli* strains carrying the respective plasmid were stored as 25% glycerol stocks

at -80 °C. Glycerol stocks were created from fresh overnight cultures mixed 1:1 with 50% sterile glycerol and then transferred to -80 °C. Whenever possible, cryoconserved stocks were also generated from cyanobacterial deletion or chromosomal insertion strains grown in liquid medium essentially as described above for *E. coli* from freshly grown cultures or with 5% DMSO (final) instead of glycerol.

6.2.15 Construction of mutant strains

A popular method to study the function of a respective gene is by removing that gene from an organism and then compare the properties of the mutant strain to the wt strain. In this study, several gene replacement and gene deletion approaches were employed, including the CRISPR Cpf1-based system described by Ungerer and Pakrasi (2016). For gene replacements with an antibiotic resistance gene, two antibiotic resistance-providing gene cassettes were used in this study: the *nptII* gene, which mediates resistance to kanamycin and neomycin and the CS.3 cassette that conveys resistance to spectinomycin and streptomycin (Beck *et al.*, 1982; Sandvang, 1999). The target gene is replaced by the antibiotic resistance cassette by double homologous recombination of the flanking regions from the knockout plasmid with the genomic region (Fig. 1). Homologous flanking regions (HFR) were designed to consist of about 1000 bp, except for gene knockout constructs in *Fischerella* where 2000 bp were chosen. Besides gene replacement and gene deletion constructs aiming for a double homologous recombination event, other gene disruption vectors were constructed, which were designed to contain homologous regions upstream of the gene as well as parts of the gene to be disrupted, intending to insert the plasmid after this short gene sequence and thereby interrupting the original gene. However, all fully segregated knockout strains obtained in this study were based on a gene replacement by double homologous recombination.

6.2.16 Verification of gene replacements

Employing double homologous recombination for targeted gene knockout includes some error sources. For instance, single homologous recombination events are far more likely to occur in *Anabaena* and based on the cyanobacterial polyploidy, full segregation of mutant alleles is a rather unlikely event (Cai and Wolk, 1990; Griese, Lange and Soppa, 2011). For this reason, a PCR-based screening for clones that underwent double homologous recombination is indispensable. The use of the conditionally lethal *sacB* gene, present in the employed pRL278 plasmid, was shown to aid this screening by excluding sucrose sensitive mutants that underwent single homologous recombination (Cai and Wolk, 1990). Gene replacements were then either verified by cPCR or by PCR from isolated gDNA of mutant clones as template. To confirm full segregation of mutant strains, a set of different primer pairs were used for analytical PCR reactions. First, the absence of the target gene was tested with gene-specific primers (G1

and G2, red arrows in Figure 7) and further confirmed by two additional PCR reactions. One reaction contained a forward primer flanking the 5' homologous flanking region (5' HFR) upstream of the gene (H1 in Figure 7) with a gene reverse primer (G2 in Figure 7) and another PCR reaction contained a gene forward primer (G1 in Figure 7) and a reverse primer flanking the 3' HFR downstream of the gene (H2 in Figure 7). Additionally, the correct placement of the introduced antibiotic resistance cassette was tested by two additional PCR reactions. The first reaction targeted the 5' end of the antibiotic resistance cassette (R1 in Figure 7) and the 3' HFR (H2 in Figure 7). The second PCR reaction was designed to amplify the 5' HFR (H1 in Figure 7) and the 3' end of the antibiotic resistance cassette (Primer R2 in Figure 7).

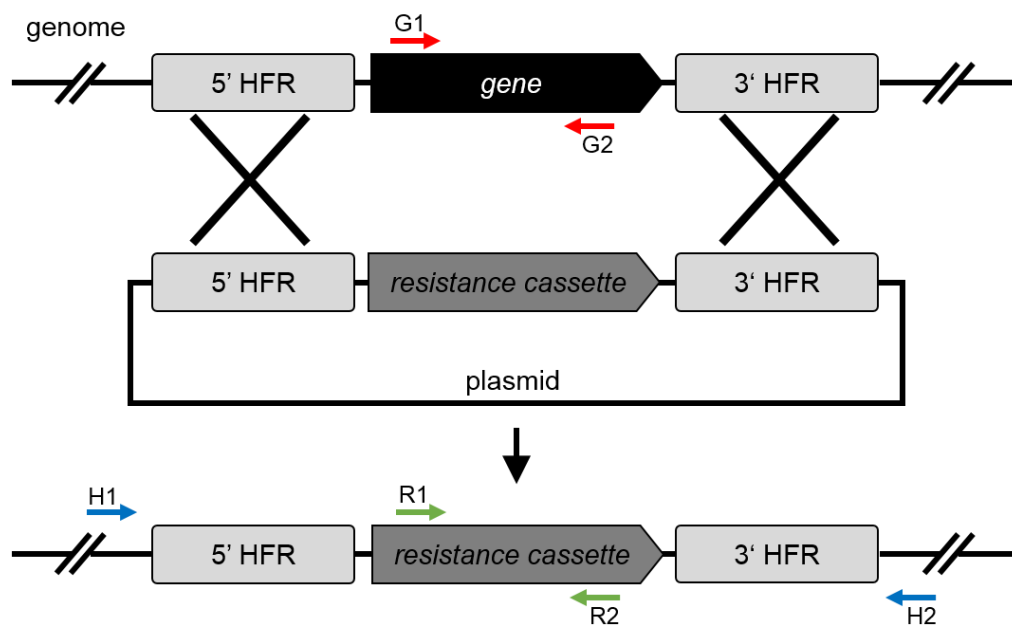


Fig. 7: Schematic representation of a double homologous recombination-based gene replacement

Gene replacement by double homologous recombination of a target gene on the genome with a knockout plasmid containing upstream (5' HFR) and downstream (3' HFR) homologous regions that are employed by the intrinsic enzymatic repair machinery to mediate the double homologous recombination event (Alberts *et al.*, 2014). Target gene-specific primers are depicted with red arrows (G1, G2), primers encompassing the 5' and 3' HFR are depicted in blue arrows (H1, H2) and specific primers targeting the resistance cassette are shown in green arrows (R1, R2).

6.3 Cell biology methods

6.3.1 Bacterial strains and growth conditions

Fischerella, *Anabaena* and *Synechocystis* GT-Kazusa substrain were obtained from the Pasteur Culture Collection (PCC) of cyanobacteria (France). *Synechococcus* was a gift from Martin Hagemann (University Rostock). Glucose tolerant *Synechocystis* PCC-M substrain was a gift from Annegret Wilde (University Freiburg). Cells were grown photoautotrophically in BG11 or without combined nitrogen (BG11-0) at a 16h/8h light/dark regime (*Fischerella*) or at constant light (*Anabaena*, *Synechococcus* and *Synechocystis*) with a light intensity of

30 $\mu\text{mol m}^{-2} \text{s}^{-1}$. When appropriate, 50 $\mu\text{g ml}^{-1}$ kanamycin (Km), 2.5 $\mu\text{g ml}^{-1}$ spectinomycin (Sp), 2.5 $\mu\text{g ml}^{-1}$ streptomycin (Sm) or 30 $\mu\text{g ml}^{-1}$ neomycin (Nm) was added to strains carrying respective plasmids or chromosomal insertions/deletions. In some cases, basal copper-regulated *petE*-driven expression of gene candidates in *Anabaena* and *Fischerella* cells turned out to be lethal or growth inhibiting, therefore these strains were grown in BG11 (or BG11-0) without copper and protein expression was later induced by the addition of CuSO_4 at indicated concentrations to the culture.

E. coli strains DH5 α , DH5 α MCR, XL1-blue and HB101 were used for cloning and conjugation by triparental mating. BTH101 was used for BACTH system and BL21 (DE3) was used for expression of His- and GFP-tagged proteins in *E. coli*. All strains were grown in LB medium containing the appropriate antibiotics at standard concentrations.

6.3.2 Cell viability tests

Growth defects of cyanobacterial deletion strains were evaluated by comparative growth curves or spot assays. For growth curves, *Synechocystis* wt cells, $\Delta\text{slr1301}$ cells and $\Delta\text{slr7083}$ cells were grown in liquid BG11 pre-cultures to an OD_{750} of about 2.0 and then diluted in BG11 to an OD_{750} of approximately 0.01. Cells were then grown at standard growth conditions in quadruple biological replicates and OD_{750} was recorded once a day. As another method to assess the viability of deletion strains and the susceptibility of these strains to certain substances, spot assays adapted from Dörrich *et al.* (2014) were performed. Spot assays of *Synechocystis* and *Synechococcus* wt and deletion strains were performed with cultures grown in BG11 to an OD_{750} of about 2.0, which were then diluted to an OD_{750} of 0.4. Cells were spotted in triplicates of 5 μl onto the respective growth plates containing either no additives (BG11 or BG11-0), BG11-0 supplemented with 2 mM NH_4Cl , Proteinase K or Lysozyme at indicated concentrations in serial dilutions of factor 1/10 and incubated under standard growth conditions until no further colonies arose in the highest dilution.

Since the majority of *Anabaena* knockout strains were incapable of growth in liquid culture, spot assays of *Anabaena* wt and knockout strains were performed from cells grown on BG11 agar plates (supplemented with antibiotics if applicable). For this purpose, cells were streaked from growth plates and resuspended in BG11 liquid medium. Cell suspensions were then diluted to an OD_{750} of 0.4, spotted on indicated growth plates with or without supplements in triplicates of 5 μl in serial dilutions of factor 1/10 and grown until no further colonies arose in the highest dilution.

6.3.3 Influence of osmotic factors on cell growth

Cytoskeletal proteins and specifically IF proteins are known to stabilize cellular structures and intercellular connections (Alberts *et al.*, 2014). Deletion of the respective genes might therefore impact the ability of deletion strains to resist certain environmental factors and specifically osmotic stress factors, which can impact the cell structure due to alterations in the turgor pressure (Fricke, 2017). The lack of stability-providing genes can thus lead to growth defects under these conditions. To examine any existing cell-stability defects, *Synechocystis*, *Synechococcus* and *Anabaena* wt and knockout strains were grown on BG11 agar plates (containing the respective antibiotics) and were then transferred to BG11 or BG11-0 liquid medium and grown under standard growth conditions with or without one of the following additives:

- 5 mM glucose
- 200 mM glucose
- 2 mM NH₄Cl
- 200 mM maltose
- 500 mM NaCl

6.3.4 Motility test

There are various known substrains of *Synechocystis* which are characterized by slight genome alterations, tolerance to glucose and motility (Trautmann *et al.*, 2012). In this study, we compared the impact of gene knockouts in two *Synechocystis* substrains. The first strain is the glucose-tolerant non-motile *Synechocystis* strain commonly referred to as the GT-Kazusa substrain (Kaneko *et al.*, 1996). This strain contains a one base pair insertion into the *spkA* gene rendering it non-motile (Trautmann *et al.*, 2012). The other strain is the motile and glucose-tolerant “Moscow” substrain called *Synechocystis* sp. PCC-M 6803 (PCC-M). This strain migrates towards the direction of a specific light source or into an area with richer nutrients (Wilde and Mullineaux, 2017). To evaluate the motility of the knockout strains, especially for the motile PCC-M substrain, three single colonies of the respective wt and knockout strain were streaked on a line on a BG11 growth plate, which was then placed into the standard culture incubator but with illumination limited to one direction. Cells were grown for a few days and motility of strains was assessed by the traveled distance across the agar plate.

6.3.5 Transformation of cyanobacteria

As *Synechocystis* and *Synechococcus* are naturally competent cyanobacteria, they are capable to take up foreign DNA and integrate it into their genome by homologous

recombination (Grigorieva and Shestakov, 1982; Golden, Brusslan and Haselkorn, 1987). The transformation efficiency of these cells is highest during the exponential growth phase (Grigorieva and Shestakov, 1982) which is why transformations were usually performed with exponentially growing cultures. However, transformation was also successfully performed with stationary phase cultures. For natural transformation of *Synechocystis* and *Synechococcus*, 500 µl cells grown in BG11 were incubated for 6 hours at 30 °C (*Synechocystis*) or 34 °C (*Synechococcus*) in the dark with 1-4 µg plasmid DNA and brief mixing every 30 min. Afterwards, cells were plated on sterilized nitrocellulose filters on BG11 agar plates. The plates were incubated for 2 days at growth conditions and then transferred to BG11 plates containing the appropriate antibiotics. After 1-2 weeks of incubation at growth conditions, single colonies arose on the filter, which were then picked and re-streaked onto fresh BG11 plates containing the respective antibiotics. Visualization of fluorescently tagged proteins was done as described in section 6.3.6. Verification of gene deletions was performed by cPCR or PCR on isolated genomic DNA as described in section 6.2.11. However, transformation of RSF1010 ori-based plasmids (i.e. pRL153-based plasmids) into *Synechocystis* required a conjugation-based triparental mating system as described below.

No natural competence has yet been described in *Anabaena* or *Fischerella*. Therefore, transformation of these strains was achieved by conjugation in a triparental mating system. This system involves three bacterial strains; two *E. coli* strains and the respective cyanobacterial acceptor strain. One of the *E. coli* strains carries a derivative of the RP4 conjugational plasmid called pRL443. This plasmid encodes all essential *mob* genes for the conjugal transfer of mobilizable plasmids (Elhai *et al.*, 1997). The other *E. coli* strain harbors the mobilizable cargo plasmid as well as the mobilizable pRL623 helper plasmid. The helper plasmid encodes the *mob* genes from ColK and mediates the methylation of the cargo plasmid by three encoded methylases: M.AvaI, M.Eco47II and M.EcoT22I (Tacon *et al.*, 1981; Elhai *et al.*, 1997). The pre-conjugational methylation of cargo plasmids was shown to drastically increase the transformation efficiency of *Anabaena* (Elhai *et al.*, 1997).

Transformation of *Anabaena* was then performed essentially as described by Ungerer and Pakrasi (2016). For this, 100 µl of overnight cultures of DH5α carrying the conjugal plasmid pRL443 and DH5αMCR carrying the cargo plasmid (pRL25c, pRL271, pRL278 or pSL2680-based) and the helper plasmid pRL623 were mixed with 200 µl of a young *Anabaena* culture. This mixture was directly applied onto sterilized nitrocellulose membranes placed on top of BG11 plates supplemented with 5% LB medium. Cells were incubated in the dark at 30 °C for 6-8 hours with subsequent transfer of the membranes to BG11 plates containing the respective antibiotics.

Fischerella, as well as other species of subsection V are characterized by a thick exopolysaccharide sheath, which was shown to diminish the transformation efficiency of these strains (Stucken *et al.*, 2012). This obstacle can be overcome by a previous high salt treatment to wash off the exopolysaccharide sheath. The conjugational transfer was then performed according to Stucken *et al.* (2012). For this aim, one day prior transformation, *Fischerella* cells were subjected to sonication in a water bath (Elmasonic S60, Elma) at maximum intensity for 10 min. This procedure results in the disruption of cell filaments and therefore poses a harsh treatment. Cells were washed in BG11 by centrifugation and returned to their growth conditions to recover overnight. The next day, cells were treated with 1 M NaCl (final concentration) for 1 h at growth conditions and then washed four times in BG11 and left to recover under light without shaking for about 5 h. *E. coli* strains carrying the conjugal plasmid or cargo and helper plasmid were washed three times in LB medium, concentrated to an OD₆₀₀ of 0.9 and mixed. 2 ml treated *Fischerella* cells were combined with 1 ml of mixed *E. coli* suspension, incubated for 1.5 h under light and plated on sterilized nitrocellulose membranes placed on top of BG11 agar plates supplemented with 5% LB medium and 2.5 mM NH₄Cl. Cells were grown for 24 h at 37 °C under low light and then transferred to BG11 plates containing 2.5 mM NH₄Cl. Finally, after 72 h of recovery, membranes were transferred to BG11 plates supplemented with the appropriate antibiotics. After one to two weeks colonies arose, which were then picked, re-streaked and evaluated depending on the respective transformed construct. Transformation of sonicated (fragmented) *Fischerella* cells using the methods developed by Ungerer and Pakrasi (2016) was also feasible for *Fischerella*, albeit with a lower transformation frequency.

6.3.6 Microscopic procedures

Bacterial strains grown in liquid culture were either directly applied to a microscope slide and then observed with an Axio Imager 2 light microscope (Carl Zeiss) or previously immobilized on a 2% low melting agarose in BG11 agarose pad (hereafter: agarose pad) and air dried before microscopic analysis. When applicable, cells were previously incubated in the dark at RT for about 5 min with 10 µg ml⁻¹ DAPI (final concentration) to stain intracellular DNA. Also, to investigate putative alterations of the polysaccharide sheath of *Anabaena* mutants, cells were grown on BG11 or BG11-0 agar plates, re-suspended in BG11 or BG11-0 liquid medium and stained with 0.05% alcian blue (final concentration). Polysaccharide staining of *Anabaena* cells immobilized on an agarose pad was then observed with an Axiocam ERc 5s color camera (Carl Zeiss).

For time lapse experiments of *E. coli* BL21 (DE3) expressing GFP-tagged protein candidates, cells were grown over night in LB Amp at 37 °C and 250 rpm. The next day, cells were diluted 1:40 in the same medium, incubated at 37 °C and 250 rpm until an OD₆₀₀ of 0.5 was reached

and then applied to an agarose pad (1.5% low melting agarose in M9 medium supplemented with Amp and 0.5 mM IPTG) and pictures were taken in intervals.

Additionally, time course experiments of *E. coli* BL21 (DE3) cells expressing C-terminally GFP-tagged protein candidates were also performed. Therefore, the respective strains were grown over night in LB and then diluted 1:40 in the same medium the following day. Cells were grown for 2 h at 37 °C, briefly acclimated to 20 °C for 10 min and induced with 0.05 mM IPTG at 20 °C. Cell morphology and localization of GFP-tagged proteins was then observed after indicated time points of cells immobilized on an agarose pad.

6.3.7 Fluorescence recovery after photobleaching (FRAP)

The calcein-staining and microscopic procedures of this technique were performed by Dr. Dennis J. Nürnberg (Imperial College London) while the subsequent calculation was done by the candidate.

$\Delta alr0931$, $\Delta all2460$ and $\Delta alr4504\Delta alr4505$ *Anabaena* strains all displayed defects in trichome integrity, albeit to a different extent. In order to evaluate whether the observed phenotype was, in part, caused by an impaired cell-cell communication mechanism, we employed the fluorescence recovery after photobleaching (FRAP) method in cooperation with Dr. Dennis J. Nürnberg (Imperial College London). This method is based on a small fluorescent tracer molecule, in this case calcein, which is able to diffuse through cell membranes. In the cells, calcein is then activated by esterases, producing a hydrophilic calcein product unable to leave the cells (Mullineaux *et al.*, 2008; Nürnberg *et al.*, 2015). Using a confocal microscope, the calcein dye can be bleached by a strong laser and the diffusion rate of calcein from neighboring cells within a trichome is then measured according to Mullineaux *et al.* (2008) and given as exchange coefficient (E , indicated in s^{-1}). The exchange coefficient relates the diffusion rate of neighboring cells to the differences in dye of those cells (Mullineaux *et al.*, 2008; Nürnberg *et al.*, 2015). In brief, the experimental procedure is as follows. Cells were either grown on BG11 plates and resuspended in BG11 or directly taken from liquid cultures, washed several times in BG11, resuspended in 0.5 ml BG11 and incubated with 10 μ l calcein-AM (1 mg ml^{-1} in DMSO). The cells were incubated in the dark at 30 °C for 1h and then subjected to four washing steps with 1 ml BG11. Subsequently, the cells were resuspended in a small volume of BG11, spotted on BG11 plates and air dried. Using an inverted confocal microscope (Leica TCS SP8), selected cells were bleached by two high power laser pulses (80% of the maximum laser intensity) and fluorescence recovery was recorded every 0.5 s for about half a minute. Exchange coefficients were then calculated according to Mullineaux *et al.* (2008).

6.3.8 Determination and calculation of cell morphological features

Cell length, volume and roundness were determined using the imaging software ImageJ. Cell volume was calculated based on the assumption of an elliptic cell shape of *Anabaena* cells

using the Major Axis and Minor Axis values given by ImageJ and the formula for the volume of an ellipse ($V = \frac{4}{3}\pi abc$):

- $$V = \frac{4}{3}\pi \left(\left(\frac{\text{Major Axis}}{2} \right)^2 \frac{\text{Minor Axis}}{2} \right)$$

6.4 Protein and biochemical methods

6.4.1 Discontinuous SDS polyacrylamide gel electrophoresis

In this study, SDS polyacrylamide gel electrophoresis (Sambrook and Green, 2012) was employed to either verify overexpression of protein candidates from *E. coli*, to explore the purity of His-tagged protein candidates upon Ni-NTA-based purification or for subsequent immobilization of resolved proteins on a nitrocellulose membrane for immunodetection by western blotting with specific antibodies (Renart, Reiser and Stark, 1979; Towbin, Staehelin and Gordon, 1979). In this study, 10% or 12% self-cast polyacrylamide gels or 4-15% TGX precast gels (Bio-Rad) were employed and, if applicable, protein bands were visualized using the Quick Coomassie® stain (SERVA). In order to estimate the molecular weight of the proteins in the samples, a protein marker (PageRuler™ Prestained Protein Ladder, Thermo Fischer Scientific) with proteins of known molecular weight was also added to the gels. Western blotting in a semi-dry approach was performed using the Trans-Blot Turbo system (Bio-Rad) and proteins were immobilized on 0.45 µm nitrocellulose blotting membrane (Sartorius).

6.4.2 Immunological detection of immobilized proteins

After the electrophoretic immobilization of proteins on a nitrocellulose membrane, free membrane binding sites were saturated for 30 min at RT with 5 % dry skim milk in TBST (blocking buffer). Thereafter, the membrane was incubated with the respective primary antibody (Table 6) over night at 4°C or for 1-2 h at RT. The primary antibody was decanted and the remaining unbound primary antibody was removed by 3x washing with TBST. Subsequently, the membrane was incubated for 1 h at RT with HRP-conjugated secondary antibody (Table 6) that specifically binds to the respective primary antibody. Again, remaining and nonspecifically bound antibodies were removed by three times washing with TBST. For the detection of specifically bound antibodies, the membrane was incubated in the dark with SuperSignal® West Pico Chemiluminescent Substrate (Thermo Fischer Scientific) for 4 minutes and chemiluminescence was then recorded in a chemiluminescent reader (ChemiDoc XRS+, Bio-Rad).

6.4.3 Evaluation of protein-protein interactions

During this study, a variety of different tests were applied to investigate protein-protein interactions of protein candidates with themselves, with each other and with already described cytoskeletal proteins and a septal junction protein (SepJ). For this purpose, we performed bacterial two hybrid, GFP reassembly and *in vitro* filamentation assays as well as co-immunoprecipitations (co-IP) followed by subsequent mass spectrometry analyses.

6.4.3.1 Bacterial two hybrid assay

The bacterial adenylate cyclase-based two hybrid (BACTH) system is a simple and reliable *E. coli*-based method for the evaluation of protein-protein interactions in an *in vivo* environment. In this study, the Euromedex BACTH system was employed (Karimova *et al.*, 1998; Karimova, Davi and Ladant, 2012). This system allows to identify interactions of any two given proteins. It is based on the interaction-mediated restoration of the adenylate cyclase (CyaA) activity from *Bordetella pertussis* in a *cya*-deficient (Δcya) *E. coli* strain. The catalytic domain of the CyaA protein consists of two domains (T25 and T18) and is only active when those domains are physically connected. Functional complementation of the CyaA protein by physical interaction of two proteins of interest can then be identified on selective media containing X-gal, which is a chromogenic substrate for the β -galactosidase and cleavage of X-gal results in the formation of an intensely blue product within the cells rendering the bacterial colonies blue. When two non-interacting proteins are fused to the T25 and T18 domain, the colonies will remain white. As a verification and quantification of this so called blue-white screening, a subsequent beta galactosidase assay was performed. This assay is a mean to indirectly quantify the interaction strength of the two invested proteins by quantifying the β -galactosidase-mediated hydrolyzation of ONPG (ortho-Nitrophenyl- β -galactoside), which is then recorded in Miller units (Miller, 1992).

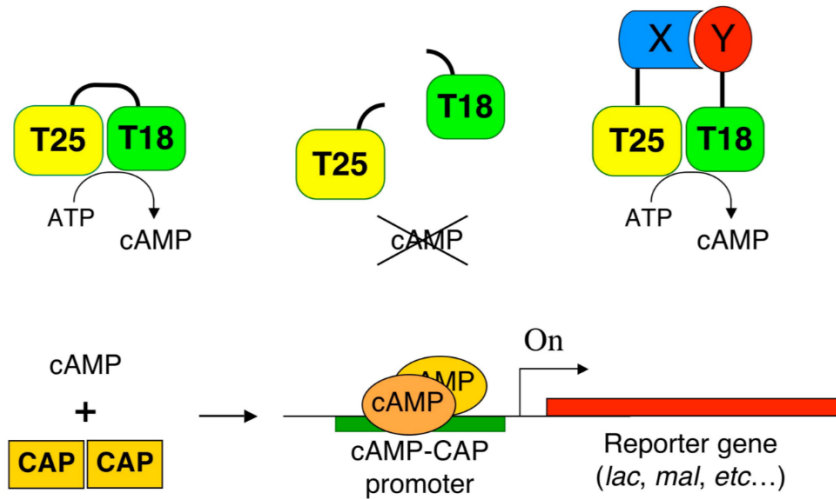


Fig. 8: Principle of the bacterial adenylate cyclase two hybrid system

In an active state, in which the T25 and T18 subunit are physically connected, the CyaA protein mediates the conversion of ATP to cyclic AMP (cAMP), which then binds to the catabolite activator protein (CAP) and functions as an allosteric effector that increases the affinity of CAP for the DNA (Busby and Ebright, 1999). For the BACTH assay, both subunits are separated and can thus not perform the enzymatic activity of the CyaA protein. When the two catalytic domains are translationally fused to two interacting proteins (X and Y), the described catalytic activity is restored and cAMP is produced. This elevation in cAMP levels induces the expression of several genes involved in lactose and maltose catabolism (*lac* and *mal* operons), including the β -galactosidase encoded by the *lacZ* gene. Picture taken from Euromedex (BACTH system Kit).

Gene candidates were cloned into the expression vectors pKNT25, pKT25, pUT18 and pUT18C (Euromedex) by GIBSON assembly, thereby generating C- and N-terminal translational fusions to the T25 or T18 subunit. Chemically competent *E. coli* BTH101 cells were co-transformed with 5 ng of the indicated plasmids, plated onto LB plates supplemented with 200 $\mu\text{g ml}^{-1}$ X-gal, 0.5 mM IPTG, Amp, Km and grown at 30°C for 24-36 h. Interactions were quantified by beta-galactosidase assays from three colonies for each combination according to the protocol described by Euromedex or in a 96 well format according to Karimova, Davi and Ladant (2012). For this aim, cultures were either grown over night at 30 °C or for two days at 20 °C in LB Amp, Km, 0.5 mM IPTG.

6.4.3.2 Identification of protein-protein interactions using GFP-reassembly

Similarly to the bacterial two hybrid system, in the GFP-fragment reassembly assay developed by Wilson, Magliery and Regan (2004), proteins to be evaluated for direct interaction are each fused to a fragmented protein, in this case the GFP protein, which only re-assembles into a functional protein upon direct binding of the two proteins of interest. This assay not only allows to detect protein-protein interactions in *E. coli* (and thus *in vivo*) but simultaneously provides a mean to assess the (co-)localization of two given proteins *in vivo* by visualization of the fluorescence signal of the re-assembled GFP with a fluorescence microscope. The assay was employed to further characterize the interaction of Alr4504 and Alr4505 and based on previous results from the bacterial two hybrid system, not all possible plasmid combinations were

constructed. Using Gibson assembly, *alr4504* was cloned into XhoI and BamHI-digested pET11a-link-NGFP, thereby fusing *alr4504* with an N-terminal *ngfp*-fragment. Additionally, *alr4504*, together with a 12 base pair linker sequence (encoding for Ala-Ser-Ala-Ser), was inserted into NheI digested pET11a-link-NGFP, equipping *alr4504* with a C-terminal *ngfp*-fragment. Furthermore, *alr4505* was inserted into NcoI and AatII-digested pMRBAD-link-CGFP by Gibson assembly, equipping *alr4505* with a C-terminal *cgfp*-fragment. *E. coli* BL21 (DE3) cells were then co-transformed with indicated plasmid combinations, plated on LB Amp, Km plated and grown over night at 37 °C. Subsequently, liquid overnight cultures of single colonies of the respective plasmid-bearing *E. coli* strains were performed in LB Amp, Km at 37°C and diluted 1:40 in the same medium the next day. Cells were grown for 2 h at 37 °C, briefly acclimated to 20 °C for 10 min and protein expression was then induced with 0.05 mM IPTG and 0.2% L-arabinose. Pictures of induced cultures grown at 20 °C were taken at indicated time points.

6.4.3.3 Protein purification and in vitro filamentation assay

Cytoskeletal proteins and especially intermediate filament proteins are not only able to interact and form polymers *in vivo*, but based on their strong intrinsic self-binding capacity, polymerization can also be observed in a cell free environment (*in vitro*). In order to obtain the necessary amount of proteins for *in vitro* polymerizations, gene candidates were cloned into pET21a(+), thereby equipping them with a C-terminal hexahistidine tag (His6-tag). Employing this His6-tag, purification of overexpressed proteins can be achieved using Ni-NTA matrixes. For protein purification, *E. coli* BL21 (DE3) cells carrying His-tagged protein candidates were grown in overnight cultures at 37 °C and 250 rpm. The next day, overnight cultures were diluted 1:40 in the same medium and grown at 37 °C until they reached an OD₆₀₀ of 0.5-0.6. Protein expression was induced with 0.5 mM IPTG for 3-4 hours at 37 °C and 250 rpm and cells were subsequently harvested by centrifugation, washed once in PBS and stored at -80 °C. For expression of MBP-Fm7001-His, DH5α cells carrying empty pMAL-c2x (control) or pMAL-c2x-Fm7001-His were grown in the same medium but supplemented with 0.2% glucose.

For *in vitro* polymerization assays of purified proteins, cell pellets were resuspended in urea lysis buffer (ULB; 50 mM NaH₂PO₄, 300 mM NaCl, 25 mM imidazole, 6 M urea; pH 8.0) and lysed in a Precellys® 24 homogenizer using the 2 ml microorganism lysis kit (VK01; Bertin) or self-packed Precellys tubes with 0.1 mm glass beads. The resulting cell debris was pelleted by centrifugation at 21,000 x *g* (30 min, 4 °C) and the supernatant was incubated with HisPur™ Ni-NTA resin (Thermo Fischer Scientific) for 1 h at 4°C with mild agitation. The resin was washed 5 times with 4 resin-bed volumes ULB and eluted in urea elution buffer (UEB; 50 mM NaH₂PO₄, 300 mM NaCl, 250 mM imidazole, 6 M urea; pH 8.0). Total protein concentration was measured using the Qubit® 3.0 Fluorometer (Thermo Fischer Scientific) and generally

adjusted to 0.5 mg ml⁻¹ before dialysis. Filament formation of purified proteins was induced by overnight dialysis against polymerization buffer (PLB: 50 mM PIPES, 100 mM KCl, pH 7.0; HLB: 25 mM HEPES, 150 mM NaCl, pH 7.4; or 25 mM HEPES pH 7.5) at 4°C or 20 °C and 180 rpm with three bath changes using a Slide-A-Lyzer™ MINI Dialysis Device (10K MWCO, 0.5 ml or 2 ml; Thermo Fischer Scientific). Purified proteins were stained with an excess of NHS-Fluorescein (Thermo Fischer Scientific) and *in vitro* filamentation was analyzed by epifluorescence microscopy.

In contrast to all tested proteins, Fm7001-His was slowly dialyzed against 2 mM Tris-HCl, 4.5 M urea, pH 7.5 (18°C, 200 rpm) decreasing 0.5 M urea every two hours (from 6 M to 4.5 M urea). The resulting filamentous web floating on top of the dialyzed solution was then applied to bright field microscopy.

Induction of Synpcc7942_2039-His in *E. coli* BL21 (DE3) cells inhibited cell growth without expression of the target protein. To bypass this, Synpcc7942_2039-GFP-His, under the control of an IPTG-inducible *P_{trc}* promoter, was inserted into a neutral locus of *Synechococcus*. Cells were grown till and OD₇₅₀ of about 0.8 and protein expression was induced with 0.05 mM IPTG for 3 days. Induced cells were harvested by centrifugation (4800 x g, 4 °C, 10 min) and stored at -80 °C. Protein purification, dialysis and labeling was then performed as described above with the exception that BG11 growth medium was used as dialysate.

Purification and dialysis of FmFtsZ-His was essentially performed according to the above described system, however, cell lysis was achieved in a native lysis buffer containing Triton X-100 (NLB-T: 50 mM NaH₂PO₄, 300 mM NaCl, 25 mM imidazole, 1% Triton X-100, pH 8.0) and eluted in a native elution buffer (NEB-T: 50 mM NaH₂PO₄, 300 mM NaCl, 250 mM imidazole, 0.5% Triton X-100, pH 8.0). The resulting protein fraction was dialyzed against FtsZ storage buffer (50 mM Tris pH 7.4, 50 mM KCl, 1 mM EDTA and 10% glycerol) and stored at -80 °C.

6.4.3.4 Protein concentration measurement

Protein concentration of cell-free cyanobacterial lysates was estimated with a Bradford assay using the Bio-Rad Protein Assay Dye Reagent Concentrate (Bio-Rad; Bradford, 1976). For this, 200 µl of dye concentrate were mixed with 800 µl of H₂O and incubated for 10 min at RT with 2 µl of cell-free lysate. The protein concentration was calculated based on previously recorded standard curves based on solutions of defined bovine serum albumin. Protein concentration of isolated and purified His6-tagged proteins in the respective elution buffer was measured using the Qubit® 3.0 Fluorometer (Thermo Fischer Scientific) according to the manufacturer's instructions with 2 µl of sample input.

6.4.3.5 Co-immunoprecipitation

Another approach to verify and assess protein-protein interactions is the so-called co-immunoprecipitation (co-IP). The co-IP is essentially based on the same principle as a normal immunoprecipitation but in a co-IP the focus of downstream analyses is shifted to the co-precipitated molecules (the interacting proteins) instead of the precipitated antigen. In these cases, eluted samples can also be investigated by SDS-Page and western blot analysis, however, another feasible approach is to sequence the interacting proteins by mass spectrometry. Thus, to further characterize the function of the investigated protein candidates, co-IPs of fluorescently tagged protein candidates were performed in this study. For this, cyanobacterial strains expressing the respective YFP or GFP-tagged protein candidates were grown in BG11 or BG11-0 liquid growth medium supplemented with the appropriate antibiotics. In some cases, growth of protein candidate-expressing strains in normal growth media was inhibited by the basal expression driven by the copper-inducible *petE* promoter. By default, copper is included in the BG11 growth medium, thus, special non-copper containing growth medium (BG11/BG11-0-Cu) was used for cell growth in those cases. Protein expression was then induced by addition of copper at indicated concentration. Also, Synpcc7942_2039-GFP-His expression at young culture stages appeared to be growth inhibitory, therefore, *Synechococcus* strains expressing Synpcc7942_2039-GFP-His were grown to an OD₇₅₀ of 0.7 and thereupon, protein expression was induced with 0.05 mM IPTG for 3 days before co-IP. Generally, about 20-30 ml of the respective cyanobacterial culture was pelleted by centrifugation (4800 x g, 10 min, RT), cells were washed by centrifugation (4800 x g, 10 min, RT) with 40 ml PBS and then resuspended in one of the following lysis buffers supplemented with protease inhibitor cocktail (PIC; cOmplete™, EDTA-free Protease Inhibitor Cocktail, Sigma-Aldrich):

- PBS-N: 10 mM Na₂HPO₄, 140 mM NaCl, 2.7 mM KCl, 1.8 mM KH₂PO₄, pH 7.4, 1% NP-40
- HSLB: 50 mM Na₂HPO₄, 500 mM NaCl, 1% NP-40, pH 7.2
- CLB: 50 mM HEPES, 200 mM NaCl, 10 mM MgCl₂, 5% glycerol, 1% Triton X-100, pH 7.2

Cells were lysed using the VK05 lysis kit (Bertin) in a Precellys® 24 homogenizer (3 strokes for 30 seconds at 6500 rpm) and cell debris was pelleted by centrifugation (30 min, 21,100 x g, 4 °C). 50 µl µMACS anti-GFP MicroBeads (Miltenyl Biotec) was added to the resulting cell-free supernatant and incubated for 1 h at 4 °C with mild rotation. Afterwards, the sample was loaded onto µColumns (Miltenyl Biotec), washed two times with 1 ml lysis buffer and eluted in 50 µl elution Buffer (50 mM Tris HCl pH 6.8, 50 mM DTT, 1% SDS, 1 mM EDTA, 0.005% bromphenol blue, 10% glycerol; Miltenyl Biotec). Samples were stored at -80 °C.

In case of *Anabaena* cells expressing Alr3364-GFP, cells were either treated as described above and lysed in PSB-N or HSLB and, if applicable, fixed in formaldehyde before cell lysis. Therefore, Alr3364-GFP expressing *Anabaena* cultures were pelleted by centrifugation and resuspended in 1 ml BG11 containing 0.6% formaldehyde. Cells were incubated for 20 min at 37 °C and the crosslinking reaction was terminated by addition of 125 mM glycine (final concentration) for 5 min at RT. Cells were washed three times in PBS by centrifugation (10,000 x g, 5 min, RT) and resuspended in 1 ml CLB supplemented with PIC. Co-IP was executed as described above, and precipitated samples in elution buffer were subjected to SDS-PAGE and subsequent western blot analysis using rabbit anti-FtsZ antibody (Agrisera; 1:2000 diluted). As a control, *Anabaena* wt cells were treated accordingly.

6.4.3.6 Mass spectrometry analysis

Raw mass spectrometry data are listed in the attached Supplementary File 3.

The following samples were analyzed by mass spectrometry in cooperation with Prof. Dr. Andreas Tholey and executed by Dr. Andreas Helbig (University of Kiel, Germany):

- *Anabaena* wt
- *Anabaena* expressing All4981-GFP
- *Anabaena* expressing YFP-All4981
- *Anabaena* expressing Alr4504-GFP
- *Anabaena* expressing All2460-GFP

The following samples were analyzed in cooperation with Prof. Dr. Martin Thanbichler (University of Marburg, Germany):

- *Fischerella* wt
- *Fischerella* expressing YFP-Fm7001
- *Anabaena* wt
- *Anabaena* expressing Alr0931-GFP
- *Anabaena* expressing Alr3364-GFP
- *Synechocystis* wt and PCC-M wt
- *Synechocystis* expressing Slr1301-YFP
- *Synechocystis* expressing Slr7083-GFP
- *Synechococcus* wt
- *Synechococcus* expressing Synpcc7942_2039-GFP
- *Synechococcus* expressing Synpcc7942_1139-GFP

Prior to the mass spectrometry analysis, the precipitated samples were applied to a 4–15% Mini-PROTEAN® TGX™ Precast Protein Gel (Bio-Rad) just until the whole sample had entered the gel. The gel electrophoresis was halted and proteins within the SDS-gels were precipitated and stained using a Colloidal Coomassie staining solution without acetic acid (20% methanol, 10% citric acid, 8% ammonium sulfate, 0.08% Coomassie Brilliant Blue G250) for 8 hours at room temperature. Upon extensive destaining in purified water with several bath changes, protein-containing gel slices were cut, transferred to 1.5 ml reaction tubes and covered with sterile and purified water. Samples were finally sent by mail on cool packs and protein sequencing was performed by the mass spectrometry facility of the University of Marburg in cooperation with Prof. Dr. Martin Thanbichler.

6.4.4 *In vivo* immunodetection of protein candidates

6.4.4.1 Immunofluorescence of *Anabaena*

In the course of this study, three different *Anabaena* knockout strains were generated that all showed defects in trichome integrity. FtsZ is a key player of the cyanobacterial cytoskeleton and is essential for proper cell division. It is also debated to be the defining factor for perpendicular or branching growth pattern of cells within a filament of multicellular cyanobacteria (unpublished data by Springstein *et al.*). Thus, the influence of the absence of the respective genes in *Anabaena* were investigated by anti-FtsZ immunolocalization essentially as described by Ramos-León *et al.* (2015). For this aim, *Anabaena* gene knockout strains as well as *Anabaena* wt control cells were streaked from growth plates (BG11 and BG11-0 plates), resuspended in a small volume of distilled water, applied to Polysine® adhesion slides (Menzel) and then let air dry for about 30 min at RT followed by fixation and permeabilization with 70% ethanol for 30 min at -20 °C. Cells were allowed to air dry for 30 min at RT and then washed 2x with PBST for 2 min. Unspecific binding sites were blocked for 30 min at RT with blocking buffer (1x Roti®-ImmunoBlock in PBST; Roth) and afterwards, rabbit anti-FtsZ (Agrisera; 1:150 diluted) antibody in blocking buffer was added to the cells and incubated for 1.5 h at RT in a self-made humidity chamber followed by five washing steps with PBST. 7.5 µg ml⁻¹ Alexa Fluor488 conjugated goat anti-rabbit IgG (H+L) secondary antibody (Thermo Fischer Scientific) in blocking buffer was added to the cells and incubated for 1 h at RT in the dark in a self-made humidity chamber. Subsequently, cells were washed 5x with PBST, air dried and mounted with ProLong™ Diamond Antifade Mountant (Thermo Fischer Scientific) overnight at 4 °C. Immunolocalization of FtsZ was then analyzed by epifluorescence microscopy. Similarly, *in vivo* localization of Alr0931-His expressed in *Anabaena* was evaluated by immunolocalization of BG11-0 grown liquid cultures and compared to *Anabaena* wt cells using mouse anti-His primary antibody (1:500 diluted; Thermo Fischer Scientific).

6.4.4.2 Immunofluorescence of *Synechococcus*

In a similar approach, the FtsZ localization in *Synechococcus* gene deletion strains was evaluated by immunofluorescence using a modified protocol from Heinz *et al.* (2016). First, *Synechococcus* wt and mutant strains grown on growth plates were resuspended in 1 ml BG11 and then fixed in 3.7% formaldehyde (final concentration) for 20 min at RT. Cells were washed 2x by centrifugation (5000 x *g*, RT, 8 min) with 1 ml PBS. Afterwards, the cells were permeabilized in PBST for 20 min at RT, centrifuged and incubated in 50 mM Tris-HCl pH 7.4, 10 mM EDTA and 0.2 mg ml⁻¹ Lysozyme for 30 min at 37 °C. After two washing steps with 1 ml PBS (5000 x *g*, RT, 8 min) the cells were blocked in blocking buffer for 30 min at RT and then incubated for 1.5 h at 30 °C with rabbit anti-FtsZ (Agisera; 1:250 diluted) primary antibody in blocking buffer. The cells were washed two times by centrifugation (5000 x *g*, RT, 8 min) with 1 ml blocking buffer and incubated for 1 h at 30 °C with 7.5 µg ml⁻¹ Alexa Fluor 488-conjugated goat anti-rabbit IgG (H+L) secondary antibody (Thermo Fischer Scientific) in blocking buffer. Unbound secondary antibody was removed by two washing steps with 1 ml PBS (5000 x *g*, RT, 8 min) and cells were resuspended in PBS containing 10 µg ml⁻¹ DAPI (final concentration) and fluorescence signals were analyzed by epifluorescence microscopy of cells immobilized on an agarose pad.

7 Chapter I: Identification and characterization of coiled-coil rich cytoskeletal proteins from cyanobacteria

7.1 Abstract

Prokaryotes, like eukaryotes possess a distinct cytoskeleton comprised of actin, tubulin and intermediate filament(IF)-like proteins. Additionally, prokaryotes have also evolved their own specific subset of cytoskeletal proteins with no eukaryotic homologs. The IF-like and coiled-coil rich proteins (CCRPs) CreS from *C. crescentus* and FilP from *S. coelicolor* determine the cell shape and provide resistance to mechanical deformations. Prediction of coiled-coil rich proteins using the COILS algorithm led to the identification of further cytoskeletal CCRPs from diverse species, suggesting a predictive property of the number of coiled-coil domains for IF-like functions. Unlike other bacteria, the Cyanobacteria phylum is characterized by an immense morphological diversity. However, little is known about the cell shape-determining factors in cyanobacteria as there have only been limited functional studies on FtsZ and MreB that constitute the bacterial tubulin and actin homologs. Here we show that CCRPs perform IF-like functions in cyanobacteria and that these proteins form diverse polymeric structures *in vitro* and *in vivo*. We identified CCRPs in each of the 141 investigated cyanobacterial genomes using the COILS algorithm and characterized five novel cytoskeletal CCRPs from 21 investigated candidates with varying levels of conservation. The IF-like protein Fm7001 polymerizes into two-dimensional structures and is involved in the phenotypic plasticity in *Fischerella*. Similarly, Slr7083 assembled into filamentous sheaths and gene deletions affected the motile *Synechocystis* substrain but were neutral in the non-motile strain, revealing a contribution to cell motility. Synpcc7942_2039 formed small and unclear polymers *in vitro* but showed clear filamentous networks *in vivo* in several bacterial species. Deletion mutants showed impaired DNA placement within the cell. Likewise, Alr3364 formed unclear polymers *in vitro* but localized as mid cell rings *in vivo*. We hypothesize that Alr3364 is associated with the septosomes and the Z-ring in *Anabaena*. Our results demonstrate that cyanobacteria of different morphotypes developed specialized CCRP-based cytoskeletal elements adapted to their respective requirements, providing further insights into the underlying principles of cyanobacterial morphological diversity. Our results hence constitute a significant starting point for further elucidation of the function and evolution of the cyanobacterial cytoskeleton.

7.2 Introduction

Eukaryotic cells are characterized by an enormous phenotypic diversity, a property that they owe to the functions of a multitude of cytoskeletal proteins that orchestrate basically every cellular behavior, including cellular motility, multicellularity, chromosome segregation and endocytosis (Alberts *et al.*, 2014). Similar, albeit neglected for a long time, cytoskeletal proteins

also exist in the less-complex bacterial and archaeal domains, with comparable, if not even greater degree of diversity (Löwe and Amos, 2017). Additionally, prokaryotes evolved their own specific cytoskeletal systems, such as Walker A Cytoskeletal ATPases (e.g. ParA, MinD), bactofilins (e.g. BacA, BacB), or pole-organizing scaffolding proteins (PopZ), which are not present in eukaryotes (reviewed by Wagstaff and Löwe, 2018). It is assumed that the high degree of variation of prokaryotic cytoskeletal elements is at least partially due to HGT and a more pronounced pressure on their genome sizes (Wickstead and Gull, 2011; Löwe and Amos, 2017). While actin (MreB) and tubulin (FtsZ) homologs rely on ATP and GTP for polymerization, IF proteins exhibit an intrinsic nucleotide-independent polymerization capability *in vivo* as well as *in vitro* (Löwe and Amos, 2009; Wagstaff and Löwe, 2018). Eukaryotic IF proteins are generally characterized by a conserved domain buildup consisting of discontinuous coiled-coil segments interspaced by so-called linker sequences which together form the central rod domain (Lin and Thanbichler, 2013). This rod domain is N- and C-terminally flanked by globular head and tail domains of different length (Köster *et al.*, 2015). CreS, a bacterial IF-like protein from *C. crescentus*, exhibits a striking domain similarity to eukaryotic IF proteins and performs cell shape-determining functions, possibly by locally exerting a constriction force which coordinates the peptidoglycan (PG) synthesis machinery (Ausmees, Kuhn and Jacobs-Wagner, 2003; Cabeen *et al.*, 2009; Charbon, Cabeen and Jacobs-Wagner, 2009). So far, no CreS homologs have been found in any other species, indicating that other non-spherical or rod-shaped prokaryotic morphologies are putatively controlled by other cytoskeletal proteins of assumed IF-like origin. Apart from CreS, many other CCRPs have been identified to polymerize into filamentous structures and/or to perform cytoskeletal roles, however, none of them resembled the eukaryotic IF domain architectures (Lin and Thanbichler, 2013). Among those proteins, two proteins from *S. coelicolor* have been subjected to a more detailed functional evaluation, namely FilP and Scy, which both exhibit an atypical IF-like coiled-coil domain architecture (Wagstaff and Löwe, 2018). In the growing hyphae, FilP filaments localize mainly to the tip in a gradient-like pattern and contribute to the general cellular stiffness. In contrast, Scy forms patchy clusters at the sites of tip-formation and recruits the scaffolding CCRP DivIVA, with which it orchestrates polar hyphal growth (Lin and Thanbichler, 2013). Like Scy, FilP also interacts with DivIVA, thereby forming an interconnected cytoskeletal network, the so-called polarisome that guides hyphal tip growth in cooperation with a cellulose-synthase (Holmes *et al.*, 2013; Lin and Thanbichler, 2013). Unlike other prokaryotic families, the Cyanobacteria phylum is characterized by an enormous morphological complexity, which ranges from unicellular cyanobacteria of subsection I to multicellular, cell-differentiating and branching cyanobacteria of subsection V (Rippka *et al.*, 1979). Even cells within one single trichome (chain of cells) of a multicellular cyanobacterium can differ in size, form or even cell wall composition (Rippka *et al.*, 1979). The molecular basis

of cyanobacterial morphogenesis is so far unknown and besides MreB and FtsZ little is known about cytoskeletal proteins in these bacteria. FtsZ, like in most other prokaryotes, is essential in the multicellular and nitrogen-fixing cyanobacterium *Anabaena*. In this cyanobacterium, FtsZ regulation is controlled at the posttranslational level by a so far unknown protease and was shown to mediate cell differentiation into heterocysts (specialized cells for nitrogen fixation) (Zhang *et al.*, 1995; Sakr, Jeanjean, *et al.*, 2006; Lopes Pinto *et al.*, 2011). Cells in an *Anabaena* trichome are linked by a common peptidoglycan sheath and outer membrane. Within this trichomes, those cells perform intercellular cell-cell communication using septosomal complexes comprised of, among others, SepJ, FraC and FraD (reviewed by Herrero, Stavans and Flores, 2016). The septosomes are functional analogs to eukaryotic gap-junctions and permit the transport of small fluorescent tracers like calcein or sugar analogs from one cell to another (Nürnberg *et al.*, 2015). Notably, the FtsZ-driven divisome influences cellular localization of SepJ, suggesting an involvement of the cytoskeleton in cell-cell communication, a phenomenon well described for adherence junctions in eukaryotic cells (Alberts *et al.*, 2014; Ramos-León *et al.*, 2015). MreB was shown to be dispensable for the growth of *Anabaena*, albeit its involvement in cell shape determination (Hu *et al.*, 2007). In contrast, MreB is essential in the rod-shaped unicellular cyanobacterium *Synechococcus* and partially segregated mutants display a coccoid morphology, resembling *E. coli mreB* deletion strains (Kruse, Bork-Jensen and Gerdes, 2005; Jain, Vijayan and O'Shea, 2012). Curiously for such complex organisms, no cell shape stabilizing elements of IF-like origin have been described so far. Strain-specific CCRPs with limited distribution determine numerous prokaryotic morphologies and considering the relatively high levels of HGT in cyanobacteria (Dagan *et al.*, 2013), it is conceivable that the extremely diverse Cyanobacteria phylum has also evolved species or phylum-specific IF-like CCRPs. Thus, we here predict and functionally characterize putative IF-like cytoskeletal CCRPs from a diverse set of cyanobacterial species and evaluate their impact on cellular morphology.

7.3 Results

Prediction of intermediate filament-like proteins

We employed the COILS algorithm from Lupas *et al.* (1991) on 141 cyanobacterial genomes to predict coiled-coil rich and putative IF-like cyanobacterial proteins. Coiled coils were selected using a window of 21 with a cut-off of at least 80 amino acids in coiled-coil conformation as described by Bagchi *et al.* (2008). The algorithm yielded a list of 15885 proteins with high coiled-coil content. CCRPs were predicted in every cyanobacterial species, indicating that they are widespread in cyanobacteria (Supplementary File 1). On average ~63 CCRPs were predicted in the unicellular subsection I cyanobacteria while ~160 CCRPs were predicted for the more complex subsections (II-V). This suggests that coiled-coil rich proteins

are involved in the manifestation of the more complex cell-division pattern and morphotype of higher order cyanobacteria (Rippka *et al.*, 1979). The obtained list of proteins was narrowed down to protein candidates from model organisms available in our laboratory namely *Thermosynechococcus elongatus* BP-1 (*BP-1*), *Synechocystis*, *Synechococcus*, *Anabaena* and *Fischerella*. Using publicly available online bioinformatic tools (NCBI Blast, NCBI CD search, PSORTb, TMHMM, InterPro, PSIPRED and I-TASSER), proteins with an assigned function or predicted to be involved in other cellular processes were excluded. CreS, FilP and other eukaryotic IF proteins (Vimentin, Desmin, Lamin) were chosen as reference points for these predictions, and proteins displaying similar results were selected. Based on this evaluation, we ended up with a list of 20 hypothetical proteins (Fig. 9 and Table 7). In addition, we included Fm7001, a protein from *Fischerella*, as it was previously identified as a putative filament forming protein in a comparative genome analysis in our group. We identified CCRPs of various sizes, ranging from only a little more than 200 amino acids (Alr0347) to more than 1000 amino acids (Alr3988). Only a few proteins exhibited a somewhat characteristic domain architecture reminiscent of eukaryotic IF proteins (Slr7083 and Alr4505), whereas the coiled-coil domain distribution in the other candidates had major differences in coiled-coil domain count and length. None of the predicted IF-like protein candidates exhibited a stutter-like structure in the last coiled-coil segment. Besides coiled-coil domains, the COILS algorithm also predicted tetratricopeptide repeats (TRPs) as coiled-coils, thus we also included All4981 into our analysis, even though conserved domain searches reliably predicted these domains as TRPs and not coiled-coils. Many predicted proteins contained conserved domains from eukaryotic IF proteins or domains found in CreS and FilP. The presence of these domains can be regarded as support for our classification. The structural maintenance of chromosomes (SMC) domains were predicted in almost all cyanobacterial IF-like protein candidates (Table 7), all eukaryotic IF proteins as well as in CreS and FilP. The MscS_TM domains from desmin were found in Slr70831 and Tlr0420. Alr0931 contains Neuromodulin_N as well as a CCDC158 domains, both present in FilP or CreS, respectively. Furthermore, Alr0347 was assigned as a member of the Filament superfamily to which all tested eukaryotic cytoskeletal proteins belong to. Additionally, structural similarities were identified by the I-TASSER tool which assigned Alr0931, Alr4505, Alr4393, All2460, All4935, Slr6096, Slr1301 and Synpcc7942_1139 with structural similarities to the bacterial cell division protein EzrA, a feature also predicted for CreS. Fm7001, unlike the other predicted CCRPs, reveals domain similarities to a metabolic enzyme (acetyl-CoA carboxylase). Many CCRP candidates were found to be highly conserved among all cyanobacterial subsections (e.g. Alr0931, Alr4504, Alr4505 and All2460) while others were restricted to only a few or even just one subsection in the case of Slr7083, Synpcc7942_2039, All4935, Alr2043 and Fm6009 (Table 7). Alr3364 and its respective homologs (sequence similarity of 46%), on the other hand, are absent from unicellular

cyanobacteria of subsection I. A conservation across all cyanobacterial morphotypes hints for a universal protein function while restrictions to certain subsections and morphotypes hints for a functional diversification to the specific needs their respective cyanobacteria of origin. Like *parM* and *tubZ* (Wagstaff and Löwe, 2018), *slr7083* is encoded on a plasmid, the large pSYSA toxin-antitoxin plasmid from *Synechocystis*.

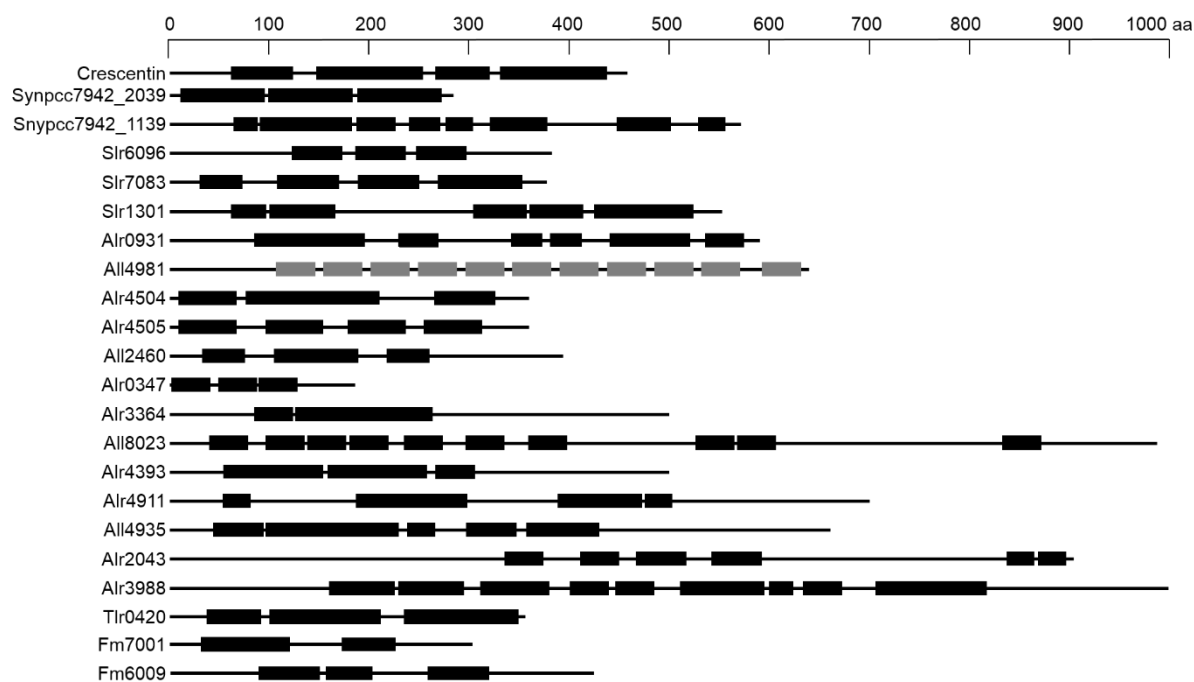


Fig. 9: Domain architecture of IF-like protein candidates

Depiction of coiled-coil domains of protein candidates and Crescentin from *C. crescentus* based on the COILS algorithm with a window with of 21. The scale on top is given in amino acid residues and amino acid sequences in coiled-coil conformation are depicted by black bars, while non-coiled-coil sequences are represented by black lines. Tetratricopeptide repeats (TRP) are shown as grey bars. Proteins are given as cyanobase locus tags. Fm7001 and Fm6009 correspond to NCBI accession numbers WP_016868005.1 and WP_020476706, respectively.

Analysis of the genomic surroundings of IF-like gene candidates revealed putative regulatory mechanisms. Subsection IV and V-specific and plus strand-located *fm7001* exhibits a 3' end 9 bp overlap to the 3' end of the minus strand-located *fm7000* (Fig. S1). While *fm7001* is constantly highly expressed, *fm7000* was upregulated under conditions that induced a change in morphology (Koch *et al.*, 2017), suggesting a putative RNAi property of *fm7000*. *fm7000* is not present in all cyanobacteria that exhibit *fm7001* homologs, and with the exception of the subsection V cyanobacterium *Mastigocladus laminosus* UU774, *fm7000* is absent from subsection IV cyanobacteria (Fig. S2). Additionally, Fm7001 and Fm7000 both display the same comparably high levels of sequence conservation (64%) among homologous proteins, strengthening the idea of a fine-tuned interplay of both proteins. Of further interest seems *fm7002*, predicted to be a protease, which is also upregulated in the treatment sample from Koch *et al.* (2017), and thus could act proteolytically to regulate Fm7001. However, Fm7002 homologs were also identified in cyanobacterial species lacking Fm7001 homologs.

A similar schematic can be identified for All4981, which is restricted to multicellular cyanobacteria of subsection III-V and which has a sequence identity to its homologs of around 46%. The 5' end of *all4981* overlaps with 4 bp with the 3' end of *all4982*. The same holds true for the overlap of *all4982* with its upstream gene *all4983* (Fig. S3). Interestingly, All4982 is predicted to belong to the large family of P-loop NTPases that also comprises the bacterial-specific cytoskeletal class of Walker A Cytoskeletal ATPases (WACAs).

Locus tag	Genus	Subsection	Homologs distribution	I-TASSER	Conserved domains	Others
<i>synpcc7942_2039</i>	<i>Synechococcus</i>	I	I	Tropomyosin in the spermine-induced crystal form	SMC_N, MukB, CALCOCO1	N-terminal TMH; present only in <i>Synechococcus sp.</i>
<i>synpcc7942_1139</i>	<i>Synechococcus</i>	I	I, II, III, IV, V	Cytoplasmic domain of bacterial cell division protein EzrA	SMC_N, MukB, Spc7	
<i>slr6096</i>	<i>Synechocystis</i>	I	I, III, IV	Cytoplasmic domain of bacterial cell division protein EzrA	SMC_N	
<i>slr7083</i>	<i>Synechocystis</i>	I	I	Structure of the spectrin repeats 7, 8, and 9 of the plakin domain of plectin	SMC_N, MscS_TM	Encoded on pSYSA plasmid
<i>slr1301</i>	<i>Synechocystis</i>	I	I, II, III, IV, V	Cytoplasmic domain of bacterial cell division protein EzrA	SMC_N, SbcC, APG6, DUF3552	
<i>alr0931</i>	<i>Anabaena</i>	IV	I, II, III, IV, V	Cytoplasmic domain of bacterial cell division protein EzrA	SMC_N, CCDC158, DUF3084, Neuromodulin_N	
<i>all4981</i>	<i>Anabaena</i>	IV	III, IV, V	Moderate: Structure of the TTC7B/Hyccin Complex or Clathrin coat	TPR	4 bp overlap to <i>all4982</i>
<i>alr4504</i>	<i>Anabaena</i>	IV	I, II, III, IV, V	Moderate: Structure of the spectrin repeats 7, 8, and 9 of the plakin domain of plectin	SMC_N	<i>alr4505</i> is localized immediately downstream of <i>alr4504</i>
<i>alr4505</i>	<i>Anabaena</i>	IV	I, II, III, IV, V	Cytoplasmic domain of bacterial cell division protein EzrA	SMC_N, DUF3552	
<i>all2460</i>	<i>Anabaena</i>	IV	I, II, III, IV, V	Cytoplasmic domain of bacterial cell division protein EzrA	SMC_N, TerB_C, CALCOCO1, Spc7	Two N-terminal TMHs

Locus tag	Genus	Subsection	Homologs distribution	I-TASSER	Conserved domains	Others
<i>alr0347</i>	<i>Anabaena</i>	IV	I, II, III, IV, V	<i>Bacillus subtilis</i> Smc coiled-coil middle fragment	Filament superfamily	
<i>alr3364</i>	<i>Anabaena</i>	IV	II, III, IV, V		SMC_N, FtsK, DUF4696	
<i>all8023</i>	<i>Anabaena</i>	IV	IV	Human ATR-ATRIP complex (replication stress response)	SMC_N, Pentapeptide, Yjbl	
<i>alr4393</i>	<i>Anabaena</i>	IV	I, II, III, IV, V	Cytoplasmic domain of bacterial cell division protein EzrA	SMC_N, DUF3084	
<i>alr4911</i>	<i>Anabaena</i>	IV	I, II, III, IV, V	Structure of the Smc head domain with a coiled coil and joint derived from <i>Pyrococcus yayanosii</i>	SMC_N, P-loop_NTPase DNA_S_dndD, Spc7, SbcC	
<i>all4935</i>	<i>Anabaena</i>	IV	IV	Cytoplasmic domain of bacterial cell division protein EzrA	DUF4114, DUF3084	
<i>alr2043</i>	<i>Anabaena</i>	IV	IV, V	human ATR-ATRIP complex (replication stress response)	SMC_N, Tubulin_2	
<i>alr3988</i>	<i>Anabaena</i>	IV	I, II, III, IV, V		SMC_N, SbcC	
<i>tlr0420</i>	<i>BP-1</i>	I	I, III	Moderate: Structure of the spectrin repeats 7, 8, and 9 of the plakin domain of plectin	SMC_N, MscS_TM	
<i>fm7001</i>	<i>Fischerella</i>	V	IV, V	Structure of α -catenin or vinculin; similar EC to acyl-CoA dehydrogenase	Acetyl-CoA carboxylase carboxyl transferase (PLN0322)	Highly expressed; 3' end 9 bp overlap to <i>fm7000</i>
<i>fm6009</i>	<i>Fischerella</i>	V	V	Structure of β -catenin and HTCF-4	COG0610	

Table 7: Characteristics of protein candidates

The first column indicates the respective locus tags of protein candidates. The second and third column indicate the respective subsection of the corresponding genus. Column four lists the subsections that contain homologous proteins to the respective candidate. Column five contains proteins predicted to be structurally close to the candidate in the PDB (Protein Data Bank) based on I-TASSER. The sixth column indicates predicted sub-domains of protein candidates identified by BLAST CDS. Column seven states other features of interest. Abbreviations: (TMH) Transmembrane helix; (EC) Enzyme Commission; (DUF) Domain of unknown function; (CCDC158) Coiled-coil domain-containing protein 158; (SMC) Structural maintenance of chromosomes; (MukB) The hinge domain of chromosome partition protein MukB; (APG6) Autophagy protein Apg6, (SbcC) DNA repair exonuclease SbcCD ATPase; (CALCOCO1) Calcium binding and coiled-coil domain; (TRP): Tetratricopeptide repeat; (Spc7) Spc7 kinetochore protein; (TerB_C) TerB-C occurs C-terminal of TerB in TerB-N containing proteins, putative metal chelating; (Filament superfamily) Intermediate filament protein; (FtsK) DNA segregation ATPase FtsK; (Pentapeptide) Pentapeptide repeats often found in many cyanobacterial proteins with unknown function (predicted to be a β -helix); (Yjbl) Uncharacterized protein containing pentapeptide repeats; (DNA_S_dndD) DNA sulfur modification protein DndD; (Tubulin_2 superfamily) Tubulin like; Many of the residues conserved in Tubulin (pfam00091) are also conserved in this family; (P-loop_NTPase) P-loop containing Nucleoside Triphosphate Hydrolases superfamily; (PLN0322) Acetyl-CoA carboxylase carboxyl transferase; (COG0610) Type I site-specific restriction-modification system.

Putative cytoskeletal proteins form diverse structures *in vitro*

One of the major characteristics of cytoskeletal proteins is their ability to self-polymerize intra and extra-cellularly (Köster *et al.*, 2015). Unlike microtubules and microfilaments, intermediate filaments are able to form filamentous structures *in vitro* in a nucleotide-independent manner and without additional co-factors upon renaturation from a denaturing buffer environment (Herrmann and Aebi, 2000; Köster *et al.*, 2015). For this reason, we investigated all 21 proteins shown in Fig. 1 for their *in vitro* polymerization capacity. Proteins equipped with a C-terminal His₆-tag were purified under denaturing conditions using a Ni-NTA matrix and subsequently renatured by dialysis. If applicable, purified proteins were labeled with an excess of NHS-Fluorescein and *in vitro* filamentation was assessed by epifluorescence or bright field microscopy. The intermediate filament-like protein CreS from *C. crescentus* (Ausmees, Kuhn and Jacobs-Wagner, 2003) was included as a positive control. Slr6096, Alr0347, All8023, Alr4393, All4911, All4935, Alr2043, Alr3988, Tlr0420 and Fm6009 failed to be expressed in *E. coli* or to form filaments *in vitro* under all tested buffer conditions and were thus not further investigated. Three proteins, namely Alr0931, Slr1301 and Synpcc7942_1139 will be discussed in Chapter 2 and another three proteins, namely Alr4504, Alr4505 and All2460, will be explored in Chapter 3. Therefore, in the following paragraphs we will be limiting our findings to a subset of five predicted IF-like CCRPs (Fm7001, Slr7083, All4981, Synpcc7942_2039 and Alr3364).

In vitro polymerization assays revealed that putative IF-like CCRPs assembled into highly diverse structures (Fig. 10), ranging from huge two-dimensional sheath-like filaments of Fm7001 (Fig. 10A inlay) to low abundant small filaments of Alr3364 (Fig. 10D). Protein polymerization required different buffer compositions, which were adjusted individually for the needs of each protein, but the majority of proteins formed filaments in Hepes or Pipes polymerization buffers (HLB or PLB). Direct dialysis of Fm7001 from a high urea-containing buffer to a physiological buffer led to protein precipitation. However, upon slow step-wise urea removal, Fm7001 polymerized into a flat two-dimensional object floating on top of the dialysate in a 4,5 M urea containing buffer (Fig. S4A). The NHS-Fluorescein dye binds primary amines and is thus incompatible with urea, which is why Fm7001 filaments were only investigated by bright field microscopy. Fm7001 mainly produced extensive two-dimensional filamentous sheaths (Fig. 10A inlay) but also single filamentous fibers aligned laterally were detected (Fig. 10A). We also addressed the eventuality that these structures could be the product of crystallized urea, but control experiments did not form filaments (data not shown). Cell-free lysates of *E. coli* overexpressing Fm7001-GFP, lysed under denaturing conditions and subjected to the same step-wise renaturation produced comparable two-dimensional filaments (Fig. S4B). When fused to the solubilizing N-terminal MBP-tag (maltose binding protein),

Fm7001 formed an interconnected filamentous meshwork (Fig. S4C). A similar two-dimensional filamentation pattern was also detected for Slr7083, which formed single, long and straight filaments, interconnected by two-dimensional sheaths, thereby producing a honeycomb-like structure (Fig. 10B). A filamentous network was observed for purified All4981 with thin single filaments (Fig. 10C). Even though filaments were present in Alr3364 (Fig. 10D), most of the protein precipitated, suggesting that optimal buffer conditions are not yet met or that other proteins are required for proper polymerization. This observation also holds true for Synpcc7942_2039, which formed shell-like polymers with the shape of rod-shaped bacteria, however, also only to a minor extent (Fig. 10E). We also found evidence that CreS filamentation, in contrast to previous results (Ausmees, Kuhn and Jacobs-Wagner, 2003), is strongly dependent on the presence of monovalent ions (NaCl) in the polymerization buffer. CreS dialyzed into a salt-free buffer formed filamentous aggregates (Fig. S5B) whereas filigree and smooth filaments were formed in a saline buffer (Fig. 10F). Thus, these data further highlight the importance of proper buffer conditions for polymerization of IF-like proteins (Herrmann, Kreplak and Aebi, 2004). Considering that these proteins belong to entirely different cyanobacterial species, the diverse architectures formed *in vitro* could indicate a structural and functional adaptation of the proteins adjusted to the needs of their cyanobacteria of origin. Nevertheless, a two-dimensional polymerization pattern appears to be a new and unique pattern for cyanobacterial IF-like proteins.

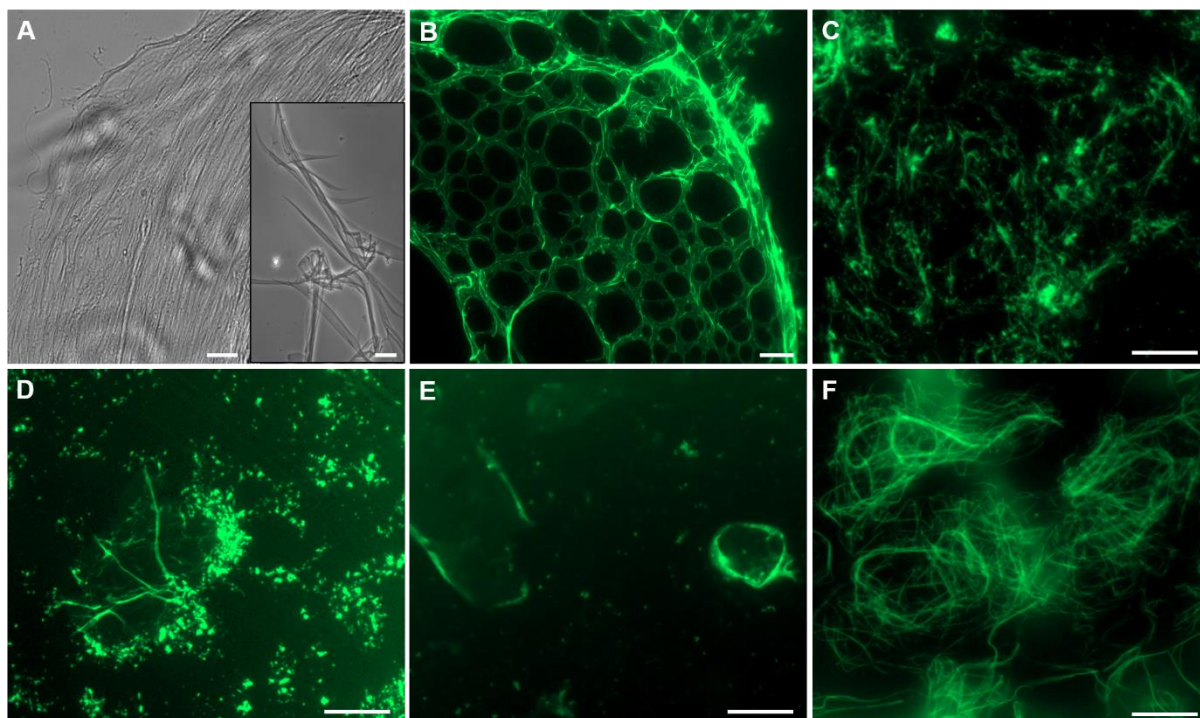


Fig. 10: *In vitro* polymerization of protein candidates into diverse filamentous structures

(A) Bright field and (C-F) epifluorescence micrographs of filamentous structures formed by purified and renatured (A) Fm7001 (0.7 mg ml^{-1}), (B) Slr7083 (1 mg ml^{-1}), (C) AlI4981 (0.5 mg ml^{-1}), (D) Alr3364 (0.5 mg ml^{-1}), (E) Synpcc7942_2039 (0.3 mg ml^{-1}) or (F) CreS (0.7 mg ml^{-1}) in (A) 2 mM Tris-HCl, 4.5 M urea pH 7.5, (B,D) HLB, (C,F) PLB or (E) BG11. Proteins were either analyzed by (A) bright field microscopy or (B-F) stained with an excess of NHS-Fluorescein and analyzed by epifluorescence microscopy. (A) Fm7001 was gradually dialyzed in a step-wise urea-decreasing manner, reducing 0.5 M urea every two hours. Scale bars: (A,C,D,E,F) 10 μm or (A inset,B) 20 μm .

Self-assembly of IF-like proteins in a bacterial two-hybrid assay

For further verification of cyanobacterial IF-like protein self-assembly, we employed the bacterial adenylate cyclase two-hybrid assay (BACTH). To quantify the interaction strength, beta-galactosidase activity in Miller units of protein candidates N- and C-terminally fused to the T25 and T18 subunit of the *Bordetella pertussis* adenylate cyclase was measured essentially as described by Karimova, Davi and Ladant (2012) of all possible pair-wise combinations. In further support for the *in vitro* polymerization results, strong self-binding properties were detected for the majority of investigated proteins (Fig. 11A-D), thereby proving one of the major hallmark of cytoskeletal proteins: to be able to self-interact. However, Alr3364 failed to self-interact, indicating a non-IF-like function (Fig. 11E).

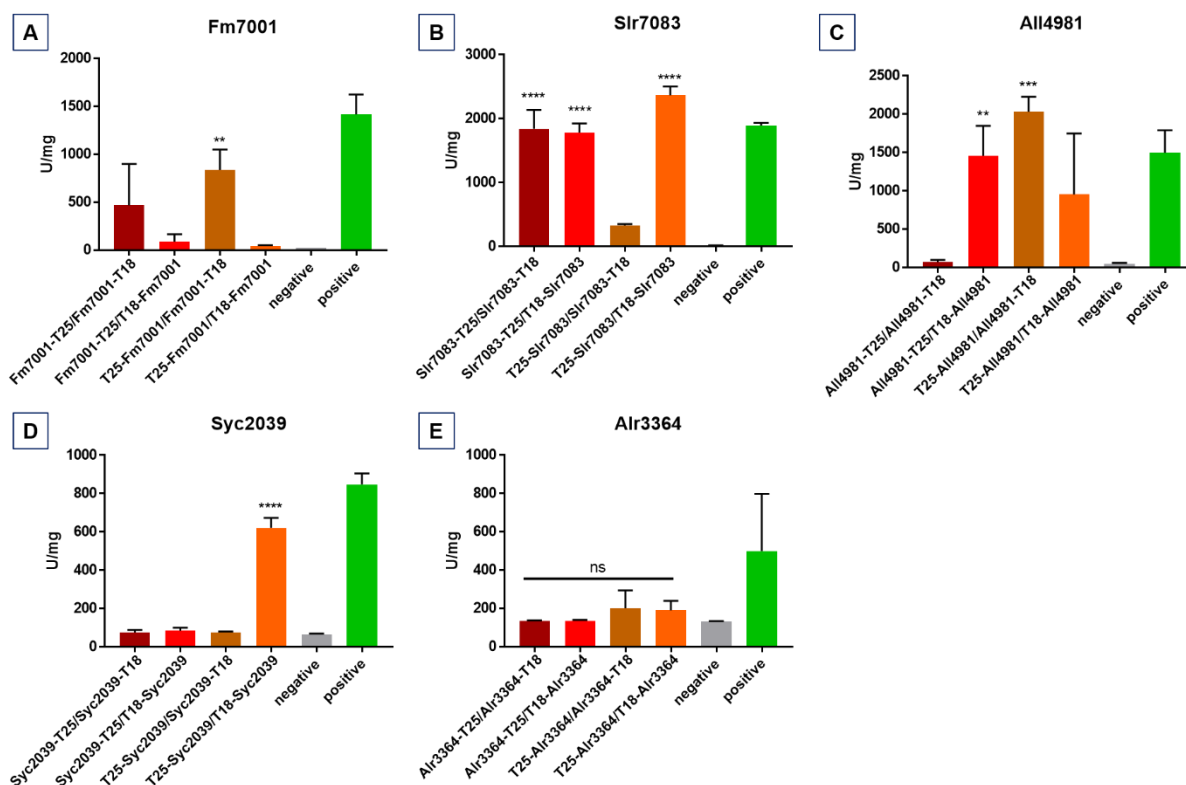


Fig. 11: Interaction of IF-like proteins in a beta-galactosidase assay

Beta-galactosidase assays of *E. coli* cells co-expressing indicated translational fusion constructs of all possible pairwise combinations of (A) Fm7001, (B) Sir7083, (C) All4981, (D) Synpcc7942_2039 and (E) Alr3364. Cells were grown for 1 day at 30 °C or 2 days at 20 °C. Quantity values are given in Miller Units per milligram LacZ of the mean results from three independent colonies. Error bars indicate standard deviations. Synpcc7942_2039 is abbreviated Syc2039. Neg: pKNT25 plasmid carrying the respective gene insert co-transformed with empty pUT18C. Pos: Zip/Zip control. *: $P < 0.05$, **: $P < 0.01$, ***: $P < 0.001$, ****: $P < 0.0001$ (Dunnett's multiple comparison test and one-way ANOVA).

IF-like proteins alter cell shape in *E. coli*

The interactions identified in the BACTH system only prove dimerization of investigated proteins and not the ability to self-polymerize. Therefore, to further explore the putative intrinsic self-assembly capability of IF-like proteins in the absence of other cyanobacterial proteins, we next studied the behavior of these proteins in a heterologous *E. coli* system. For this, gene candidates fused to a C-terminal *gfp*-tag were cloned into pET21a(+) and *in vivo* protein filamentation was assessed by epifluorescence microscopy.

Heterologous expression of Fm7001-GFP induced a swollen and elongated phenotype where GFP fluorescence localized partially to the cell envelope and in a meshwork-like pattern throughout the cells (Fig. 12B). A similar impact on the morphotype of *E. coli* cells was also detected upon heterologous expression of MBP-Fm7001. Cells expressing this construct were filamentous and partially curved (Fig. S6B) compared to control cells (Fig. S6A). It is noteworthy that DAPI staining indicated a limitation of cellular DNA to certain parts of the cells,

specifically excluding it from the tip of the cells (Fig. S6B). Slr7083-GFP predominantly localized to the cell poles with, in some cases, a U-shaped pattern (white arrows in Fig. 12C). These distinct accumulations could indicate a scaffolding function analogous to bactofilins or PopZ (Ebersbach *et al.*, 2008; Kühn *et al.*, 2010). All4981-GFP expression did not have any effect on cellular morphology as cells displayed wt phenotype. The GFP localization pattern suggested accumulation of All4981-GFP in inclusion bodies (Fig. 12C). Expression of GFP-tagged Synpcc7942_2039 (Fig. 12E) and Alr3364 (Fig. 12F) occasionally induced a filamentous cell phenotype as observed in *E. coli* cells overexpressing the ClpXP protease (Camberg, Hoskins and Wickner, 2009), which could indicate its involvement with the divisome. Indeed, cellular DNA was restricted from parts of the cell where Alr3364-GFP accumulated (translucent triangles). No such observations were made for Synpcc7942_2039-GFP. Synpcc7942_2039-GFP appears to attach to the bacterial cell envelope resembling MreB-GFP localization (Swulius and Jensen, 2012). Protein filaments traversing the cells in a helical pattern (white triangles) were identified although also GFP-signals localized opposite to one another were observed, indicating a banded localization pattern (white stars). These data suggest that IF-like protein candidates are either able to directly influence cellular morphology and/or form filamentous structures within a surrogate species, demonstrating their species-independent cytoskeletal properties.

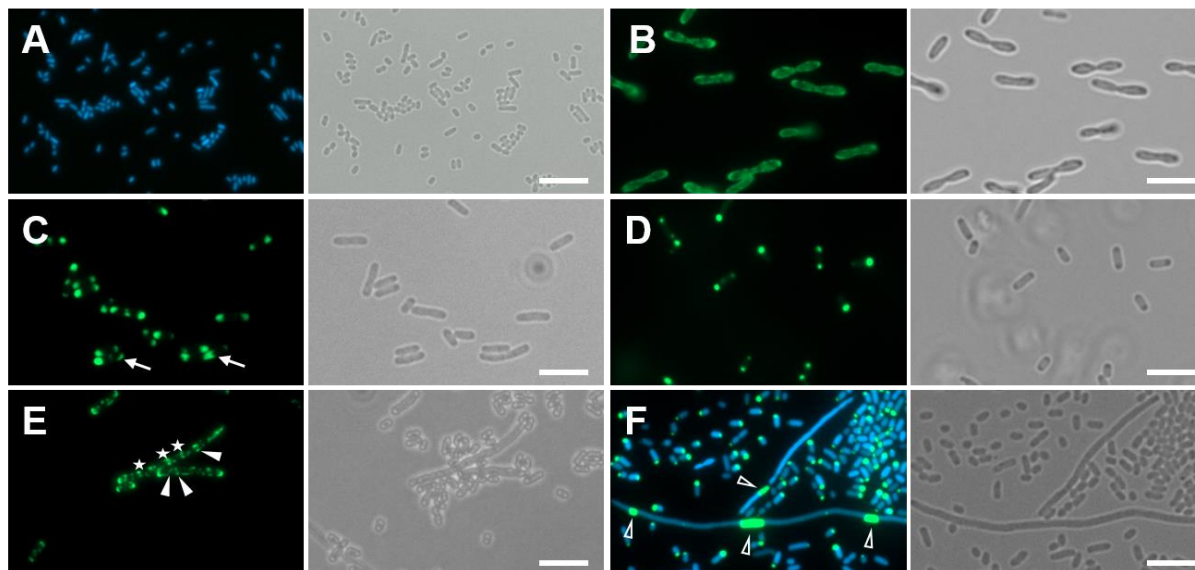


Fig. 12: *In vivo* localization of protein candidates heterologously expressed in *E. coli*

(A,F) overlay of GFP and DAPI fluorescence and bright field micrographs or (B-E) GFP fluorescence and bright field micrographs of (A) *E. coli* wt cells or *E. coli* cells expressing (B) Fm7001-GFP, (C) Slr7083-GFP, (D) All4981-GFP, (E) Synpcc7942_2039-GFP or (F) Alr3364-GFP. (E) Maximum intensity projection of a Z-stack. Protein expression of cells grown at (B) 16 °C or (A,C-E) at 20 °C was induced with 0.05 mM IPTG and, if applicable, cells were stained with 10 $\mu\text{g ml}^{-1}$ DAPI and immobilized on an agarose pad. White arrows show curved GFP-signals. White stars mark banded GFP localizations. Translucent triangles highlight areas of denied DNA distribution. White triangles indicate helix-like filaments. Scale bars: 5 μm .

IF-like protein candidates form filaments in cyanobacteria

In order to investigate whether the genetic background influences filamentation properties, we expressed *gfp* or *yfp* translational fusion constructs of IF-like protein candidates in their cyanobacterium of origin and in cyanobacteria with different morphologies. Gene expression was driven by inducible or constitutive promoters commonly used cyanobacteria. These included *Pcpc560* (*Synechocystis*), *Ptrc* (*Synechococcus*) or *PpetE* (*Anabaena*, *Fischerella*). Fluorescence pattern was analyzed by fluorescence microscopy. As a positive control, we also investigated the protein filamentation of CreS-GFP in a multicellular cyanobacterium.

Fm7001 forms species-independent filaments *in vivo*

C. crescentus CreS protein has a strong self-affinity and forms polymers under a wide range of polymerization buffers. Thus, we expected that its ability to form polymers would remain upon expression in distantly related organisms, as cyanobacteria. As such, CreS-GFP formed round (white stars in Fig. 13A) and helical filaments that can even traverse through cell-cell connections of neighboring cells in *Anabaena* (white triangles in Fig. 13A). This finding simultaneously provided the first evidence for the ability of septosomal junctions, made of SepJ among others (Nürnberg *et al.*, 2015), to allow proteins and even large filamentous structures pass through cell-cell connections. Fm7001 localization was inevitably linked to the orientation of the attached fluorescence tag. While C-terminally GFP-tagged Fm7001 induced a swollen morphotype in a subpopulation of *Synechocystis* cells (Fig. 13B), the protein localization appeared to be patchy throughout the cells with certain accumulation of fluorescence signals at the cell envelope. No filamentous structures of Fm7001-GFP were observed in any analyzed cells and the morphological impact of Fm7001-GFP was only present in the unicellular cyanobacterium *Synechocystis* (Fig. 13B,D,F). *Fischerella* cells expressing Fm7001-GFP (Fig. 13F) only exhibited fluorescence signals in a minority of cells, which was rapidly lost upon growth in liquid culture. However, localization of the N-terminal YFP-tagged Fm7001 showed an entirely different pattern (Fig. 13C,E,G). Expression in *Synechocystis* revealed cell-traversing, straight and curved filaments (white triangles in Fig. 13C). Similar, albeit to a larger extent, YFP-Fm7001 expressed in *Anabaena* formed abundant short filamentous strings often accumulating at the cell poles, which then extended into the interior of the cells (white triangles in Fig. 13E). Filaments localized to the cell center with no apparent septal origin were also present in various cells, indicating that Fm7001 not necessarily arises from the cell poles. As observed in *Anabaena*, heterologous YFP-tagged expression of Fm7001 in its cyanobacterium of origin - *Fischerella* – led to the formation of small filaments three-dimensionally traversing the cells (Fig. 13G inlay). The occurrence of those filaments was, however, relatively low compared to the observations from *Anabaena* and the majority of proteins localized in a patchy pattern throughout the cells or accumulated at the septa (Fig. 13G,G inlay). And yet this

construct was able to alter the morphotype of *Fischerella*. Trichomes became swollen and often divided in more than one plane, inducing a multiseriate phenotype (Fig. 13G) resembling the morphology of *Chlorogloeopsis fritschii* PCC 6912. Transfer of *Fischerella* cells expressing YFP-Fm7001 from growth plate into liquid BG11 medium resulted in cell death. Standard BG11 by default contains copper, which induces the expression of *petE*-regulated genes. YFP-Fm7001 expressing cells had to be grown in a non-inducing environment and protein expression could only be induced in a pre-developed culture. Apart from its species-independent filamentation capability and morphogenic properties, this indicates an involvement of this protein in early culture developmental stages.

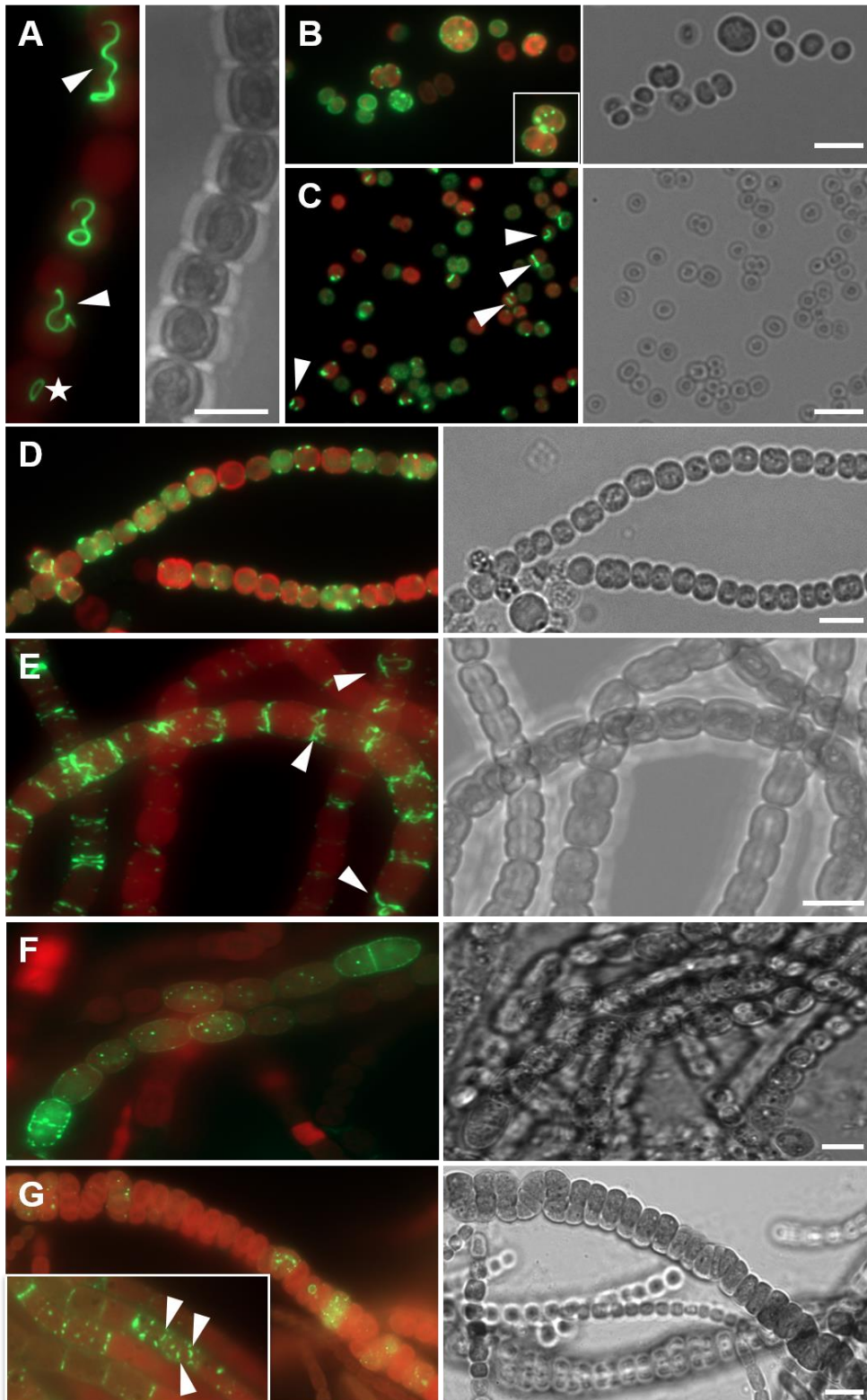


Fig. 13: Fm7001 and CreS form filaments in cyanobacteria

Merged GFP fluorescence and chlorophyll auto-fluorescence and bright field micrographs of (A,D,E) *Anabaena*, (B,C) *Synechocystis* or (F,G) *Fischerella* cells expressing (A) CreS-GFP, (B,D,F) Fm7001-GFP or (C,E,G) YFP-Fm7001. Cells were either grown in (A,B,C) liquid BG11, (D) liquid BG11-0 supplemented with 0.2 μM CuSO_4 or liquid BG11 supplemented with (E) 5 μM or (F,G) 0.5 μM CuSO_4 . White triangles point to selected filamentous strings (A) traversing through neighboring cells or (C,E,G) within the cells. (A,E): maximum intensity projection of a Z-stack. Scale bars: (A-F) 5 μm or (G) 10 μm .

Fm7001 interacts with proteins involved in the phenotypic plasticity in *Fischerella*

Attempts to generate a $\Delta fm7001$ strain remained unsuccessful, presumably due to a lacking functional gene knockout system in *Fischerella* and not as a result of an essential function of Fm7001 for *Fischerella* viability. Although, we cannot rule out that Fm7001 is in fact essential for cell growth as we observed *fm7001* expression already in young *Fischerella* cultures, independent of the availability of fixed nitrogen sources in the growth medium (Fig. S7). Additionally, Koch *et al.* (2017) showed that *fm7001* is constantly highly expressed. Thus, in order to further characterize Fm7001's cellular function, we performed co-IPs of *Fischerella* wt and *Fischerella* expressing YFP-Fm7001 grown in full growth medium (BG11) and nitrogen-deprived growth medium (BG11-0) using anti-GFP μ Beads (Fig. 14) with a subsequent analysis of co-precipitated proteins by mass spectrometry.

YFP-Fm7001 specifically interacted with various hypothetical or so far uncharacterized proteins involved in phenotypic plasticity (Koch *et al.*, 2017 and unpublished results by Robin Koch). However, only interactions with WP_016868221.1, a hypothetical protein conserved in cyanobacteria from the BG11 sample and FtsH (WP_016858941.1) from the BG11-0 sample were identified as significant hits. Nevertheless, we also found several non-significant hits of unknown and hypothetical proteins, which co-precipitated in both growth conditions. Some of the corresponding genes were significantly upregulated or downregulated (among the 5% highest fold change) in the conditions leading to morphology changes (Koch *et al.*, 2017), indicating a role of those proteins in cellular morphology. Taking into account that purification of overexpressed Fm7001-His in *E. coli* was also possible with the addition of detergents (1% Triton X-100) in the lysis buffer – however to a lesser extent than with urea - we found an interesting interaction of Fm7001 with Fm5958 (WP_016869785.1). Fm5958 is a predicted membrane protein, which was co-precipitated in both growth conditions. Additionally, it is significantly upregulated in the morphology changing conditions from Koch *et al.* (2017). This protein could function as a linker of Fm7001 to the cell envelope. Due to Fm7001's morphogenetic properties, we also addressed the possibility of a direct interaction with FtsZ and MreB in a bacterial two hybrid system as these proteins are known to be essential for cell morphology (Wagstaff and Löwe, 2018). However, no such interactions were identified, demonstrating that Fm7001-driven morphogenesis relies on other pathways. Taken together, these data further highlight the contribution of Fm7001 to *Fischerella* morphogenesis as it interacts with proteins involved in phenotypic plasticity such as Fm5958 or Fm3835 (WP_016860646.1).

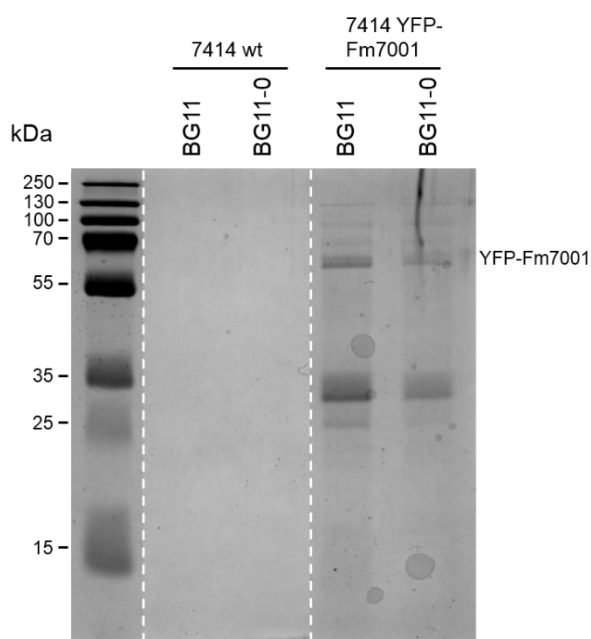


Fig. 14: Identification of proteins interacting with YFP-Fm7001

Cell-free lysates of *Fischerella* wt and *Fischerella* expressing YFP-Fm7001 cells grown in BG11 or BG11-0 were subjected to co-immunoprecipitation using anti-GFP magnetic beads. YFP-Fm7001 cells were initially grown under non-inducing copper-depleted growth conditions, transferred to BG11 or BG11-0 medium and then supplemented for 1 day with 0.5 μM CuSO_4 before co-IP. 25 μl of the precipitate were resolved in a 10% SDS-polyacrylamide gel and detected by Quick Coomassie stain (Serva).

Plasmid-encoded Slr7083 forms sheath-like filaments *in vivo*

slr7083 expression is restricted to later culture growth stages (OD_{750} 1.2) while no *slr7083* transcripts were detected in exponentially growing cultures (OD_{750} 0.7) or in later stationary phase cultures (OD_{750} 1.5) (Fig. S8). Expression of Slr7083-GFP in its cyanobacterium of origin *Synechocystis* usually localized to the cell envelope (Fig. 15A) but in some occasions also S-shaped filamentous sheaths were observed (Fig. 15A inlay). This further supported the observed two-dimensional *in vitro* structures (Fig. 10C). A similar membrane-associated localization pattern was identified in *Anabaena* expressing Slr7083-GFP (Fig. 15B). In addition, a minority of cells also displayed filamentous structures traversing through the cells (white arrow in Fig. 15B). On the contrary, N-terminally YFP-tagged Slr7083 was only associated to the membrane. The orientation of the tag influenced *Anabaena* morphology; YFP-Slr7083 expressing cells became spherical and slightly enlarged compared to *Anabaena* expressing Slr7083-GFP or *Anabaena* wt cells. Further indications for a tag-orientation-dependent localization were given by the lack of Slr7083-GFP expression in heterocysts, since YFP-Slr7083 expressing cells illustrated a pronounced accumulation of fluorescence signal in these cell types (white arrows in Fig. S 9A,B). Besides cell rounding, other morphogenetic properties were also shown to be specific to *Anabaena* expressing YFP-Slr7083. Upon extended cultivation for 2 days in liquid BG11 medium, cells started to lose their elliptical shape and

formed a rather compressed cell phenotype (Fig. S9C). This phenomenon was more pronounced upon prolonged growth where cells tended to form multiseriate trichomes with growth in more than just one plane (white triangles Fig. S9D). Comparable observations were made in cells equilibrated in non-inducing growth media with subsequent induction of protein expression (Fig. S9E,F), promoting the idea that Slr7083 possesses intrinsic and culture age-independent morphogenic properties. Even though overexpression of Slr7083-GFP did not lead to multiplanar cell division in *Anabaena*, extended cultivation sporadically resulted in cell lysis upon which Slr7083-GFP formed extracellular filaments in the growth medium (Fig. 15D). Taken together, Slr7083 holds *in vivo* polymerization and morphogenic properties, which were shown to be tag-orientation-dependent but not species-specific.

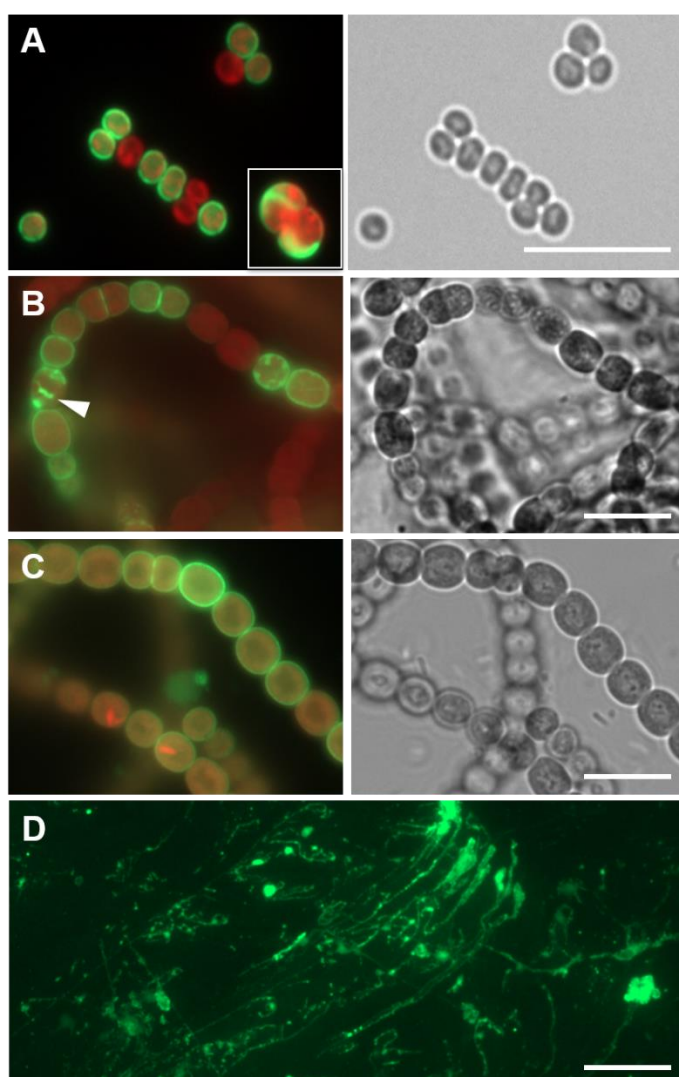


Fig. 15: *In vivo* localization of Slr7083

Merged GFP fluorescence and chlorophyll auto-fluorescence and bright field micrographs of (A) *Synechocystis* and (B,C,D) *Anabaena* cells expressing (A,B,D) Slr7083-GFP or (C) YFP-Slr7083. Cells were either grown in (A) BG11 or (B,C) taken from mating filters. (D) Extracellular filaments formed upon cell lysis of *Anabaena* cells expressing Slr7083-GFP grown in BG11-0 and induced with 0.5 μM CuSO_4 for 28 hours. Trichome-like growth of (A) *Synechocystis* expressing Slr7083-GFP is an artifact of the cell immobilization on an agarose pad. White triangles indicate filamentous *in vivo* structure. Scale bars: 10 μm .

Slr7083 is involved in cell motility in the *Synechocystis* PCC-M substrain

In contrast to *Fischerella*, a functional gene knockout system is available for *Synechocystis* (Grigorieva and Shestakov, 1982). Thus, *slr7083* gene deletion strains of the non-motile *Synechocystis* GT-Kazusa (hereafter GT-Kazusa) as well as the motile *Synechocystis* PCC-M (hereafter PCC-M) substrain were generated by gene replacement with an antibiotic resistance cassette (Fig. S10).

Gene deletion of *slr7083* in the GT-Kazusa substrain showed no apparent phenotype compared to wt cells (Fig. 16A,B) and cell growth was not impaired confirming unaltered viability (data not shown). Similar results were obtained for spot assay-based viability tests of $\Delta slr7083$ GT-Kazusa, however, a slightly elevated sensitivity to Proteinase K was detected (Fig. S11F). Interestingly, *slr7083* gene deletion in the PCC-M substrain was not silent. Cell size and shape appeared to be unaltered, however, a substantial proportion of $\Delta slr7083$ PCC-M cells entirely lacked the chlorophyll auto-fluorescence signal (white triangles in Fig. 16D). Dividing cells displayed chlorophyll auto-fluorescence in just one of the daughter cells, indicating that equal distribution of chlorophyll content in dividing daughter cells is impaired (white stars in Fig. 16D). Furthermore, we investigated the impact on twitching motility in $\Delta slr7083$ PCC-M in a motility test and found that, even though cell motility is not entirely abrogated, $\Delta slr7083$ PCC-M showed a decreased motility compared to PCC-M wt cells (Fig. 16G,H). In order to assess the viability of $\Delta slr7083$ PCC-M we also performed spot assays on growth plates with different supplements and observed a decrease fitness of $\Delta slr7083$ PCC-M (Fig. S11A). The mutant had also an elevated sensitivity to Lysozyme compared to PCC-M wt indicating a defect of the cell wall (Fig. S11B). Consistent with this observation, non-motile *Synechocystis* expressing Slr7083-GFP showed decreased colony size and an impaired colony morphology, suggesting an influence of Slr7083 on cellular integrity or colony maintenance (Fig. S11G,H). Apart from this, we generally observed that 30 $\mu\text{g ml}^{-1}$ Proteinase K entirely inhibited cell growth of the PCC-M substrain (wt and mutants) while the non-motile GT-Kazusa substrain (wt and mutants) showed a less detrimental impact of Proteinase K (Fig. S11C,F). Additionally, Lysozyme was found to abrogate motility in PCC-M strains (Fig. S11B and Chapter 2 Fig. S30B). These findings suggest that structures that enable twitching motility simultaneously increase the sensitivity of cells to extracellular proteases and muramidases, and that proper activity of pili structures relies on an intact cell wall. The clear difference between $\Delta slr7083$ PCC-M and $\Delta slr7083$ GT-Kazusa is apparent and indicative for an involvement in cellular motility. Colony viability data suggest an influence in cell and culture stability or integrity. However, whether this effect is direct or indirect remains to be elucidated.

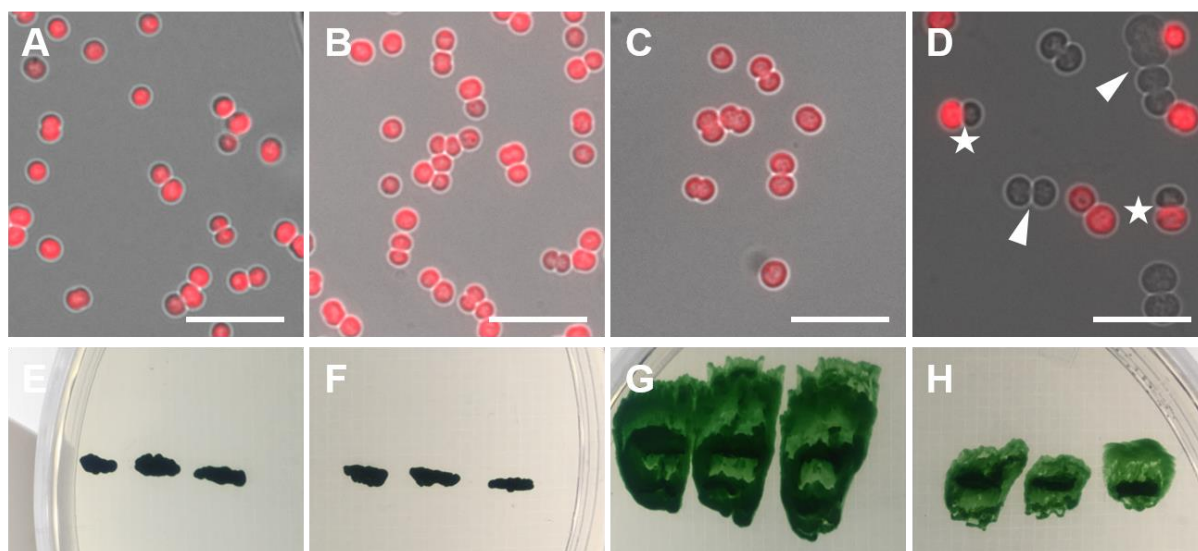


Fig. 16: Impact of $\Delta slr7083$ on motile and non-motile *Synechocystis* substrains

(A,B,C,D) Merged bright field and chlorophyll auto-fluorescence micrographs of (A) the non-motile GT-Kazusa substrain wt, (B) $\Delta slr7083$ GT-Kazusa, (C) the motile PCC-M substrain wt and (D) $\Delta slr7083$ PCC-M. (E,F,G,H) motility test of (E) GT-Kazusa wt, (F) $\Delta slr7083$ GT-Kazusa, (G) PCC-M wt or (H) $\Delta slr7083$ PCC-M of three single colonies each, streaked on a BG11 growth plate and illuminated from one direction adapted from Schuergers *et al.* (2015). White triangles indicate chlorophyll-lacking cells. White stars mark dividing cells with chlorophyll restricted to one daughter cell. Scale 5 μ m.

All4981 – an essential protein specific to multicellular and cell-differentiating cyanobacteria

Unlike Fm7001 and Slr7083, All4981 polymerization and localization showed only a minor tag-orientation dependency. Tag orientation-dependency was mainly seen in *Synechocystis*, where protein filaments formed only in cells carrying C-terminally GFP-tagged All4981 (white triangles in Fig. 17A) whereas YFP-All4981 showed a patchy localization. Tag-orientation slightly affected All4981 polymers and intracellular localization within its cyanobacterium of origin, *Anabaena*. Both, All4981-GFP and YFP-All4981 expressing strains exhibited numerous cell-traversing and septal-arising filaments (white triangles in Fig. 17C-E), which sometimes spread in a star-like pattern into the cytosol (right white triangles in Fig. 17C and upper and lower triangle in Fig. 17D). The only observable tag-dependent difference was the large filamentous network formed by YFP-All4981 in a cell subpopulation (middle white triangle in Fig. 17D). Notably, All4981 also formed bridge-like formations (white stars in Fig 17C,D) between neighboring cells suggesting its involvement in cell-cell communication or stabilization of cell-cell connections. We addressed this option by a bacterial two hybrid system and found weak, albeit significant physical interactions with SepJ, the septosomal protein from *Anabaena* (Fig. S12B). In agreement with the filamentous network seen in Fig. 8D, we also identified strong interactions of All4981 with MreB (Fig. S12A), which was previously shown to form similar structures in *Anabaena* (Hu *et al.*, 2007). Unlike MreBCD overexpression-induced cell abominations (Hu *et al.*, 2007), no direct morphogenic influence was detected for All4981,

although extended protein expression in liquid cultures caused cell lysis of a subpopulation of cells, thereby releasing their intracellular components into the growth medium. In fact, filamentous structures were seen in freshly lysed All4981-GFP expressing cells (Fig. S13A). The released filaments further assembled in the medium into higher order and strongly interconnected cytoskeletal networks resembling the *in vitro* polymerization pattern of All4981 (Fig. S13B). Extracellular filaments were also identified in growth medium from *Anabaena* cells expressing YFP-All4981, however, to a less well-defined extent. These results show that All4981 filamentation is mostly tag-independent, non-morphogenic and, like Slr7083, extracellular filaments from lysed cells can assemble in the growth medium.

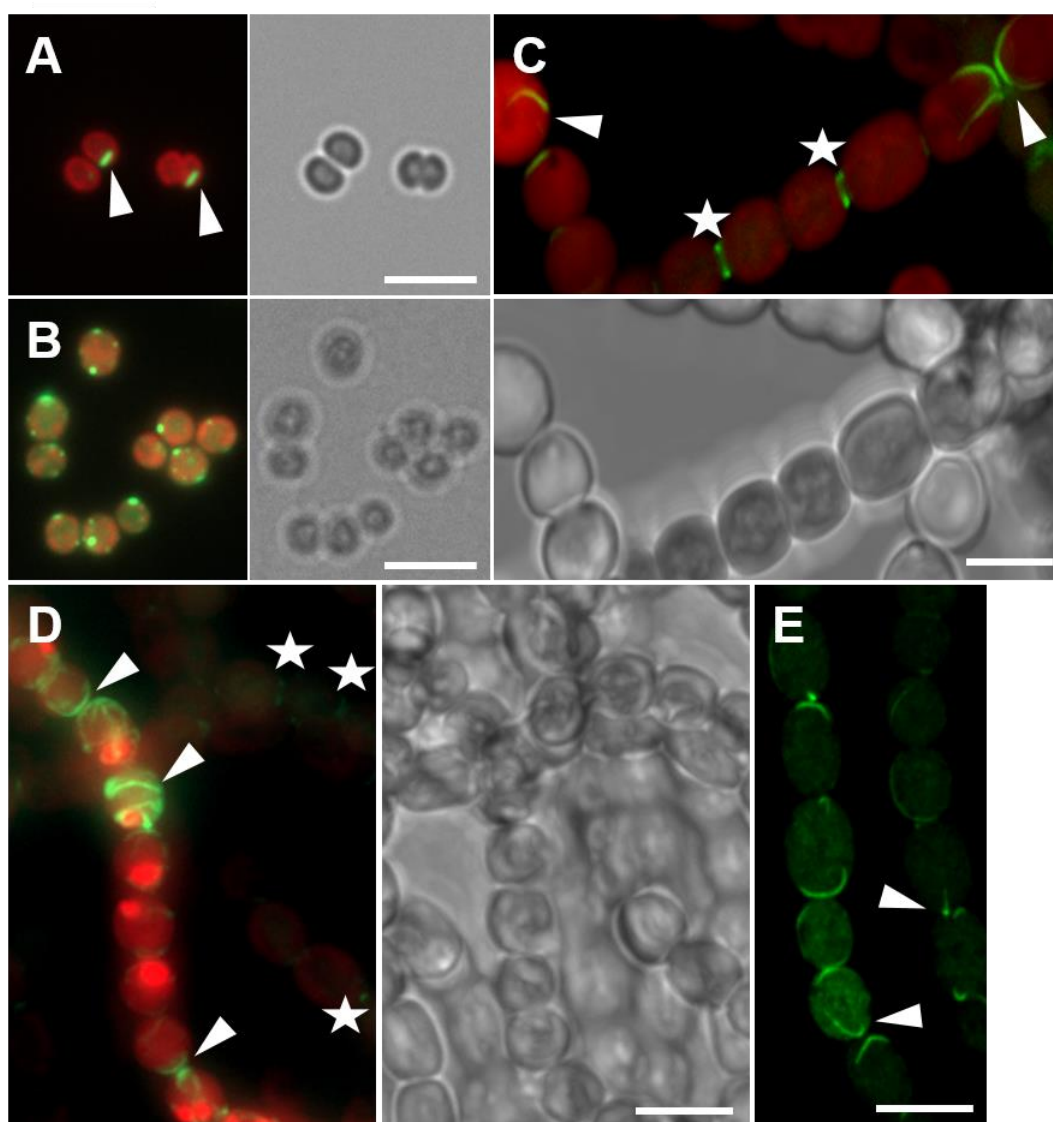


Fig. 17: All4981 forms species-independent cell-traversing filaments in cyanobacteria

GFP fluorescence and merged GFP fluorescence and chlorophyll auto-fluorescence and bright field micrographs of (A,B) *Synechocystis* and (C,D,E) *Anabaena* cells expressing (A,C) All4981-GFP or (B,D,E) YFP-All4981. Strains were grown in (A,B) BG11 or BG11-0 supplemented with (C) 0.25 μM CuSO_4 for 8 days, (D) for 1 day with 2 μM CuSO_4 or (E) without further induction. (C-E): Maximum intensity projections of a Z-stack. White triangles indicate selected filaments traversing through the cells. White stars mark bridge-like formations between two neighboring cells. Scale bars: 5 μm .

All4981 interacts with known cytoskeletal proteins and predicted S-layer proteins

Gene deletions by double homologous recombination in *Anabaena* was previously shown to be functional and reliable in several cases (Cai and Wolk, 1990; Hu *et al.*, 2007; Ramos-León *et al.*, 2015). In fact, using a pRL278-based system, we were able to delete several *Anabaena* genes (Chapters 2 and 3). However, neither employing a double homologous replacement with an antibiotic resistance cassette nor gene disruption by single homologous insertion yielded any segregated $\Delta allr4981$ strain. Colony PCRs of antibiotic resistant exconjugants using flanking gene primers consistently resulted in only one PCR product corresponding to the wt allele. Additionally, we also employed the CRISPR-Cpf1-based system developed by Ungerer and Pakrasi (2016), which also failed to produce gene deletion strains. We even transferred the functional CRISPR-Cpf1 cassette from pSL2680 into pRL25C, a plasmid known to be reliably replicated in *Anabaena* (Wolk *et al.*, 1988; Wang and Xu, 2005; Sakr, Thyssen, *et al.*, 2006) but also this approach failed to generate a gene deletion strain. As none of our approaches resulted in a segregated or even partially segregated mutant, we assume that *all4981* is essential and that even minor reductions in protein levels are lethal for *Anabaena*. Since we were unable to deduce the cellular function of All4981 by its absence, we wanted to pinpoint its putative cellular implications through the identification of interaction partners. Therefore, we performed co-IPs of *Anabaena* wt and *Anabaena* expressing YFP-All4981 grown in BG11 and BG11-0 using anti-GFP μ Beads (Fig. 18) and subsequently analyzed the co-precipitated proteins by mass spectrometry

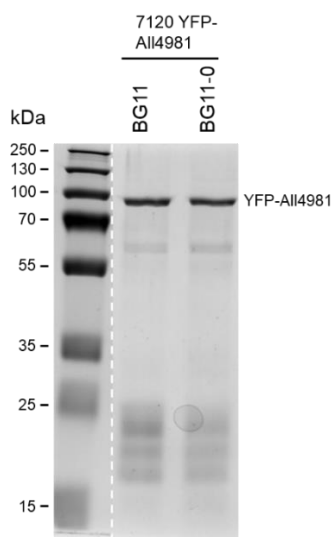


Fig. 18: Identification of proteins interacting with YFP-All4981

Cell-free lysates of *Anabaena* strain expressing YFP-All4981 grown in BG11 or BG11-0, both supplemented with 5 μ M CuSO_4 for two days, were subjected to co-immunoprecipitation using anti-GFP magnetic beads. Pooled duplicates of precipitated proteins of two independent experiments were analyzed by mass spectrometry and 25 μ l of the precipitate were resolved in a 10% SDS-polyacrylamide gel and detected by Quick Coomassie stain (Serva). Wt control samples grown in BG11 and BG11-0 were directly provided to the mass spectrometry facility and not resolved on an SDS-polyacrylamide gel.

All4981 was found to associate with a wide range of cytoskeletal proteins, such as ParB (Alr7083) specifically found in BG11 growth conditions. Further interactions with FtsH (Alr1261) were established in BG11 and BG11-0 samples and MinD (Alr3456) was found to interact with All4981 under nitrogen-deprived growth conditions. In agreement with the bacterial two-hybrid assays and the *in vivo* localization of YFP-All4981 in *Anabaena*, we identified MreB (All0087) as an interactor in the BG11-0 sample. Under both growth conditions, we further identified physical contact with the endopeptidase ClpB (Alr2999), which could function as a proteolytic regulatory protein of All4981. Further significant interactions in both samples were found with a variety of putative S-layer proteins, including Alr4550, All4499, Alr0834. Samples from complete medium further revealed binding of All4981 with another S-layer or fascilin repeat protein (Alr1819) and a prohibitin-like protein (Alr1295). We also obtained evidence for the interaction with DevH (Alr3952), a protein essential for heterocyst glycolipid layer synthesis, further strengthening the putative involvement of All4981 in the buildup of a protective and cell-stabilizing cell envelope. Curiously, we were able to identify All4982 as an interactor of All4981 in both samples. No interaction was detected with All4983, however, direct association of All4981 with a protein in its direct genetic neighborhood suggests an involvement of those proteins in All4981 polymerization. Intrigued by this observation, we explored the possibility of a common transcripts of those genes but couldn't identify any (i.e. operon structure). The obtained results demonstrate that All4981 is strongly connected to the cytoskeletal network and the protective S-layer of *Anabaena* and might perform its function jointly with All4982.

Synechococcus*-specific protein Synpcc7942_2039 assembles into filaments *in vivo

Like *slr7083*, *synpcc7942_2039* is primarily expressed in stationary phase cultures and not in exponentially growing cells (Fig. S14). *In vivo* localization of Synpcc7942_2039-GFP contrasted the ambiguous *in vitro* polymerization pattern. Cell-traversing filamentous networks were clearly visible in *Synechocystis* and *Anabaena* expressing Synpcc7942_2039-GFP, indicating a strain-independent polymerization ability (Fig. 19A,B). These filaments were long, curved and intertwined (white triangles in Fig. 19A,B) and were identified throughout the whole cell. In addition, the polymerization pattern partially resembled the spindle apparatus from eukaryotes (Reece *et al.*, 2013; white stars in Fig. 19A). Such a filament network was not detectable in its cyanobacterium of origin, *Synechococcus*. Instead, Synpcc7942_2039-GFP formed long filaments that often aligned with or in close proximity to the cell membrane (white triangles in Fig. 19C,D). Furthermore, a partial banded filamentation pattern was also detected, reminiscent of Synpcc7942_2039-GFP localization upon heterologous expression in *E. coli* (white arrows in Fig. 19C,D). Besides a banded arrangement, Synpcc7942_2039-GFP formed helices resembling MreB filaments as seen for this protein in *E. coli* (Fig. 12E). Attempts to translationally fuse a YFP-tag to the N-terminus of Synpcc7942_2039 were unsuccessful and

were thus not pursued any further. Remarkably, overexpression of Synpcc7942_2039-GFP with medium to high induction levels (0.5 or 1 mM IPTG) led to growth arrest of *Synechococcus*, suggesting that Synpcc7942_2039 is involved in the cell cycle. Taken together, the species-independent and complex *in vivo* filamentation pattern of Synpcc7942_2039 indicates that optimal buffer conditions for *in vitro* filamentation are yet to be found or that conserved bacterial proteins collaborate with Synpcc7942_2039 to form polymers *in vivo*.

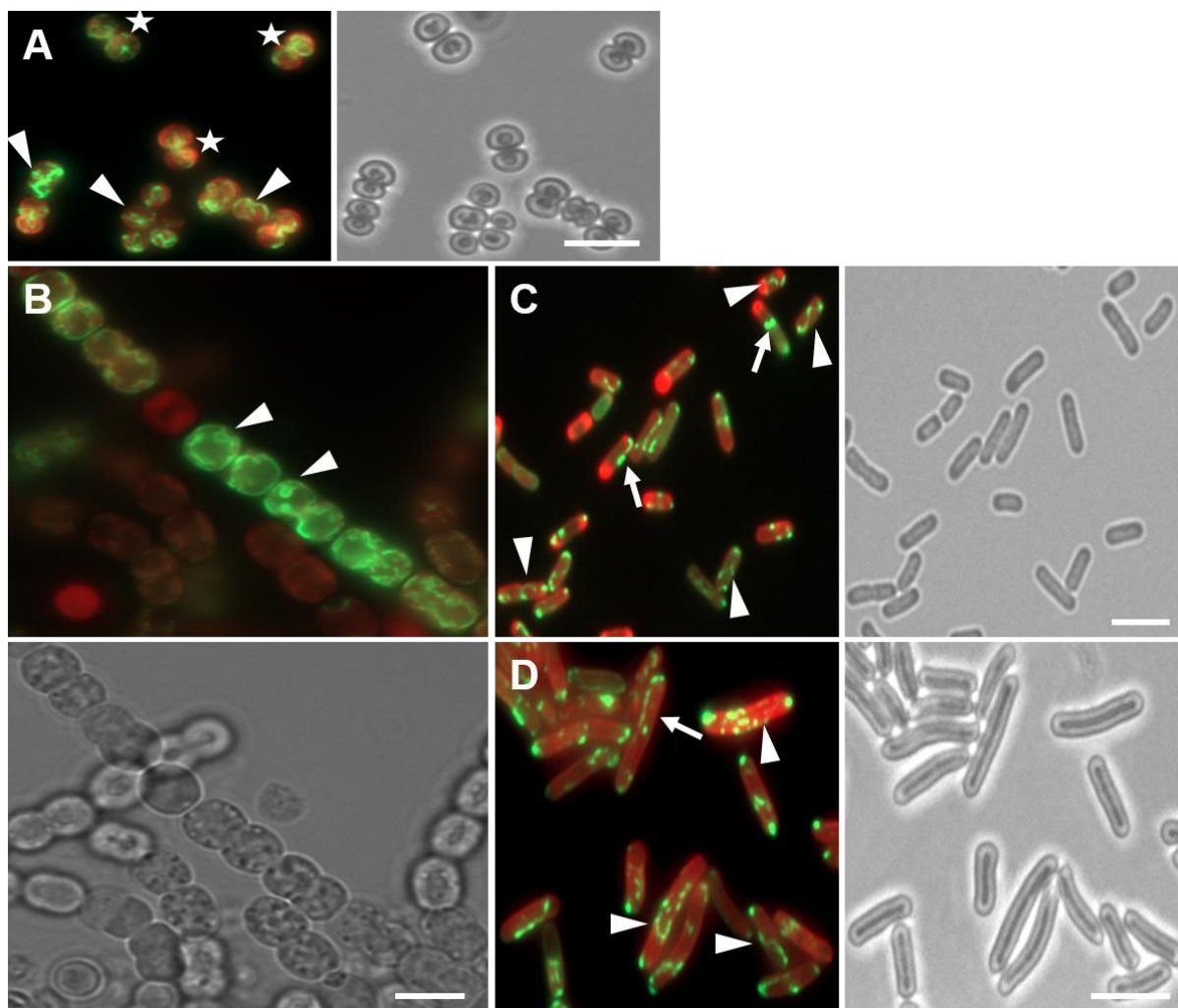


Fig. 19: Synpcc7942_2039 forms filamentous polymers *in vivo*

Merged GFP fluorescence and chlorophyll auto-fluorescence and bright field micrographs of (A) *Synechocystis*, (B) *Anabaena* and (C,D) *Synechococcus* cells expressing Synpcc7942_2039-GFP. Cells were either grown in (A) BG11 medium, (B) BG11-0 supplemented with 0.25 μM CuSO_4 for 1 day or on BG11 agar plates containing either (C) 0.05 mM or (D) 0.01 mM IPTG. (A,D): Maximum intensity projections of a Z-stack. White triangles indicate selected intracellular filaments. White stars show spindle-like localizations within cells and white arrows point to straight or banded filaments. Scale bars: 5 μm .

Synpcc7942_2039 is involved in cell division in *Synechococcus*

As *Synechocystis*, *Synechococcus* is genetically tractable and plasmids for gene deletions or gene expression can be transferred to *Synechococcus* by natural transformation or by conjugation from *E. coli* (Golden, Brusslan and Haselkorn, 1987; Ducat, Sachdeva and Silver, 2011). Using double homologous gene replacement, we generated $\Delta\text{synpcc7942_2039}$ (Fig. S15).

Colony formation on growth plates and cell size phenotype of $\Delta\text{synpcc7942_2039}$ was unaltered, however, epifluorescence microscopy of DAPI-stained cells revealed detrimental alterations in this gene deletion strain. A proportion of $\Delta\text{synpcc7942_2039}$ cells exhibited a segregated DNA distribution either to both cell poles or to just one pole (white triangles in Fig. 20B). Furthermore, we observed cells without any discernible intracellular DNA (white arrows in Fig. 20B) or perceptible chlorophyll (white stars in Fig. 20B). Upon transfer into liquid growth medium we consistently observed that $\Delta\text{synpcc7942_2039}$ possess a growth advantage over wt cells, which we confirmed by a comparative growth experiment of three different liquid cultures of *Synechococcus* wt and $\Delta\text{synpcc7942_2039}$. $\Delta\text{synpcc7942_2039}$ grown for 4 days at standard growth conditions already showed a clearly noticeable green color, while wt cultures required longer incubation times (Fig. 20C). This effect, albeit at a lesser extent, was confirmed with spot assays. Remarkably and in agreement with the growth experiment, $\Delta\text{synpcc7942_2039}$ cell density was higher than wt density up to a dilution of 10^{-3} , while at higher dilutions (dilution of 10^{-5}), wt cells displayed a higher cell density compared to $\Delta\text{synpcc7942_2039}$ (Fig. S16). In order to explore the altered DNA distribution, we also addressed the possibility of FtsZ mislocalization in $\Delta\text{synpcc7942_2039}$. However, immunolocalization of FtsZ with an anti-FtsZ antibody revealed an unaltered Z-ring placement compared to wt cells (Fig. S17). Taken together, our results suggest that $\Delta\text{synpcc7942_2039}$ cells increase their fitness at the expense of a disturbed cytokinesis or cell-division control system, putatively inducing cell division at an earlier time point than in wt cells.

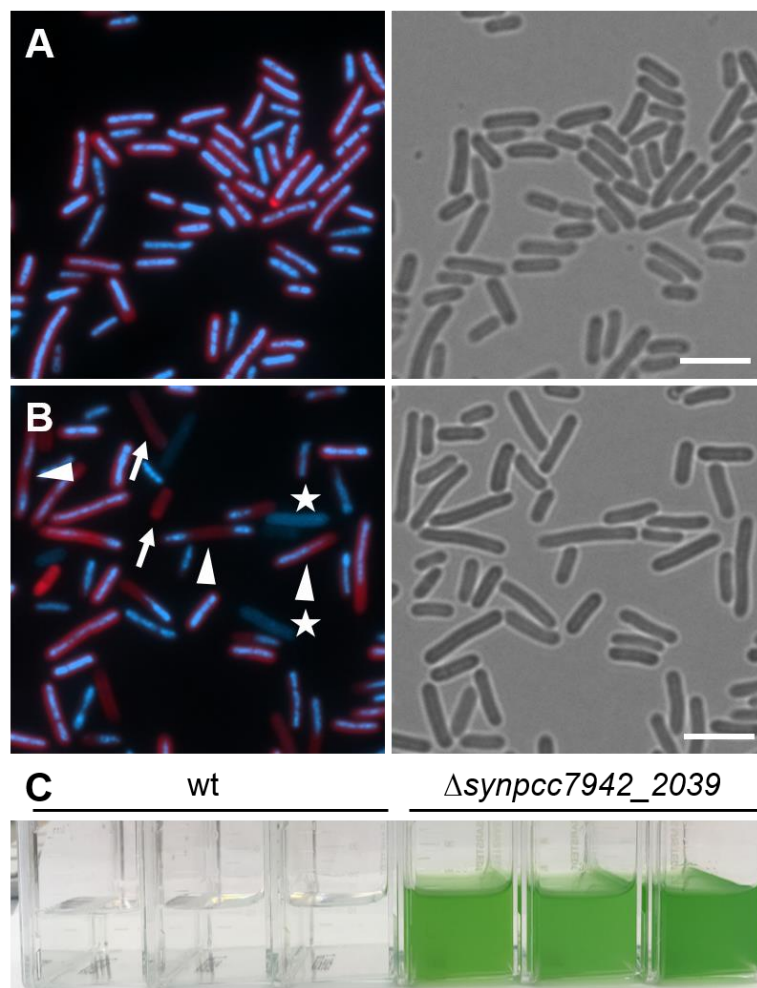


Fig. 20: Impact of $\Delta\text{synpcc7942_2039}$ on *Synechococcus* viability

(A,B) Merged DAPI fluorescence and chlorophyll auto-fluorescence and bright field micrographs of *Synechococcus* (A) wt or (B) $\Delta\text{synpcc7942_2039}$ grown on BG11 plates and stained with $10 \mu\text{g ml}^{-1}$ DAPI. White triangles indicate non-dividing cells with segregated DNA content. White stars mark cells without chlorophyll auto-fluorescence and white arrows point to cells lacking DNA. (C,D) Three independent *Synechococcus* wt or $\Delta\text{synpcc7942_2039}$ colonies were transferred to BG11 medium and grown for four days at standard growth conditions. Scale bars: 5 μm .

Alr3364 is a putative interactor of the *Anabaena* divisome

In contrast to the previous described proteins, Alr3364 specifically localizes to the Z-ring of *Anabaena* cells (white triangles in Fig. 21A,B) and also to the cell septa of two neighboring cells (white stars). In accordance with the missing self-binding ability, based on a bacterial two hybrid system, this suggests that Alr3364 is part of the divisome rather than a novel *Anabaena* IF-like cytoskeletal protein. In stationary cultures Alr3364-GFP localization shifted towards the cell septa (Fig. 21B), although Z-rings were still perceptible (white triangles Fig. 21B). Interaction of Alr3364 with FtsZ would explain why only a small proportion of purified Alr3364 formed filaments *in vitro*, as Alr3364 might require other binding partners like FtsZ for polymerization. To test this and a potential interaction with the septosome, we investigated the interaction of Alr3364 with FtsZ and SepJ in a bacterial two hybrid system. We identified

physical interactions of Alr3364 with SepJ but could not detect any direct interaction with FtsZ (Fig. S18A,B). Based on the septal localization of Alr3364, we also addressed a putative interaction with All4981 but found none (Fig. S18C). To further validate the bacterial two-hybrid assay results, we performed co-immunoprecipitations (Co-IPs) of formaldehyde fixed *Anabaena* cultures expressing Alr3364-GFP followed by western blot analysis using anti-FtsZ antibodies. In this experiment, input samples of wt and Alr3364-GFP expressing strain were only taken after the incubation with the anti-GFP μ Beads and not before addition of the beads. Strangely, FtsZ was still detectable in the wt input control samples (see Fig. S19) while no FtsZ was detected in any of the three Alr3364-GFP input control samples nor in any co-IP sample. These results raised the idea that Alr3364 could be a FtsZ-specific protease. However, FtsZ-His degradation assays showed no increased proteolytic activity in cell-free extracts of Alr3364-GFP expressing strains compared to wt (Fig.S20). We also attempted an indirect co-IP with immobilized Alr3364-His and cell-free extract of *Anabaena* wt. But again, no interaction with FtsZ was detected (Fig. S21). Remarkably, though, *E. coli* FtsZ co-precipitated with Alr3364-His when overexpressed in *E. coli* followed by native Ni-NTA purification, while no such interaction was detected under denaturing conditions (Fig. S21). Therefore, precise association modes of Alr3364 with the divisome are yet to be elucidated.

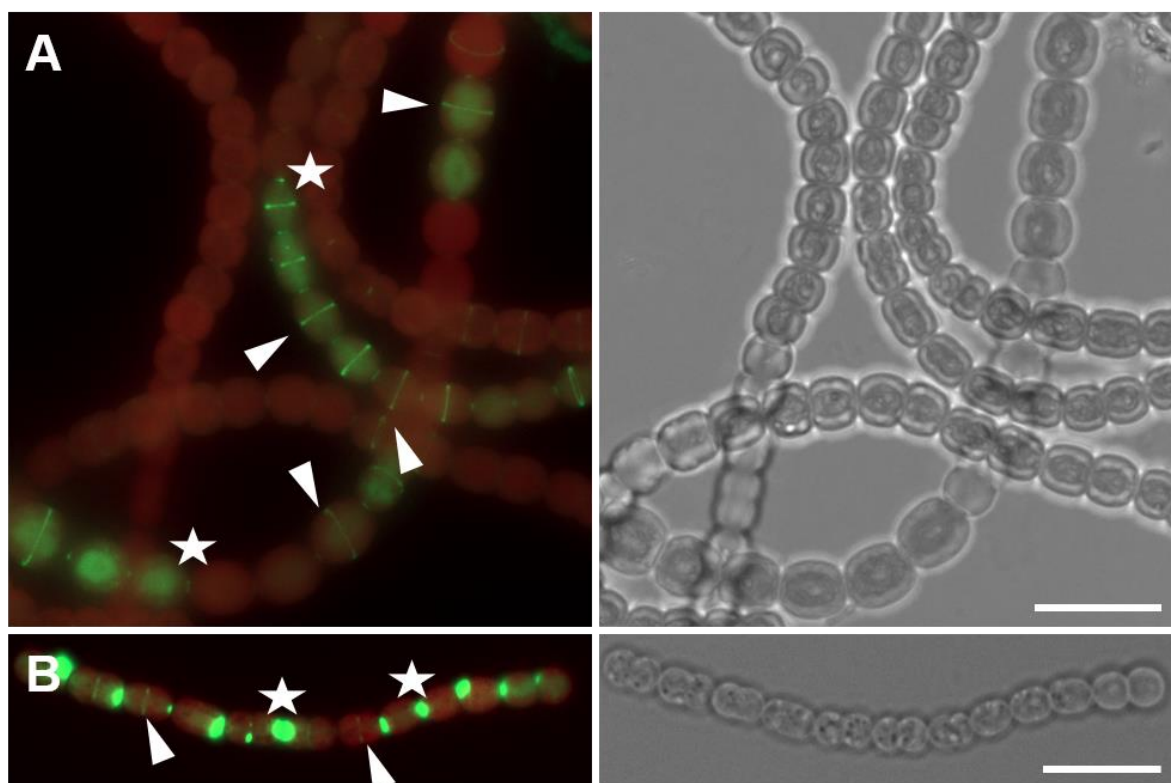


Fig. 21: Alr3364 localizes to the Z-ring in *Anabaena*

Merged GFP fluorescence and chlorophyll auto-fluorescence and bright field micrographs of *Anabaena* cells expressing Alr3364-GFP. Cells were grown in BG11 for (A) 5 days or (B) for 10 days and immobilized on an agarose pad. (A): Maximum intensity projection of a Z-stack. White triangles mark Z-rings. White stars mark septal localization. Scale bars: (A) 5 μ m or (B) 10 μ m.

7.4 Discussion

Coiled-coil rich IF-like cytoskeletal proteins with a central rod-domain are widespread in prokaryotes (Bagchi *et al.*, 2008) but, except for CreS (Ausmees, Kuhn and Jacobs-Wagner, 2003), do not follow the typical eukaryotic sub-domain architecture of IFs with their three interspaced coiled-coil domains (Coil 1A, 1B, 2; Kelemen, 2017). Ausmees and colleagues (2003), Bagchi and colleagues (2008) as well as Walshaw and colleagues (2010) hinted that there is a broad spectrum of coiled-coil rich and rod-domain containing proteins in prokaryotes with a putative IF-like function. However, to this date, only a limited amount of prokaryotic IF-like CCRPs have been more thoroughly investigated. Among those studied, functions in cell-shape determination and resistance to deformations were described, reminiscent of eukaryotic IFs (reviewed by Lin and Thanbichler (2013)). In a similar approach to Bagchi *et al.* (2008), we used the COILS algorithm from Lupas, Van Dyke and Stock (1991) and identified several thousand coiled-coil rich proteins from 141 cyanobacterial genomes. In every species investigated, CCRPs were present, providing further evidence for the wide spread dissemination of CCRPs in prokaryotes. CCRPs were about 3x more abundant in species of subsection II-V compared to subsection I, indicative for an involvement of CCRPs in the manifestation of the multicellular phenotype of subsection III-V and/or the more sophisticated cell division pattern of subsection II-V (Rippka *et al.*, 1979). It is likely that most of the here predicted proteins will not form IF-like cytoskeletal structures as indicated by the rather high amount of cyanobacterial CCRPs that failed to perform IF-like functions *in vitro* and/or *in vivo*. Nevertheless, among this subset of CCRPs, we identified four novel IF-like cytoskeletal proteins from species with simple and complex morphologies in which we found them to be involved in different cellular processes.

Fm7001 modulates phenotypic plasticity in *Fischerella*

Fm7001 and its homologs are strictly restricted to cell-differentiating and multicellular cyanobacteria of subsection IV and V (Rippka *et al.*, 1979). Based on its constant expression level even at early growth stages, we assume that Fm7001 constitutes an essential protein for *Fischerella* viability which is supported by the fact that we were not able to obtain any *fm7001* knockout strain. However, due to a lack of proper genome modification systems, the latter statement is inevitably connected with a touch of skepticism, because so far, a successful gene knockout was only accomplished once in subsection V cyanobacteria (Zhao *et al.*, 2015). Apart from that, the genomic region of *fm7001* is characterized by a large number of repetitive sequences which can be deleterious for homologous recombination events. In contrast to all studied prokaryotic CCRPs and to our knowledge also to all eukaryotic IF proteins, the floating Fm7001 polymer sheet in high molar urea indicates a unique and enormous intrinsic self-association capacity of Fm7001. For instance, eukaryotic vimentin exists only as tetramers in

5 M urea (Köster *et al.*, 2015). *In vivo*, Fm7001 species-independently forms filaments or filamentous meshworks that we identified to be tag-orientation dependent, revealing an essential role of the C-terminus for protein polymerization and function. Tag-orientation-dependency for filamentation and execution of cellular functions is a known factor for many proteins, including MreB (Swulius and Jensen, 2012) and IF-like proteins like CreS (Ausmees, Kuhn and Jacobs-Wagner, 2003). YFP-Fm7001 consistently formed filaments in *Synechocystis*, *Anabaena* and *Fischerella* and even induced a swollen and multiseriate phenotype in *Fischerella*, reminiscent of the morphotype of *C. fritschii*. Thus, Fm7001 shows phenotype-determining properties. By using mass spectrometry, we identified the membrane protein Fm5958 (WP_016869785.1) of the PspA/IM30 protein family that interacts with Fm7001 and which is upregulated in a morphotype-changing treatment (Koch *et al.*, 2017). Members of the PspA/IM30 family are known to bind and strengthen cellular membranes (Thurotte *et al.*, 2017). Based on the solubility of Fm7001 in detergent-containing buffers, a membrane linking function of Fm5958 for Fm7001 might provide an explanation as to how Fm7001 influences cell morphology. Upon certain stimuli (10 mM sucrose in the case of Koch *et al.* (2017)), elevated levels of Fm5958 are present in the cell, thus providing more membrane anchoring spots for the Fm7001 cytoskeleton, ultimately enabling the stabilization of the changing phenotype. The genomic surroundings of *fm7001* provide further insights into putative regulatory mechanisms of Fm7001 function (Fig. S2). Two genes, *fm7000* and *fm7002*, located on the minus strand, were upregulated in the morphology changing treatment by Koch *et al.* (2017). The 9 bp overlap of the 3' ends of *fm7001* with *fm7000* could hint for putative posttranscriptional RNAi function (Alberts *et al.*, 2014) of *fm7000* for *fm7001*, while Fm7002 is predicted to execute proteolytic functions and might further control Fm7001 quantity on a posttranslational level. Interestingly, homologs of *fm7000* are only present in subsection V and in one subsection IV cyanobacterium, suggesting that a tight control of Fm7001 might be necessary for the establishment of the branching phenotype of subsection V cyanobacteria. This hypothesis is supported by an analysis in our group which identified Fm7001 as a potential cytoskeletal protein putatively involved in the manifestation of the subsection V-specific phenotype. I-TASSER and NCBI CDS predictions further revealed a potential acetyl-CoA-carboxylase-like function for Fm7001. It is hence attributed to enzymatic functions in the citric acid cycle. Remarkably, the eukaryotic acetyl-CoA-carboxylase was previously already reported to polymerize into catalytically active protein filaments *in vitro* (Gregolin *et al.*, 1966; Kleinschmidt, Moss and Lane, 1969). Thus, Fm7001 polymerization and cytoskeletal properties provide further evidence for the theory that cytoskeletal proteins originate from metabolic enzymes that obtained polymerization features (Ingerson-Mahar and Gitai, 2012). Therefore, future studies should elucidate the putative enzymatic function of Fm7001 in order

to establish whether Fm7001, like CtpS (Ingerson-Mahar *et al.*, 2010), has still retained its enzymatic function.

A plasmid-encoded and *Synechocystis*-specific CCRP performs IF-like functions

Many prokaryotic tubulin- and actin-like cytoskeletal proteins, such as ParM, are known to be encoded on plasmids or on bacteriophages (Wagstaff and Löwe, 2018) but only very few CCRPs were identified on bacterial plasmids (Hurme *et al.*, 1994). Here we identified another IF-like CCRP encoded on the large toxin-antitoxin defense plasmid (pSYSA; Kopfmann and Hess (2013)) from *Synechocystis*. Consequently, a similar ParM-like plasmid-segregation role is conceivable. However, Slr7083 showed no indications of dynamic properties *in vitro*, which would be indispensable to plasmid segregation. Furthermore, unlike ParM (Carballido-Lopez, 2006), Slr7083 did not localize in a spindle-like pattern *in vivo* and was only expressed at later growth phases which would be contradictory to an involvement in the cell cycle. We also identified a direct interaction of Slr7083 with Slr1301 (Chapter 2), inevitably linking Slr7083 to the motility phenotype of the PCC-M substrain. *In vivo*, Slr7083 forms septal scaffold-like structures in *E. coli* and is associated with the cell envelope in *Synechocystis* and *Anabaena*, which is in accordance with its two-dimensional net-like *in vitro* structure, suggesting that Slr7083 forms a protective layer below the cell membrane. Slr7083 *in vitro* structures resemble the nuclear lamina formed by nuclear lamins and FilP lace-like filaments. It is thus conceivable that Slr7083 regulates cellular stiffness as well as rigidity and mediates mechanical cell stabilization (Stuurman, Heins and Aebi, 1998; Bagchi *et al.*, 2008; Fuchino *et al.*, 2013). Therefore, future work should explore putative mechanical resistance defects of $\Delta slr7083$ strains by, for example, atomic force microscopy. In a very low minority of cases, Slr7083 filaments were present in *Anabaena* and *Synechocystis* cells and, like Fm7001, a certain degree of tag-orientation-dependency was identified. Slr7083-GFP was excluded from heterocysts in *Anabaena* while YFP-Slr7083 specifically accumulated in heterocysts. Considering that those specialized cell types are absent in *Synechocystis*, the extent of this observation for Slr7083 function is questionable. Slr7083 shows morphogenic and cell shape-determining properties which we observed in *Anabaena*. Overexpression of YFP-Slr7083 induced an aberrant morphotype in *Anabaena* and an impaired perpendicular growth of cells within a trichome ultimately leading to a local multiseriate phenotype with cells dividing in more than one plane. YFP-Slr7083 partially impairs complete segregation of daughter cells, suggesting that overrepresented Slr7083 sheets prevent proper cell segregation. The presumed stable protective proteinaceous Slr7083 sheet could provide resistance to deformation and rigidity but, as indicated in *Anabaena*, might also impair cell division if not properly controlled. Therefore, it will be interesting to see whether Slr7083 interacts with FtsZ and whether it is proteolytically regulated during cell division. The absence of such a layer

should have tremendous effects on the cellular morphology, although such effect was not identified in the $\Delta slr7083$ GT-Kazusa strain. Therefore, it is debatable whether the observed feature in *Anabaena* reflects a morphology-determining property or whether it is simply caused by steric hindrance for other cell shape-determining factors in *Anabaena*. Even though no direct cell phenotype could be observed, the $\Delta slr7083$ GT-Kazusa strain showed an increased susceptibility to Proteinase K which suggests that Slr7083 sheets protect *Synechocystis* from external harmful substances, like proteases. Otherwise, no other impairments of cellular viability were identified in $\Delta slr7083$ GT-Kazusa. Interestingly, a clear cellular phenotype was identified upon *slr7083* gene deletion in the motile PCC-M substrain, revealing a motility-associated role of Slr7083, reminiscent of the essential role of the eukaryotic cytoskeleton in cell migration (Alberts *et al.*, 2014). $\Delta slr7083$ exhibited a reduced twitching motility and revealed defects in cytokinesis as daughter cells readily lacked chlorophyll signals. In accordance with an impaired cell division mechanism and a direct link of *slr7083* to the motile phenotype of the PCC-M strain, only the $\Delta slr7083$ PCC-M and not the $\Delta slr7083$ GT-Kazusa strain revealed a reduced cell viability and an increased sensitivity to Lysozyme. Together, those results imply that other factors, presumably involved in cell motility, regulate cell permeability and cell wall integrity in the PCC-M strain (Salazar and Asenjo, 2007; Kelemen, 2017). Notably, we also identified a generally higher susceptibility to Proteinase K for the PCC-M substrain compared to the GT-Kazusa substrain. In contrast to the non-motile GT-Kazusa substrain, we were not able to generate a Slr7083-GFP overexpressing PCC-M strain, indicating that *slr7083* expression is tightly regulated in this strain and alterations of cellular protein content have detrimental effects for the cells. This idea is further strengthened by the altered colony morphology of the Slr7083-GFP expressing GT-Kazusa substrain. Taken together, Slr7083 performs its motility-associated cytoskeletal function in a highly strain-specific manner, which is also underscored by the fact that its only homolog is present in another *Synechocystis* strain (PCC 6714).

The TPR protein All4981 bridges the S-layer, the septosomes and the elongasomes

All4981 is primarily predicted to contain 11 TRP repeats rather than coiled-coil repeats, even though those TRP-repeats are also recognized as coiled-coils by the COILS algorithm. TRP repeats are degenerate repeats of 34 amino acids, exhibiting only a few conserved amino acid positions and unlike left-handed coiled-coil motifs, consisting of heptad-repeats, these repeats assemble into right-handed α -helices (Blatch and Lässle, 1999; Mason and Arndt, 2004). TRP proteins are known to mediate protein-protein interactions and can assemble into multimers, but so far no filamentous phenotype was described (Blatch and Lässle, 1999). Like Fm7001, All4981 is restricted to cell-differentiating and multicellular cyanobacteria of subsection IV and V and reveals a particularly insightful genomic surrounding. The upstream gene *all4982*

overlaps with *all4981* and *all4983* in turn overlaps with *all4982*, all exhibiting a 4 bp overlap of their 3' end to the 5' end of the following gene. In accordance with a joint function, pull down analysis identified All4982 as an interactor of All4981. Apart from the inclusion body-like accumulations in *E. coli*, All4981 formed cell-traversing single or intertwined filaments that are largely strain and fluorescent tag-orientation independent. Based on this observation together with its capacity to assemble into a vast filamentous network *in vitro* and even extracellularly upon cell lysis of All4981-GFP overexpressing cells, All4981 fulfills basic IF-like functions (Kelemen, 2017). Dempwolff *et al.* (2011) showed that MreB can form extracellular filaments, indicating that this property resides within cytoskeletal proteins. Considering the high affinity of IF proteins to each other and their self-binding capacity in a cell free environment (Köster *et al.*, 2015), it is very well conceivable that IF-like proteins possess the ability to assemble in the extracellular space as well. Using a variety of different gene knockout approaches, we were not able to generate any gene deletion strain in an organism known to be reliably genetically modifiable (Cai and Wolk, 1990; Flores *et al.*, 2007; Nayar *et al.*, 2007). These results imply that All4981 performs essential cellular functions, reminiscent of the important role of vertebrate IFs for normal tissue development and integrity (Hesse *et al.*, 2000; Eriksson *et al.*, 2009). Homologs of All4981 are only present in multicellular cyanobacteria of subsection III, IV and V where they putatively perform indispensable functions for trichome-integrity. In the absence of a gene deletion strain, we tried to tackle the cellular function of All4981 by co-IP following mass spectrometry and identified interactions with a broad range of cytoskeletal proteins including ParB, MinD, MreB. Interestingly, also several putative S-layer proteins co-precipitated with All4981. S-layer proteins make up the crystalline two-dimensional layer covering the cell of archaea and bacteria and act as a protective shield and communication arrays of the prokaryote with its surroundings, thus functioning as adhesion and signal transduction sites as well as cell shape-determining factors (Sára and Sleytr, 2000; Pum, Toca-Herrera and Sleytr, 2013). An involvement of All4981 in signaling cascades would be in concert with the signal transduction role of eukaryotic IF proteins (Eriksson *et al.*, 2009) and the predicted phospholipid binding protein All4983 might provide a membrane-recruiting linker for All4981. Although, no physical interaction with All4983 was identified in co-precipitated samples. All4982 is another consistent interactor of All4981 and co-precipitated in both tested growth conditions. All4982 is a predicted Walker A Cytoskeletal ATPase (WACA) and a member of the large P-type NTPase superfamily, which also includes MinD and ParA (Ingerson-Mahar and Gitai, 2012; Lutkenhaus, 2012). Members of this group perform cytoskeletal functions in prokaryotes and some of them form filamentous polymers, often involved in cell division or cytokinesis (Ingerson-Mahar and Gitai, 2012). Thus, All4982 could aid or co-polymerize with All4981 but does not appear to be essential for All4981 filamentation as indicated by All4981 *in vitro* filaments and All4981 filaments present in *Synechocystis*, which

doesn't possess any All4982 or All4981 homologs. In accordance with the septal bridge-like localization pattern together with septum-arising All4981 filaments, we identified modest interactions with the septosomal junction protein SepJ. Taken together, it is conceivable that All4981 functions as a signal transducer or conductor of cell stability from the outermost cellular compartment - the S-layer – to the intracellular cell shape-determining MreB cytoskeleton, allowing cells to alter their growth behavior according to their external surroundings. By means of its interaction with SepJ, All4981 might further couple the MreB cytoskeleton to sites of cell-cell connections and cell-cell communication, putatively transmitting the aforementioned extracellular signals to neighboring cells within an *Anabaena* trichome.

Synpcc7942_2039 is involved in cell cycle control and chromosome segregation

Synpcc7942_2039 has only one homologous protein which is present in another *Synechococcus elongatus* strain (PCC 6301) and is thus a highly strain-specific protein. Although the *in vitro* polymerization assays were not entirely conclusive, revealing more aggregates than polymers, it appears to form a two-dimensional sheet-like structure reminiscent of the *Synechococcus* cell envelope. Thus, besides Fm7001 and Slr7083, Synpcc7942_2039 constitutes another CCRP that forms sheet-like structures, indicative for a common property of IF-like cyanobacterial proteins to assemble into multidimensional layers. *E. coli* cells expressing C-terminally GFP-tagged Synpcc7942_2039 revealed a similar banded and helical pattern as described for *E. coli* and *Bacillus subtilis* expressing YFP-MreB (Jones, Carballido-López and Errington, 2001; Swulius and Jensen, 2012). However, Swulius and Jensen (2012) showed that helical MreB structures are artifacts of the N-terminal YFP tag. Thus, it cannot be ruled out that Synpcc7942_2039-GFP localization in *E. coli* might as well be an artifact of the GFP tag. However, besides helical and banded structures, Synpcc7942_2039-GFP also reveals a patchy localization pattern along the membrane with several fluorescence puncta reminiscent of the sandwich MreB-mCherry translational fusion strain FB76 (Swulius and Jensen, 2012). The observed Synpcc7942_2039 filaments in *Synechocystis* and *Anabaena* resemble scattered GFP-MreB filaments in the subsection V cyanobacterium *C. fritschii* (unpublished data by Springstein *et al.*). The localization pattern in *Anabaena* and *Synechocystis* somewhat resembles thylakoid membrane placement in these organisms (Liberton *et al.*, 2006; Hu *et al.*, 2007) and as a result it cannot be ruled out that Synpcc7942_2039 rather associates with the thylakoid membrane instead of forming polymers on its own. Taking into consideration that Synpcc7942_2039-GFP is clearly not associated with the thylakoid membrane system in *Synechococcus*, it is likely that the observed localization pattern in *Synechocystis* and *Anabaena* is in fact a result of its intrinsic polymerization and not based on an association with the thylakoid membrane. Expression of

Synpcc7942_2039-GFP in the rod-shaped *Synechococcus* leads to a similar helical, banded and patchy localization pattern compared to *E. coli*, suggesting a direct contribution of Synpcc7942_2039 to the rod-shaped cell phenotype of both species. In rod-shaped bacteria, the cell shape is determined and maintained by the elongasome (Wagstaff and Löwe, 2018), a MreB-guided multi-enzyme complex. The similar distribution of Synpcc7942_2039-GFP in rod-shaped bacteria, suggests a direct involvement of Synpcc7942_2039 with the elongasome. The structural resemblance of Synpcc7942_2039 to tropomyosin (I-TASSER prediction) suggests that Synpcc7942_2039 polymers, like tropomyosin polymers, act on and stabilize actin-like MreB filaments preventing its depolymerization (Bryce *et al.*, 2003). A MreB-system modified in such way might also explain why (over)expression of Synpcc7942_2039-GFP inhibits growth of young *Synechococcus* cultures since an overprotective Synpcc7942_2039 polymer layer could impair elongasome dynamics, essential for cell wall synthesis (reviewed by Ingerson-Mahar and Gitai, 2012). However, no direct association with MreB was detected for Synpcc7942_2039 in a bacterial two hybrid system and MreB is absent from *Synechocystis* sp. (Hu *et al.*, 2007). Thus, together with the self-binding capacity identified in a bacterial two-hybrid assay, the spindle-like structures observed in *Synechocystis* and likely also the filaments observed *Anabaena* are MreB-independent, questioning a tropomyosin-like function and simultaneously promoting IF-like functions for Synpcc7942_2039. Remarkably, removal of Synpcc7942_2039 increased cell growth of Δ *synpcc7942_2039* strains in early growth phases but revealed a decrease in cell viability at later stages. This observation is in harmony with the recently identified correlation of cell density to cell division by Esteves-Ferreira *et al.* (2017), hinting for a disturbed intercellular communication in Δ *synpcc7942_2039*. Fluorescence microscopy of DAPI-stained Δ *Synpcc7942_2039* cells revealed cells lacking any discernible chlorophyll or DNA, suggesting a disturbed cell-cycle control system with uncontrolled cell division and cytokinesis. But like MreB, no interaction with FtsZ could be detected in a bacterial two hybrid assay, thus the function of Synpcc7942_2039 remains to be elucidated.

Alr3364 is associated with the divisome and the septosome

The lack of a clear Alr3364 *in vitro* polymerization pattern together with its *in vivo* localization reveals a non-IF-like cytoskeletal role for Alr3364. Alr3364-GFP localized to the Z-ring in *Anabaena* and *E. coli* FtsZ co-precipitated upon Alr3364 purification. However, no co-precipitation of FtsZ from Alr3364-GFP expressing *Anabaena* cells was identified, and no physical interaction of both proteins were discovered in a bacterial two hybrid assay, suggesting that Alr3364 does not directly interact with FtsZ but requires further linker proteins. As FtsZ from *E. coli* but not from *Anabaena* is co-precipitated, it is conceivable that other *Anabaena*-specific adaptor proteins mediate the association of Alr3364 and FtsZ, and that this

indirect association is not stable enough to be pulled-down. However, this does not explain why Alr3364 can be co-precipitated in *E. coli* but does not co-localize with the Z-ring in *E. coli* and still leads to a partial cell filamentous phenotype. Camberg, Hoskins and Wickner (2009) showed that the ClpXP protease specifically degrades *E. coli* FtsZ and cells overexpressing ClpXP exhibit a filamentous phenotype. However, no such degradation of FtsZ was detected in cell-free lysates of Alr3364-GFP expressing *Anabaena* cells. In accordance with the partial septal localization of Alr3364-GFP, we identified an interaction with SepJ, whose localization was previously shown to be dependent on the FtsZ-driven divisome (Ramos-León *et al.*, 2015). The septal localization and the Z-ring association, together with the direct interaction with SepJ suggests that Alr3364 is also involved in the interplay between the divisome and the septosomes. The apparent link of the septosomes and divisome is in accordance with the restriction of Alr3364 to cyanobacteria of subsection II-V, excluding unicellular cyanobacteria of subsection I that only exhibit a simple binary fission division pattern (Rippka *et al.*, 1979). Regardless, further research is needed in order to pinpoint the nature of the association of Alr3364 with the Z-ring and the septosomes.

Taken together, using the COILS algorithm, we have identified four IF-like coiled-coil rich cytoskeletal proteins in cyanobacteria and identified another protein putatively involved in the crosstalk between divisome and septosome in *Anabaena*. However, regardless of the reliable predictive power of the COILS algorithm, in the absence of more sophisticated prediction systems, the identification of novel IF-like cytoskeletal proteins in prokaryotes will remain a Sisyphean task as the vast majority of CCRPs does not perform cytoskeletal functions. The different filamentation and *in vivo* localization pattern of cyanobacterial coiled-coil rich cytoskeletal proteins together with their different cellular roles reveal that CCRPs have evolved in order to adjust to specific requirements. Many cyanobacterial CCRPs exhibit a clear restriction to only a subset of cyanobacterial species, and some appear to be involved in the multicellular phenotype while others were shown to be associated with the elongasome and/or divisome, thus being involved in cell shape, cell growth and cell division. Further phylogenetic analysis will have to show the evolutionary relationships of the here identified CCRPs. However, since the five here studied proteins do not reveal any sequence similarity to each other it is unlikely that they have evolved from a common ancestor and thus presumably arose by convergent evolution. Despite the unlikely relationship, cyanobacterial CCRPs have evolved a common property to polymerize into two-dimensional sheet-like structures, which distinguishes them from other CCRPs (Lin and Thanbichler, 2013).

8 Chapter II: Evolutionary diversification of cytoskeletal networks in cyanobacteria

8.1 Abstract

The properties of the eukaryotic cytoskeletal systems (MTs, MFs, IFs) are largely dependent on accessory proteins that regulate their function, localization or shape and even link them to junctional complexes. In the multicellular and heterocyst-forming cyanobacterium *Anabaena* a similar linkage of the FtsZ-driven tubulin-like cytoskeleton to the septosomes (i.e. cyanobacterial gap junctions) was described. Most of the CCPR families in our dataset have a conserved amino-acid sequence and are predicted to form polymers; nonetheless, whether their function in the cell is also conserved is currently unknown. Here we study the evolutionary and functional diversification of three members of a conserved cyanobacterial CCRP family. The three proteins are Slr1301 from the unicellular coccoid *Synechocystis*, Synpcc7942_1139 from the unicellular rod-shaped *Synechococcus* and Alr0931 from the filamentous *Anabaena*. We find that the three proteins polymerize into dissimilar structures *in vitro* and show different localization patterns *in vivo* in a species-independent manner. Furthermore, they represent different levels of essentiality. *Synechocystis slr1301* mutants are impaired in twitching motility whereas *synpcc7942_1139* is essential for *Synechococcus* viability and *Anabaena* cells lacking *alr0931* are unable to grow in liquid culture. Despite their different cellular roles, homologous CCRPs have retained the ability to interact with each other and to form cytoskeletal networks with other IF-like cytoskeletal CCRPs. Taken together, homologous cyanobacterial CCRPs constitute a novel class of conserved prokaryotic IF-like cytoskeletal proteins that exhibit different functional properties suggesting species-specific evolutionary adaptations.

8.2 Introduction

Apart from microtubules and microfilaments, the intermediate filament (IF) superfamily comprises the third major and largely diverse cytoskeletal system in some metazoans, which consists of 70 different genes in humans (Alberts *et al.*, 2014). In contrast to actin and tubulin homologs, IF proteins exhibit only low levels of sequence conservations, sometimes only displaying as little as 20% sequence similarity (Fuchs and Weber, 1994). Instead, the IF superfamily is mainly characterized by their conserved structural and biochemical properties that enable them to assemble into similar 10 nm filaments in a co-factor independent manner (Shoeman and Traub, 1993; Eriksson *et al.*, 2009). Intermediate filaments are thinner than microtubules but thicker than microfilaments, hence their name “intermediate filament”. IF proteins exhibit tissue-specific expression patterns and hence cell type-specific biological functions (Fuchs and Weber, 1994). Although long considered to function purely as stiff cellular stabilization systems it has become evident that IFs, like the other cytoskeletal systems, are

dynamic structures that act as intracellular orchestrators of various processes (Eriksson *et al.*, 2009). Furthermore, the function, localization and polymerization of these cytoskeletal systems is often dependent on other accessory or other cytoskeletal proteins, highlighting the importance of the cytoskeletal network as a whole for proper cytoskeletal functions (Green *et al.*, 2005; Alberts *et al.*, 2014). For example, accurate Z-ring placement in *E. coli* is dependent on the MinCDE system, with MinC acting as a capping protein that inhibits FtsZ polymerization (Lutkenhaus, 2012). Furthermore, the metabolic enzyme CtpS, which itself is able to polymerize, acts as a negative regulator for CreS polymerization and thus controls the degree of cell curvature in *C. crescentus* (Ingerson-Mahar *et al.*, 2010). It is assumed that all IF proteins are derived from a lamin-like common ancestor by gene duplication and subsequent functional diversifications (Shoeman and Traub, 1993; Alberts *et al.*, 2014). In contrast, CreS, the first identified prokaryotic IF-like protein lacks any discernible homologs outside of *C. crescentus* (Ausmees, Kuhn and Jacobs-Wagner, 2003; Wickstead and Gull, 2011). CreS determines the crescent cell curvature in *C. crescentus* where it forms cell-traversing filaments that line up at the inner cell (Ausmees, Kuhn and Jacobs-Wagner, 2003). CreS's domain building block resembles the eukaryotic tripartite architecture albeit having only 25% sequence identity to eukaryotic IF proteins. Shortly after the discovery of CreS other IF-like CCRPs were identified in *S. coelicolor* and *Helicobacter pylori* that share essential biochemical and functional properties with eukaryotic IF proteins, albeit lacking the characteristic rod domain structure consisting of three sub-domains - coil 1A,1B and 2 (Bagchi *et al.*, 2008; Specht *et al.*, 2011; Holmes *et al.*, 2013). Although they exhibit a huge difference in amino acid (aa) sequence length, FilP (310 aa) and Scy (1326 aa) from the polar growing *S. coelicolor* are putative paralogs that have evolved from gene duplications (Walshaw, Gillespie and Kelemen, 2010). Unlike CreS, both proteins possess homologous proteins distributed across the Actinobacteria phylum (Walshaw, Gillespie and Kelemen, 2010). Given their paralogous state, both proteins have evolved and fulfill different, but simultaneously also adjunctive functions in the cells. FilP mechanically stabilizes *S. coelicolor* hyphae whereas Scy orchestrates polar growth by recruiting DivIVA to sites of novel tip formation (Bagchi *et al.*, 2008; Holmes *et al.*, 2013). DivIVA is another widely conserved prokaryotic CCRP often involved in cell division that, together with FilP, Scy and a cellulose synthase, forms the so-called polarisome and guides polar growth by directed peptidoglycan synthesis (Holmes *et al.*, 2013; Lin and Thanbichler, 2013). The polarisome, together with the elongasome and the divisome are prominent examples for highly organized cytoskeletal networks where cytoskeletal proteins readily provide the basic building-block (i.e. scaffold) in order to mediate, for example, cell wall synthesis or to provide structural stability (Typas *et al.*, 2012; Lin and Thanbichler, 2013; Löwe and Amos, 2017). Another example for a genus-specific cytoskeletal IF-like CCRP is RsmP, which is exclusively present in *Corynebacterium* and which is involved cell shape-maintenance

(Fiuza *et al.*, 2010). Whether the above described proteins are actual relatives of eukaryotic IF proteins or whether they display functional analogs is still largely obscure (Lin and Thanbichler, 2013). The recently identified IF-like CCRPs from morphologically diverse cyanobacterial species further highlighted the broad distribution of cytoskeletal proteins of the large CCRP family (Chapter 1), supporting the need of a revision of the definition of IF proteins. CCRPs of morphologically different cyanobacterial species were identified, including the subsection IV and V-specific Fm7001 protein from the multicellular, true branching and heterocyst-forming cyanobacterium *Fischerella* (Chapter 1) that formed filaments *in vivo* and planar, two-dimensional polymers *in vitro*. Another protein with a restricted distribution among cyanobacteria, which is only present on the large toxin-antitoxin plasmid pSYSA from *Synechocystis*, polymerized into net-like structures *in vitro* reminiscent of FilP *in vitro* lattices (Fuchino *et al.*, 2013), suggesting a cell stability or cell rigidity maintenance function (Chapter 1). Together with the subsection I-specific Synpcc7942_2039 and the subsection III, IV and V-specific AlI4981, these proteins are examples for subsection and morphotype-specific cytoskeletal proteins in cyanobacteria. Besides subsection-specific proteins, we also identified several conserved CCRPs present in all cyanobacterial subsections and hence in all different morphotypes. Here we study the evolutionary diversification of three members of a large family of conserved cyanobacterial CCRPs, namely Alr0931, Slr1301 and Synpcc7942_1139 and investigate whether these proteins have retained similar properties or if they have adapted in a species-specific manner. We further elucidate the involvement of a cytoskeletal network for correct cytoskeletal functions.

8.3 Results

In Chapter 1 we identified 21 cyanobacterial IF-like protein candidates with a high probability of adopting a coiled-coil conformation. Based on their high coiled-coil content, reminiscent of the IF-like cytoskeletal protein CreS, and in the absence of other predicted cellular functions, an IF-like cytoskeletal role for these proteins was hypothesized and validated for four out of the 21 proteins (Chapter 1). In this chapter, we look deeper into three homologous proteins, Alr0931, Slr1301 and Synpcc7942_1139 that are members of a large group of cyanobacterial CCRPs conserved among all different cyanobacterial subsections and hence morphotypes. The group comprises 168 members, all of them predicted to be hypothetical proteins that share moderate levels of sequence conservations (39%). The genomic surrounding shows no highly conserved gene neighbors but in many cases homologous proteins are surrounded by genes encoding for the CheY-like or methyl-accepting chemotaxis proteins, thought to regulate cellular movement in cyanobacteria (Schuergers, Mullineaux and Wilde, 2017). However, no such proteins are located in the vicinity of *slr1301*. As in most of the 21 cyanobacterial CCRPs, I-TASSER-based prediction revealed structural similarities of Alr0931, Slr1301 and

Synpcc7942_1139 to the cell division protein EzrA (Chapter 1), strengthening an IF-like function of the three homologous proteins. Coiled-coil motif count and length is not fixed among the homologs and can vary substantially. Alr0931 exhibits six coiled-coil motifs, five were predicted for Slr1301, while eight coiled-coil motifs were predicted for Synpcc7942_1139 (Chapter 1). Characteristic for this group is a highly conserved N-terminus with a M-L-Y-L-A-E-V motif present in nearly all homologs, followed by a moderately conserved N-terminal region of the first 120 amino acids (Fig. 22). Two other highly conserved domains are present in this group, one located around the center of the proteins (between the 340th and 370th amino acid), and another one shortly thereafter between the 400th and 420th amino acid (Fig. 22).

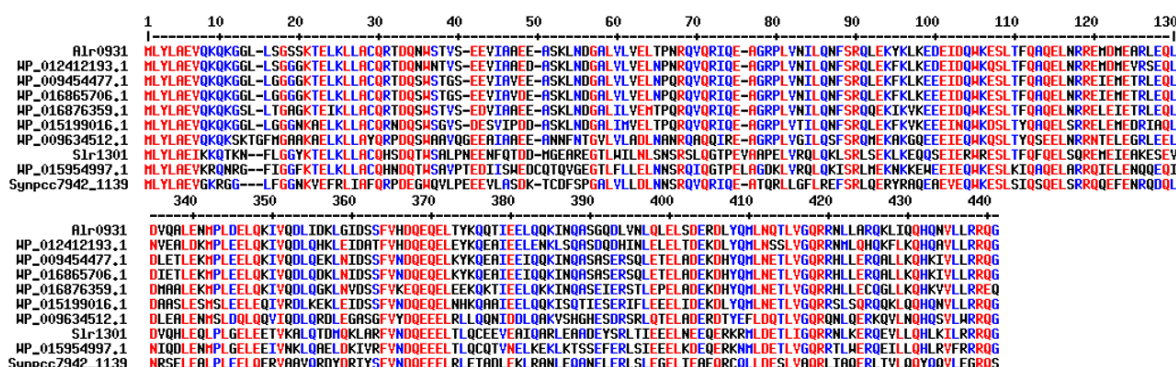


Fig. 22: Conserved sequence motifs of homologous proteins

Multiple sequence alignment of selected cyanobacterial homologous CCRPs using MULTALIGN (Corpet, 1988) with default settings and sorted according to relatedness. Alr0931 (*Anabaena*), Slr1301 (*Synechocystis*) and Synpcc7942_1139 (*Synechococcus*) are identified by their designated cyanobase locus tag. Other proteins are given as NCBI accession numbers. WP_012412193.1 (*Nostoc punctiforme* PCC 73102), WP_009454477.1 (*Fischerella thermalis* PCC 7521), WP_016865706.1 (*Fischerella*), WP_016876359.1 (*C. fritschii* PCC 9212), WP_015199016.1 (*Calothrix* sp. PCC 6303), WP_009634512.1 (*Synechocystis* sp. PCC 7509), and WP_015954997.1 (*Cyanothece* sp. PCC 7424). Amino acids from 1-130 and 334 to 441 are depicted. Red highlighted amino acid residues are conserved among all species while amino acid residues highlighted in blue are mostly conserved. Amino acids depicted in black show no conservation.

Members of this homologous group are present in cyanobacteria of all morphotypes which gave rise to the question if these proteins, albeit being evolutionary related, have undergone evolutionary diversifications. In order to pinpoint their evolutionary path, we performed *in vitro* polymerization, *in vivo* protein localization in *Synechocystis*, *Anabaena* and *Synechococcus* and compared the phenotypes of the respective gene deletion strains.

Homologous proteins assemble into manifold structures *in vitro*

Although evolutionary related to one another, homologous proteins polymerize into a highly diverse set of structures *in vitro*. Alr0931 assembled into abundant short and thin filaments, revealing no tendencies to assemble into higher order structural networks (Fig. 23A). However, when subjected to a different polymerization buffer with a higher pH, Alr0931 formed a strongly interconnected filamentous networks (Fig. S22). Synpcc7942_1139 did not polymerize into single filaments but assembled into three-dimensional continuous sheets reminiscent of the

cell envelope of rod-shaped bacteria (Fig. 23B). Unlike its homologs, Slr1301 merely formed tiny filamentous networks with a very low abundance in the sample (Fig. 23C).

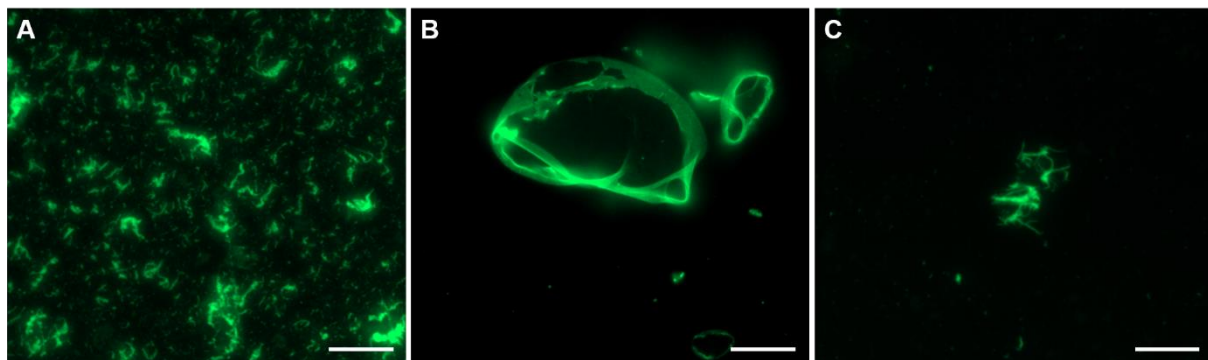


Fig. 23: *In vitro* polymerization of homologous proteins

Epifluorescence micrographs of filamentous structures formed by purified and renatured 0.5 mg ml^{-1} (A) Alr0931, (B) Slr1301 or (C) Synpcc7942_1139 in PLB. Proteins were stained with an excess of NHS-Fluorescein and analyzed by epifluorescence microscopy. Scale bars: $10 \mu\text{m}$.

Despite different polymerization properties, the obtained filaments fulfill one of the major criteria for IF-like cytoskeletal proteins, namely to be able to self-assemble in a nucleotide independent manner *in vitro* (Köster *et al.*, 2015). A strong self-binding affinity of the homologous proteins was further validated by subsequent bacterial two hybrid assays (Fig. 24).

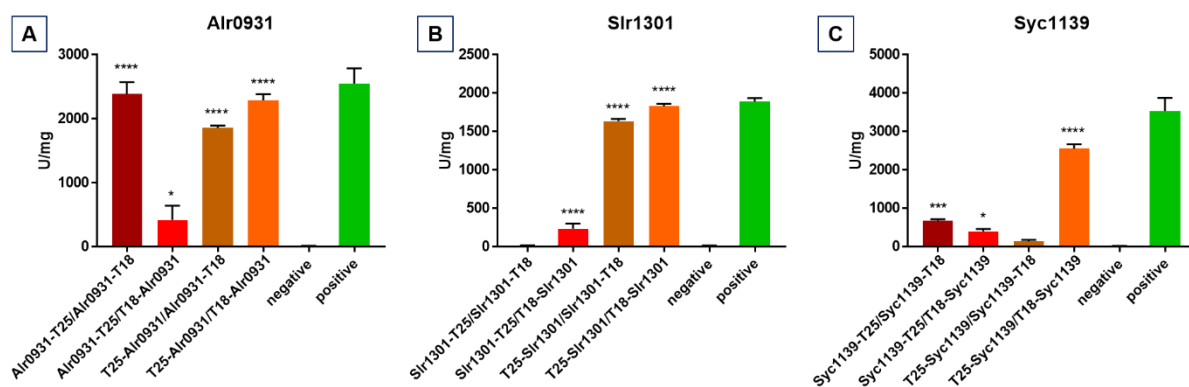


Fig. 24: Interactions of IF-like homologous proteins in a beta-galactosidase assay

Beta-galactosidase assays of *E. coli* cells co-expressing indicated translational fusion constructs of all possible pairwise combinations of (A) Alr0931, (B) Slr1301 and (C) Synpcc7942_1139 (abbreviated Syc1139). Cells were grown for 1 day at $30 \text{ }^\circ\text{C}$. Quantity values are given in Miller Units per milligram LacZ of the mean results from three independent colonies. Error bars indicate standard deviations. Neg: pKNT25 plasmid carrying the respective gene insert co-transformed with empty pUT18C. Pos: Zip/Zip control. *: $P < 0.05$, **: $P < 0.01$, ***: $P < 0.001$, ****: $P < 0.0001$ (Dunnnett's multiple comparison test and one-way ANOVA).

Localization pattern of Alr0931, Slr1301 and Synpcc7942_1139 differs *in vivo*

To further explore the role of each homologous protein, we compared their localization pattern in *E. coli*, *Anabaena*, *Synechocystis* and *Synechococcus*. Initially, and in order to address

phyla-independent *in vivo* localization of homologous proteins, we expressed C-terminally *gfp* tagged translational fusion constructs of homologous proteins in *E. coli* and assessed *in vivo* localization by epifluorescence microscopy.

In *E. coli*, GFP tagged Alr0931 and Slr1301 showed bright fluorescence signals that accumulated at the cell poles (Fig. 25B,C). These structures resembled the polar scaffold-like assemblies formed by bactofilins (Kühn *et al.*, 2010) and showed a similar localization pattern to Slr7083-GFP expressed in *E. coli* (Chapter 1). Slr1301-GFP was present only at the cell poles where it formed U-shaped structures whereas Alr0931-GFP was also distributed in the cytoplasm with focal accumulations at the poles ending in a straight line (Fig. 25B). In contrast to Alr0931 and Slr1301, Synpcc7942_1139 mainly localized to the membrane but was also present at the cytoplasm and showed only slight polar orientation (Fig. 25C). These findings indicate a different localization pattern with different degrees of polarity of the three homologs in a heterologous expression system.

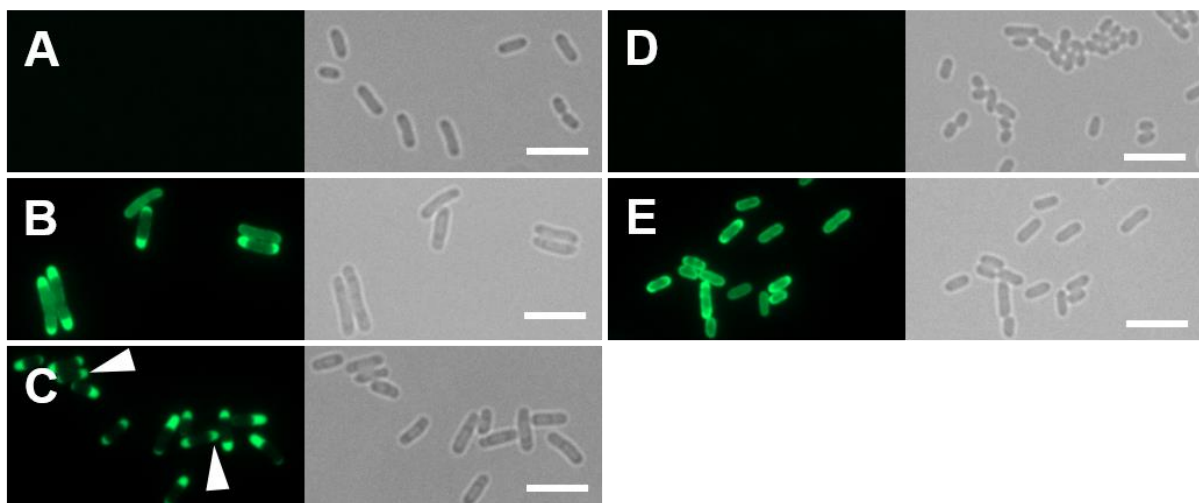


Fig. 25: *In vivo* localization of homologous proteins in *E. coli*

GFP-fluorescence and bright field micrographs of *E. coli* BL21 (DE3) (A,D) wt cells or *E. coli* expressing (B) Alr0931-GFP, (C) Slr1301-GFP or (E) Synpcc7942_1139-GFP. Cells were grown till an OD₆₀₀ of 0.5 and then induced for (A,B,C) 5.5 hours or (D,E) 24 hours at 20 °C with 0.05 mM IPTG. White triangles point to U-shaped GFP localization pattern. Scale bars: 5 µm.

Given the difference in localization patterns observed in *E. coli*, we next wanted to compare the localization of the homologs in their respective cyanobacteria of origin. We were interested if cyanobacterial-specific proteins can alter the cellular localization of homologous CCRPs and if homologous CCRPs have any effect on the species morphotype. To this end, we expressed C-terminally *gfp* or *yfp*-tagged homologous proteins in *Synechocystis* under the control of the *cpc560* or *trc* promoter and evaluated *in vivo* localization by fluorescence microscopy.

Unlike heterologously expressed in *E. coli*, Alr0931-GFP did not accumulate as focal patches and was homogeneously associated to the membrane but also revealed a partial

cytoplasmic localization (Fig. 26A). Slr1301-YFP displayed a similar localization pattern as in *E. coli*. Membrane-associated focal protein accumulations were detectable throughout the cells with no obvious site preference except for certain crescent-like formations seemingly underlying the cell membrane (white stars in Fig. 26B). Sheet-like S-shaped filaments within a minority of cells were also detectable, resembling the sheets formed by Slr7083-GFP in *Synechocystis* from Chapter 1 (Fig. 26B inlay). In Chapter 1, we showed that $\Delta slr7083$ decreased twitching motility of the motile *Synechocystis* PCC-M substrain (PCC-M) and affected cytokinesis only in the PCC-M strain. Inspired by the different effects of $\Delta slr7083$ on the motile and non-motile *Synechocystis* substrains, we also expressed Slr1301-YFP in the PCC-M substrain and found intracellular focal accumulations and crescent-like fluorescence signals comparable to those seen in the non-motile *Synechocystis* GT-Kazusa strain (GT-Kazusa; white arrows in Fig. S23A,B). However, few thin single filamentous strings could be identified in the PCC-M substrain (white triangles in Fig. S23A). These findings indicate that Slr1301 function differs in the motile and non-motile *Synechocystis* substrains. Like Alr0931-GFP, Synpcc7942_1139-GFP was membrane-bound (Fig. 26C) but did not underlie the whole cell envelope and was rather distributed in a patchy pattern. None of the proteins had a morphogenic effect on *Synechocystis* and were found to be mainly associated with the cell envelope, reminiscent of their localization in *E. coli*.

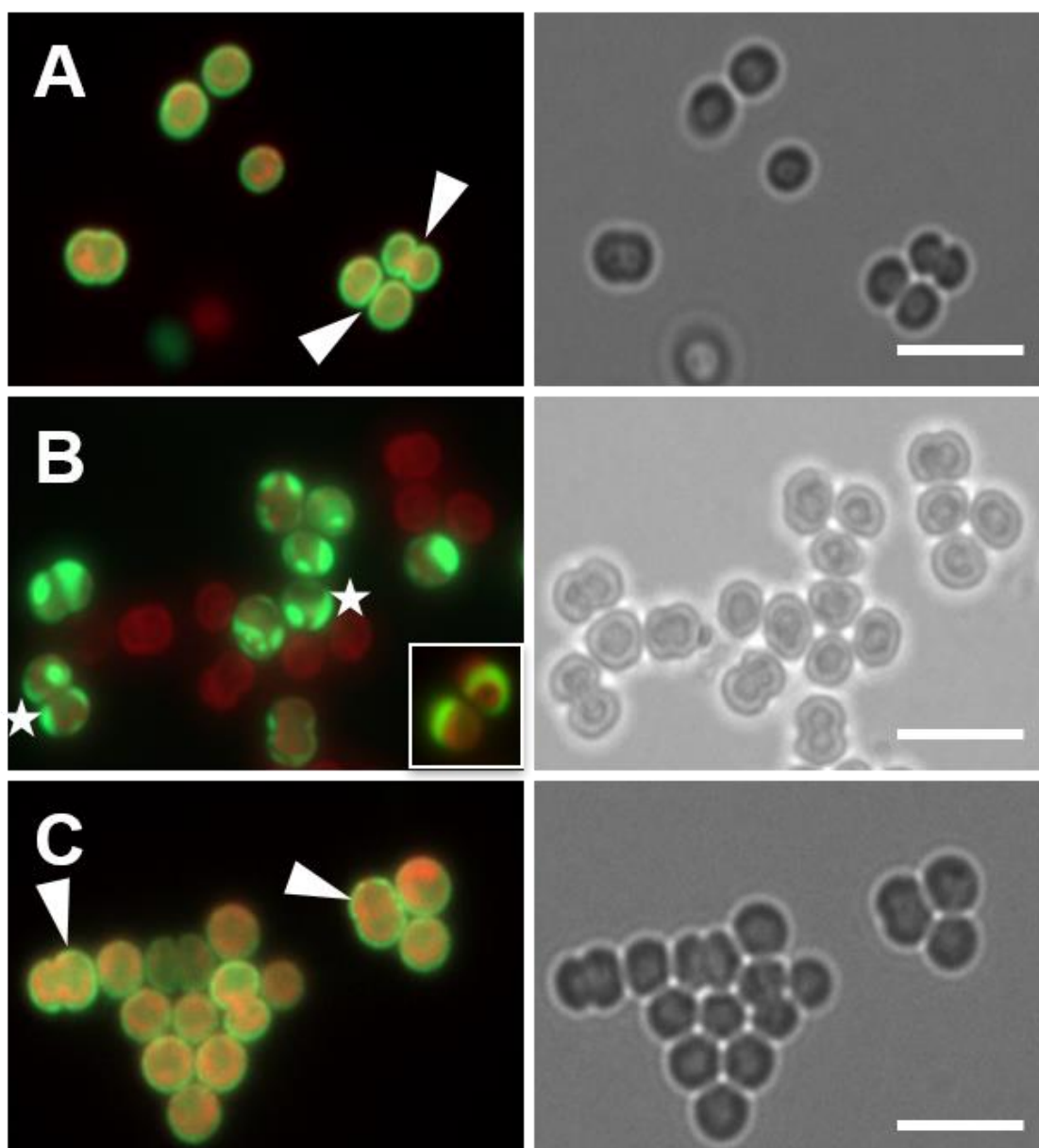


Fig. 26: *In vivo* localization of homologous proteins in *Synechocystis*

Merged GFP or YFP fluorescence and chlorophyll auto-fluorescence and bright field micrographs of non-motile *Synechocystis* GT-Kazusa expressing (A) Alr0931-GFP, (B) Slr1301-YFP and (C) Synpcc7942_1139-GFP. Cells were grown under standard growth conditions in liquid culture and immobilized on agarose pads. (B): Maximum intensity projection of a Z-stack. (B inlay) A selected Slr1301-YFP expressing cell showing sheet-like filaments. White triangles indicated selected cells with cell envelope-localized GFP fluorescence. White stars mark crescent-like localization of Slr1301-GFP. Scale bars: 5 μ m.

Localization of homologous proteins was assessed in a similar manner in *Synechococcus* with chromosomally inserted homologous proteins expressed from an inducible *trc* promoter. In contrast to the localization pattern in *Synechocystis* but in line with the distribution pattern from *E. coli*, Alr0931-GFP and Slr1301-GFP formed predominantly polar accumulations where Alr0931-GFP was distributed to both poles and Slr1301-GFP restricted to one cell pole (Fig. 27A,B). A proportion of Alr0931-GFP was localized to the cytoplasm (Fig. 27A) while Slr1301-GFP showed no such diffuse localization, reminiscent of

their localization in *E. coli* and *Synechocystis*. Alr0931 formed internal spots which sometimes formed diffuse, sheet-like structures (white star in Fig. 27A). Alr0931-GFP and Slr1301-GFP accumulations were found to replace the cellular chlorophyll (Fig. S24), preventing it from cell-wide distribution. This localization pattern could further hint to a scaffolding function with overexpressed proteins creating a massive and impenetrable filamentous layer. Expression of Synpcc7942_1139-GFP was hardly detectable and only discernable as small spots at the cell envelope of certain cells with 10x longer exposure time (white triangles in Fig. 27C).

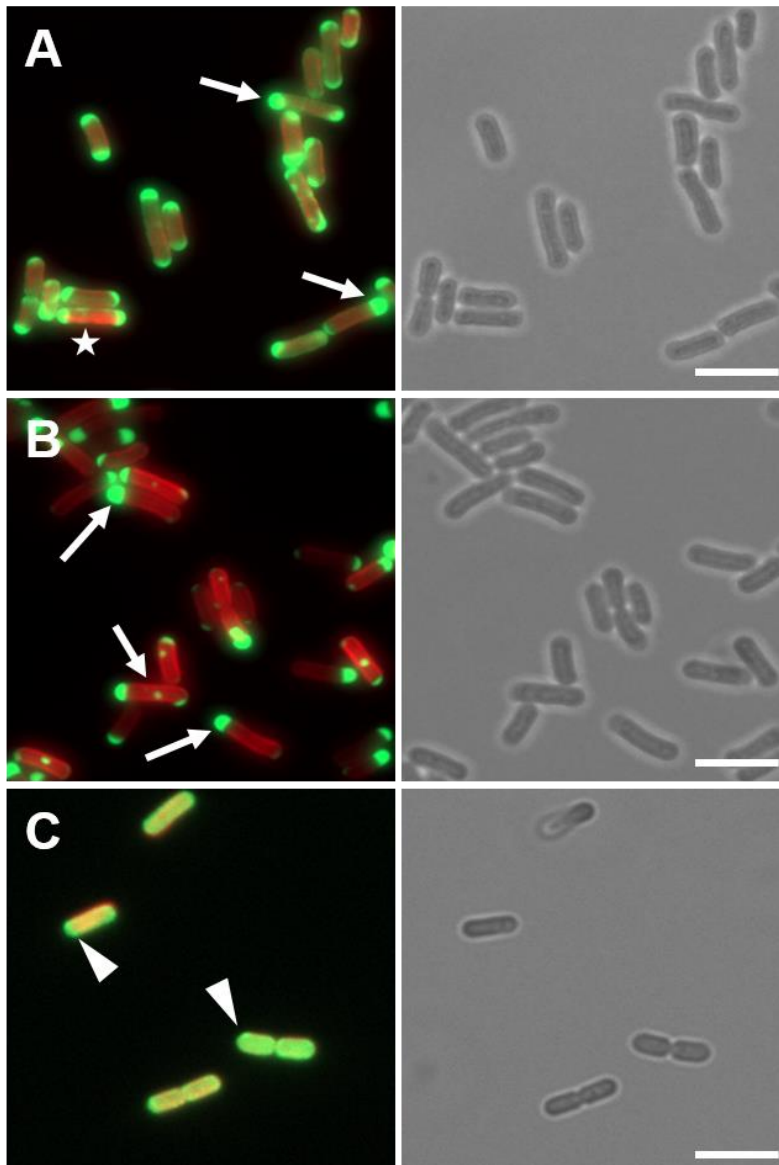


Fig. 27: *In vivo* localization of homologous proteins in *Synechococcus*

Merged GFP fluorescence and chlorophyll auto-fluorescence and bright field micrographs of *Synechococcus* cells expressing (A) Alr0931-GFP, (B) Slr1301-GFP and (C) Synpcc7942_1139-GFP. Cells were either grown on BG11 plates supplemented with (A) 0.5 mM, (B) 0.05 mM IPTG or in (C) BG11 liquid cultures supplemented with 1 mM IPTG and immobilized on agarose pads. (A,B) Maximum intensity projection of a Z-stack. White triangles indicate Synpcc7942_1139-GFP spots. White star points to internal diffuse GFP signals. White arrows mark selected cells with restricted chlorophyll distribution. Scale bars: 5 μ m.

Finally, we were interested in the behavior of the homologs in a more complex cellular environment such as the multicellular and heterocyst-forming cyanobacterium *Anabaena*. Localization of the homologous proteins in *Anabaena* was more complex than in the unicellular *Synechocystis* and *Synechococcus*. Alr0931-GFP showed two localization patterns that appeared to be mutually exclusive. Initially, Alr0931-GFP was homogeneously distributed throughout the cytoplasm in all vegetative cells and was excluded from heterocysts (Fig. S25). However, upon progression of culture age, Alr0931-GFP localization shifted to cell envelope-associated patches (Fig. 28A). Interestingly, fluorescence intensity differed between groups of dividing cells (white triangles in Fig. 28A) whereas heterocysts remained devoid of fluorescence (white arrows in Fig. 28A). As in all other investigated bacterial strains, Slr1301-GFP formed focal accumulations of different sizes in *Anabaena* (white stars in Fig. 28B). Additionally, filamentous protein strings traversing the cells were detected (white triangles in Fig. 28B,C). Some cells only displayed rather thin single filaments (Fig. 28B and 28B upper inlay) while others exhibited sheet-like and cell-cell traversing filaments often scattering throughout the cell (white triangles in Fig. 28B,C and 28B lower inlay). Additionally, overexpression of Slr1301-GFP was associated with a morphogenic impact on the cells as we observed a proportion of swollen and enlarged cells (blue triangles in Fig. 28B). We were not able to localize Synpcc7942_1139-GFP in *Anabaena*, as cells carrying the expression plasmid never displayed any discernible fluorescence signal, not even upon strong induction of *P_{petE}*. Likewise, no fluorescence signal was recorded for any N-terminally YFP-tagged homolog, indicating a tag-orientation dependency of these proteins.

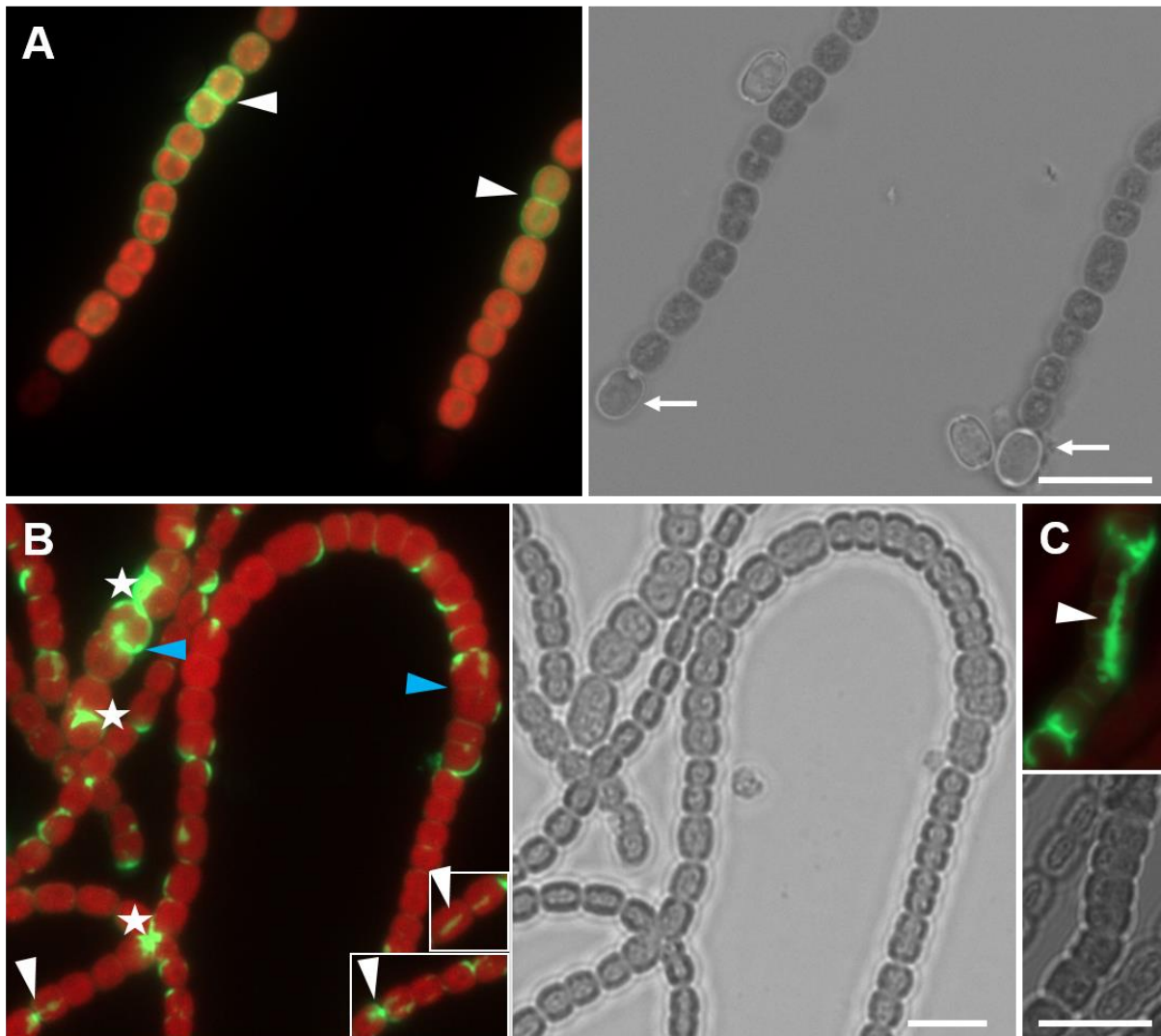


Fig. 28: *In vivo* localization of homologous proteins in *Anabaena*

Merged GFP fluorescence and chlorophyll auto-fluorescence and bright field micrographs of *Anabaena* strains expressing (A) Alr0931-GFP or (B,C) Slr1301-GFP grown on (A) BG11-0 or (B,C) BG11 growth plates. White triangles mark (A) cell envelope and septal accumulations or (B,C) *in vivo* filaments. Blue triangles indicate selected enlarged cells. White stars point to selected focal accumulations of fluorescence signal. White arrows show heterocysts. Scale: 10 μ m.

In summary, Alr0931 tends to associate, species-independently, with cellular envelopes of different bacterial species with certain cytoplasmic localizations. Slr1301 consistently and species-independently formed focal accumulations and filamentous sheets. Expression of Synpcc7942_1139 is often strongly restricted and, if present at all, only envelope-associated patches can be detected. Thus, all obtained *in vivo* results further highlight a functional diversification of homologous proteins and suggest that the expression of Synpcc7942_1139 must be tightly regulated in different cyanobacterial morphotypes.

Homologous proteins show conserved interactions with each other and bind other cytoskeletal proteins

The three homologs form different polymeric structures *in vitro* and show strong self-interaction capabilities in bacterial two-hybrid assays. However, it is still unknown if the homologous proteins have retained the capacity to interact with each other despite their different localization properties. Furthermore, the similar *in vivo* localization signals of Slr1301 and Slr7083 in *E. coli* and *Synechocystis* as well as the comparable *in vitro* assemblies of Synpcc7942_1139 and Synpcc7942_2039 suggest that these proteins might interact with each other. To test this, we performed bacterial two hybrid assays of each homolog looking for cross interactions with each other and with Slr7083 and Synpcc7942_2039.

Alr0931, Slr1301 and Synpcc7942_1139 are all able to interact with each other (Fig. 29A-C). This shows that, despite the apparent evolutionary diversification of homologous IF-like cyanobacterial proteins based on *in vitro* and *in vivo* experiments, the ability to physically interact with one another has still been preserved. Remarkably, and in accordance with previously observed *in vivo* and *in vitro* patterns, we also found positive associations of Slr1301 with Slr7083 (Fig. 29D) as well as Synpcc7942_1139 with Synpcc7942_2039 (Fig. 29E). These results indicate that cyanobacterial cytoskeletal proteins form interconnected cytoskeletal networks.

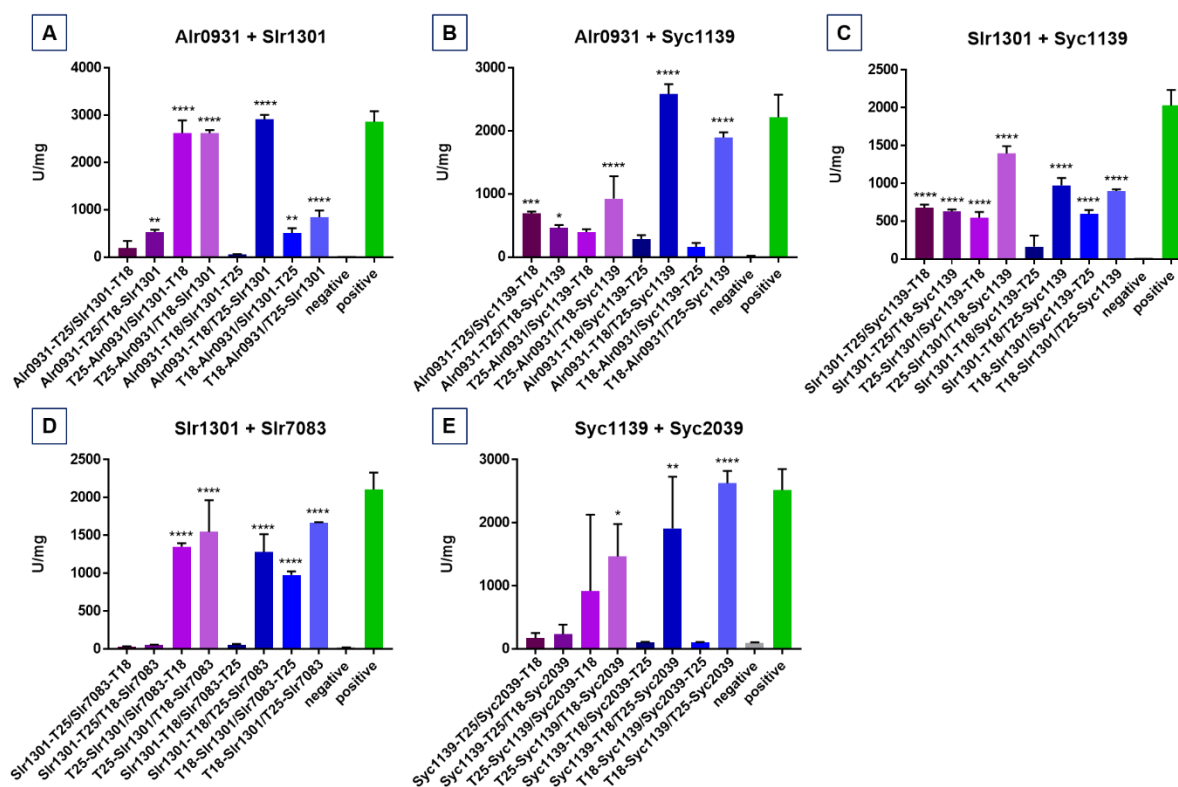


Fig. 29: Homologous proteins interact with each other and other CCRPs

Beta-galactosidase assays of *E. coli* cells co-expressing indicated translational fusion constructs of all possible pairwise combinations of (A) Alr0931+Slr1301, (B) Alr0931+Synpcc7942_1139 (abbreviated Syc1139), (C) Slr1301+Synpcc7942_1139, (D) Slr1301+Slr7083 and (E) Synpcc7942_1139+Synpcc7942_2039 (abbreviated Syc2039). Cells were grown for 2 days at 20 °C. Quantity values are given in Miller Units per milligram LacZ of the mean results from three independent colonies. Error bars indicate standard deviations. Neg: pKNT25 plasmid carrying the respective gene insert co-transformed with empty pUT18C. Pos: Zip/Zip control. *: P < 0.05, **: P < 0.01, ***: P < 0.001, ****: P < 0.0001 (Dunnett's multiple comparison test and one-way ANOVA).

Gene deletions of homologous proteins reveal different levels of essentiality

To gain further information about putative cellular functions, we attempted to generate gene deletions of the homologous proteins by double homologous recombination, replacing the gene with an antibiotic resistance cassette (Allele segregation was evaluated by colony PCR; Figs. S26-28). These strains were then subjected to different viability tests and their respective cellular morphology was explored by microscopy.

The *alr0931* deletion strain shows defects in cell-cell connectivity

The $\Delta alr0931$ strain lost the ability to grow in liquid culture (Fig. 30C). Grown on solid media, $\Delta alr0931$ appeared to grow slower than the wt, however, these observations could not be confirmed by a spot assay. Microscopy analysis revealed that a proportion of cells immediately lysed upon transfer into liquid medium (not shown). Cells were enlarged in volume ($33.956 \pm 11.499 \mu\text{m}^3$ compared to wt $32,794 \pm 15,379 \mu\text{m}^3$; One Way ANOVA using Dunns's test: P < 0.05; white star in Fig. 30B) showed a rounded morphotype (roundness 0.871 ± 0.0996

compared to wt 0.802 ± 0.123 ; One Way ANOVA using Dunns's test: $P < 0.05$) and *Anabaena* trichomes often lost their perpendicular growth pattern, switching to a zig-zag pattern (white triangles in Fig. 30B). To further tackle the function of Alr0931, we performed co-IPs of *Anabaena* cells expressing Alr0931-GFP grown in BG11 and BG11-0 using anti-GFP μ Beads followed by mass spectrometry analysis of co-precipitated proteins (Fig. S29). However, growth of Alr0931-GFP expressing *Anabaena* cells on nitrogen-deprived solid medium (BG11-0) was only tolerated for a few days followed by rapid culture death. Similarly, no growth was observed in BG11-0 liquid medium. Therefore, cultures were raised under non-inducing nitrogen-deprived conditions and protein expression was induced prior to co-IP. We also subjected *Synechocystis* cells expressing Alr0931-GFP to the same analysis. Alr0931-GFP ectopically expressed in *Synechocystis* yielded none but one interactor of interest. We found associations of Alr0931-GFP with Slr1301, thereby confirming our above described interaction tests. The Alr0931-GFP expressing strain grown in BG11 revealed no interactions of interest, however, we were able to identify ParA (AlI1075) and different iron and redox-homeostasis proteins to be associated with Alr0931-GFP in BG11-0 grown cells. We found proteins that were either upregulated (AlI1783 and Alr2783) or downregulated (Alr1144 and Alr2309) in the ferric uptake regulator (FurA) mutant and a significant hit for AlI4145, a putative DNA-binding ferritin-like protein, indicative for a role of Alr0931 in iron homeostasis or transcriptional regulation.

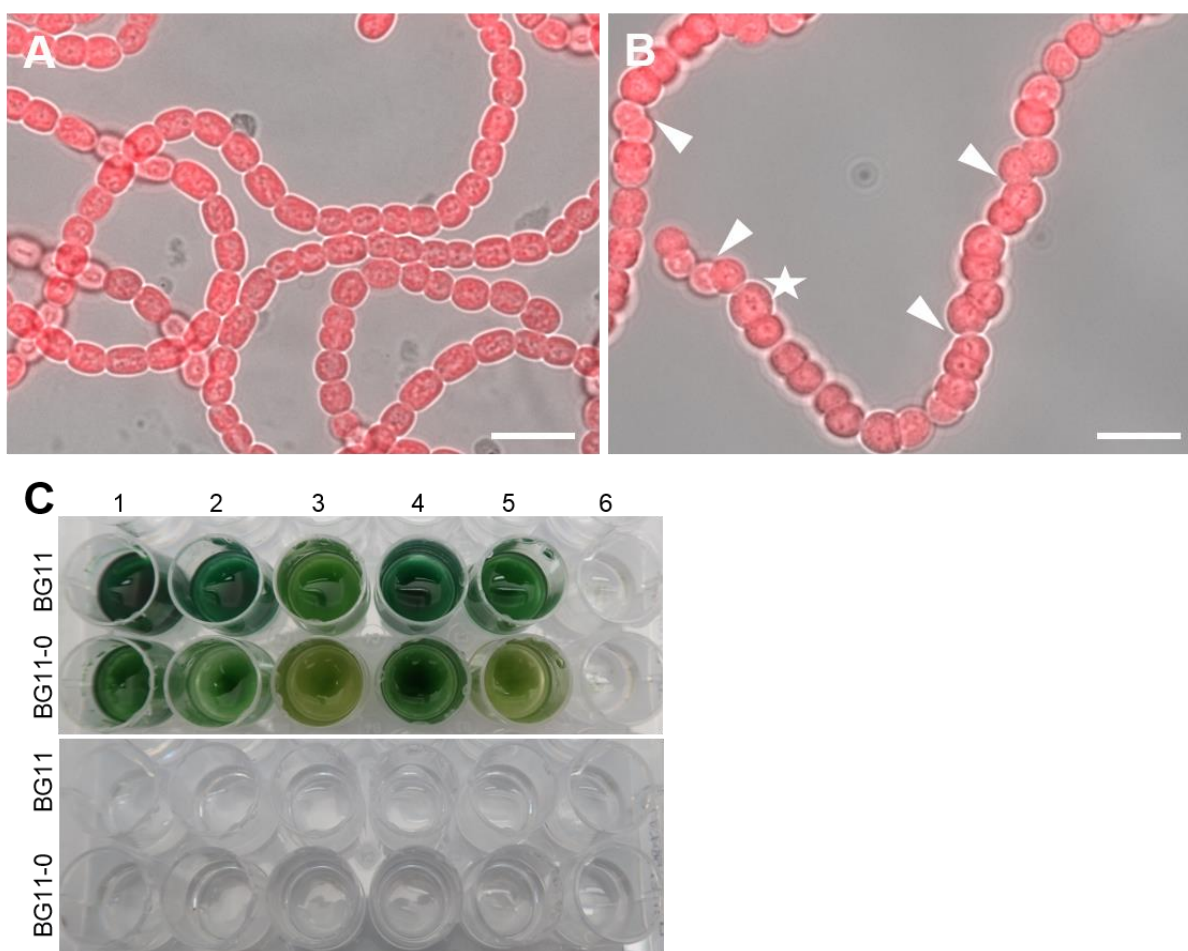


Fig. 30: Phenotypic effects of $\Delta alr0931$ in *Anabaena*

(A,B) Merged bright field and chlorophyll auto-fluorescence of (A) *Anabaena* wt and (B) $\Delta alr0931$ strains grown on BG11 plates. (C) Viability of *Anabaena* wt and $\Delta alr0931$ grown in (1) BG11/BG11-0 or BG11/BG11-0 supplemented with (2) 5 mM glucose, (3) 200 mM glucose, (4) 2 mM NH_4Cl , (5) 200 mM maltose or (6) 500 mM NaCl. White triangles mark zig-zag growth. White star indicates swollen cells. Scale bar: 10 μm .

Gene deletion of *slr1301* impairs cell motility in the motile *Synechocystis* substrain

Morphologically, no difference between the motile and non-motile $\Delta slr1301$ strain was discernable (Fig. 31A-D). However, $\Delta slr1301$ PCC-M completely lost its motility (Fig. 31G). Notably, overexpression of Slr1301-YFP in the PCC-M substrain also led to a decrease in cellular motility (Fig. 31F). Loss of motility was not related to a decrease in viability under standard growth conditions, but $\Delta slr1301$ PCC-M, like $\Delta slr7083$ PCC-M (Chapter 1), was more sensitive to Proteinase K than PCC-M wt (Fig. S30).

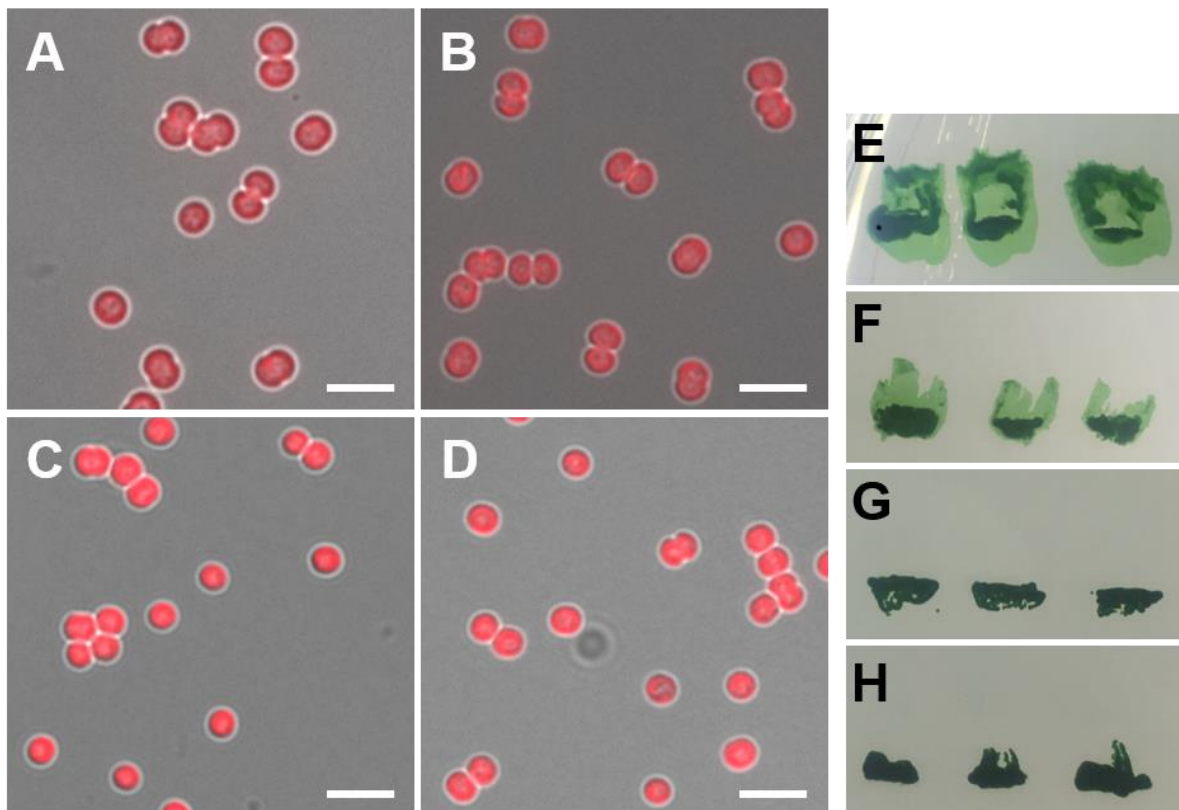


Fig. 31: $\Delta slr1301$ impairs cell motility in the PCC-M substrain

(A-D) Merged bright field and chlorophyll auto-fluorescence of (A) GT-Kazusa wt, (B) $\Delta slr1301$ GT-Kazusa, (C) PCC-M wt and (D) $\Delta slr1301$ PCC-M. (E,F,G,H) Motility test of (E) PCC-M wt, (F) PCC-M expressing Slr1301-YFP, (G) $\Delta slr1301$ PCC-M and (H) GT-Kazusa wt of three single colonies each streaked on a BG11 growth plate and illuminated from only one direction. Scale bars: 5 μ m.

In order to identify putative interaction partners of Slr1301, we performed co-IPs of motile and non-motile *Synechocystis* cells expressing Slr1301-YFP using anti-GFP antibodies and sequenced precipitated proteins by mass spectrometry. Using a PBS-based lysis buffer, Slr1301 was found to associate with Slr0161, a twitching motility protein. In a second sample, using a high salt-containing (500 mM NaCl) lysis buffer, Slr1301 was found to interact with a bandwidth of motility and cytoskeletal proteins. Among those proteins, FtsZ (SII1633), MinD (SII0289) and a Walker-A-type ATPase (Slr0374) as well as two methyl-accepting chemotaxis proteins (McpA and SYNGTS_0624) and PilB, a type IV fimbrial assembly ATPase were

identified. Taken together, Slr1301 is essential for twitching motility in the PCC-M substrain, possibly through direct interaction with pili and chemotaxis proteins and might be linked to the FtsZ cytoskeleton. Unfortunately, due to cross contaminations, co-IP samples from motile PCC-M substrain expressing Slr1301-YFP were unusable.

Non-segregated Δ *synpcc7942_1139* reveals an impairment in colony cohesion

Attempting to generate *synpcc7942_1149* mutants by double homologous recombination always resulted in a high transformation efficiency. After one round of re-streaking on selective media, all colonies displayed notorious changes in colony morphology and viability (Fig. S31), suggesting these were fully segregated gene deletion strains. However, colony PCR revealed that all these strains still retained at least one copy of the *synpcc7942_1139* allele (Fig. S28B). Therefore, and to avoid a reversal to wt genotype, non-segregated Δ *synpcc7942_1139* was always grown in the presence of kanamycin. Epifluorescence microscopy of DAPI-stained cells showed that non-segregated Δ *synpcc7942_1139* cells were elongated ($4,665 \pm 1.762 \mu\text{m}$, $n=417$ compared to wt cells with $3,156 \pm 0.74 \mu\text{m}$, $n=648$, unpaired t-test: $P < 0.0001$; Fig. S32) and that many cells lacked cellular DNA (white stars in Fig. 32B) or chlorophyll autofluorescence (white arrows in Fig. 32B), reminiscent of Δ *synpcc7942_2039* cells (Chapter 1). This suggests that decreasing levels of *Synpcc7942_1139* impair proper cell division. We addressed a putative deficiency of septum site-determination through altered Z-ring placement by immunofluorescence but found no alterations in the localization of FtsZ (Fig. S33). Brightfield microscopy of wt and non-segregated mutants revealed a loss of proper cell network connectivity and a failure to form round colonies (Fig. 32C,D). The cellular and colony morphotypes were observed in all PCR-validated non-segregated Δ *synpcc7942_1139* clones. Additionally, non-segregated Δ *synpcc7942_1139* failed to grow in liquid media (Fig. 32E) and showed decreased cell viability in spot assays (Fig. S34). Colonies required at least ten times longer to grow to a discernible size and were unable to grow in the presence of Lysozyme (Fig. S34C). Taken together, these results show that the cellular integrity, the intercellular connectivity and the colony formation of non-segregated Δ *synpcc7942_1139* cells is strongly impaired. We also attempted to sequence interactors of *Synpcc7942_1139*-GFP by mass spectrometry of co-precipitated proteins, however, as a result of a cross contamination, these samples could not be used.

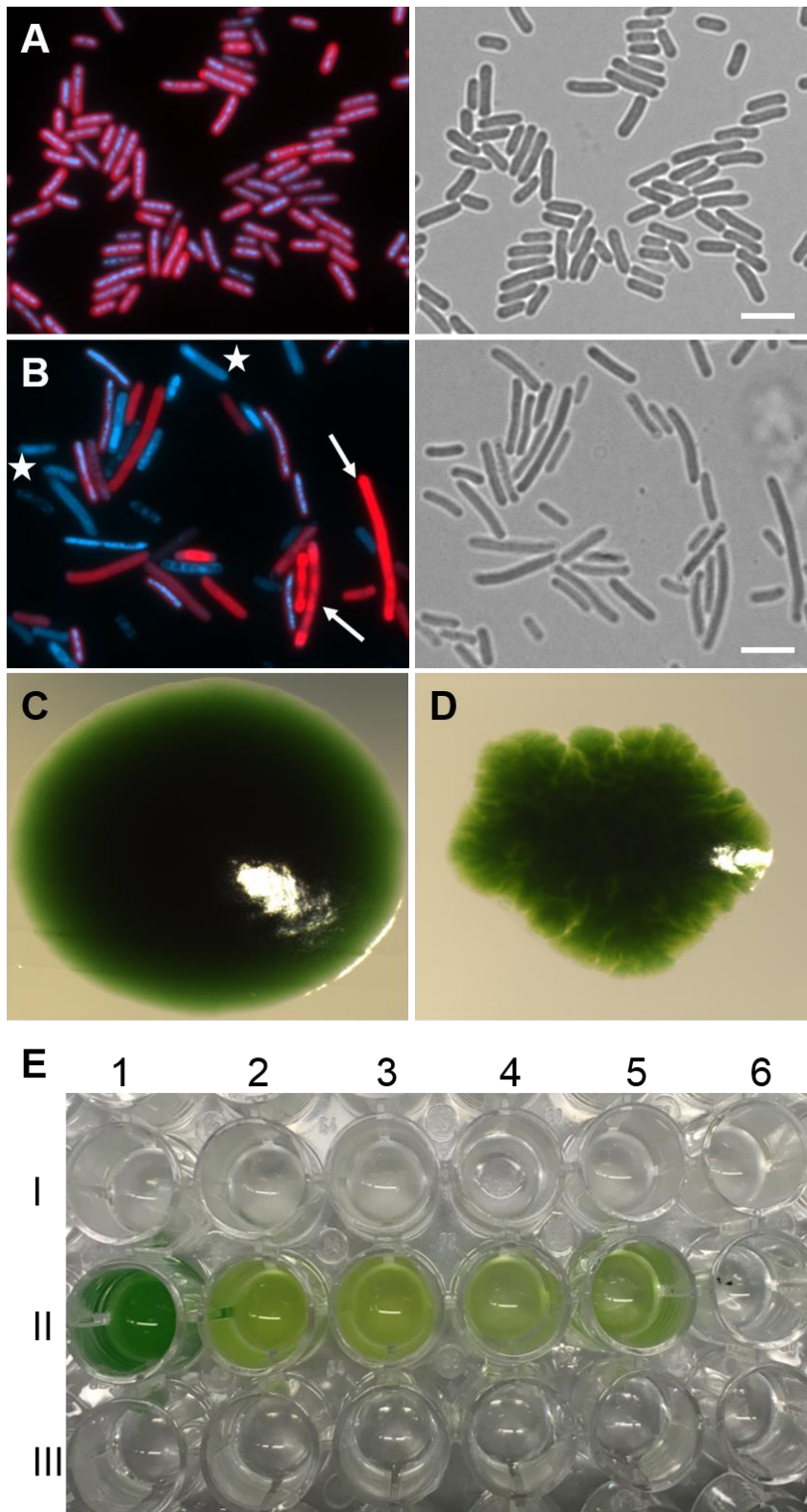


Fig. 32: Non-segregated $\Delta\text{synpcc7942_1139}$ displays decreased culture viability

(A,B) Bright field and merged DAPI fluorescence and chlorophyll auto-fluorescence of (A) *Synechococcus* wt and (B) non-segregated $\Delta\text{synpcc7942_1139}$ strains stained with $10\ \mu\text{g ml}^{-1}$ DAPI. (C,D) Colony morphology of (C) *Synechococcus* wt and (D) non-segregated $\Delta\text{synpcc7942_1139}$ grown on (C) BG11 or (D) BG11 supplemented with kanamycin ($50\ \mu\text{g ml}^{-1}$) growth plates. (E) Cell viability of *Synechococcus* (II) wt and (I,III) non-segregated $\Delta\text{synpcc7942_1139}$ grown in (1) BG11 or BG11 supplemented with (2) 5 mM glucose, (3) 200 mM glucose, (4) 2 mM NH_4Cl , (5) 200 mM maltose or (6) or 500 mM NaCl. White arrows indicate selected cells without cellular DNA. White stars mark selected chlorophyll-lacking cells. Scale bars: 5 μm .

8.4 Discussion

We have identified a group of 168 homologous cyanobacterial CCRPs that are present in all cyanobacterial subsections and further functionally characterized three of those proteins from *Synechocystis*, *Synechococcus* and *Anabaena* using *in vitro* and *in vivo* approaches. Our goal was to analyze if members of this homologous group are IF-like cytoskeletal proteins and whether they have retained similar functional and structural properties across the different species or if they have evolved in a species-specific manner. Furthermore, we wanted to evaluate whether their presumed cytoskeletal properties are regulated by other species-specific accessory or cytoskeletal proteins. The I-TASSER tool reliably predicted all three investigated CCRPs with similarities to the bacterial cell division protein EzrA, which was also predicted for CreS from *C. crescentus* (Chapter 1), providing a first clue for an IF-like function. With a sequence conservation of about 39%, homologous CCRPs fit into the framework of the metazoan IF protein conservation (Fuchs and Weber, 1994; Schaffeld *et al.*, 2001). Using the COILS algorithm, Bagchi *et al.* (2008) identified a group of homologous CCRPs of Actinomycetes with a conserved sequence motif. Three of them were identified as IF-like proteins although, information about the exact level of sequence conservations are not available. Besides the moderate sequence identity of the cyanobacterial group of homologous CCRPs, members of this group vary evidently in coiled-coil motif count and length of the individual domain (Chapter 1). It is therefore not surprising that the three studied members of this group polymerized each into entirely different structures *in vitro*. This already indicates a functional diversification of these proteins. For Alr0931, we observed two polymerization states. In a near-physiological buffer system (pH 7.4) Alr0931 formed a strongly interconnected filamentous network, while short and abundant polymers were identified in a slightly more acidic buffer system (pH 7.0). These polymeric structures resemble the protein filamentation pattern of bactofilins (Kühn *et al.*, 2010; Lin and Thanbichler, 2013). It is hence possible that Alr0931, like BacA and BacB, evolved to fulfill scaffolding functions within *Anabaena* cells. Like Alr0931, albeit to a vanishingly low amount, Slr1301 formed small and short filaments, questioning Slr1301's general IF-like properties. However, bacterial two hybrid assays revealed a high degree of self-binding affinity for Slr1301, suggesting that a suitable *in vitro* polymerization buffer system remains to be identified. A high self-interaction affinity was also quantified for Alr0931 and Synpcc7942_1139, further strengthening a putative IF-like function for this group. Reminiscent of the cell envelope-like filaments formed by Synpcc7942_2039 (Chapter 1), Synpcc7942_1139 assembled into the same structures *in vitro*, albeit to a much higher degree and without any discernible protein aggregates. Taking into account that we had to purify Synpcc7942_2039 from *Synechococcus* cells, since we could not overexpress it in *E. coli* (Chapter 1), it is possible that the observed Synpcc7942_2039 envelope-like filaments rather constitute co-precipitated and polymerized Synpcc7942_1139. A reasonable argument

for this hypothesis is that Synpcc7942_1139 alone showed the intrinsic ability to form polymers *in vitro*. This was not the case for Synpcc7942_2039. However, considering Synpcc7942_2039's self-binding capacity (Chapter 1) we cannot rule out that Synpcc7942_2039 co-polymerized with or on Synpcc7942_1139 sheets. This assumption is supported by the identified physical interaction between Synpcc7942_1139 and Synpcc7942_2039, suggesting that those two form a connected cytoskeletal network of at least two CCRPs in *Synechococcus*. The observed interaction of Slr1301 with the plasmid-encoded IF-like CCRP Slr7083 (Chapter 1), strengthens the idea that cyanobacterial CCRPs bind each other in order to form multi-protein cytoskeletal complexes. This would allow similar regulatory mechanisms as observed for the interconnected eukaryotic cytoskeleton (Herrmann and Aebi, 2000; Green *et al.*, 2005; Alberts *et al.*, 2014). The specific interaction of Slr1301 and Synpcc7942_1139 with two other species-specific CCRPs identified in Chapter 1 (Slr7083 and Synpcc7942_2039, respectively) reveals that species-specific functional adaption in cyanobacteria does not only comprise the group of homologous CCRPs but also their species-specific accessory proteins. Similarly, Alr0931 and Slr1301 were found to interact with entirely different cellular proteins, giving rise to the idea that the whole cytoskeletal network, including non-cytoskeletal accessory proteins, plays a crucial role for the properties of the cellular cytoskeleton. Notably, and despite their different *in vitro* and *in vivo* properties, all three homologous proteins were able to bind each other. Further studies could focus on identifying the amino acid sequences that mediate this prevailed interaction, likely residing within the highly conserved amino acid sequence motifs identified in this group. In fact, none of the homologous proteins showed any discernable expression upon N-terminal YFP translational fusion, reminiscent of the essential function for oligomerization of the N-terminal head domain of eukaryotic IF proteins (Heins and Aebi, 1994; Herrmann *et al.*, 1996) and CreS from *C. crescentus* (Cabeen, Herrmann and Jacobs-Wagner, 2011). An indispensable function for polymerization of the N-terminus for this group of homologous CCRPs is also in agreement with their highly conserved N-terminal head domain, indicating that specifically this part of the proteins is indispensable for protein function. The tail domain of eukaryotic IF proteins, however, is mainly involved in the limitation of lateral associations and thus defining the 10 nm width of IF proteins but not affecting the general assembly property (Nakamura *et al.*, 1993). Therefore, it is not surprising that we obtained functional C-terminal translational fusion constructs of the three CCRPs. Consequently, it is conceivable that the identified functional diversification of the three studied proteins relies on the variable and non-conserved amino acid sequences identified in this group. These regions are putatively employed by other species-specific proteins, ultimately regulating their cellular features. Moreover, this implies that the conserved IF-like properties of this group (*in vitro* and *in vivo* polymerization), are

dependent on their conserved sequence motifs. Therefore, it is likely that these conserved motifs also mediate the interaction of the three CCRPs with each other.

Cyanobacterial homologous CCRPs perform different cellular tasks

We obtained further important clues for a functional diversification from *in vivo* studies. These revealed alternative localization patterns for the homologs in varying organisms. Alr0931-GFP was either uniformly distributed throughout the cells or localized to the cell envelope in stationary phase cultures, suggesting that Alr0931 localization to the membranes is growth stage dependent and likely relies on other so far unidentified interaction partners. Growth of Alr0931-GFP expressing *Anabaena* cultures was inhibited in nitrogen-deprived liquid growth medium and cells had to be pre-cultivated under non-inducing conditions before protein expression could be induced. Furthermore, Alr0931-GFP was restricted from heterocysts, but RNA data did not reveal any differences in the expression pattern of *alr0931* under different growth conditions. A direct involvement in heterocyst formation is thus unlikely and overexpressed Alr0931 might rather constitute a steric hindrance that hamper proper cell-differentiation or cell-cell communication. Like eukaryotic IF-proteins, a scaffolding function for Alr0931 is thus possible (Green *et al.*, 2005). $\Delta alr0931$ revealed detrimental defects in cell viability and trichome integrity, with cells showing a zig-zag-like growth pattern and an increase in cell roundness and cell volume. This suggests that Alr0931 is involved in intercellular trichome stability. The inflated and round cell phenotype resembles $\Delta mreB$ *Anabaena* strain (Hu *et al.*, 2007), providing supportive evidence for a cytoskeletal function of Alr0931 as a cell shape-determining protein. Since the MreB-driven elongasome is responsible for the peptidoglycan (PG) synthesis (Errington and Wu, 2017), it is also conceivable that Alr0931 performs a similar function or is at least partially involved in PG synthesis. Pulldown experiments of Alr0931-GFP identified various proteins involved in iron homeostasis and transcription (Oliveira *et al.*, 2015; González *et al.*, 2016), and although IF proteins were long thought to only provide structural properties to the cells, it is now evident that IF proteins function also as signal transducers (Eriksson *et al.*, 2009). Consequently, Alr0931 scaffolds might signal in response to changing iron concentrations to downstream molecules, possibly resulting in a change in their own abundance by altered *alr0931* expression (negative or positive feedback loop). Alternatively, they could provide an anchoring platform for other proteins that are involved in iron homeostasis. Comparative transcriptomic or proteomic data of the *alr0931* gene deletion strain will provide further insights into this uncertainty. Considering a missing structure-providing scaffold within $\Delta alr0931$ cells, it is not unprecedented that the inflated phenotype is the result of a decreased resistance of the cells to the turgor pressure. In *Streptomyces spp.*, turgor pressure was shown to affect the distribution of CCRPs revealing a significant impact of the external environment on the intracellular organization (Fuchino *et al.*,

2017). Among others, turgor pressure affects the cell shape and cellular mechanical resistance-providing cytoskeletal systems (Fuchino *et al.*, 2017). The notion that $\Delta alr0931$ is sensitive to extracellular influence was further supported by its inability to grow in liquid culture, possibly as this strain is no longer able to cope with the elevated fluid shear stress (FSS) imposed on cells grown in liquid cultures (Joshi, Elias and Patole, 1996). FSS, like turgor pressure, induces cell shape modifications due to a remodeling of the cytoskeleton (Malek and Izumo, 1996). Therefore, the lack of a mechanical resistance-providing cytoskeletal scaffold in the $\Delta alr0931$ strain might cause the combined deficiency to FSS and turgor pressure ultimately resulting in the observed aberrant phenotype.

In contrast to the observed negligible *in vitro* filamentation capacity of Slr1301, *in vivo* localization studies revealed filamentous structures in *Synechocystis* and *Anabaena*, albeit the majority of Slr1301 formed focal accumulations. Interestingly, single protein filaments were only observed in *Anabaena* or upon heterologous expression of Slr1301-YFP in the motile PCC-M substrain and not in the non-motile GT-Kazusa strain. This is indicative for an involvement of Slr1301 in cell motility. It is also in accordance with previous studies by Bhaya *et al.* (2001) who identified $\Delta slr1301$ as a non-motile strain. However, no further experiments were performed to identify the nature of this loss of function. We created gene deletion strains of the GT-Kazusa and the PCC-M substrain and observed no phenotypic changes in any of them, revealing that Slr1301 is not directly involved in cell shape determination. We confirmed the non-motile nature of the $\Delta slr1301$ strain by motility assays and identified twitching motility proteins as Slr1301 interactors, for which Slr1301 could function as a stabilizing or scaffolding structure. So far it is unknown how photoreceptors transduce the perceived light stimuli to the motility apparatus in *Synechocystis* ultimately resulting in phototactic movements (Schuergers, Mullineaux and Wilde, 2017). The missing link between the two systems could be provided by the Slr1301 cytoskeleton. This hypothesis is supported both by the physical interaction of Slr1301 with PilB in a pulldown experiment and with the focal accumulations and crescent-shaped signals of Slr1301-GFP, specifically in the PCC-M substrain. This localization strikingly resembles the PilB-GFP localization in *Synechocystis* (Schuergers *et al.*, 2015). In a similar manner, FimL (a proposed scaffolding protein) was shown to connect the chemosensory receptor system to the type IV pili apparatus, regulating the chemotactic and virulence pathways in *Pseudomonas aeruginosa* (Inclan *et al.*, 2016). If Slr1301 in fact constitutes a relay station between the photoreceptors and the motility apparatus, it would imply certain signal transduction properties of Slr1301, reminiscent of the signaling roles of eukaryotic IF proteins (Eriksson *et al.*, 2009). Cellular motility of eukaryotic cells is strongly dependent on the cytoskeleton (Cappuccinelli, 1980), thus it is not unprecedented that the cytoskeleton is a key factor for cell movements in prokaryotes as well. Although, IFs do not directly participate in cell motility in eukaryotes (Lodish *et al.*, 2000), an adaptation of CCRPs in prokaryotes for

this task is imaginable. Bactofilins constitute a separate class of prokaryotic-specific cytoskeletal proteins and were proposed to be involved in social motility in *Myxococcus xanthus* (Kühn *et al.*, 2010). The interaction of Slr1301 with twitching motility proteins was prevailed in the non-motile GT-Kazusa strain, hinting for additional beneficial functions of this interaction besides motility. Otherwise, this interaction would have likely been lost during evolution. Based on the interaction of Slr1301 with Slr7083, Slr1301 could also be involved in cellular rigidity and resistance to deformation, reminiscent of FilP (Chapter 1; Bagchi *et al.*, 2008). In harmony with a physical interaction of Slr1301 with Slr7083, we also observed sheet-like Slr7083-YFP filaments within *Synechocystis*, providing further evidence for a cytoskeletal network of both proteins in *Synechocystis*. The $\Delta slr7083$ PCC-M strain revealed increased sensitivity to Lysozyme (Chapter 1), which was not the case for the $\Delta slr1301$ PCC-M. Thus suggests that Slr1301, unlike Slr7083, is not directly involved in cell wall integrity. The $\Delta slr7083$ and $\Delta slr1301$ GT-Kazusa strains both showed higher sensitivity to Proteinase K, demonstrating that both proteins might somehow regulate membrane protein localization or constitution in *Synechocystis* (Besingi and Clark, 2015). In Chapter 1, we showed that $\Delta slr7083$ had reduced motility. In the light of the interaction with Slr1301, a coordinated action of both, Slr7083 and Slr1301, seems to be important for motility in *Synechocystis*. In further support for a cytoskeletal function of Slr1301, we observed an inflated *Anabaena* phenotype upon overexpression of Slr1301-GFP, reminiscent of the irregular *Anabaena* cells observed in the MreBCD overexpression strain (Hu *et al.*, 2007). Whether this phenotype is the result of an inflated intracellular cytoskeleton remains to be elucidated.

Like Alr0931, fluorescently tagged Synpcc7942_1139 was shown to be associated with the cell envelope which is in concert with the identified cell envelope-like *in vitro* structure. It suggests that Synpcc7942_1139 performs cell shape-determining or cell-protective functions. Although, *in vivo* studies did not reveal a complete coating of the inner membrane but rather patchy spots at different membrane sites. The absence of any discernible expression of Synpcc7942_1139-GFP in *Anabaena* and only minor expression levels in *Synechocystis* and *Synechococcus* indicates that the abundance of Synpcc7942_1139 must be tightly regulated and is detrimental to multicellular cyanobacteria or harmful at higher cellular concentrations. Notably, no such detrimental influences were detected for the other two proteins. Removal of *alr0931* impaired trichome integrity and disabled growth in liquid culture while gene deletion of *slr1301* merely abrogated cellular motility and only slightly affected cellular viability. The inability to create a *synpcc7942_1139* gene deletion strain demonstrates an entire different level of significance of this protein for *Synechococcus* viability. Even non-segregated $\Delta synpcc7942_1139$ cells displayed tremendous impairments in cell growth, cell viability and colony integrity. Non-segregated $\Delta synpcc7942_1139$ cells are highly sensitive to Proteinase K, indicating a protective role of Synpcc7942_1139 by possibly providing a protease-resistant

proteinaceous layer. A comparable resistance has also been described for the pathogenic PrP (prion protein) that exhibits a partial resistance to proteolytic degradation in its polymeric state (Cronier *et al.*, 2008). A protective and stabilizing protein layer function is also supported by the distorted colony morphology of non-segregated $\Delta\text{synpcc7942_1139}$ mutants, resembling the colony phenotype Slr7083-GFP overexpressing colonies (Chapter 1). This observation could be also explained by the adherence of colony formation-supporting proteins to the Synpcc7942_1139 sheet. Thus, the sheet would function as a signal transduction platform for the cell in order to control colony growth through interaction with the extracellular space. This would be in agreement with the signal transduction function of eukaryotic IF proteins (Eriksson *et al.*, 2009). In metazoans, cell-cell and cell-matrix interaction is a cytoskeleton-controlled process by means of junctional complexes, the so called desmosomes and hemidesmosomes (Alberts *et al.*, 2014). Non-segregated $\Delta\text{synpcc7942_1139}$ mutants exhibit an elongated phenotype with a distorted distribution of DNA and chlorophyll, however no alteration of the Z-ring was detected. This elongated phenotype could also be due to a disturbed MreB-driven elongasome, which is no longer properly regulated by contact inhibition, by for example Synpcc7942_1139 sheets. This could then lead to uncontrolled PG synthesis and hence longer cells. Such a connection of the IF-like cytoskeleton to the MreB cytoskeleton was shown to be responsible for the cell shape-determining mechanical properties of CreS filaments in *C. crescentus*, revealing a joint collaboration of two cytoskeletal systems for cellular morphology (Charbon, Cabeen and Jacobs-Wagner, 2009). Future studies will attempt to unravel this presumed connection of the cyanobacterial IF-like cytoskeleton to the MreB cytoskeleton. Since MreB is absent from *Synechocystis* (Hu *et al.*, 2007), it is possible that other species-specific proteins have evolved a collaborative function with Slr1301 apart from MreB. Future studies shall also aim to elucidate a potential interplay between Alr0931 and MreB in *Anabaena*.

Here, we characterized three proteins from a homologous group of cyanobacterial CCRPs that differ in cellular localization, cellular function, *in vitro* polymerization and the level of essentiality. Our obtained results indicate that these proteins have undergone species-specific evolution. Additionally, we identified different species-specific interactors of cytoskeletal and non-cytoskeletal origin for these proteins that highlight the importance of a cytoskeletal network for proper cytoskeletal function. Our study shows that not only the respective function of a single protein is relevant, but that the entire proteinaceous context has to be considered. Thus, this study provides valuable insights into the essential interplay of different cellular components in prokaryotes, reminiscent of the crucial role of accessory proteins for the eukaryotic cytoskeleton.

9 Chapter III: A cytoskeletal network stabilizes cell-cell connections in the multicellular cyanobacterium *Anabaena*

9.1 Abstract

The eukaryotic cytoskeleton is a highly interconnected network of different polymeric fibers that are linked to each other and that stabilize and orchestrate junctional complexes. In prokaryotes, similar interconnected cytoskeletal systems can be detected in the divisomes, elongasome and polarisomes which are dependent on the actions of the prokaryotic homologs to microtubules, actin filaments and intermediate filaments (IFs). The polarisome of *S. coelicolor* is, among others, composed of three IF-like coiled-coil rich proteins (CCRPs) which govern polar hyphal growth. In the multicellular cyanobacterium *Anabaena*, parts of the septosomes, a gap-junction-like pore complex, are composed of SepJ whose localization is dependent on the FtsZ-driven divisome. However, the underlying mechanisms that stabilize these cell-cell connections are still to be elucidated. Here we describe three cyanobacterial IF-like CCRPs whose polymers form an interconnected cytoskeletal network that stabilizes the *Anabaena* trichome through direct interactions with the septosomal complex. Alr4504 and Alr4505 jointly form cell-traversing polymers that anchor to the scaffolding protein Alr0931 and the septosomal protein SepJ, thereby connecting the two opposite cell poles and neighboring cells. Strains lacking either Alr0931 or Alr4504 and Alr4505 show severe growth impairments in liquid culture and cells in a trichome lose their perpendicular growth pattern. Additionally, the presence of both Alr4504 and Alr4505 is required for *in vitro* polymerization. We thus propose that this cytoskeletal network is an essential system for the development of multicellularity in cyanobacteria.

9.2 Introduction

The divisome, the elongasome and the polarisome are prokaryotic cell wall modulation machineries that mediate cell division, cell elongation and polar cell growth, respectively (Lin and Thanbichler, 2013; Löwe and Amos, 2017). These major cellular tasks are executed by multi-protein complexes that rely on the actions of cytoskeletal elements to govern the precise localization of peptidoglycan (PG) synthesis and integration (Lin and Thanbichler, 2013; Löwe and Amos, 2017). The divisome machinery assembles upon Z-ring formation of polymerized FtsZ monomers at future septum sites and is comprised of numerous proteins including membrane-tethering proteins FtsA and ZipA. These link the Z-ring to the cell membrane and recruit other downstream proteins like the transmembrane protein FtsN that constitutes the last essential component of the divisome and initiates the PG synthesis (reviewed by Löwe & Amos, 2017). Similar to the Z-ring formed by FtsZ, FtsA, a member of the actin superfamily, can form actin-like polymeric protofilaments by binding to the lipid bilayer by means of its

amphipathic C-terminus (Szwedziak *et al.*, 2012). The resulting A-ring or short stretches of polymerized FtsA bind to the C-terminus of FtsZ and this bilateral interaction is sufficient for FtsZ treadmilling (Loose and Mitchison, 2014). Although the precise mechanism for cell constriction is still under debate, it is known that the process of cell division in prokaryotes is a finely tuned process and depends on the tubulin-like cytoskeleton (Wagstaff and Löwe, 2018). Similarly, cell elongation driven by the elongasome is dependent on the action of the actin-like cytoskeletal protein MreB whose filaments are circumferentially directed around the cell in a patchy pattern by the motor activity of the PG synthesis machinery (Swulius and Jensen, 2012; Wagstaff and Löwe, 2018). The elongasome comprises functional analogs of divisome components and several penicillin-binding proteins (PBPs) and it was further shown that MreB directly interacts with FtsZ in *E. coli*, thereby providing a direct link of the two cytoskeletal systems in prokaryotes (Typas *et al.*, 2012; Fenton and Gerdes, 2013). The joint action of MreB and FtsZ is essential for cell division, possibly due to the MreB-mediated transfer of several PBPs to the divisome (Fenton and Gerdes, 2013). The polarisome of *S. coelicolor* is another prominent prokaryotic example for a multi-protein complex governed by the action of at least three intermediate filament (IF)-like coiled-coil rich proteins (CCRPs) - called DivIVA, Scy and FilP - that together orchestrate proper polar hyphal growth (Lin and Thanbichler, 2013). Unlike eukaryotic IF proteins, these three CCRPs exhibit unconventional rod-domain architectures and do not follow the typical coiled-coil repeat pattern (Coil 1A, 1B and 2), although all of them form filaments *in vitro* and *in vivo* and regulate cell morphology (Stahlberg *et al.*, 2004; Bagchi *et al.*, 2008; Holmes *et al.*, 2013; Kelemen, 2017). The function of the filament-forming protein DivIVA varies among different bacterial species and often determines future septum sites in cooperation with the MinCDE system (Lin and Thanbichler, 2013). DivIVA functions as a polar tip-associated scaffold for the PG synthesis machinery in *S. coelicolor* (Lin and Thanbichler, 2013). The localization of DivIVA is controlled by the comparably large CCRP Scy (1326 amino acids) which, together with FilP - a protein that contributes to hyphal stiffness - and a cellulose synthase forms the polarisome and organizes polar extension in *S. coelicolor* (Lin and Thanbichler, 2013). These examples show that essential prokaryotic multi-enzyme complexes are governed, controlled and guided by several cytoskeletal proteins reminiscent of their eukaryotic counterparts. The multicellular cyanobacterium *Anabaena*, often used to study nitrogen fixation, has recently gained more attention as septosomes, prokaryotic pore-complexes, resembling eukaryotic gap-junctions, were discovered and found to enable cell-cell communications (Flores *et al.*, 2016). So far, three integral membrane proteins (SepJ, FraC and FraD) were identified to modulate septosomal structures and are thought to form the identified pore complexes that span the PG layer of two neighboring cells (Flores *et al.*, 2016). SepJ forms multimers reminiscent of the hexamer formed by connexin proteins in gap junctions (Alberts *et al.*, 2014; Ramos-León *et*

al., 2017). The localization of SepJ is dependent on the FtsZ-driven divisome but no physical interaction of SepJ and FtsZ was identified (Ramos-León *et al.*, 2015). It has been shown that in the absence of SepJ, FraC and/or FraD *Anabaena* trichomes fragment which stresses the major importance of septosomal integrity for trichome stability in *Anabaena* (Nürnberg *et al.*, 2015). In eukaryotes, cellular junctions are essential communication and interaction platforms that establish the linkage between neighboring cells in a tissue as well as to the extracellular surroundings, enabling the sensing of the environment (Alberts *et al.*, 2014). This connection is mediated and stabilized by the actin cytoskeleton and IF proteins that are linked to special junctional multi-protein complexes by cytolinker proteins like plakins or catenins (Alberts *et al.*, 2014). However, unlike in eukaryotes, so far, no direct cytoskeletal interactions were discovered in cyanobacterial septosomes and it is unclear how SepJ and other pore-complex proteins are transported to and maintained at the cell septa. Here we study the trichome integrity-maintaining effect of CCRPs in *Anabaena* and investigate the extent of a putative septosome-associated IF-like cytoskeletal network.

9.3 Results

We have previously identified 21 putative IF-like CCRPs in cyanobacteria (Chapter 1). In this chapter, we further characterize in *Anabaena* four proteins that are conserved across the cyanobacterial phylum: Alr4504, Alr4505, Alr0931 and All2460. We investigate their involvement in the manifestation of a cytoskeletal network that stabilizes cell-cell connections within the *Anabaena* trichome. For this purpose, protein localization experiments as well as various protein-protein interaction assays were applied, and gene deletion strains were generated.

Conservation and structure of cyanobacterial IF-like CCRPs

Alr4504 and Alr4505 homologs are present in all cyanobacterial subsections (Chapter 1) and exhibit similar levels of sequence similarity to their respective homologs (~55%). On the genome, *alr4504* and *alr4505* reside on the same strand and are only separated by 39 bp, suggesting that both genes may be transcribed as an operon or perform their functions in a cooperative manner. To test this, we performed RT-PCR from whole RNA isolated from *Anabaena* cells grown in BG11 and BG11-0 using primers encompassing both genes and each single gene. No common transcript could be detected by this approach while transcripts for each single gene were obtained under nitrogen-deprived growth conditions (Fig. S35). Consistent with these results, *in silico* analysis of the upstream regions of *alr4504* and *alr4505* identified two promoter regions for each gene (Fig. S36). The predicted promoters for *alr4505* both at least partially resided within the *alr4504* open reading frame (Fig. S36). The genomic environment upstream of *alr4504* includes a predicted histidine kinase and a two-component

system response regulator while the *alr4505* downstream region encodes a gene involved in the histidine biosynthesis pathway and a hypothetical DUF3593 domain-containing protein. Protein structure predictions by I-TASSER and the domain prediction by the NCBI conserved domain tool (NCBI CDS) revealed similarities of Alr4504 and Alr4505 to cell division, cytoskeletal and cytoskeleton-related proteins. The structure of Alr4504 is similar to plectin, a crucial cytolinker protein of the IF protein desmin in myofibers (Goldmann, 2018), Alr4505's predicted structure is similar to the cytoplasmic domain of the bacterial cell division protein EzrA. I-TASSER prediction of CreS also revealed similarities to EzrA. Both Alr4504 and Alr4505 have a conserved SMC_N domain associated to structural maintenance of chromosomes (SMC) while Alr4505 has an additional DUF3552 domain.

All2460, like Alr4504 and Alr4505, is present in all cyanobacterial subsections and shows a medium level of sequence identity with its homologs (51%). In many species, *all2460* homologs are encompassed by genes encoding for a member of the large family of P-loop NTPases (comprising the cytoskeletal class of Walker A Cytoskeletal ATPases, among others) and a biotin carboxylase. This is reminiscent to the genomic surrounding of *all4981* (Chapter 1). Even though All2460 consists of several coiled-coil domains (Chapter 1) and its I-TASSER-based predictions revealed similar properties to CreS, it is unlikely that All2460 has an IF-like function as two N-terminal transmembrane domains were predicted (Fig. S37), and up to this date, no IF-like protein containing a transmembrane domain has been described.

Interdependence of Alr4504 and Alr4505 for *in vitro* polymerization

The genomic localization of *alr4504* and *alr4505* tempted us to investigate whether both proteins might directly interact with each other. To explore the putative filamentation capability of both proteins *in vitro*, Alr4504 and Alr4505 bearing a C-terminal His6-tag were purified under denaturing conditions and then allowed to renature by dialysis. Protein filamentation was assessed by epifluorescence microscopy of NHS-Fluorescein-labeled and renatured proteins.

Epifluorescence micrographs revealed that Alr4504 and Alr4505 assembled into different structures when subjected to renaturing conditions. Alr4504 formed distinct round or tunnel-like structures with a rather even spacing between each single structure which never overlapped or assembled into higher-order complexes (Fig. 33A). In contrast, Alr4505 formed huge multidimensional sheath-like structures upon renaturation into a non-salt-containing buffer (Fig. 33B) that were even visible by bright field microscopy (Fig. S38A). Albeit considerably less coordinated with visibly high amount of protein aggregates in the sample, similar Alr4505 filaments were also obtained in a salt-containing Hepes polymerization buffer (HLB) (Fig. S38B). Remarkably, co-purification/renaturation of Alr4504 and Alr4505 resulted in ring-like filaments which were traversed by smaller single filamentous strings (Fig. 33C)

comparable to the membrane skeleton of red blood cells (Fowler, 2013). The size of these structures was markedly smaller than those from Alr4505 alone but had about the same size as Alr4504 structures. However, besides these filamentous structures, a substantial amount of co-purified Alr4504 and Alr4505 formed aggregates (not shown), indicating that optimal buffer conditions remain to be elucidated. The obtained results indicate that the presence of both Alr4504 and Alr4505 is required for the more sophisticated *in vitro* polymerization into filaments. Nonetheless, Alr4505 appears to bear a certain filament-forming property.

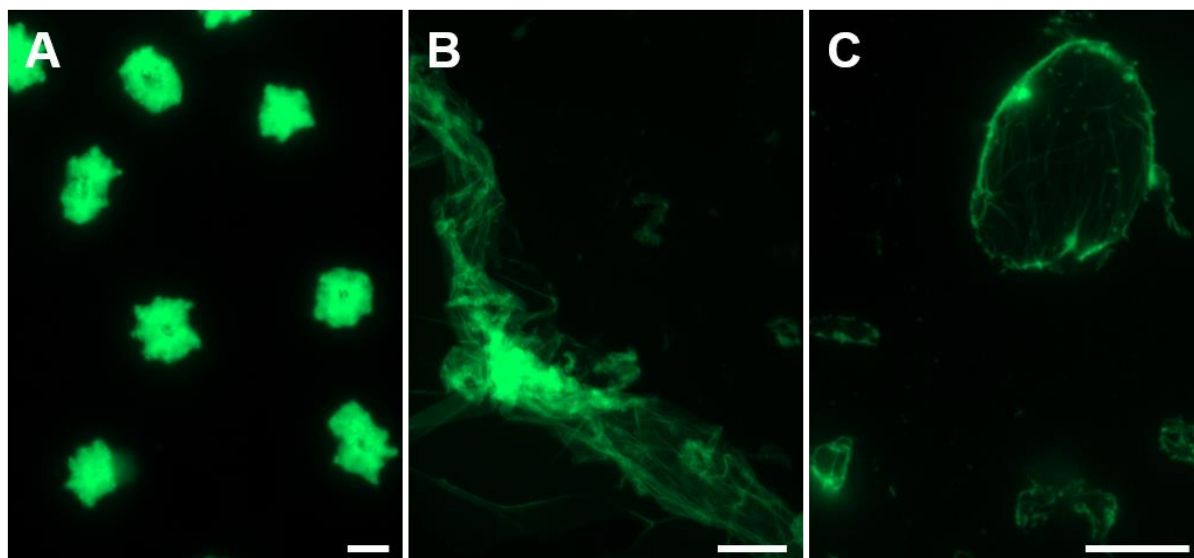


Fig. 33: *In vitro* filamentation of Alr4504 and Alr4505

Epifluorescence micrographs of filamentous structures formed by purified and renatured (A) Alr4504 (1 mg ml⁻¹), (B) Alr4505 (0.5 mg ml⁻¹) or (C) Alr4504+Alr4505 (0.25 mg ml⁻¹ each) in (A,C) HLB or (B) 25 mM HEPES pH 7.4. Proteins were stained with an excess of NHS-Fluorescein and analyzed by epifluorescence microscopy. Scale bars: (A,C) 10 μm or (B) 50 μm.

Alr4504 and Alr4505 jointly form polymers in an *E. coli* surrogate system

Since the availability of Alr4504 appears to be conducive for proper Alr4505 filamentation in an *in vitro* system, we wanted to evaluate whether this also holds true *in vivo*. To this end, we employed the GFP-fragment reassembly system developed by Wilson, Magliery and Regan (2004). This assay not only allows to detect protein-protein interactions *in vivo* but also provides valuable information about the intracellular localization of two given proteins. For this system, one protein candidate is N-terminally fused to the N-terminal GFP-fragment (NGFP) while the other protein candidate is C-terminally fused to the C-terminal GFP-fragment (CGFP). Although this system enables to detect a broad range of different interactions, it fails to investigate protein-protein interactions that require either both carboxyl-terminus or amino-terminus to be free of a tagged protein. Based on preliminary interaction tests by bacterial two-hybrid assays, we identified that Alr4504 and Alr4505 interaction required that either both N-termini or both C-termini were free of any tagged protein. Thus, in order to study N to N-terminal

interactions, we exchanged the orientation of the NGFP-tag in the expression plasmid (pET11a-link-NGFP) thereby creating an Alr4504-NGFP-encoding expression plasmid (see methods section 6.4.3.2). Since we knew from previous experiments that Alr4504 and Alr4505 interacted only through the same available termini, and that interaction was comparably strong, we limited *in vivo* assays to the below listed combinations. Co-dependency of Alr4504 and Alr4505 was then assessed by epifluorescence microscopy of *E. coli* cells bearing either N- or C-terminally NGFP-tagged Alr4504, C-terminally CGFP-tagged Alr4505 or empty vectors.

Even though the N- and C-terminal parts of the fragmented GFP proteins are not fused to any other protein, those two units can re-assemble within the cell just by pure chance which results in a uniform fluorescence signal throughout the cell (Fig. 34A). On the other hand, when only one GFP fragment is linked to another protein, a fluorescence signal corresponding to the localization of that protein will be detected (Fig. 34B,C,E). Consistent with the *in vitro* polymerization results (Fig. 33A), expression of NGFP-Alr4504 or Alr4504-NGFP with untagged CGFP leads to the formation of round or dot-like structures within the cells which were localized to the cell poles (Fig. 34C,E). Furthermore, in agreement with the *in vitro* results, similar small and undefined planar structures - often localized to the cell center - were observed upon expression of Alr4505-CGFP with untagged NGFP (Fig. 34B). A partial cell elongation was observed for cells expressing this construct, indicating an involvement of this protein in cellular morphology. Intriguingly, a subpopulation of *E. coli* cells co-expressing NGFP-Alr4504 and Alr4505-CGFP showed fluorescent polymers (white triangle in Fig. 34D) and a partially elongated filamentous cell phenotype (Fig. 34D). This phenotype was even more pronounced in cells co-expressing Alr4504-NGFP and Alr4505-CGFP with nearly all cells exhibiting an even further elongated cell filamentous phenotype and prominent protein filaments in the cells (white triangles in Fig. 34F). These results highlight that Alr4504 and Alr4505 assembly is terminus-dependent and that proper filamentation only occurs upon co-expression of both proteins.

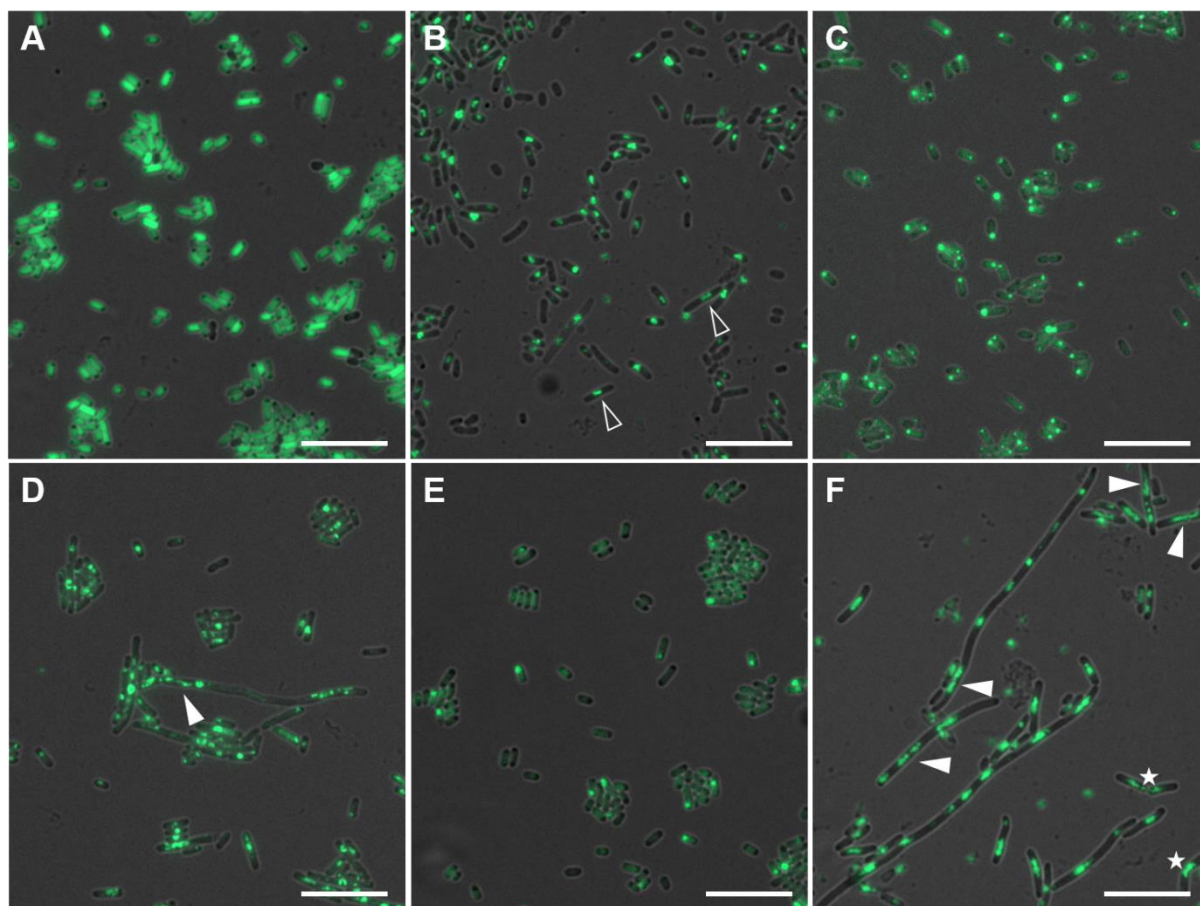


Fig. 34: Alr4504-NGFP and Alr4505-CGFP form filamentous structures in co-expressing *E. coli*

Merged GFP fluorescence and bright field micrographs of *E. coli* BL21(DE3) cells co-expressing (A) NGFP (empty pET11a-link-NGFP) and CGFP (empty pMRBAD-link-CGFP), (B) NGFP and Alr4505-CGFP, (C) NGFP-Alr4504 and CGFP, (D) NGFP-Alr4504 and Alr4505-CGFP, (E) Alr4504-NGFP and CGFP or (F) Alr4504-NGFP and Alr4505-CGFP. Cells were grown to an OD₆₀₀ of 0.5, induced with 0.2% L-arabinose and 0.05 mM IPTG and incubated for 48 h at 20 °C. For microscopy, cells were immobilized on an agarose pad. White triangles indicate filamentous structures. White stars show equal distribution of fluorescence signal to daughter cells. Transparent triangles point to structures resembling Alr4505 *in vitro* structures. Scale bars: 10 µm.

Co-expressed Alr4504 and Alr4505 polymerize into filaments *in vivo*

Inspired by the ability of Alr4504 and Alr4505 to co-polymerize into long filaments in *E. coli*, we now wanted to investigate how these proteins would behave in a unicellular cyanobacterium. Therefore, we next sought to identify the *in vivo* localization of C-terminally GFP-tagged Alr4504 and Alr4505 in the non-motile *Synechocystis* GT-Kazusa substrain and the motile *Synechocystis* PCC-M substrain (PCC-M) by epifluorescence microscopy. In order to test for co-localization we also generated a strain co-expressing Alr4504-eCFP and Alr4504-GFP by chromosomal insertion. All genes were expressed under the control of the light-inducible *cpc560* promoter.

As seen for *E. coli*, expression of only Alr4504-GFP or Alr4505-GFP in *Synechocystis* resulted in the formation of inclusion body-like structures (Fig 35A,B). However, unlike in *E.*

coli, co-expression of Alr4504-eCFP and Alr450-GFP did not promote protein filamentation in *Synechocystis* but only resulted in dot-like structures throughout the cell (Fig. 35C). On the contrary, co-expression of these proteins in the PCC-M substrain appeared to generate filamentous protein structures within the cells (white triangles in Fig. 35D). Nevertheless, it must be noted that these filaments were observed only in a minority of cells and that exposure time had to be increased tenfold to visualize the filaments. Therefore, it cannot be stated with certainty that co-expression of Alr4504 and Alr4505 induced protein polymerization in this unicellular cyanobacterium.

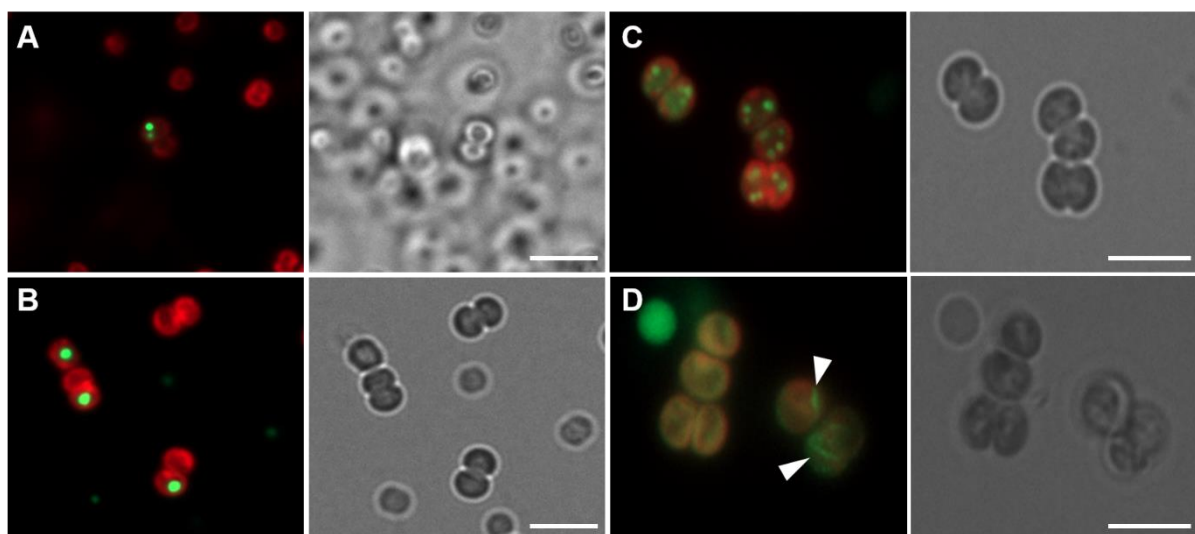


Fig. 35: Localization of Alr4504 and Alr4505 in *Synechocystis* substrains

Merged GFP fluorescence and chlorophyll auto-fluorescence and bright field micrographs of live cells expressing (A) Alr4504-GFP, (B) Alr4505-GFP, (C,D) co-expressing Alr4504-eCFP and Alr4505-GFP in (A-C) *Synechocystis* or (D) PCC-M. Cells were either (A,B) directly applied to a microscope slide or (C,D) previously immobilized on an agarose pad. White triangles indicate putative protein filaments. Scale bars: 10 μ m.

Consequently, we were now wondering how both proteins would behave in their cyanobacterium of origin, *Anabaena*. For this, we employed epifluorescence microscopy in order to assess *in vivo* polymerization in *Anabaena* cells expressing Alr4504-GFP or Alr4505-GFP and to identify co-localization in Alr4504-eCFP and Alr4505-GFP co-expressing cells. Expression of translational fusion constructs was under the control of the copper-inducible *petE* promoter.

The localization pattern of Alr4504-GFP and Alr4505-GFP (Fig. 36A, B) strongly resembled that observed in *E. coli* and *Synechocystis* (Figs. 34 and 35). Alr4504-GFP formed small aggregations within the cells without any apparent localization pattern (Fig. 36A). Likewise, Alr4505-GFP mainly formed focal aggregations, although in rare occasions, structures resembling Alr4505 *in vitro* polymers could be identified (white triangle in Fig. 36B). Besides these rather large accumulations of Alr4504-GFP and Alr4505-GFP, both proteins also formed small motile dots that moved through the cells (Fig. S39). Co-expression of

Alr4504-eCFP and Alr4505-GFP in *Anabaena* did not only lead to the formation of filamentous-like structures as observed for example in *E. coli* but also resulted in clear and cell-traversing filaments in *Anabaena* (Fig. 36C,D). In most cases, filaments formed straight lines spanning the whole cell with the tendency to arise from one cell pole and to attach to the opposite cell pole. In some cases, filaments traversing through almost divided daughter cells could be identified (white stars), however, no filaments connecting fully divided cells were observed in any sample. A proportion of co-expressing cells also displayed protein filaments that arose from the cell pole and then spread in a star-like fashion with radiating filaments which appeared to anchor or attach to different parts of the cell envelope in the vicinity (white arrows). Noteworthy, unlike other *petE*-driven translational fusions, the co-expression of Alr4504-eCFP and Alr4505-GFP was persistent over time. Despite our observations that fluorescence signals of *petE*-driven constructs are rapidly lost with advanced culture age, *Anabaena* cells co-expressing Alr4504-eCFP and Alr4505-GFP retained their fluorescence signal for several months. This indicates a beneficial effect of the cell-traversing and cell pole-docking structures for trichome growth, stability or cell viability. Notably, we did not observe any expression of YFP-Alr4504 or YFP-Alr4505. Cells expressing N-terminally tagged *yfp* translational fusions exhibited no fluorescence signal, indicating that tag-orientation is crucial for their expression or localization. These findings, together with the *in vitro* polymerization pattern and localization in *E. coli*, suggest that the presence of both proteins, Alr4504 and Alr4505, is crucial for proper filament formation.

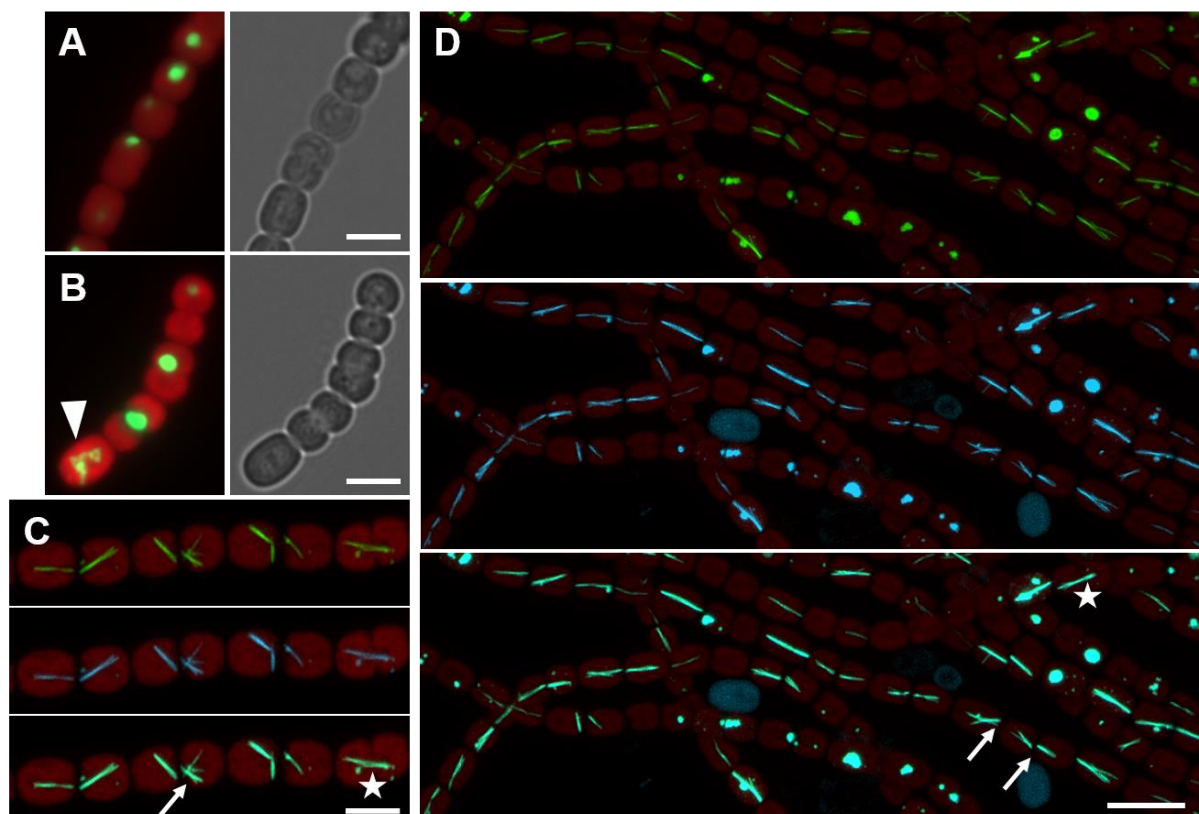


Fig. 36: Co-expressed Alr4504-eCFP and Alr4505-GFP polymerize into heteropolymers in *Anabaena*

Merged GFP and/or enhanced cyan fluorescent protein (eCFP) fluorescence and chlorophyll auto-fluorescence and bright field micrographs of *Anabaena* cells expressing (A) Alr4504-GFP, (B) Alr4505-GFP or (C,D) co-expressing Alr4504-eCFP and Alr4505-GFP. Cells were grown in (A) BG11 and induced for two days with 10 μM CuSO₄ or in (B,C,D) BG11-0 for 36 hours. White stars show cell-traversing filaments of not yet fully divided cells. White arrows indicate star-like formations arising from cell poles. White triangle indicates Alr4505-GFP structures resembling Alr4505 *in vitro* polymerization pattern. Scale bars: 5 μm .

Deletion of putative cytoskeletal proteins alters cell shape and cell filament growth of *Anabaena*

In order to pinpoint the function of Alr4504 and Alr4505 in trichome integrity, we attempted to generate gene deletion strains of *alr4504*, *alr4505* and an *alr4504-alr4505* double deletion strain.

The $\Delta alr4504\Delta alr4505$ strain (Fig. S40) showed severe defects in perpendicular trichome growth compared to the wt strain (Fig 37A,B). $\Delta alr4504\Delta alr4505$ tended to grow in a zig-zag fashion in more than just one plane. Furthermore, cells became more spherical compared to the elliptical cell shape of wt cells (roundness 0.853 ± 0.113 compared to wt 0.802 ± 0.123 (Chapter 2); one-way ANOVA using Dunns's test: $P < 0.05$). This observation is reminiscent of the rounding of $\Delta alr0931$ (Chapter 2) although no increase in cell volume was detected for $\Delta alr4504\Delta alr4505$. However, it must be noted that these phenotypes are not permanent because $\Delta alr4504\Delta alr4505$ and $\Delta alr0931$ tended to return to a normal perpendicular trichome growth pattern with elliptical cells upon extended culture age. Growth

of $\Delta alr4504\Delta alr4505$ in liquid media was strongly impaired, reinforcing the hypothesis that Alr4504 and Alr4505 are involved in cell-cell stability and trichome integrity as *Anabaena* cells encounter stronger forces when grown in a shaking liquid culture compared to growth on agar plates. Moreover, $\Delta alr4504\Delta alr4505$ hardly grew in liquid BG11 and completely failed to grow in liquid BG11-0 (Fig. S41C). Ultimately, the addition of osmotic stress factors entirely inhibited growth in liquid media (Fig. S41C column 3,5,6). We were not able to generate any single $\Delta alr4504$ or $\Delta alr4505$ strain, neither by double homologous recombination nor by the pSL2680-based CRISPR-Cpf1 system described by Ungerer and Pakrasi (2016). We also tried to disrupt the genes by single homologous recombination via plasmid integration into the open reading frame of the genes which was also unsuccessful. Taken together, Alr4504 and Alr4505 play an important role in *Anabaena* trichome integrity.

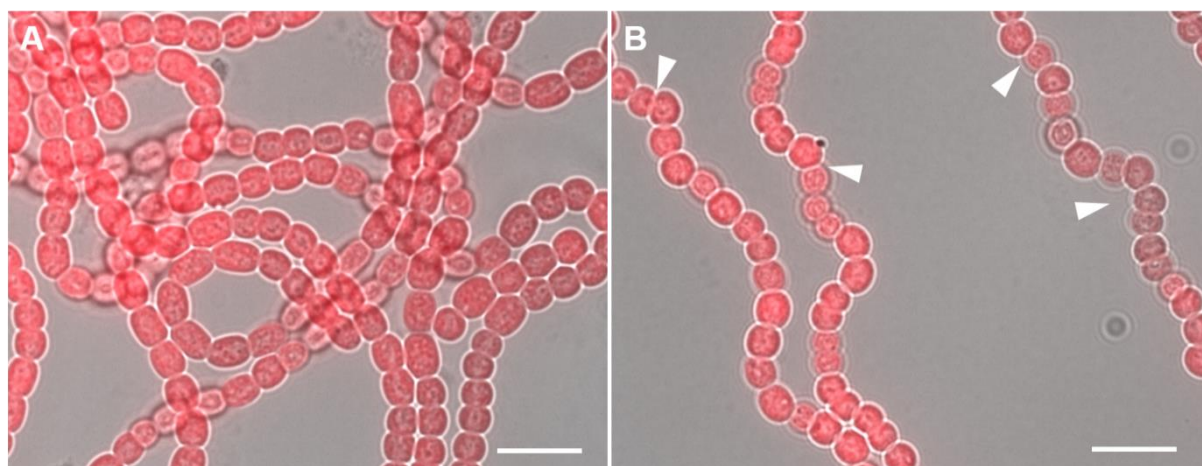


Fig. 37: $\Delta alr4504\Delta alr4505$ affects perpendicular growth of *Anabaena* trichomes

Merged bright field and chlorophyll auto-fluorescence micrographs of (A) *Anabaena* wt and (B) $\Delta alr4504\Delta alr4505$ cells grown on BG11 plates. White triangles indicate zig-zag growth of selected trichome sections. Scale bars: 10 μ m.

Alr0931 localizes to cell septa and forms scaffold-like structures *in vivo*

$\Delta alr0931$ revealed a comparable phenotype as $\Delta alr4504\Delta alr4505$, suggesting a similar role in cell stability (Chapter 2). *In vitro*, Alr0931 assembled into numerous small filaments which can only partially be reconciled with the localization of Alr0931-GFP in *Anabaena*. Thus, to explore putative misguiding effects of the large GFP-tag on Alr0931 localization, we replaced the GFP-tag with a His6-tag.

Alr0931-His expressing cultures grown in BG11-0 displayed reduced chlorophyll auto-fluorescence signals specifically at sites of cell-cell connections and cell septa (white triangles in Fig 38B). Further induction of protein expression for two days with 0.25 μ M CuSO₄ altered the cell morphology leading to swollen and sometimes pear-shaped cells (white stars in Fig. 38D). However, induction with a tenfold concentration of CuSO₄ eventually also resulted in

septal low-chlorophyll containing regions and cell distortions on BG11 grown cells (Fig. S42). This suggests that the effect is not specific for nitrogen-deprivation. Anti-His6 immunofluorescence revealed the nature of these chlorophyll-less regions. Cell poles of neighboring cells showed prominent Alr0931-His signals and a gradient-like mitigation from the septa to the cell center (Fig. 38F). This staining pattern correlated with the decrease in chlorophyll auto-fluorescence signals in close proximity to the cell septa. Thus, it is plausible that abundant Alr0931-His polymers displace the thylakoid membranes at the sites of cell septa.

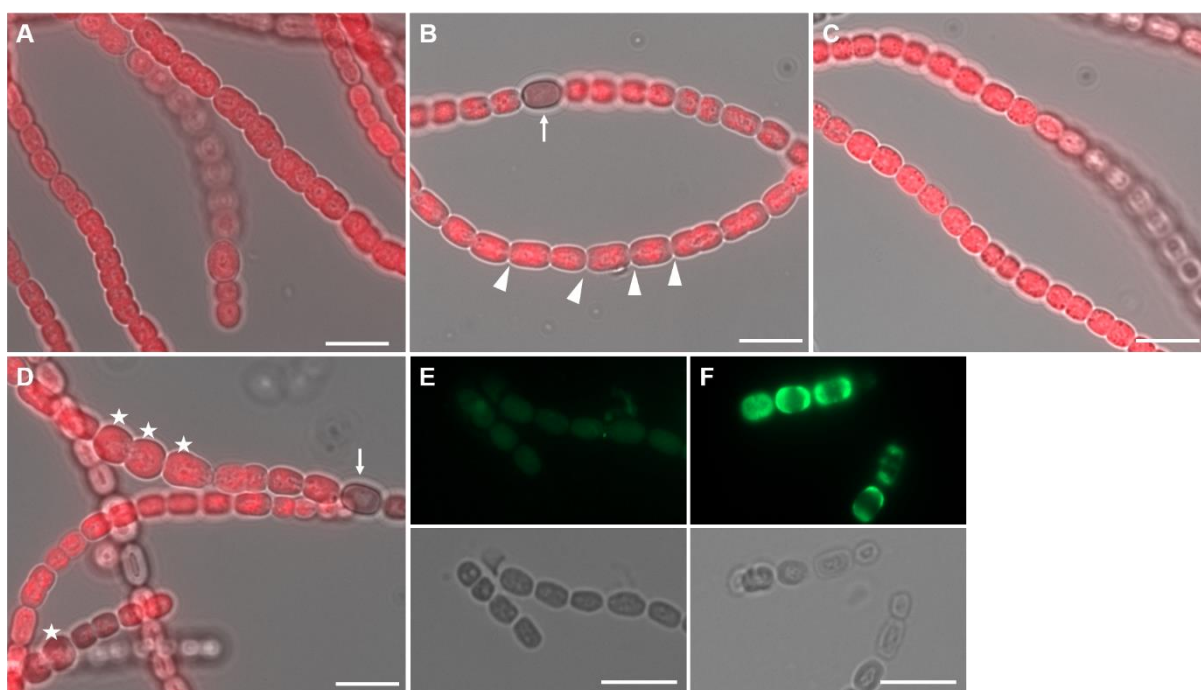


Fig. 38: Expression of Alr0931-His induces morphological defects

(A-D) Merged bright field and chlorophyll auto-fluorescence or (E,F) bright field and Alexa Fluor-488 fluorescence micrographs of (A-D,F) *Anabaena* cells expressing Alr0931-His or (E) *Anabaena* wt cells grown in (A) BG11, (B) BG11-0, (C) BG11 supplemented with 0.25 μM CuSO_4 for 2 days or (D,E,F) BG11-0 supplemented with 0.25 μM CuSO_4 for two days. (E,F) Cells were treated as described by Ramos-León *et al.* (2015), incubated with anti-His6 primary antibody and Alexa Fluor-488 conjugated secondary antibody. Cells were mounted in Prolong Diamond antifade mountant (Thermo Fischer Scientific). White triangles mark cell septa with the most prominent reduction in chlorophyll signal. White stars indicate swollen cells. White arrows point to heterocysts. Scale bars: 5 μm .

Expression of All2460 alters cell shape in *Anabaena*

In Chapter 1, we identified All2460, a putative IF-like cytoskeletal CCRP. The TMHMM online tool predicted two N-terminal transmembrane helices within the first 52 amino acids of All2460 which is in accordance with the membrane-localization of All2460-GFP in *E. coli* and *Anabaena* (Fig. 39A-D). Besides its association to the cell envelope, All2460-GFP also formed a banded and helical pattern in *E. coli* (see white triangles) with a striking resemblance to MreB (Swulius and Jensen, 2012) and Synpcc7942_2039-GFP in *E. coli* (Chapter 1). In *Anabaena*, All2460-GFP was often most pronounced at sites of cell-cell connections of two neighboring cells (white

stars in Fig. 39C) although this might be related to the superposition of the two septal signals. Overexpression of All2460-GFP caused swelling of the cells in a small proportion of the cell population (Fig. 39B). The association of All2460-GFP to the cell envelope presents itself in patches rather than in a uniform pattern (Fig. 39D), suggesting that All2460 functions as an anchor point for other proteins. While *Anabaena* cells expressing All2460-GFP are able to grow in BG11, growth is inhibited under nitrogen-deprived growth conditions (Fig. S43C). This inhibitory effect was also observed in strains expressing Alr4504-GFP (Fig. S43A), Alr4505-GFP (Fig. S43B), Alr0931-GFP (data not shown) but not in Alr4504-eCFP and Alr4505-GFP co-expressing strains (Fig. S43D) further implying an affiliation with cell-cell connections and possibly intercellular transport. No fluorescence signal was detected in *Anabaena* expressing YFP-All2460 (data not shown), indicative for a tag-orientation dependency of All2460 as also seen in N-terminally YFP-tagged Alr0931, Alr4504 and Alr4505. We were not able to overexpress All2460-GFP in *Synechocystis*, suggesting that (over)expression of this protein is toxic in this species. Similarly, upon ectopic expression of All2460-His in *E. coli* cell division immediately halted, possibly due to a toxic effect. Taken together, All2460 associates with the cell membrane in patches and exerts an effect on cellular morphology and cell viability.

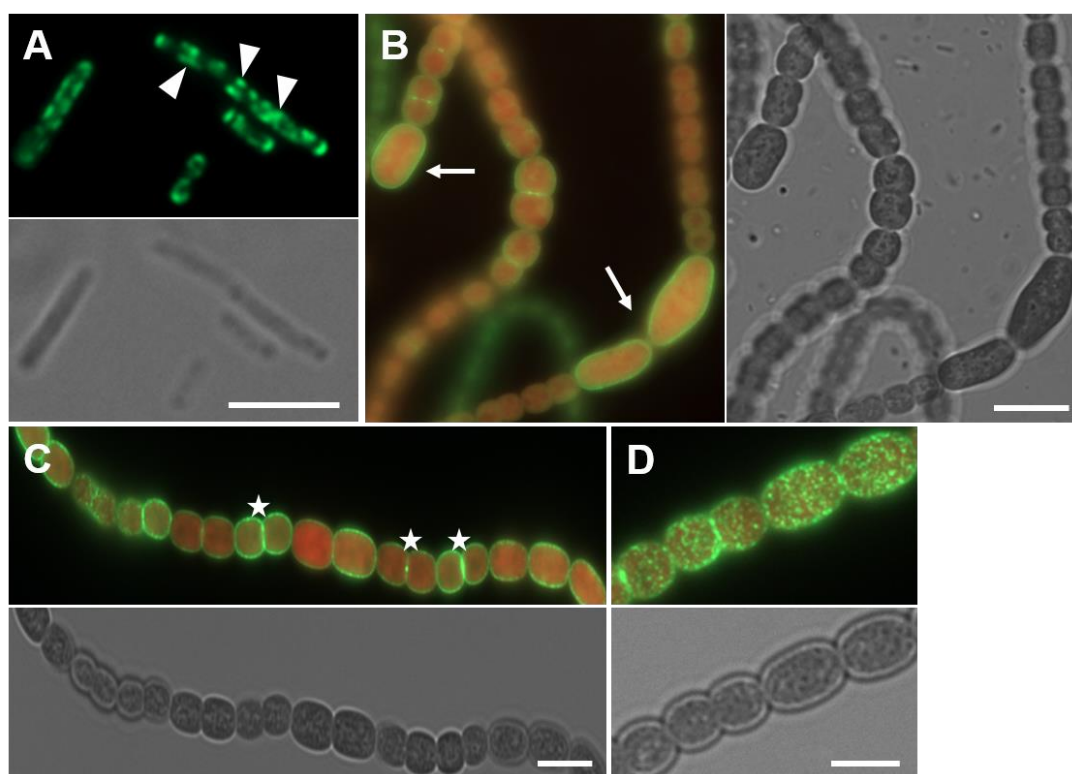


Fig. 39: Heterologous expression of All2460-GFP affects *Anabaena* morphology

GFP fluorescence, bright field and merged GFP fluorescence and chlorophyll auto-fluorescence micrographs of (A) *E. coli* BL21 (DE3) and (B,C,D) *Anabaena* expressing All2460-GFP. (A) *E. coli* cells were induced with 0.05 mM IPTG and grown for 48 hours at 20 °C. *Anabaena* cells were either grown (B) on BG11 plates or (C,D) in BG11 without copper supplemented with 5 μ M CuSO₄ for 1 day and immobilized on an agarose pad. White arrows point to markedly swollen cells. White triangles indicate banded and helical-like fluorescence signals. White stars mark accumulations of fluorescence signal at septum sites. Scale bars: 5 μ m.

Gene deletion of *all2460* induces *Anabaena* trichome fragmentation

To further explore the cellular function of All2460, we generated an *all2460* deletion strain ($\Delta all2460$; Fig S44) by double homologous recombination and assessed its morphotype by epifluorescence microscopy.

In contrast to the $\Delta al0931$ and $\Delta alr4504\Delta 4505$ strains, $\Delta all2460$ cells were able to grow in liquid BG11 (Fig S41A) and did not exhibit a rounded or enlarged phenotype (roundness 0.806 ± 0.117 compared to wt 0.806 ± 0.132 ; one-way ANOVA using Dunns's test: $P > 0.05$). Although cells were able to grow in nitrogen-deprived medium and even formed heterocysts, cells died within a few days (usually around 4-5 days) after nitrogen stepdown. Compared to the wt, $\Delta all2460$ cells showed a fragmented growth pattern in early culture stages. This fragmentation phenotype was seen in BG11 but it was more pronounced under nitrogen-deprivation where trichomes rarely exceeded more than 20 cells in a row (Fig. 40C,D). Furthermore, $\Delta all2460$ cells exhibited reduced chlorophyll auto-fluorescence signals (Fig. 40D). Noteworthy, reminiscent of $\Delta al0931$ and $\Delta alr4504\Delta 4505$, trichome structure of $\Delta all2460$ cells returned to wt phenotype in later culture stages. Given the differences in trichome integrity, we investigated the impact of these gene deletion strains on intracellular FtsZ localization by immunofluorescence microscopy. However, none of the mutants showed alterations of Z-ring placement (Fig. S45). DAPI staining of cellular DNA and Alcian blue staining of heterocysts also revealed no differences compared to the wt (Figs. S46 and S47) showing that heterocyst development and integrity is not impaired in these mutants. Heterocyst formation was, however, delayed in the $\Delta all2460$ strain in which they appeared 3-4 days after nitrogen step-down compared to 24-48h in the wt (not shown). All these evidences point to a function of All2460 downstream of heterocyst differentiation. We also addressed the possibility that some of these gene deletions might impact other viability parameters by comparing cell viability using spot assays under a variety of different growth conditions. However, none of them could be shown to influence cell viability in a spot assay (Fig. S48). Trichome integrity was severely impaired in all gene deletion strains, suggesting defects in cell-cell connectivity. $\Delta all2460$ trichome readily fragmented in liquid cultures comparable to $\Delta sepJ$ (Flores *et al.*, 2007; Nayar *et al.*, 2007). In *Anabaena*, SepJ is an essential component of the septosomal complexes that regulate cell-cell communication (Flores *et al.*, 2016) and *sepJ* mutants exhibited defects in intercellular communication (Nürnberg *et al.*, 2015). Prompted by this resemblance, we next performed fluorescence recovery after photobleaching (FRAP) experiments with the small fluorescent tracer calcein (Fig. S49).

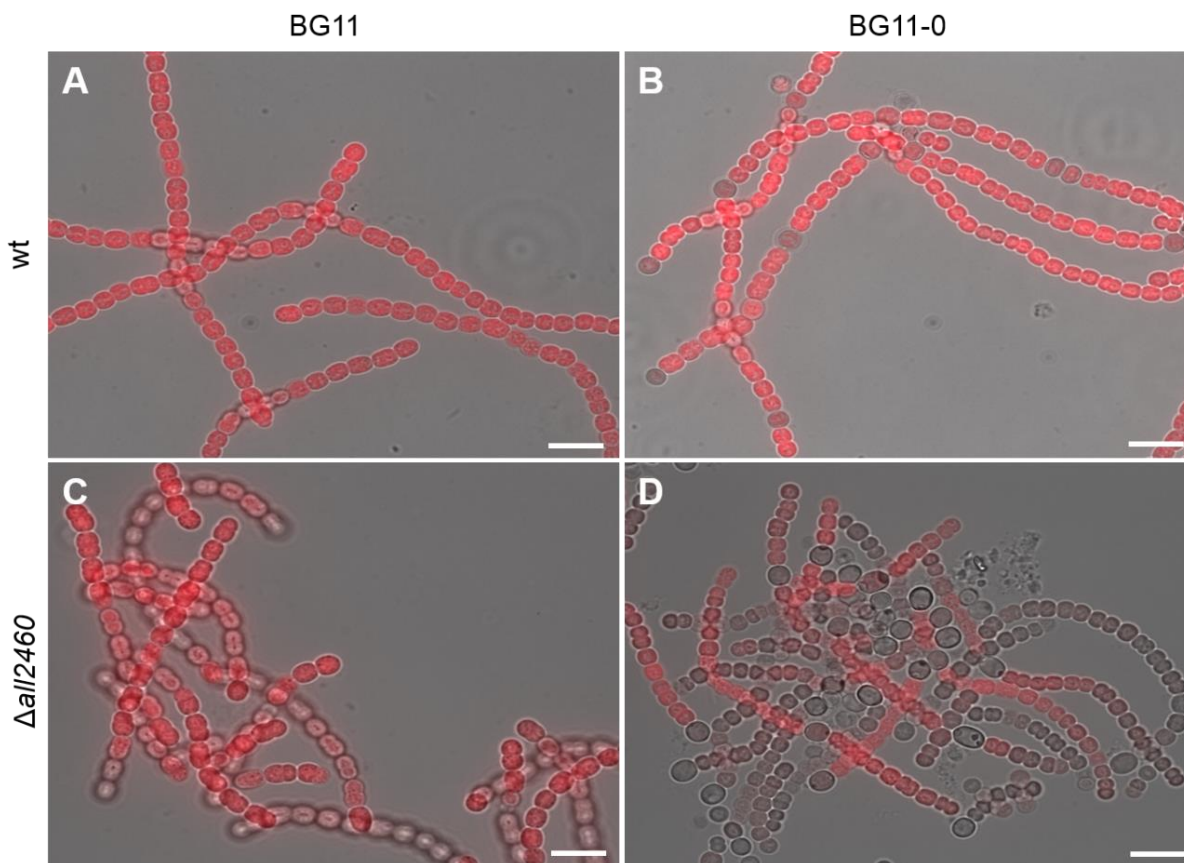


Fig. 40: $\Delta all2460$ leads to cell fragmentation

Merged bright field and chlorophyll auto-fluorescence micrographs of (A,B) *Anabaena* wt or (C,D) $\Delta all2460$ cells grown in (A,C) BG11 or (B,D) BG11-0. Cells from growth plates were transferred to liquid media and grown for five days before micrographs were obtained. Scale bar: 10 μ m.

In accordance with the observed fragmentation phenotype of $\Delta all2460$, molecular exchange between neighboring cells decreased in a 1/18 factor compared to *Anabaena* wt (Table 8). Likewise, albeit not as pronounced, a decrease in cell-cell communication was also detected for $\Delta alr0931$ (by about 40%) while no difference was identified for $\Delta alr4504\Delta alr4505$ (Table 8). Liquid BG11-grown $\Delta all2460$ cells furthermore exhibited uneven calcein dispersions which were accumulated in some cells but nearly depleted from others of the same trichome, indicative for a diffusion blockade (translucent triangles in Fig S49C). This clearly shows that the intercellular transport is markedly impaired in the *all2460* and *alr0931* mutants.

Table 8: *Anabaena* mutant strains reveal defects in calcein exchange rates between cells in a trichome

Strain	Mean E (s^{-1}) (\pm s.d.)	Growth condition
<i>Anabaena</i> wt	0.124 \pm 0.05	BG11 plate
Δ <i>alr0931</i>	0.079 \pm 0.03	BG11 plate
Δ <i>alr4504Δ<i>alr4505</i></i>	0.128 \pm 0.05	BG11 plate
<i>Anabaena</i> wt	0.126 \pm 0.06	Liquid BG11
<i>Anabaena</i> wt	0.124 \pm 0.03	Liquid BG11-0
Δ <i>all2460</i>	0.007 \pm 0.007	Liquid BG11
Δ <i>all2460</i>	0.0046 \pm 0.005	Liquid BG11-0

Anabaena wt was either grown on BG11 plates or in BG11 or BG11-0 liquid medium, Δ *alr0931* and Δ *alr4504 Δ *alr4505* were grown on BG11 plates and Δ *all2460* was grown in BG11 or BG11-0 liquid medium. One-way ANOVA using Dunns's test indicates that E values are significantly different between *Anabaena* wt and Δ *alr0931* and Δ *all2460* (BG11 and BG11-0) ($P < 0.05$) but not between *Anabaena* wt and Δ *alr4504 Δ *alr4505* ($P > 0.05$). Number of experiments performed for *Anabaena* wt BG11 plate: 21; *Anabaena* wt liquid BG11: 10; *Anabaena* wt liquid BG11-0: 10; Δ *alr0931*: 23; Δ *alr4504 Δ *alr4505*: 17; Δ *all2460* liquid BG11: 16; Δ *all2460* liquid BG11-0: 6. Representative fluorescence recovery curves for bleached cells are shown in Fig. S50.***

Alr4504, Alr4504, Alr0931 and All2460 form a cytoskeletal network that interacts with the septosomal protein SepJ

The defects on morphology, trichome stability and intercellular transport prompted us to presume that these proteins play an important role in filament integrity and as such, they might interact with SepJ or other cytoskeletal components. To test this and to identify further interaction partners, we performed bacterial two hybrid assays and looked for self-interaction of Alr4505, Alr4504, Alr0931 and All2460, interaction with each other, with the cytoskeletal proteins MreB and FtsZ and with the septal junction protein SepJ. Additionally, we performed co-immunoprecipitations (co-IPs) of *Anabaena* strains overexpressing GFP-tagged All2460 and Alr4504 using anti-GFP antibodies with subsequent sequencing of interactors by mass spectrometry.

Two hybrid assays revealed that Alr0931, Alr4504, Alr4505 and All2460 are able to self-interact (Chapter 2 and Fig. S51A,B,C, respectively) confirming the *in vitro* polymerization assays (Alr4504, Alr4505 and Alr0931, Fig. 33 and Chapter 2). All four proteins were also able to cross-interact with each of the remaining CCRPs (Fig. S51D-I) showing the potential of cyanobacterial IF-like CCRPs to form a vastly interconnected cytoskeletal web. To support this, Alr4504, Alr4505 and All2460 but not Alr0931, were found to interact with the major cytoskeletal component, the actin-like protein MreB (Fig. S52A-D) and only All2460 faintly interacted with FtsZ (Fig. S52E-H). Finally, all proteins were identified as interaction partners of the septosomal junction protein SepJ (Fig. S53A-D). Thus, the observed fragmented and zig-zag growth phenotypes of the *Anabaena* deletion strains might be directly linked to impaired cell-cell connections and a disturbed cell-cell communication with IF-like cytoskeletal proteins forming a cell-septa anchored physical stabilization network. In Chapter 1 we

described Alr3364, a protein that localized to the septa in *Anabaena*. We thus investigated whether this protein might also be part of the cytoskeletal network. However, no interactions were revealed for Alr3364 with Alr0931, Alr4505 and All2460 and only a weak interaction was verified with Alr4504 (Fig. S53E-H).

Co-immunoprecipitation (co-IP) assays of All2460-GFP showed several putative interactor proteins, seen as different protein bands on the SDS-gel (Figure 41A). Qualitatively, co-IP of Alr4504-GFP showed less possible interaction partners than All2460 (Fig. 41B). All bands were sequenced by mass spectrometry. Among the identified interactors, All2460-GFP specifically interacted with numerous already characterized cytoskeletal proteins, including MinD, ParA and MreB. In additional support of the identified interaction of All2460 with SepJ by two hybrid assays, SepJ also co-precipitated with All2460-GFP. Further identified interaction partners were Alr4981 (see Chapter 1), the protease ClpB and three penicillin binding proteins (PbP; All2952, All2981, All0718). Alr4504-GFP was found to associate with Alr4505, thereby further confirming the direct interaction of Alr4504 and Alr4505 *in vivo* and *in vitro*. Moreover, interactions with a ParA-family protein (All1075), a few hypothetical proteins or proteins of unknown function and MreB were found. The number of interacting proteins involved in the peptidoglycan synthesis machinery or of cytoskeletal origin, together with the self-interaction capacity of all investigated CCRPs led us to propose that these proteins form a strongly inter-linked cytoskeletal network in *Anabaena*, with coiled-coil rich proteins playing a major role in maintaining the phenotypic architecture of this cyanobacterium.

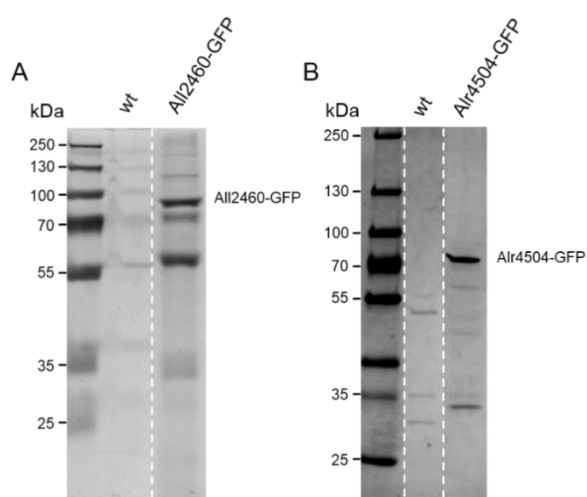


Fig. 41: Identification of proteins interacting with All2460-GFP and Alr4504-GFP

Cell-free lysates of *Anabaena* strains expressing All2460-GFP or Alr4504-GFP were subjected to co-immunoprecipitation using anti-GFP magnetic beads. (A) All2460-GFP expressing cells were grown in BG11 without copper and protein expression was induced for 1 day with 5 μM CuSO_4 . (B) Alr4504-GFP expressing cells were grown in BG11-0 without copper and protein expression was induced for 5 days with 0.5 μM CuSO_4 . Pooled duplicates of precipitated proteins of two independent experiments were analyzed by mass spectrometry and 25 μl of those fractions were resolved in a (A) 10% SDS-polyacrylamide gel or (B) 4-15% TGX precast gel and detected by Quick Coomassie stain (Serva).

9.4 Discussion

We have identified a strongly interconnected cytoskeletal network in the multicellular and N_2 -fixing cyanobacterium *Anabaena* that we showed to stabilize the connection of neighboring cells within a trichome. This network comprises at least four different IF-like CCRPs and is directly linked to the septosomes and the actin-like cytoskeleton in *Anabaena*. Based on our findings, we propose a model in which trichome integrity in *Anabaena* is regulated by a web of several cytoskeletal components including the CCRPs Alr0931, Alr4504, Alr4505 and All2460 and the MreB cytoskeleton. Together with the septosomes that are comprised of SepJ, among others, this network relays stabilizing properties to neighboring cells (Fig 42).

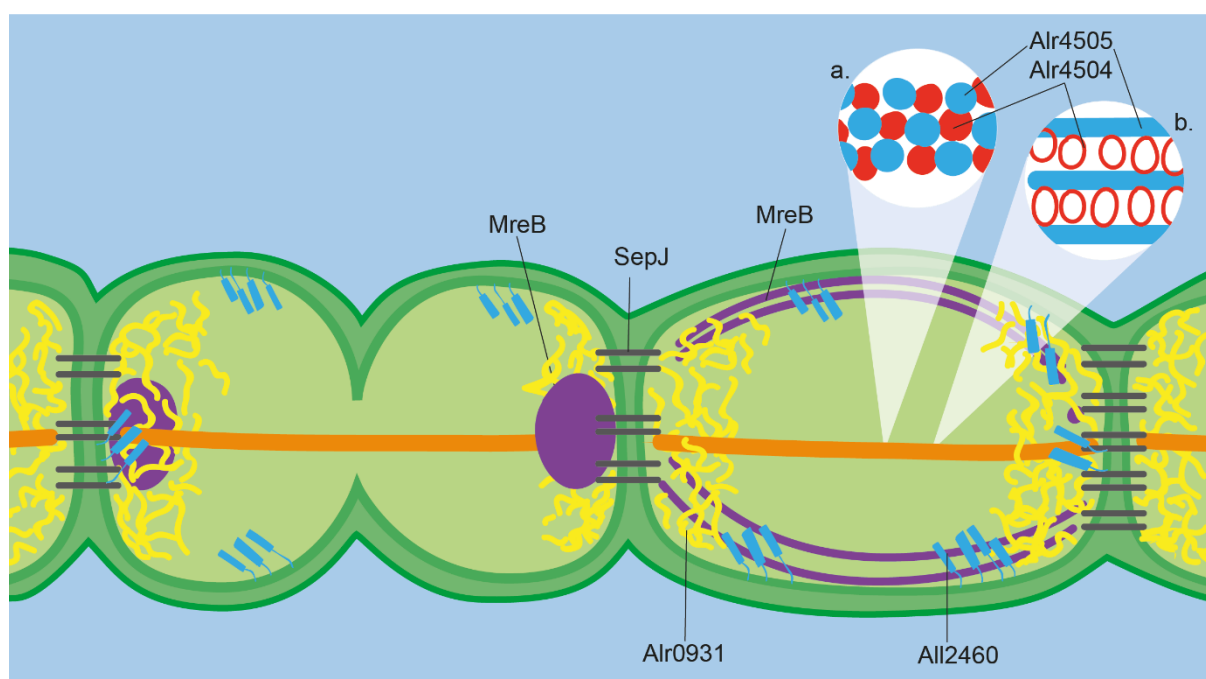


Fig. 42: Interconnected cytoskeletal network stabilizing cell-cell connections

Septosomes, comprised of SepJ (grey), are directly connected to the Alr0931 scaffolding cytoskeleton (yellow) that provides anchoring sites for the Alr4504/Alr4505 filaments (orange). (a) Similar to α -tubulin and β -tubulin (Alberts *et al.*, 2014), the Alr4504/Alr4505 heteropolymer could be composed of alternating Alr4504 (red) and Alr4505 (blue) monomers. (b) However, based on *in vivo* localizations, *in vitro* polymerization, domain predictions and structural similarities to eukaryotic plectin, it is likely that Alr4504 acts as a cytolinker protein for Alr4505, enabling proper polymerization. The Alr4504/Alr4505 filament can span through nearly divided cells as indicated in the dividing cell on the left of the figure. However, it cannot pass through the septosomes of fully divided cells (right cell). The stabilizing effect of Alr4504/Alr4505 is then linked to the neighboring cell via interactions with Alr0931, All2460 (light blue), SepJ and MreB (purple). MreB localizes to the septa (indicated in the dividing cell on the left) but also forms cell-traversing filaments (right cell) (Hu *et al.*, 2007), which are possibly anchored to the cell envelope through All2460. Furthermore, according to FRAP results, it is conceivable that All2460 regulates septosomal and trichome integrity through interaction with SepJ, possibly by organizing septosomal placements.

The proposed cytoskeletal functions of the CCRPs are supported by the mutant phenotypes which revealed impairments in trichome integrity, increased cell volume, changes in cell shape and zig-zag cell filament growth pattern. All of these phenotypes are partly reminiscent of the phenotype of *Anabaena*'s $\Delta mreB$ strain (Hu *et al.*, 2007) and the $\Delta sepJ$

strain (Flores *et al.*, 2007). Despite the prominent phenotypic changes, all deletion mutant strains returned to a wt-like morphology at later growth stages. We hypothesize that this phenomenon is based on other stabilizing structures or cell envelope components that rescue the wt phenotype in developed cultures. In support of this notion, *Anabaena* cell envelope mutants lacking genes that regulate cell envelope components reveal analogous morphotypic alterations and trichome fragmentation phenotypes (Burnat, Schleiff and Flores, 2014). Thus, cell envelope components exhibit a striking relevance for trichome integrity and might be able to complement the mutant phenotypes of the here characterized mutant strains. Trichome growth defects of all here studied deletion strains were most prominent at early culture stages, indicative for a function of these genes in early stage cell-cell stability. Additionally, the pronounced fragmentation phenotype of the $\Delta all2460$ strain resembles the phenotype from $\Delta sepJ$, and the filament fragmentation-related genes *fraC* and *fraD* deletion strains (Flores *et al.*, 2007; Nayar *et al.*, 2007; Nürnberg *et al.*, 2015). Those similarities suggest a direct involvement of All2460 in cell-cell communication. In fact, using the small fluorescent tracer calcein, we identified severe impairments in cell to cell communication of the $\Delta all2460$ strain and a moderate, albeit significantly reduced exchange rate in the $\Delta alr0931$ strain. Although exhibiting a similar phenotype as the $\Delta alr0931$ mutant, the dye exchange rate of the $\Delta alr4504\Delta alr4505$ strain was comparable to *Anabaena* wt. Heterocyst development of mutant strains grown on nitrogen-deprived growth plates was not affected and alcian blue staining of heterocyst-specific polysaccharides was unaltered, suggesting that none of the CCRPs is directly involved in heterocyst formation. Nevertheless, based on the delayed heterocyst-development of the $\Delta all2460$ strain in BG11-0 and the reduced chlorophyll fluorescence similar to the reduced cell pigmentations in the $\Delta sepJ$ strain (Nayar *et al.*, 2007), we propose that All2460 functions downstream of heterocyst differentiation which further supports its role in cell-cell communication. The phenotype is, however, not as pronounced as in the *sepJ* mutant strain where heterocyst development was entirely abrogated (Flores *et al.*, 2007; Nayar *et al.*, 2007). All2460 possesses two N-terminal transmembrane domains and interacts with the rod shape-determining protein MreB and several Pbps, pointing to a complement function of All2460 for the MreB cytoskeleton by recruiting the peptidoglycan synthesis machinery to sites of cell growth. Interaction of All2460 with MreB and the Pbps could indicate that the detected All2460-GFP patches in the *Anabaena* cell envelope function as putative anchoring sites for the elongasome. In accordance with this hypothesis, we observed analogous localization of All2460-GFP and MreB (Swulius and Jensen, 2012) in *E. coli* and a swollen cell phenotype of All2460-GFP expressing *Anabaena* cells, putatively the result of an uncontrolled recruitment of the PG synthesis machinery to the cell membrane. This observation is in concert with the inflated and aberrant phenotype of *Anabaena* cells overexpressing MreBCD (Hu *et al.*, 2007). However, the precise role of All2460 in cell wall synthesis remains to be elucidated and so far,

no *in vitro* protein filaments were detected for Alr2460, suggesting a non-IF like cytoskeletal function.

Strikingly, GFP-tagged Alr4504 and Alr4505 alone are insufficient for polymerization into filaments *in vivo*. Species-independent polymerization in *E. coli* or *Anabaena* cells was only observed upon co-expression of both proteins. No clear filaments were observed upon co-expression in *Synechocystis*, although this might be due to the very strong *cpc560* promoter (Zhou *et al.*, 2014) which might cause high accumulations of Alr4504 and Alr4505. This high-level expression does not seem to favor the formation into filaments since the proteins are rather stored in inclusion bodies to avoid cell damage. A similar observation was made from *in vitro* polymerization assays with protein filaments detected only upon co-polymerization, even though, a certain sheath-like polymerization pattern was identified for Alr4505. The I-TASSER online prediction tool detected moderate similarities of Alr4504 with the spectrin repeat structure of plectin (Chapter 1), a well-described eukaryotic cytolinker protein. Plectins link the three cytoskeletal systems (microfilaments, microtubules and IFs), thereby contributing to the resistance to deformation of vertebrate cells (Herrmann and Aebi, 2000; Alberts *et al.*, 2014). They furthermore stabilize desmosomes and hemidesmosomes and are thus directly involved in cell-cell and cell-matrix integrity (Leung, Green and Liem, 2002). An analogous cytolinker property of Alr4504 could explain why Alr4505 alone is not proficient for filamentation *in vivo* as it might require linker proteins (i.e. Alr4504) for directed polymerization. The cylindrical *in vitro* structure of Alr4504 could therefore hint to an Alr4505-embracing structure, providing guidance for correct Alr4505 polymerization. Based on the given structural similarity to spectrin, it is also conceivable that Alr4504 and Alr4505 evolved comparable functions to α -spectrin and β -spectrin that produce the so-called red blood cell ghost (spectre), an interconnected cytoskeletal network below the plasma membrane of erythrocytes (Zhang *et al.*, 2013). The spectrin cytoskeleton is involved in cell shape maintenance and provides mechanical stiffness to red blood cells (Alberts *et al.*, 2014), reminiscent of the trichome-stabilizing effect of Alr4504 and Alr4505. Furthermore, assembly of the spectrin cytoskeleton is dependent on heteropolymerization of α - and β -subunits, thus resembling the interdependency of Alr4504 and Alr4505 for protein filamentation. Interestingly, like Alr4504 and Alr4505, spectrin is directly linked to the actin cytoskeleton (Alberts *et al.*, 2014). However, the *in vitro* co-polymerization properties of Alr4504 and Alr4505 in an MreB-free environment and the different localization pattern of Alr4504 and Alr4505 co-expressed in *E. coli* compared to the patchy, helical or banded structures of MreB in *E. coli* (Swulius and Jensen, 2012) show that Alr4504 and Alr4505 together are sufficient for polymerization and do not merely associate to MreB filaments. Cyanobacterial septosomes are thought to be analogs of eukaryotic gap junctions, which, unlike desmosomes, are not associated with the intermediate filament cytoskeleton but with actin filaments, microtubules and cytolinker proteins like spectrin and

catenin (Giepmans, 2004). The absence of other known junctional complexes in cyanobacteria could indicate that IF-like CCRPs might have evolved to implement that function in cyanobacteria.

In accordance with a putative cell-cell stabilizing effect, the $\Delta alr0931$ and $\Delta alr4504\Delta alr4505$ strains are incapable of growth in liquid growth medium, suggesting that the trichome integrity and resistance to deformation of those mutant strains is strongly impaired and that they cannot withstand the increased shear stress in a liquid culture (Joshi, Elias and Patole, 1996). The so-called fluid shear stress (FSS), which inevitably acts upon cells grown in liquid culture, affects cell-cell communication within a biofilm (Park *et al.*, 2011), alters cellular morphology in the green algae *Chlamydomonas reinhardtii* as well as trichome length in *Spirulina platensis* (Bronnenmeier and Märkl, 1982) and can even directly induce remodeling of the cytoskeleton (Malek and Izumo, 1996). Thus, the resistance to FSS is strongly dependent on a scatheless protective apparatus against external mechanical deformation forces (i.e. the cell envelope and the cytoskeleton) and impairments of these systems result in detrimental shear injuries (Joshi, Elias and Patole, 1996). Besides reduced resistance to FSS, a higher sensitivity to turgor pressure of the mutant strains is also conceivable which only becomes apparent under liquid growth conditions (Fricke, 2017). In fact, a proportion of $\Delta alr0931$ cells immediately bursted upon transfer into liquid medium (Chapter 2). Turgor pressure regulates cell growth, cell movement and cell wall remodeling and increases membrane tension thus inflicting an elevated mechanical stress on cells (Fricke, 2017; Rojas and Huang, 2018). In *Bacillus subtilis*, reminiscent of plants, turgor pressure is assumed to drive cellular deformation during cell growth and it has been indicated that an equilibrium of cell wall stress and membrane tension is crucial for this process (Rojas and Huang, 2018). Consequently, growth defects of *Anabaena* mutants could indicate a distorted equilibrium of turgor pressure and the mechanical resistance to deformation of the cells.

Remarkably, unlike other *petE*-driven translational fusion constructs that are rapidly lost in *Anabaena*, expression of Alr4504/Alr4505 filaments was remarkably persistent with cultures exhibiting protein filaments for several months. This observation is in agreement with the hypothesized trichome-stabilizing effect of Alr4504 and Alr4505 since the cells benefit from Alr4504/Alr4505 filament expression. Furthermore, in previous studies it was shown that the localization of SepJ, which is essential for the multicellular phenotype of *Anabaena*, is dependent on the divisome (Ramos-León *et al.*, 2015). This suggests that the tubulin-like FtsZ cytoskeleton, like in eukaryotes, is involved in the manifestation of multicellularity (Alberts *et al.*, 2014; Ramos-León *et al.*, 2015). Here we obtained further evidence for the interaction of four CCRPs with each other and with SepJ as well as with MreB. Hence, CCRPs putatively provide a crucial interconnected cytoskeletal structure needed in order to stabilize the

septosomes within the cells of a trichome. This network of CCRPs consequently also links the septosomes to the MreB cytoskeleton. The lack of growth of GFP-fusion constructs under nitrogen-deprived conditions for any of the described proteins could therefore be the result of an impaired cell-cell communication by overrepresentation of cytoskeletal proteins at septosomes by physically blocking molecular exchange. Although a similar cell filamentation phenotype as described by Camberg, Hoskins and Wickner (2009) was detected for *E. coli* cells co-expressing Alr4504 and Alr4505, the functional properties of the cyanobacterial network-forming CCRPs are independent of the tubulin-like cytoskeleton since we did not identify any interactions with FtsZ for the four CCRPs and immunolocalization of FtsZ as well as intracellular DNA distribution in *Anabaena* mutants was unaltered. N-terminal YFP-fusions of network-forming CCRPs failed to produce discernible fluorescence signals, suggesting that the N-terminus is essential for their cytoskeletal functions. Similarly, CreS-GFP and mCherry-CtpS were found to be non-functional albeit they retained their filamentation properties (Ausmees, Kuhn and Jacobs-Wagner, 2003; Ingerson-Mahar *et al.*, 2010). Alr0931-GFP localized either diffusely throughout the cytosol or was associated with the cell envelope. However, immunolocalization of Alr0931-His revealed that Alr0931 rather likely forms polar accumulations with a gradient-like decrease of fluorescence towards the cell center, reminiscent of the gradient-like decrease of FilP in *S. coelicolor* hyphal tips or ParA in *C. crescentus* (Bagchi *et al.*, 2008; Lin and Thanbichler, 2013; Sundararajan and Goley, 2017). Based on this observation, and the matching phenotype of the $\Delta alr4504\Delta alr4505$ and $\Delta alr0931$ strains, it is conceivable that Alr0931 might act as a scaffold-like anchor that bridges the septosomal complex via SepJ interaction with the cell-traversing Alr4504/Alr4505 filaments. In further support for a scaffolding function of Alr0931, we recently showed that Alr0931 polymerizes into short and small filaments *in vitro* (Chapter 2) which could provide a suitable meshwork required for scaffolding functions (Kühn *et al.*, 2010). As no direct cell-cell spanning Alr4504/Alr4505 filaments were observed in fully divided cells, the Alr0931 scaffolding system could provide a relay station that transmits the stabilizing properties of the Alr4504/Alr4505 filaments through neighboring cells within an *Anabaena* trichome through the septosomes. The analogous growth impairment of $\Delta alr4504\Delta alr4505$ and $\Delta alr0931$ strains in liquid medium would be in agreement with this interdependency. An identified neuromodulin domain motif for Alr0931, as indicated by the conserved domain search (NCBI CDS), further supports this hypothesis. Neuromodulin (or Gap-43) is thought to modulate the function of the presynaptic terminal in neurons by acting as an adapter protein for the membrane cytoskeleton through interaction with brain spectrin (BS) and actin filaments (Riederer and Routtenberg, 1999). Thereby, Gap-43, like Alr0931, is directly linked to the actin-like cytoskeleton and indirectly connected to microtubules and intermediate filaments through BSs. It was further shown to module the synaptic vesicle exocytosis (Riederer and Goodman, 1990; Riederer and

Routtenberg, 1999), reminiscent of the role of Alr0931 in cell-cell communication as shown by FRAP experiments. The fact that intercellular communication was not affected in the $\Delta alr4504\Delta alr4505$ strain but only in the $\Delta alr0931$ and $\Delta all2460$ strain further indicates a septosomal complex-organizing role for the corresponding two proteins while Alr4504 and Alr4505 possibly only anchor to those septosomal complexes in order to provide trichome stability but are not directly involved in septosome maintenance.

Furthermore, expression of Alr4504-GFP or Alr4505-GFP alone revealed a certain subpopulation of fluorescent patches that moved through the cells. Whether this motion is the direct result of an intrinsic dynamic property or relies on other cellular factors is not yet established. Preliminary FRAP experiments showed a possible, albeit not yet conclusive recovery of bleached Alr4504/Alr4505 filaments with a rather long recovery rate of more than > 20 min. This rate is within the framework of the recovery rate of eukaryotic IF proteins of about 23 min (Vikstrom *et al.*, 1992; Yoon *et al.*, 1998) and similar to CreS dynamics (Esue *et al.*, 2010). Additional bleaching experiments could thus provide further insight into the dynamic nature of these heteropolymers. To our surprise, we were not able to generate $\Delta alr4504$ or $\Delta alr4505$ strains. Whether this was due to pure chance or a toxic effect for the cells when only one of both proteins is present remains to be elucidated. Cytoskeletal complexes and networks are common in eukaryotes but were also shown to exist in prokaryotes, albeit with different properties. Networks of cytoskeletal proteins govern essential cellular functions including cell division (the FtsZ-driven divisome; reviewed by Lutkenhaus and Du (2017)), cell shape-maintenance (the MreB-dependent elongasome; reviewed by Wagstaff and Löwe (2018)) and polar growth (Scy, DivIVA and FilP orchestrated polarisome; reviewed by Lin and Thanbichler (2013)). The so-called polarisome resembles the trichome-stabilizing CCRPs studied here in so far as it also consists of an interconnected cytoskeletal network of IF-like CCRPs involved in crucial cellular functions (Holmes *et al.*, 2013). Like the Alr4504/Alr4505-filament, FilP was shown to provide a stabilizing structure that resisted mechanical stress. Our investigations revealed a pronounced interconnected cyanobacterial IF-like cytoskeleton comprised of numerous IF-like CCRPs from which certain cytoskeletal proteins are specifically adapted to the needs of their cyanobacteria of origin (Chapter 1+2). Interconnection and interactions of several of those IF-like cytoskeletal components like Slr1301 with Slr7083, Synpcc7942_2039 with Synpcc7942_1139 or All4981 with MreB and SepJ reveals an alleged advantage of a coordinated collaboration of the cytoskeleton. Therefore, the orchestration of essential cellular functions by cytoskeletal complexes in prokaryotes is more common than previously thought and appears to be rather the rule than the exception.

10 General Discussion

CCRPs with IF-like function are widespread among various cyanobacterial morphotypes and govern numerous cellular functions, often associated with cellular stability, motility or even signaling. In accordance with CreS (Ausmees, Kuhn and Jacobs-Wagner, 2003) and the conserved rod-domain protein family in Actinomycetes (Bagchi *et al.*, 2008), no homology and thus no relationship to eukaryotic IF proteins were identified for any of the investigated cyanobacterial proteins. This supports the idea that prokaryotic IF-like proteins evolved by convergent evolution rather than a vertical inheritance (Waidner *et al.*, 2009; Wickstead and Gull, 2011). At present, it is unknown from which ancestors cytoskeletal proteins originally arose. Current hypotheses suggest that they may have evolved from metabolic enzymes that had gained filament formation properties and later lost their enzymatic activity (Ingerson-Mahar and Gitai, 2012). In this study, Fm7001, an acetyl-CoA-carboxylase-like protein, was found to inhabit cytoskeletal properties which further strengthens the enzyme evolution theory. Cyanobacterial CCRPs assembled into diverse filamentous forms *in vitro* and *in vivo*, often forming multidimensional sheet-like structures. Although lace-like and net-like structures have been previously described for FilP (Fuchino *et al.*, 2017), CreS (Ausmees, Kuhn and Jacobs-Wagner, 2003), eukaryotic spectrin (Morrow *et al.*, 2011) or for so far uncharacterized proteins with a putative cytoskeletal function (Dobro *et al.*, 2017), cyanobacterial CCRPs revealed the unique tendency to form continuous layers rather than nets. This observation was specifically pronounced for Fm7001, Synpcc7942_2039, Synpcc7942_1139 and partially for Slr7083, which exhibited single filaments but also sheets that seemed to connect these filaments. Among those identified IF-like cyanobacterial cytoskeletal proteins, some were restricted to only few subsections while others were more broadly distributed, displaying homologous proteins in most or all cyanobacterial subsections. Like CreS (Ausmees, Kuhn and Jacobs-Wagner, 2003), Synpcc7942_2039 and Slr7083 are restricted to only one cyanobacterial genus where they exhibit particular species-specific cytoskeletal functions. Other proteins, like Fm7001, seem to have adapted to certain cyanobacterial morphotypes, being only present in cell-differentiating and multicellular cyanobacteria. On the other hand, proteins from a conserved group of homologous proteins (Alr0931, Slr1301 and Synpcc7942_1139) showed functional and structural diversification properties despite their direct relationship. Bagchi *et al.* (2008) identified a similar family of homologous proteins in actinomycetes but apart from *in vitro* data, functional studies were only performed for FilP from *S. coelicolor*. Although not belonging to the steadily growing group of coiled-coil rich cytoskeletal proteins, functional diversification was reported for bactofilins, which represent a unique class of prokaryotic-specific cytoskeletal proteins (Kühn *et al.*, 2010; Koch, McHugh and Hoiczky, 2011). The eukaryotic cytoskeletal systems are strongly interconnected, among others by so-called cytolinker proteins, inevitably linking their respective functions to one another (Herrmann and

Aebi, 2000; Alberts *et al.*, 2014). In prokaryotes, jointly operating cytoskeletal networks were described for the divisome (Löwe and Amos, 2017) and the polarisome that consist of at least three bacterial CCRPs (Lin and Thanbichler, 2013). Furthermore, a direct interplay of the MreB cytoskeleton and the IF-like protein CreS was described in *C. crescentus*, revealing a crosstalk of the different cytoskeletal systems (Charbon, Cabeen and Jacobs-Wagner, 2009). In the present study, we further identified a vastly interconnected cytoskeletal network comprising at least four IF-like CCRPs (Alr0931, Alr4504, Alr4505 and AlI2460) and the MreB cytoskeleton. Together they mediate cell-cell stability in the multicellular cyanobacterium *Anabaena* through the septosomes, which are sites of cell-cell connections composed of the membrane protein SepJ. The cytoskeletal network, which we hypothesize to be essential for the multicellular phenotype in cyanobacteria, provides another resemblance of the prokaryotic to the eukaryotic cytoskeleton. In eukaryotes, cell-cell communication and stabilization are facilitated by several cellular junctions that are essential for the development of higher order cellular assemblies and which are all directly or indirectly associated and regulated by the three cytoskeletal systems (Alberts *et al.*, 2014). Among the cyanobacterial CCRP network in *Anabaena*, two proteins (Alr4504 and Alr4505), showed interdependency for filamentation *in vitro* and *in vivo*, a phenomenon that has not yet been described for any IF-like cytoskeletal system in prokaryotes. It is therefore conceivable that cyanobacteria, owed to their long evolutionary history on earth (Schirromeister *et al.*, 2013) developed a unique cytoskeletal system that is not present in other species.

Taken together, we here identified several sophisticated cytoskeletal IF-like systems present in cyanobacteria of different morphotypes which are comprised of numerous CCRPs that have the tendency to assemble into sheet-like structures and that jointly perform various cellular tasks by forming interconnected cytoskeletal networks.

11 Outlook

This study lays the foundation for future research not only on cyanobacterial morphology but also on the underlying principles of the morphological diversity of the cyanobacterial phylum. Previous studies mainly focused only on one aspect of cyanobacterial morphology by studying MreB, FtsZ or SepJ isolated from one another. There are only a few exceptions where, for example, the connection between the FtsZ-driven elongasome and the SepJ-comprised septosomes were investigated or which superficially addressed putative collaboration of the FtsZ and MreB cytoskeleton. Here we showed that, like in eukaryotes, a one-sided approach focusing only on individual cytoskeletal systems alone does not meet the requirements of this complex phylum, most evident for multicellular cyanobacteria. Cytoskeletal systems of different origin (MreB, FtsZ, IF-like) are highly intertwined and interdependent and can thus only be assessed as a collective. The identified link of the MreB cytoskeleton to sites of cell-cell connections and trichome stability encourages to further evaluate the precise role of each of the participating components. An interesting question would be whether all these proteins are simultaneously expressed and immediately act together or if there is a certain chronology that is required in order to establish the precise functions and localizations within the cells. Time lapse gene expression analyses or genomically inserted fluorescently tagged CCRPs under the control of their native promoter might provide further insight into this. Interestingly, albeit all three obtained *Anabaena* mutant strains revealed temporary tremendous phenotypic changes, they all returned to a wt-like phenotype after prolonged culturing. The responsible mechanism for this observation is still unknown. Are single cytoskeletal components able to adopt functions of a missing component or are, for instance, changes in the cell envelope composition sufficient to stabilize the mutant phenotype? To tackle this question, lipid and polysaccharide compositions of wt and mutant strains could be compared at different time points in order to shed light on this transient phenotype.

Despite their moderate sequence similarity of about 39%, members of a group of conserved cyanobacterial IF-like homologous proteins were found to have retained their interaction capacity with each other. The precise domains that mediate this interaction are so far still unknown but four conserved amino acid sequence motifs were identified. Mutational analysis of those domains would supply us with further information about domains essential for polymerization and presumably also protein function. Likewise, essential protein domains for filamentation could be identified in other cyanobacterial cytoskeletal proteins which may lead to the identification of key motifs for cytoskeletal functions of cyanobacterial CCRPs. Additionally, albeit being involved in the multicellular phenotype of *Anabaena*, homologs of Alr4504 and Alr4505 were also identified in unicellular cyanobacteria belonging to *Cyanothece* spp.. Since these species lack cell-cell connections, it will be interesting to see whether the

polymerization capability of Alr4504/Alr4505 homologs in those bacteria was retained, lost or evolutionary adapted for other purposes. Alr4504/Alr4505 filaments showed incipient traits of dynamic turnovers within *Anabaena* cells, reminiscent of eukaryotic IF proteins and prokaryotic CreS. In order to explore the precise dynamic nature of those proteins, further FRAP experiments should be carried out including other fluorescently tagged cytoskeletal proteins like MreB, FtsZ or other here identified CCRPs to assess and compare intrinsic dynamic properties. This would additionally provide further indications for their cellular function within the cells; stable polymers would indicate structural or mechanical resistance features while highly dynamic structures would rather be involved in cellular processes that require more flexible polymers like chromosome segregation, peptidoglycan incorporation or cell division.

In the study at hand, we focused our research on about two dozen coiled-coil rich protein candidates from a few cyanobacterial species. The COILS algorithm, however, provided us with a set of several thousand proteins with a high coiled-coil content. By dint of including additional domain and motif characteristics - like the SMC domain or similarities to the cell division protein EzrA - that are partially predictive for cytoskeletal function, the *in silico* prediction strength could be increased even further. Additionally, coiled-coil rich proteins predicted by the COILS algorithm often contained domain features clearly linking them to membrane-bound pore-forming proteins. Precluding those proteins would further narrow down the list of predicted proteins. The morphotypes present in cyanobacterial species extend far beyond the ones employed in this thesis. For example, subsection III cyanobacteria of the order Spirulinales exhibit a coiled trichome morphotype. It would be interesting to investigate whether CreS-like CCRPs might also govern trichome curvature in those cells. Finally, little is known about the evolutionary relationship of cyanobacterial cytoskeletal proteins, specifically of those proteins exhibiting homologous proteins in other cyanobacterial morphotypes and subsections. Thus, phylogenetic studies could shed light on the evolutionary history of cyanobacterial CCRPs and link them to specific morphotypes or even the evolution of the cyanobacterial phylum.

12 References

- Alberts, B. *et al.* (2002) *Molecular Biology of the Cell, 4th edition*. New York: Garland Science.
- Alberts, B. *et al.* (2014) *Molecular Biology of the Cell*. 6th editio. Garland Science.
- Ausmees, N., Kuhn, J. R. and Jacobs-Wagner, C. (2003) 'The bacterial cytoskeleton: An intermediate filament-like function in cell shape', *Cell*, pp. 705–713. doi: 10.1016/S0092-8674(03)00935-8.
- Bagchi, S. *et al.* (2008) 'Intermediate filament-like proteins in bacteria and a cytoskeletal function in *Streptomyces*', *Molecular Microbiology*, 70(4), pp. 1037–1050. doi: 10.1111/j.1365-2958.2008.06473.x.
- Beck, E. *et al.* (1982) 'Nucleotide sequence and exact localization of the neomycin phosphotransferase gene from transposon Tn5', *Gene*, 19(3), pp. 327–336. doi: 10.1016/0378-1119(82)90023-3.
- Besingi, R. N. and Clark, P. L. (2015) 'Extracellular protease digestion to evaluate membrane protein cell surface localization', *Nature Protocols*. Nature Publishing Group, 10(12), pp. 2074–2080. doi: 10.1038/nprot.2015.131.
- Bhaya, D. *et al.* (2001) 'Novel Motility Mutants of *Synechocystis* Strain PCC 6803 Generated by *In Vitro* Transposon Mutagenesis', *Journal of Bacteriology*, 183(20), pp. 1–5. doi: 10.1128/JB.183.20.6140.
- Bi, E. and Lutkenhaus, J. (1991) 'FtsZ ring structure associated with division in *Escherichia coli*', *Nature*, 354(6349), pp. 161–164. doi: 10.1038/354161a0.
- Birnboim, H. C. and Doly, J. (1979) 'A rapid alkaline extraction procedure for screening recombinant plasmid DNA', *Nucleic Acids Research*, 7(6), pp. 1513–1523. doi: 10.1093/nar/gkn907.
- Blatch, G. L. and Lässle, M. (1999) 'The tetratricopeptide repeat: A structural motif mediating protein-protein interactions', *BioEssays*, 21(11), pp. 932–939. doi: 10.1002/(SICI)1521-1878(199911)21:11<932::AID-BIES5>3.0.CO;2-N.
- de Boer, P., Crossley, R. and Rothfield, L. (1992) 'The essential bacterial cell-division protein FtsZ is a GTPase', *Nature*, 359(6392), pp. 254–256. doi: 10.1038/359254a0.
- Bork, P., Sander, C. and Valencia, a (1992) 'An ATPase domain common to prokaryotic cell cycle proteins, sugar kinases, actin, and hsp70 heat shock proteins.', *Proceedings of the National Academy of Sciences of the United States of America*, pp. 7290–4. doi: 10.1073/pnas.89.16.7290.
- Bouameur, J. E., Favre, B. and Borradori, L. (2014) 'Plakins, a versatile family of cytolinkers: Roles in skin integrity and in human diseases', *Journal of Investigative Dermatology*. Elsevier Masson SAS, 134(4), pp. 885–894. doi: 10.1038/jid.2013.498.
- Boyer, H. and Roulland-Dessoix, D. (1969) 'A complementation analysis of the restriction and modification of DNA in *Escherichia coli*.', *J. Mol. Biol.*, 41, pp. 459–472.
- Bradford, M. M. (1976) 'A rapid and sensitive method for the quantitation of microgram quantities of protein utilizing the principle of protein-dye binding', *Analytical Biochemistry*, 72(1–2), pp. 248–254. doi: 10.1016/0003-2697(76)90527-3.
- Bronnenmeier, R. and Märkl, H. (1982) 'Hydrodynamic stress capacity of microorganisms', *Biotechnology and Bioengineering*, 24(3), pp. 553–578. doi: 10.1002/bit.260240304.

- Bryant, D. A. and Frigaard, N. U. (2006) 'Prokaryotic photosynthesis and phototrophy illuminated', *Trends in Microbiology*, 14(11), pp. 488–496. doi: 10.1016/j.tim.2006.09.001.
- Bryce, N. S. *et al.* (2003) 'Specification of actin filament function and molecular composition by tropomyosin isoforms.', *Molecular biology of the cell*. American Society for Cell Biology, 14(3), pp. 1002–16. doi: 10.1091/mbc.E02-04-0244.
- Burnat, M., Schleiff, E. and Flores, E. (2014) 'Cell envelope components influencing filament length in the heterocyst-forming cyanobacterium *Anabaena sp.* strain PCC 7120', *Journal of Bacteriology*, 196(23), pp. 4026–4035. doi: 10.1128/JB.02128-14.
- Busby, S. and Ebright, R. H. (1999) 'Transcription activation by catabolite activator protein (CAP)', *Journal of Molecular Biology*, 293(2), pp. 199–213. doi: 10.1006/jmbi.1999.3161.
- Cabeen, M. T. *et al.* (2009) 'Bacterial cell curvature through mechanical control of cell growth', *The EMBO Journal*, pp. 1208–1219. doi: 10.1038/emboj.2009.61.
- Cabeen, M. T., Herrmann, H. and Jacobs-Wagner, C. (2011) 'The domain organization of the bacterial intermediate filament-like protein crescentin is important for assembly and function', *Cytoskeleton*, pp. 205–219. doi: 10.1002/cm.20505.
- Cabeen, M. T. and Jacobs-Wagner, C. (2010) 'The Bacterial Cytoskeleton'. *Annu. Rev. Genet.*, 44, pp. 365–392. doi: 10.1146/annurev-genet-102108-134845.
- Cai, Y. and Wolk, C. P. (1990) 'Use of a conditionally lethal gene in *Anabaena sp.* strain PCC 7120 to select for double recombinants and to entrap insertion sequences', *Journal of Bacteriology*, 172(6), pp. 3138–3145.
- Camberg, J. L., Hoskins, J. R. and Wickner, S. (2009) 'ClpXP protease degrades the cytoskeletal protein, FtsZ, and modulates FtsZ polymer dynamics', *Proc Natl Acad Sci U S A*, 106(26), pp. 10614–10619. doi: 10.1073/pnas.0904886106.
- Cappuccinelli, P. (1980) 'The movement of eukaryotic cells', in *Motility of Living Cells*. Dordrecht: Springer Netherlands, pp. 59–74. doi: 10.1007/978-94-009-5812-8_4.
- Carballido-Lopez, R. (2006) 'The Bacterial Actin-Like Cytoskeleton', *Microbiology and Molecular Biology Reviews*, 70(4), pp. 888–909. doi: 10.1128/MMBR.00014-06.
- Carballido-López, R. *et al.* (2006) 'Actin Homolog MreBH Governs Cell Morphogenesis by Localization of the Cell Wall Hydrolase LytE', *Developmental Cell*, 11(3), pp. 399–409. doi: 10.1016/j.devcel.2006.07.017.
- Celler, K. *et al.* (2013) 'Multidimensional view of the bacterial cytoskeleton', *Journal of Bacteriology*, 195(8), pp. 1627–1636. doi: 10.1128/JB.02194-12.
- Charbon, G., Cabeen, M. T. and Jacobs-Wagner, C. (2009) 'Bacterial intermediate filaments: *In vivo* assembly, organization, and dynamics of crescentin', *Genes and Development*, pp. 1131–1144. doi: 10.1101/gad.1795509.
- Cohen, S. E. *et al.* (2014) 'Dynamic localization of the cyanobacterial circadian clock proteins', *Current Biology*. Elsevier Ltd, 24(16), pp. 1836–1844. doi: 10.1016/j.cub.2014.07.036.
- Corpet, F. (1988) 'Multiple sequence alignment with hierarchical clustering.', *Nucleic acids research*, 16(22), pp. 10881–90. doi: 10.1093/nar/16.22.10881.
- Corrales-Guerrero, L. *et al.* (2013) 'Functional dissection and evidence for intercellular transfer of the heterocyst-differentiation PatS morphogen', *Molecular Microbiology*, 88(6), pp. 1093–1105. doi: 10.1111/mmi.12244.

- Cronier, S. *et al.* (2008) 'Detection and characterization of proteinase K-sensitive disease-related prion protein with thermolysin', *Biochemical Journal*, 416(2), pp. 297–305. doi: 10.1042/BJ20081235.
- Dagan, T. *et al.* (2013) 'Genomes of stigonematalean cyanobacteria (subsection V) and the evolution of oxygenic photosynthesis from prokaryotes to plastids', *Genome Biology and Evolution*, 5(1), pp. 31–44. doi: 10.1093/gbe/evs117.
- Daley, D. O., Skoglund, U. and Söderström, B. (2016) 'FtsZ does not initiate membrane constriction at the onset of division', *Scientific Reports*. Nature Publishing Group, 6, pp. 1–6. doi: 10.1038/srep33138.
- Dempwolff, F. *et al.* (2011) 'Bacillus subtilis MreB orthologs self-organize into filamentous structures underneath the cell membrane in a heterologous cell system', *PLoS ONE*. doi: 10.1371/journal.pone.0027035.
- Deng, X. *et al.* (2017) 'Four-stranded mini microtubules formed by *Prostheco bacter* BtubAB show dynamic instability', *Proceedings of the National Academy of Sciences*, 114(29), pp. E5950–E5958. doi: 10.1073/pnas.1705062114.
- Derman, A. I. *et al.* (2009) 'Phylogenetic analysis identifies many uncharacterized actin-like proteins (Alps) in bacteria: Regulated polymerization, dynamic instability and treadmilling in Alp7A', *Molecular Microbiology*, 73(4), pp. 534–552. doi: 10.1111/j.1365-2958.2009.06771.x.
- Deusch, O. *et al.* (2008) 'Genes of cyanobacterial origin in plant nuclear genomes point to a heterocyst-forming plastid ancestor', *Molecular Biology and Evolution*, 25(4), pp. 748–761. doi: 10.1093/molbev/msn022.
- Dobro, M. J. *et al.* (2017) 'Uncharacterized bacterial structures revealed by electron cryotomography', *Journal of Bacteriology*, 199(17). doi: 10.1128/JB.00100-17.
- Dörrich, A. K. *et al.* (2014) 'Deletion of the *Synechocystis* sp. PCC 6803 kaiAB1C1 gene cluster causes impaired cell growth under light-dark conditions', *Microbiology (United Kingdom)*, 160(2014), pp. 2538–2550. doi: 10.1099/mic.0.081695-0.
- Ducat, D. C., Sachdeva, G. and Silver, P. A. (2011) 'Rewiring hydrogenase-dependent redox circuits in cyanobacteria', *Proceedings of the National Academy of Sciences*, 108(10), pp. 3941–3946. doi: 10.1073/pnas.1016026108.
- Ebersbach, G. *et al.* (2006) 'Regular cellular distribution of plasmids by oscillating and filament-forming para ATPase of plasmid pB171', *Molecular Microbiology*, 61(6), pp. 1428–1442. doi: 10.1111/j.1365-2958.2006.05322.x.
- Ebersbach, G. *et al.* (2008) 'A Self-Associating Protein Critical for Chromosome Attachment, Division, and Polar Organization in *Caulobacter*', *Cell*, 134(6), pp. 956–968. doi: 10.1016/j.cell.2008.07.016.
- Eisenbach, M. (2011) 'Bacterial Chemotaxis', *eLS*. doi: 10.1002/9780470015902.a0001251.pub3.
- Elhai, J. *et al.* (1997) 'Reduction of conjugal transfer efficiency by three restriction activities of *Anabaena* sp. strain PCC 7120.', *Journal of bacteriology*, 179(6), pp. 1998–2005.
- van den Ent, F. *et al.* (2014) 'Bacterial actin MreB forms antiparallel double filaments', *eLife*, 2014(3), pp. 1–22. doi: 10.7554/eLife.02634.
- Van den Ent, F. *et al.* (2002) 'F-actin-like filaments formed by plasmid segregation protein ParM', *EMBO Journal*, 21(24), pp. 6935–6943. doi: 10.1093/emboj/cdf672.

- Ent, F. van den, Amos, L. A. and Löwe, J. (2001) 'Prokaryotic origin of the actin cytoskeleton', *Nature*, 413(9), pp. 39–44. Available at: vanDenEnt_2001_Nature_413(9)-39.pdf.
- Erber, A. *et al.* (1999) 'Characterization of the Hydra lamin and its gene: A molecular phylogeny of metazoan lamins', *Journal of Molecular Evolution*, 49(2), pp. 260–271. doi: 10.1007/PL00006548.
- Erickson, H. P. (2007) 'Evolution of the cytoskeleton', *Bioessays*, 29(7), pp. 668–677. doi: 10.1002/bies.20601.
- Erickson, H. P. and Osawa, M. (2017) 'FtsZ Constriction Force – Curved Protofilaments Bending Membranes', 84, pp. 139–160. doi: 10.1007/978-3-319-53047-5.
- Eriksson, J. E. *et al.* (2009) 'Introducing intermediate filaments: from discovery to disease.', *The Journal of clinical investigation*, 119(7), pp. 1763–71. doi: 10.1172/JCI38339.
- Errington, J. and Wu, L. J. (2017) 'Cell Cycle Machinery in *Bacillus subtilis*', in: Springer, Cham, pp. 67–101. doi: 10.1007/978-3-319-53047-5_3.
- Esteves-Ferreira, A. A. *et al.* (2017) 'A Novel Mechanism, Linked to Cell Density, Largely Controls Cell Division in *Synechocystis*', *Plant Physiology*, 174(4), pp. 2166–2182. doi: 10.1104/pp.17.00729.
- Esue, O. *et al.* (2010) 'Dynamics of the Bacterial Intermediate Filament Crescentin *In Vitro* and *In Vivo*', *PLoS ONE*, 5(1), p. e8855. doi: 10.1371/journal.pone.0008855.
- Fenton, A. K. and Gerdes, K. (2013) 'Direct interaction of FtsZ and MreB is required for septum synthesis and cell division in *Escherichia coli*', *EMBO Journal*. Nature Publishing Group, 32(13), pp. 1953–1965. doi: 10.1038/emboj.2013.129.
- Fiuza, M. *et al.* (2010) 'Phosphorylation of a novel cytoskeletal protein (RsmP) regulates rod-shaped morphology in *Corynebacterium glutamicum*', *Journal of Biological Chemistry*, pp. 29387–29397. doi: 10.1074/jbc.M110.154427.
- Flores, E. *et al.* (2006) 'Is the periplasm continuous in filamentous multicellular cyanobacteria?', *Trends in Microbiology*, 14(10), pp. 439–443. doi: 10.1016/j.tim.2006.08.007.
- Flores, E. *et al.* (2007) 'Septum-localized protein required for filament integrity and diazotrophy in the heterocyst-forming cyanobacterium *Anabaena sp.* strain PCC 7120', *Journal of Bacteriology*, 189(10), pp. 3884–3890. doi: 10.1128/JB.00085-07.
- Flores, E. *et al.* (2016) 'Septal Junctions in Filamentous Heterocyst-Forming Cyanobacteria', *Trends in Microbiology*. Elsevier Ltd, 24(2), pp. 79–82. doi: 10.1016/j.tim.2015.11.011.
- Flores, E. and Herrero, A. (2010) 'Compartmentalized function through cell differentiation in filamentous cyanobacteria', *Nature Reviews Microbiology*, 8(1), pp. 39–50. doi: 10.1038/nrmicro2242.
- Fowler, V. M. (2013) 'The Human Erythrocyte Plasma Membrane: A Rosetta Stone for Decoding Membrane–Cytoskeleton Structure', *Current Topics in Membranes*. Academic Press, 72, pp. 39–88. doi: 10.1016/B978-0-12-417027-8.00002-7.
- Fricke, W. (2017) 'Turgor Pressure', *eLS*, (January), pp. 1–6. doi: 10.1002/9780470015902.a0001687.pub2.
- Fuchino, K. *et al.* (2013) 'Dynamic gradients of an intermediate filament-like cytoskeleton are recruited by a polarity landmark during apical growth', *Proceedings of the National Academy of Sciences*, pp. E1889–E1897. doi: 10.1073/pnas.1305358110.

- Fuchino, K. *et al.* (2017) 'Cell-biological studies of osmotic shock response in *Streptomyces*', *Journal of Bacteriology*, 199(1). doi: 10.1128/JB.00465-16.
- Fuchs, E. and Weber, K. (1994) 'INTERMEDIATE FILAMENTS: Structure, Dynamics, Function and Disease', *Annual Review of Biochemistry*, 63, pp. 345–382.
- Garner, E. C. *et al.* (2011) 'Circumferential Motions of the Cell Wall Synthesis Machinery Drive Cytoskeletal Dynamics in *B. subtilis*', *Science*, 333(6039), pp. 222–225.
- Garner, E. C., Campbell, C. S. and Dyce Mullins, R. (2004) 'Dynamic Instability in a DNA-Segregating Prokaryotic Actin Homolog', *Science*, 306(5698), pp. 1021–1025.
- Gayathri, P. *et al.* (2012) 'A Bipolar Spindle Of Antiparallel ParM Filaments Drives Bacterial Plasmid Segregation', 338(6112), pp. 1334–1337. doi: 10.1126/science.1229091.
- Gerdes, K., Larsen, J. E. L. and Molin, S. (1985) 'Stable inheritance of plasmid R1 requires two different loci', *Journal of Bacteriology*, 161(1), pp. 292–298.
- Giepmans, B. N. G. (2004) 'Gap junctions and connexin-interacting proteins', *Cardiovascular Research*, 62(2), pp. 233–245. doi: 10.1016/j.cardiores.2003.12.009.
- Golden, S. S., Brusslan, J. and Haselkorn, R. (1987) 'Genetic Engineering of the Cyanobacterial Chromosome', *Methods in Enzymology*, 153(C), pp. 215–231. doi: 10.1016/0076-6879(87)53055-5.
- Goldmann, W. H. (2018) 'Intermediate filaments and cellular mechanics', *Cell Biology International*, 42, pp. 132–138. doi: 10.1002/cbin.10879.
- González, A. *et al.* (2016) 'Expanding the role of FurA as essential global regulator in cyanobacteria', *PLoS ONE*, 11(3), pp. 1–22. doi: 10.1371/journal.pone.0151384.
- González, J. M. *et al.* (2003) 'Essential cell division protein FtsZ assembles into one monomer-thick ribbons under conditions resembling the crowded intracellular environment', *Journal of Biological Chemistry*, 278(39), pp. 37664–37671. doi: 10.1074/jbc.M305230200.
- Grant, S. G. *et al.* (1990) 'Differential plasmid rescue from transgenic mouse DNAs into *Escherichia coli* methylation-restriction mutants.', *Proceedings of the National Academy of Sciences*, 87(12), pp. 4645–4649. doi: 10.1073/pnas.87.12.4645.
- Green, K. J. *et al.* (2005) 'Intermediate filament associated proteins', *Fibrous Proteins: Coiled-Coils, Collagen and Elastomers*, p. 143. doi: 10.1016/S0065-3233(04)70006-6.
- Gregolin, C. *et al.* (1966) 'Molecular characteristics of liver acetyl-CoA carboxylase.', *Biochemistry*, pp. 148–155.
- Griese, M., Lange, C. and Soppa, J. (2011) 'Ploidy in cyanobacteria', *FEMS Microbiology Letters*, 323(2), pp. 124–131. doi: 10.1111/j.1574-6968.2011.02368.x.
- Grigorieva, G. and Shestakov, S. (1982) 'Transformation in the cyanobacterium *Synechocystis* sp. 6803', *FEMS Microbiology Letters*, 13(4), pp. 367–370. doi: 10.1111/j.1574-6968.1982.tb08289.x.
- Hagemann, M. and Hess, W. R. (2018) 'Systems and synthetic biology for the biotechnological application of cyanobacteria', *Current Opinion in Biotechnology*. Elsevier Ltd, 49, pp. 94–99. doi: 10.1016/j.copbio.2017.07.008.
- Hanukoglu, I. and Fuchs, E. (1983) 'The cDNA sequence of a type II cytoskeletal keratin reveals constant and variable structural domains among keratins', *Cell*, 33(3), pp. 915–924. doi: 10.1016/0092-8674(83)90034-X.

- Heins, S. and Aebi, U. (1994) 'Making heads and tails of intermediate filament assembly, dynamics and networks', *Current Opinion in Cell Biology*, 6(1), pp. 25–33. doi: 10.1016/0955-0674(94)90112-0.
- Heinz, S. *et al.* (2016) 'Thylakoid Membrane Architecture in *Synechocystis* Depends on CurT, a Homolog of the Granal CURVATURE THYLAKOID1 Proteins', *The Plant Cell*, 28(9), pp. 2238–2260. doi: 10.1105/tpc.16.00491.
- Henson, B. J. *et al.* (2004) 'Molecular phylogeny of the heterocystous cyanobacteria (subsections IV and V) based on nifD', *International Journal of Systematic and Evolutionary Microbiology*, 54(2), pp. 493–497. doi: 10.1099/ij.s.0.02821-0.
- Hering, L. *et al.* (2016) 'Novel origin of lamin-derived cytoplasmic intermediate filaments in tardigrades', *eLife*, 5(FEBRUARY2016), pp. 1–18. doi: 10.7554/eLife.11117.
- Herrero, A., Stavans, J. and Flores, E. (2016) 'The multicellular nature of filamentous heterocyst-forming cyanobacteria', *FEMS Microbiology Reviews*, 40(6), pp. 831–854. doi: 10.1093/femsre/fuw029.
- Herrmann, H. *et al.* (1996) 'Structure and assembly properties of the intermediate filament protein vimentin: The role of its head, rod and tail domains', *Journal of Molecular Biology*, 264(5), pp. 933–953. doi: 10.1006/jmbi.1996.0688.
- Herrmann, H. *et al.* (2007) 'Intermediate filaments: From cell architecture to nanomechanics', *Nature Reviews Molecular Cell Biology*, 8(7), pp. 562–573. doi: 10.1038/nrm2197.
- Herrmann, H. and Aebi, U. (2000) 'Intermediate filaments and their associates: Multi-talented structural elements specifying cytoarchitecture and cytodynamics', *Current Opinion in Cell Biology*, 12(1), pp. 79–90. doi: 10.1016/S0955-0674(99)00060-5.
- Herrmann, H. and Aebi, U. (2004) 'Intermediate Filaments: Molecular Structure, Assembly Mechanism, and Integration Into Functionally Distinct Intracellular Scaffolds', *Annual Review of Biochemistry*, 73(1), pp. 749–789. doi: 10.1146/annurev.biochem.73.011303.073823.
- Herrmann, H., Kreplak, L. and Aebi, U. (2004) 'Isolation, Characterization, and *In Vitro* Assembly of Intermediate Filaments', *Methods in Cell Biology*. Academic Press, 78, pp. 3–24. doi: 10.1016/S0091-679X(04)78001-2.
- Hesse, M. *et al.* (2000) 'Targeted deletion of keratins 18 and 19 leads to trophoblast fragility and early embryonic lethality', *EMBO Journal*, 19(19), pp. 5060–5070. doi: 10.1093/emboj/19.19.5060.
- Hoiczky, E. and Baumeister, W. (1998) 'The junctional pore complex, a prokaryotic secretion organelle, is the molecular motor underlying gliding motility in cyanobacteria', *Current Biology*, 8(21), pp. 1161–1168. doi: 10.1016/S0960-9822(07)00487-3.
- Holmes, N. A. *et al.* (2013) 'Coiled-coil protein Scy is a key component of a multiprotein assembly controlling polarized growth in *Streptomyces*', *Proceedings of the National Academy of Sciences*, pp. E397–E406. doi: 10.1073/pnas.1210657110.
- Hu, B. *et al.* (2007) 'MreB is important for cell shape but not for chromosome segregation of the filamentous cyanobacterium *Anabaena sp.* PCC 7120', *Molecular Microbiology*, 63(6), pp. 1640–1652. doi: 10.1111/j.1365-2958.2007.05618.x.
- Hu, Z., Gogol, E. P. and Lutkenhaus, J. (2002) 'Dynamic assembly of MinD on phospholipid vesicles regulated by ATP and MinE', *Proceedings of the National Academy of Sciences of the United States of America*, 99(10), pp. 6761–6766. doi: 10.1073/pnas.102059099.
- Hurme, R. *et al.* (1994) 'Intermediate filament-like network formed *in vitro* by a bacterial coiled

- coil protein', *Journal of Biological Chemistry*, pp. 10675–10682.
- Inclan, Y. F. *et al.* (2016) 'A scaffold protein connects type IV pili with the Chp chemosensory system to mediate activation of virulence signaling in *Pseudomonas aeruginosa*', *Molecular Microbiology*, 101(4), pp. 590–605. doi: 10.1111/mmi.13410.
- Ingerson-Mahar, M. *et al.* (2010) 'The metabolic enzyme CTP synthase forms cytoskeletal filaments', *Nature Cell Biology*, pp. 739–746. doi: 10.1038/ncb2087.
- Ingerson-Mahar, M. and Gitai, Z. (2012) 'A growing family: the expanding universe of the bacterial cytoskeleton', *FEMS Microbiol Rev*, 36(1), pp. 256–266. doi: 10.1111/j.1574-6976.2011.00316.x.
- Inoue, H., Nojima, H. and Okayama, H. (1990) 'High efficiency transformation of *Escherichia coli* with plasmids', *Gene*, 96(1), pp. 23–28. doi: 10.1016/0378-1119(90)90336-P.
- Jain, I. H., Vijayan, V. and O'Shea, E. K. (2012) 'Spatial ordering of chromosomes enhances the fidelity of chromosome partitioning in cyanobacteria.', *Proceedings of the National Academy of Sciences of the United States of America*, 109(34), pp. 13638–43. doi: 10.1073/pnas.1211144109.
- Jiang, X. R. and Chen, G. Q. (2016) 'Morphology engineering of bacteria for bio-production', *Biotechnology Advances*. Elsevier Inc., 34(4), pp. 435–440. doi: 10.1016/j.biotechadv.2015.12.007.
- Jinek, M. *et al.* (2012) 'A Programmable Dual-RNA – Guided DNA Endonuclease in Adaptive Bacterial Immunity', *Science*, 337(6096), pp. 816–821. doi: 10.1126/science.1225829.
- Jones, L. J. F., Carballido-López, R. and Errington, J. (2001) 'Control of cell shape in bacteria: Helical, actin-like filaments in *Bacillus subtilis*', *Cell*, 104(6), pp. 913–922. doi: 10.1016/S0092-8674(01)00287-2.
- Joshi, J. B., Elias, C. B. and Patole, M. S. (1996) 'Role of hydrodynamic shear in the cultivation of animal, plant and microbial cells', *Chemical Engineering Journal and the Biochemical Engineering Journal*, 62(2), pp. 121–141. doi: 10.1016/0923-0467(95)03062-X.
- Kabsch, W. and Holmes, K. C. (1995) 'The actin fold', *FASEB Journal*, 9(2), pp. 167–174.
- Kaneko, T. *et al.* (1996) 'Sequence Analysis of the Genome of the Unicellular Cyanobacterium *Synechocystis sp.* Strain PCC6803 . II . Sequence Determination of the Entire Genome and Assignment of Potential Protein-coding Regions', *DNA Research*, 3(January), pp. 109–136.
- Kaneko, T. (2001) 'Complete Genomic Sequence of the Filamentous Nitrogen-fixing Cyanobacterium *Anabaena sp.* Strain PCC 7120', *DNA Research*, 8(5), pp. 205–213. doi: 10.1093/dnares/8.5.205.
- Karimova, G. *et al.* (1998) 'A bacterial two-hybrid system based on a reconstituted signal transduction pathway', *Proceedings of the National Academy of Sciences*, 95(10), pp. 5752–5756. doi: 10.1073/pnas.95.10.5752.
- Karimova, G., Davi, M. and Ladant, D. (2012) 'The β -lactam resistance protein Blr, a small membrane polypeptide, is a component of the *Escherichia coli* cell division machinery', *Journal of Bacteriology*, 194(20), pp. 5576–5588. doi: 10.1128/JB.00774-12.
- Kelemen, G. H. (2017) 'Intermediate Filaments Supporting Cell Shape and Growth in Bacteria', in: Springer, Cham, pp. 161–211. doi: 10.1007/978-3-319-53047-5_6.
- Khayatan, B., Meeks, J. C. and Risser, D. D. (2015) 'Evidence that a modified type IV pilus-like system powers gliding motility and polysaccharide secretion in filamentous cyanobacteria',

Molecular Microbiology, 98(6), pp. 1021–1036. doi: 10.1111/mmi.13205.

Kleinschmidt, A. K., Moss, J. and Lane, D. M. (1969) 'Acetyl coenzyme A carboxylase: filamentous nature of the animal enzymes.', *Science (New York, NY)*, pp. 1276–1278.

Koch, M. K., McHugh, C. A. and Hoiczky, E. (2011) 'BacM, an N-terminally processed bactofilin of *Myxococcus xanthus*, is crucial for proper cell shape', *Mol Microbiol.*, 80(4), pp. 1031–1051. doi: 10.1111/j.1365-2958.2011.07629.x.

Koch, R. *et al.* (2017) 'Plasticity first: Molecular signatures of a complex morphological trait in filamentous cyanobacteria', *BMC Evolutionary Biology*. *BMC Evolutionary Biology*, 17(1), pp. 1–11. doi: 10.1186/s12862-017-1053-5.

Koonin, E. V. (2010) 'The origin and early evolution of eukaryotes in the light of phylogenomics', *Genome Biology*, 11(5). doi: 10.1186/gb-2010-11-5-209.

Koonin, E. V. (2015) 'Origin of eukaryotes from within archaea, archaeal eukaryome and bursts of gene gain: eukaryogenesis just made easier?', *Philosophical Transactions of the Royal Society B: Biological Sciences*, 370(1678), p. 20140333. doi: 10.1098/rstb.2014.0333.

Kopfmann, S. and Hess, W. R. (2013) 'Toxin-antitoxin systems on the large defense plasmid pSYSYA of *Synechocystis sp.* PCC 6803', *Journal of Biological Chemistry*, 288(10), pp. 7399–7409. doi: 10.1074/jbc.M112.434100.

Köster, S. *et al.* (2015) 'Intermediate filament mechanics *in vitro* and in the cell: From coiled coils to filaments, fibers and networks', *Current Opinion in Cell Biology*, 32, pp. 82–91. doi: 10.1016/j.ceb.2015.01.001.

Kraemer, J. A. *et al.* (2012) 'A phage tubulin assembles dynamic filaments by an atypical mechanism to center viral DNA within the host cell', *Cell*. Elsevier Inc., 149(7), pp. 1488–1499. doi: 10.1016/j.cell.2012.04.034.

Kruse, T., Bork-Jensen, J. and Gerdes, K. (2005) 'The morphogenetic MreBCD proteins of *Escherichia coli* form an essential membrane-bound complex', *Molecular Microbiology*, 55(1), pp. 78–89. doi: 10.1111/j.1365-2958.2004.04367.x.

Kühn, J. *et al.* (2010) 'Bactofilins, a ubiquitous class of cytoskeletal proteins mediating polar localization of a cell wall synthase in *Caulobacter crescentus*', *EMBO Journal*, pp. 327–339. doi: 10.1038/emboj.2009.358.

Kumar, K., Mella-Herrera, R. A. and Golden, J. W. (2010) 'Cyanobacterial heterocysts', *Cold Spring Harbor Perspectives in Biology*, 2(4), pp. 1–19. doi: 10.1101/cshperspect.a000315.

Larsen, R. A. *et al.* (2007) 'Treadmilling of a prokaryotic tubulin-like protein, TubZ, required for plasmid stability in *Bacillus thuringiensis*', *Genes and Development*, 21(11), pp. 1340–1352. doi: 10.1101/gad.1546107.

Leung, C. L., Green, K. J. and Liem, R. K. H. (2002) 'Plakins: A family of versatile cytolinker proteins', *Trends in Cell Biology*, 12(1), pp. 37–45. doi: 10.1016/S0962-8924(01)02180-8.

Liberton, M. *et al.* (2006) 'Ultrastructure of the membrane systems in the unicellular cyanobacterium *Synechocystis sp.* strain PCC 6803', *Protoplasma*, 227(2–4), pp. 129–138. doi: 10.1007/s00709-006-0145-7.

Lin, L. and Thanbichler, M. (2013) 'Nucleotide-independent cytoskeletal scaffolds in bacteria', *Cytoskeleton*, 70(8), pp. 409–423. doi: 10.1002/cm.21126.

Liu, J. L. (2010) 'Intracellular compartmentation of CTP synthase in *Drosophila*', *Journal of Genetics and Genomics*, pp. 281–296. doi: 10.1016/S1673-8527(09)60046-1.

- Lodish, H. *et al.* (2000) *Molecular Cell Biology*. 4th edn. New York: W. H. Freeman. Available at: <https://www.ncbi.nlm.nih.gov/books/NBK21560/>.
- Loose, M. and Mitchison, T. J. (2014) 'The bacterial cell division proteins FtsA and FtsZ self-organize into dynamic cytoskeletal patterns', *Nature Cell Biology*. Nature Publishing Group, 16(1), pp. 38–46. doi: 10.1038/ncb2885.
- Lopes Pinto, F. *et al.* (2011) 'FtsZ degradation in the cyanobacterium *Anabaena sp.* strain PCC 7120', *Journal of Plant Physiology*. Elsevier GmbH., 168(16), pp. 1934–1942. doi: 10.1016/j.jplph.2011.05.023.
- Löwe, J. and Amos, L. A. (1998) 'Crystal structure of the bacterial cell division protein FtsZ.', *Nature*, 391(1996), pp. 203–206.
- Löwe, J. and Amos, L. A. (2009) 'Evolution of cytomotive filaments: The cytoskeleton from prokaryotes to eukaryotes', *International Journal of Biochemistry and Cell Biology*, 41(2), pp. 323–329. doi: 10.1016/j.biocel.2008.08.010.
- Löwe, J. and Amos, L. A. (2017) Prokaryotic Cytoskeletons Filamentous Protein Polymers Active in the Cytoplasm of Bacterial and Archaeal Cells. *Springer International Publishing AG*. doi: 10.1007/978-3-319-53047-5 ISBN.
- Lu, C., Reedy, M. and Erickson, H. P. (2000) 'Straight and curved conformations of FtsZ are regulated by GTP hydrolysis', *Journal of Bacteriology*, 182(1), pp. 164–170. doi: 10.1128/JB.182.1.164-170.2000.
- Lupas, A., Van Dyke, M. and Stock, J. (1991) 'Predicting coiled coils from protein sequences', *Science*, pp. 1162–1164. doi: 10.1126/science.252.5009.1162.
- Lutkenhaus, J. (2012) 'The ParA/MinD family puts things in their place', *Trends in Microbiology*, 20(9), pp. 411–418. doi: 10.1016/j.tim.2012.05.002.
- Lutkenhaus, J. and Du, S. (2017) '*E. coli* Cell Cycle Machinery', in *Springer*, Cham, pp. 27–65. doi: 10.1007/978-3-319-53047-5_2.
- Lutkenhaus, J., Pichoff, S. and Du, S. (2012) 'Bacterial cytokinesis: From Z ring to divisome', *Cytoskeleton*, 69(10), pp. 778–790. doi: 10.1002/cm.21054.
- Maier, B. and Wong, G. C. L. (2015) 'How Bacteria Use Type IV Pili Machinery on Surfaces', *Trends in Microbiology*. Elsevier Ltd, 23(12), pp. 775–788. doi: 10.1016/j.tim.2015.09.002.
- Malek, A. M. and Izumo, S. (1996) 'Mechanism of endothelial cell shape change and cytoskeletal remodeling in response to fluid shear stress.', *Journal of cell science*, 109, pp. 713–726. doi: 10.1007/bf02623896.
- Mason, J. M. and Arndt, K. M. (2004) 'Coiled coil domains: Stability, specificity, and biological implications', *ChemBioChem*, 5(2), pp. 170–176. doi: 10.1002/cbic.200300781.
- Mazza, P. *et al.* (2006) 'MreB of *Streptomyces coelicolor* is not essential for vegetative growth but is required for the integrity of aerial hyphae and spores', *Molecular Microbiology*, 60(4), pp. 838–852. doi: 10.1111/j.1365-2958.2006.05134.x.
- Meselson, M. and Yuan, R. (1968) 'DNA restriction enzyme from *E. coli*.', *Nature*, 217(5134), pp. 1110–4. Available at: <http://www.ncbi.nlm.nih.gov/pubmed/4868368>.
- Miller, J. H. (1992) A Short Course in Bacterial Genetics – A Laboratory Manual and Handbook for *Escherichia coli* and Related Bacteria, *Cold Spring Harbor Laboratory Press*. Cold Spring Harbor. doi: 10.1002/jobm.3620330412.

- Miyagishima, S. *et al.* (2014) 'FtsZ-less prokaryotic cell division as well as FtsZ- and dynamin-less chloroplast and non-photosynthetic plastid division', *Frontiers in Plant Science*, 5(September), pp. 1–13. doi: 10.3389/fpls.2014.00459.
- Miyagishima, S. Y. *et al.* (2004) 'Two types of FtsZ proteins in mitochondria and red-lineage chloroplasts: The duplication of FtsZ is implicated in endosymbiosis', *Journal of Molecular Evolution*, 58(3), pp. 291–303. doi: 10.1007/s00239-003-2551-1.
- Møller-Jensen, J. and Löwe, J. (2005) 'Increasing complexity of the bacterial cytoskeleton', *Current Opinion in Cell Biology*, 17(1), pp. 75–81. doi: 10.1016/j.ceb.2004.11.002.
- Mori, T. and Johnson, C. H. (2001) 'Independence of Circadian Timing from Cell Division in Cyanobacteria.', *Journal of Bacteriology*, 183(8), pp. 2439–44. doi: 10.1128/JB.183.8.2439.
- Morrow, J. S. *et al.* (2011) 'Of Membrane Stability and Mosaics: The Spectrin Cytoskeleton', *Comprehensive Physiology*. doi: 10.1002/cphy.cp140111.
- Moseley, J. B. (2013) 'An expanded view of the eukaryotic cytoskeleton', *Molecular Biology of the Cell*, 24(11), pp. 1615–1618. doi: 10.1091/mbc.E12-10-0732.
- Mukherjee, A. and Lutkenhaus, J. (1994) 'Guanine nucleotide-dependent assembly of FtsZ into filaments', *Journal of Bacteriology*, 176(9), pp. 2754–2758. doi: 10.1128/jb.176.9.2754-2758.1994.
- Mullineaux, C. W. *et al.* (2008) 'Mechanism of intercellular molecular exchange in heterocyst-forming cyanobacteria', *EMBO Journal*, 27(9), pp. 1299–1308. doi: 10.1038/emboj.2008.66.
- Mullis, K. B. and Faloona, F. A. (1987) 'Specific synthesis of DNA *in vitro* via a polymerase-catalyzed chain reaction', *Methods in Enzymology*. Academic Press, 155, pp. 335–350. doi: 10.1016/0076-6879(87)55023-6.
- Nakamura, Y. *et al.* (1993) 'Acceleration of bovine neurofilament L assembly by deprivation of acidic tail domain', *European Journal of Biochemistry*, 212(2), pp. 565–571. doi: 10.1111/j.1432-1033.1993.tb17694.x.
- Nayar, A. S. *et al.* (2007) 'FraG is necessary for filament integrity and heterocyst maturation in the cyanobacterium *Anabaena sp.* strain PCC 7120', *Microbiology*, 153(2), pp. 601–607. doi: 10.1099/mic.0.2006/002535-0.
- Nieves-Mori3n, M., Mullineaux, C. W. and Flores, E. (2017) 'Molecular diffusion through cyanobacterial septal junctions', *mBio*, 8(1), pp. 1–5. doi: 10.1128/mBio.01756-16.
- Nogales, E. *et al.* (1998) 'Tubulin and FtsZ form a distinct family of GTPases', *Nature Structural Biology*, 5(6), pp. 451–458.
- Noree, C. *et al.* (2010) 'Identification of novel filament-forming proteins in *Saccharomyces cerevisiae* and *Drosophila melanogaster*', *The Journal of Cell Biology*, pp. 541–551. doi: 10.1083/jcb.201003001.
- Nürnberg, D. J. *et al.* (2015) 'Intercellular diffusion of a fluorescent sucrose analog via the septal junctions in a filamentous cyanobacterium', *mBio*, 6(2), pp. 1–12. doi: 10.1128/mBio.02109-14.
- Ochoa De Alda, J. A. G. *et al.* (2014) 'The plastid ancestor originated among one of the major cyanobacterial lineages', *Nature Communications*, 5. doi: 10.1038/ncomms5937.
- Oliveira, P. *et al.* (2015) 'The *Anabaena sp.* PCC 7120 Exoproteome: Taking a Peek outside the Box', *Life*, 5(1), pp. 130–163. doi: 10.3390/life5010130.

- Orlova, A. *et al.* (2007) 'The structure of bacterial ParM filaments', *Nature Structural and Molecular Biology*, 14(10), pp. 921–926. doi: 10.1038/nsmb1300.
- Osteryoung, K. W. and Nunnari, J. (2003) 'The Division of Endosymbiotic Organelles', *Science*, 302(5651), pp. 1698–1704. doi: 10.1126/science.1082192.
- Park, A. *et al.* (2011) 'Effect of shear stress on the formation of bacterial biofilm in a microfluidic channel', *BioChip Journal*, 5(3), pp. 236–241. doi: 10.1007/s13206-011-5307-9.
- Popp, D., Narita, A., *et al.* (2010) 'Filament structure, organization, and dynamics in MreB sheets', *Journal of Biological Chemistry*, 285(21), pp. 15858–15865. doi: 10.1074/jbc.M109.095901.
- Popp, D., Xu, W., *et al.* (2010) 'Structure and filament dynamics of the pSK41 actin-like ParM protein implications for plasmid DNA segregation', *Journal of Biological Chemistry*, 285(13), pp. 10130–10140. doi: 10.1074/jbc.M109.071613.
- Pum, D., Toca-Herrera, J. L. and Sleytr, U. B. (2013) 'S-Layer protein self-assembly', *International Journal of Molecular Sciences*, 14(2), pp. 2484–2501. doi: 10.3390/ijms14022484.
- Ramamurthi, K. S. and Losick, R. (2008) 'ATP-Driven Self-Assembly of a Morphogenetic Protein in *Bacillus subtilis*', *Molecular Cell*, 31(3), pp. 406–414. doi: 10.1016/j.molcel.2008.05.030.
- Ramos-León, F. *et al.* (2015) 'Divisome-dependent subcellular localization of cell-cell joining protein SepJ in the filamentous cyanobacterium *Anabaena*', *Molecular Microbiology*, 96(3), pp. 566–580. doi: 10.1111/mmi.12956.
- Ramos-León, F. *et al.* (2017) 'Septal protein SepJ from the heterocyst-forming cyanobacterium *Anabaena* forms multimers and interacts with peptidoglycan', *FEBS Open Bio*, 7(10), pp. 1515–1526. doi: 10.1002/2211-5463.12280.
- Reece, J. B. *et al.* (2013) *Campbell Biology*. 10th edn. Pearson.
- Renart, J., Reiser, J. and Stark, G. R. (1979) 'Transfer of proteins from gels to diazobenzoyloxymethyl-paper and detection with antisera: a method for studying antibody specificity and antigen structure.', *Proceedings of the National Academy of Sciences*, 76(7), pp. 3116–3120. doi: 10.1073/pnas.76.7.3116.
- Riederer, B. M. and Goodman, S. R. (1990) 'Association of brain spectrin isoforms with microtubules', *FEBS Letters*, 277(1–2), pp. 49–52. doi: 10.1016/0014-5793(90)80807-U.
- Riederer, B. M. and Routtenberg, A. (1999) 'Can GAP-43 interact with brain spectrin?', *Molecular Brain Research*, 71(2), pp. 345–348. doi: 10.1016/S0169-328X(99)00179-5.
- Rippka, R. *et al.* (1979) 'Generic Assignments, Strain Histories and Properties of Pure Cultures of Cyanobacteria', *Microbiology*, 111(1), pp. 1–61. doi: 10.1099/00221287-111-1-1.
- Rojas, E. R. and Huang, K. C. (2018) 'Regulation of microbial growth by turgor pressure', *Current Opinion in Microbiology*. Elsevier Ltd, 42, pp. 62–70. doi: 10.1016/j.mib.2017.10.015.
- Saiki, R. *et al.* (1988) 'Primer-directed enzymatic amplification of DNA with a thermostable DNA polymerase', *Science*, 239(4839), pp. 487–491. doi: 10.1126/science.2448875.
- Sakr, S., Jeanjean, R., *et al.* (2006) 'Inhibition of cell division suppresses heterocyst development in *Anabaena* sp. strain PCC 7120', *J. Bacteriol.*, 188(4), pp. 1396–1404. doi: 10.1128/JB.188.4.1396.

- Sakr, S., Thyssen, M., *et al.* (2006) 'Relationship among several key cell cycle events in the developmental cyanobacterium *Anabaena sp.* strain PCC 7120', *Journal of Bacteriology*, 188(16), pp. 5958–5965. doi: 10.1128/JB.00524-06.
- Salazar, O. and Asenjo, J. A. (2007) 'Enzymatic lysis of microbial cells', *Biotechnology Letters*. Kluwer Academic Publishers, 29(7), pp. 985–994. doi: 10.1007/s10529-007-9345-2.
- Sambrook, J. and Green, M. R. (2012) *Molecular Cloning: A Laboratory Manual*. 4th edn. Cold Spring Harbor Laboratory Press. Available at: www.molecularcloning.org.
- Sánchez-Baracaldo, P., Hayes, P. K. and Blank, C. E. (2005) 'Morphological and habitat evolution in the Cyanobacteria using a compartmentalization approach', *Geobiology*, 3, pp. 145–165. doi: 10.1111/j.1472-4669.2005.00050.x.
- Sandvang, D. (1999) 'Novel streptomycin and spectinomycin resistance gene as a gene cassette within a class 1 integron isolated from *Escherichia coli*', *Antimicrobial Agents and Chemotherapy*, 43(12), pp. 3036–3038. doi: 10.1128/AAC.44.2.475-475.2000.
- Sára, M. and Sleytr, U. B. U. (2000) 'S-Layer Proteins', *Journal of Bacteriology*, 182(4), pp. 859–868. doi: 10.1128/JB.182.4.859-868.2000.
- Savakis, P. and Hellingwerf, K. J. (2015) 'Engineering cyanobacteria for direct biofuel production from CO₂', *Current Opinion in Biotechnology*. Elsevier Ltd, 33, pp. 8–14. doi: 10.1016/j.copbio.2014.09.007.
- Schaffeld, M. *et al.* (2001) 'Vimentin and desmin of a cartilaginous fish, the shark *Scyliorhinus stellaris*: sequence, expression patterns and *in vitro* assembly.', *European journal of cell biology*, 80(11), pp. 692–702. doi: 10.1078/0171-9335-00206.
- Schirrmeister, B. E. *et al.* (2013) 'Evolution of multicellularity coincided with increased diversification of cyanobacteria and the Great Oxidation Event', *Proceedings of the National Academy of Sciences*, 110(5), pp. 1791–1796. doi: 10.1073/pnas.1209927110.
- Schirrmeister, B. E., Antonelli, A. and Bagheri, H. C. (2011) 'The origin of multicellularity in cyanobacteria', *BMC Evolutionary Biology*, 11(1). doi: 10.1186/1471-2148-11-45.
- Schlieper, D. *et al.* (2005) 'Structure of bacterial tubulin BtubA/B: evidence for horizontal gene transfer.', *Proceedings of the National Academy of Sciences of the United States of America*, 102(26), pp. 9170–9175. doi: 10.1073/pnas.0502859102.
- Schopf, William, J. and Packer, B. M. (1987) 'Early Archean (3.3-billion to 3.5-billion-year-old) microfossils from Warrawoona Group, Australia', *Science*, 237(4810), pp. 70–73. doi: 10.1126/science.11539686.
- Schuergers, N. *et al.* (2015) 'PilB localization correlates with the direction of twitching motility in the cyanobacterium *Synechocystis sp.* PCC 6803', *Microbiology (Reading, England)*, 161(2015), pp. 960–966. doi: 10.1099/mic.0.000064.
- Schuergers, N. *et al.* (2016) 'Cyanobacteria use micro-optics to sense light direction', *eLife*, pp. 1–16. doi: 10.7554/eLife.12620.
- Schuergers, N., Mullineaux, C. W. and Wilde, A. (2017) 'Cyanobacteria in motion', *Current Opinion in Plant Biology*. Elsevier Ltd, 37, pp. 109–115. doi: 10.1016/j.pbi.2017.03.018.
- Schuergers, N. and Wilde, A. (2015) 'Appendages of the Cyanobacterial Cell', *Life*, 5(1), pp. 700–715. doi: 10.3390/life5010700.
- Shaewitz, J. W. and Gitai, Z. (2010) 'The structure and function of bacterial actin homologs.', *Cold Spring Harbor perspectives in biology*, 2(9). doi: 10.1101/cshperspect.a000364.

- Sharma, A. D., Gill, P. K. and Singh, P. (2002) 'DNA isolation from dry and fresh samples of polysaccharide-rich plants', *Plant Molecular Biology Reporter*, 20(4), pp. 415–415. doi: 10.1007/BF02772129.
- Shih, Y.-L. and Rothfield, L. (2006) 'The bacterial cytoskeleton', *Microbiology and Molecular Biology Reviews*, 70(3), pp. 729–754. doi: 10.1128/MMBR.00017-06.
- Shoeman, R. L. and Traub, P. (1993) 'Assembly of Intermediate Filaments', *Bioessays*, 15(9), pp. 605–611. doi: 10.1002/bies.950150906.
- Singh, S. P. and Montgomery, B. L. (2014) 'Morphogenes *bolA* and *mreB* mediate the photoregulation of cellular morphology during complementary chromatic acclimation in *Fremyella diplosiphon*', *Molecular Microbiology*, 93(1), pp. 167–182. doi: 10.1111/mmi.12649.
- Solovyev, V. and Salamov, A. (2011) 'Automatic Annotation of Microbial Genomes and Metagenomic Sequences', in Robert W. Li, pp (ed.) *Metagenomics and its Applications in Agriculture, Biomedicine and Environmental Studies*. Nova Science Publishers, Inc., pp. 61–78.
- Spang, A. *et al.* (2015) 'Complex archaea that bridge the gap between prokaryotes and eukaryotes', *Nature*, 521(7551), pp. 173–179. doi: 10.1038/nature14447.
- Specht, M. *et al.* (2011) '*Helicobacter pylori* Possesses Four Coiled-Coil-Rich Proteins That Form Extended Filamentous Structures and Control Cell Shape and Motility', *Journal of Bacteriology*, 193(17), pp. 4523–4530. doi: 10.1128/JB.00231-11.
- Stahlberg, H. *et al.* (2004) 'Oligomeric structure of the *Bacillus subtilis* cell division protein DivIVA determined by transmission microscopy', *Molecular Microbiology*, 52(5), pp. 1281–1290. doi: 10.1111/j.1365-2958.2004.04074.x.
- Stucken, K. *et al.* (2012) 'Transformation and conjugal transfer of foreign genes into the filamentous multicellular cyanobacteria (subsection V) *Fischerella* and *Chlorogloeopsis*', *Current Microbiology*, 65(5), pp. 552–560. doi: 10.1007/s00284-012-0193-5.
- Studier, F. W. and Moffatt, B. A. (1986) 'Use of bacteriophage T7 RNA polymerase to direct selective high-level expression of cloned genes', *Journal of Molecular Biology*, 189(1), pp. 113–130. doi: 10.1016/0022-2836(86)90385-2.
- Stuurman, N., Heins, S. and Aebi, U. (1998) 'Nuclear lamins: Their structure, assembly, and interactions', *Journal of Structural Biology*, 122(1–2), pp. 42–66. doi: 10.1006/jsbi.1998.3987.
- Suefuji, K., Valluzzi, R. and RayChaudhuri, D. (2002) 'Dynamic assembly of MinD into filament bundles modulated by ATP, phospholipids, and MinE', *Proceedings of the National Academy of Sciences*, 99(26), pp. 16776–16781. doi: 10.1073/pnas.262671699.
- Sundararajan, K. and Goley, E. D. (2017) 'Cytoskeletal Proteins in *Caulobacter crescentus*: Spatial Orchestrators of Cell Cycle Progression, Development, and Cell Shape', in Springer, Cham, pp. 103–137. doi: 10.1007/978-3-319-53047-5_4.
- Swulius, M. T. and Jensen, G. J. (2012) 'The helical *mreB* cytoskeleton in *Escherichia coli* MC1000/pLE7 is an artifact of the N-terminal yellow fluorescent protein tag', *Journal of Bacteriology*, 194(23), pp. 6382–6386. doi: 10.1128/JB.00505-12.
- Szwedziak, P. *et al.* (2012) 'FtsA forms actin-like protofilaments', *EMBO Journal*, 31(10), pp. 2249–2260. doi: 10.1038/emboj.2012.76.
- Szwedziak, P. *et al.* (2014) 'Architecture of the ring formed by the tubulin homologue FtsZ in bacterial cell division', *eLife*, December, pp. 1–22. doi: 10.7554/eLife.04601.

- Tacon, W. *et al.* (1981) 'Structure and Function of Plasmid ColK', *Plasmid*, 6(3), pp. 358–359. doi: 10.1016/0147-619X(81)90044-5.
- Thurotte, A. *et al.* (2017) 'Membrane chaperoning by members of the PspA/IM30 protein family', *Communicative & Integrative Biology*. Taylor & Francis, 10(1), p. e1264546. doi: 10.1080/19420889.2016.1264546.
- Tomitani, A. *et al.* (2006) 'The evolutionary diversification of cyanobacteria: Molecular-phylogenetic and paleontological perspectives', *Proceedings of the National Academy of Sciences*, 103(14), pp. 5442–5447. doi: 10.1073/pnas.0600999103.
- Towbin, H., Staehelin, T. and Gordon, J. (1979) 'Electrophoretic transfer of proteins from polyacrylamide gels to nitrocellulose sheets: procedure and some applications.', *Proceedings of the National Academy of Sciences*, 76(9), pp. 4350–4354. doi: 10.1073/pnas.76.9.4350.
- Trautmann, D. *et al.* (2012) 'Microevolution in cyanobacteria: Re-sequencing a motile substrain of *Synechocystis* sp. PCC 6803', *DNA Research*, 19(6), pp. 435–448. doi: 10.1093/dnares/dss024.
- Tria, F. D. K., Landan, G. and Dagan, T. (2017) 'Phylogenetic rooting using minimal ancestor deviation', *Nature Ecology & Evolution*, 1(June), p. 193. doi: 10.1038/s41559-017-0193.
- Typas, A. *et al.* (2012) 'From the regulation of peptidoglycan synthesis to bacterial growth and morphology', *Nature Reviews Microbiology*. Nature Publishing Group, 10(2), pp. 123–136. doi: 10.1038/nrmicro2677.
- Ungerer, J. and Pakrasi, H. B. (2016) 'Cpf1 Is A Versatile Tool for CRISPR Genome Editing Across Diverse Species of Cyanobacteria', *Scientific Reports*. Nature Publishing Group, 6, pp. 1–9. doi: 10.1038/srep39681.
- Vats, P. and Rothfield, L. (2007) 'Duplication and segregation of the actin (MreB) cytoskeleton during the prokaryotic cell cycle.', *Proceedings of the National Academy of Sciences of the United States of America*, 104(45), pp. 17795–17800. doi: 10.1073/pnas.0708739104.
- Vikstrom, K. L. *et al.* (1992) 'Steady state dynamics of intermediate filament networks', *J Cell Biol*, 118(1), pp. 121–129.
- Wagstaff, J. and Löwe, J. (2018) 'Prokaryotic cytoskeletons: protein filaments organizing small cells', *Nature Reviews Microbiology*. Nature Publishing Group. doi: 10.1038/nrmicro.2017.153.
- Waidner, B. *et al.* (2009) 'A novel system of cytoskeletal elements in the human pathogen *Helicobacter pylori*', *PLoS Pathogens*. doi: 10.1371/journal.ppat.1000669.
- Walshaw, J., Gillespie, M. D. and Kelemen, G. H. (2010) 'A novel coiled-coil repeat variant in a class of bacterial cytoskeletal proteins', *Journal of Structural Biology*, pp. 202–215. doi: 10.1016/j.jsb.2010.02.008.
- Walter, J. M. *et al.* (2017) 'Ecogenomics and taxonomy of Cyanobacteria phylum', *Frontiers in Microbiology*, 8(NOV). doi: 10.3389/fmicb.2017.02132.
- Wang, Y. and Xu, X. (2005) 'Regulation by *hetC* of Genes Required for Heterocyst Differentiation and Cell Division in *Anabaena* sp. Strain PCC 7120', *Journal of Bacteriology*, 187(24), pp. 8489–8493. doi: 10.1128/JB.187.24.8489–8493.2005.
- Werner, J. N. *et al.* (2009) 'Quantitative genome-scale analysis of protein localization in an asymmetric bacterium', *Proceedings of the National Academy of Sciences*, pp. 7858–7863. doi: 10.1073/pnas.0901781106.
- Wiche, G., Osmanagic-Myers, S. and Castañón, M. J. (2015) 'Networking and anchoring

- through plectin: A key to IF functionality and mechanotransduction', *Current Opinion in Cell Biology*, 32, pp. 21–29. doi: 10.1016/j.ceb.2014.10.002.
- Wickstead, B. and Gull, K. (2011) 'The evolution of the cytoskeleton', *Journal of Cell Biology*, 194(4), pp. 513–525. doi: 10.1083/jcb.201102065.
- Wilde, A. and Mullineaux, C. W. (2017) 'Light-controlled motility in prokaryotes and the problem of directional light perception', *FEMS Microbiology Reviews*, 41(6), pp. 900–922. doi: 10.1093/femsre/fux045.
- Wilk, L. *et al.* (2011) 'Outer membrane continuity and septosome formation between vegetative cells in the filaments of *Anabaena sp.* PCC 7120', *Cellular Microbiology*, 13(11), pp. 1744–1754. doi: 10.1111/j.1462-5822.2011.01655.x.
- Wilson, C. G. M., Magliery, T. J. and Regan, L. (2004) 'Detecting protein-protein interactions with GFP-fragment reassembly', *Nature Methods*, 1(3), pp. 255–262. doi: 10.1038/nmeth1204-255.
- Wolf, Y. I. and Koonin, E. V. (2013) 'Genome reduction as the dominant mode of evolution', *BioEssays*, 35(9), pp. 829–837. doi: 10.1002/bies.201300037.
- Wolk, C. P. *et al.* (1988) 'Isolation and complementation of mutants of *Anabaena sp.* strain PCC 7120 unable to grow aerobically on dinitrogen.', *Journal of bacteriology*, 170(3), pp. 1239–1244. doi: 10.1128/jb.170.3.1239-1244.1988.
- Xiao, J. and Goley, E. D. (2016) 'Redefining the roles of the FtsZ-ring in bacterial cytokinesis', *Current Opinion in Microbiology*. Elsevier Ltd, 34, pp. 90–96. doi: 10.1016/j.mib.2016.08.008.
- Yoon, H. (1998) 'Heterocyst Pattern Formation Controlled by a Diffusible Peptide', *Science*, 282(5390), pp. 935–938. doi: 10.1126/science.282.5390.935.
- Yoon, M. *et al.* (1998) 'Motile properties of vimentin intermediate filament networks in living cells', *Journal of Cell Biology*, 143(1), pp. 147–157. doi: 10.1083/jcb.143.1.147.
- Yoshida, Y. *et al.* (2016) 'Chloroplast FtsZ assembles into a contractible ring via tubulin-like heteropolymerization', *Nature Plants*. Nature Publishing Group, 2(7), pp. 1–10. doi: 10.1038/NPLANTS.2016.95.
- Zhang, C.-C. C. *et al.* (1995) 'Analysis of genes encoding the cell division protein FtsZ and a glutathione synthetase homologue in the cyanobacterium *Anabaena sp.* PCC 7120', *Research in Microbiology*, 146(6), pp. 445–455. doi: 10.1016/0923-2508(96)80290-7.
- Zhang, R. *et al.* (2013) 'Spectrin: Structure, function and disease', *Science China Life Sciences*, 56(12), pp. 1076–1085. doi: 10.1007/s11427-013-4575-0.
- Zhao, C. *et al.* (2015) 'RfpA, RfpB, and RfpC are the master control elements of far-red light photoacclimation (FaRLiP)', *Frontiers in Microbiology*, pp. 1–13. doi: 10.3389/fmicb.2015.01303.
- Zhou, J. *et al.* (2014) 'Discovery of a super-strong promoter enables efficient production of heterologous proteins in cyanobacteria', *Scientific Reports*, 4, pp. 1–6. doi: 10.1038/srep04500.
- Zigler, J. S. J. and Rao, P. V. (1991) 'Enzyme/crystallins and extremely high pyridine nucleotide levels in the eye lens', *Faseb J.*, pp. 223–225. Available at: <http://www.fasebj.org/content/5/2/223.short>.

13 Supplementary figures Chapter I

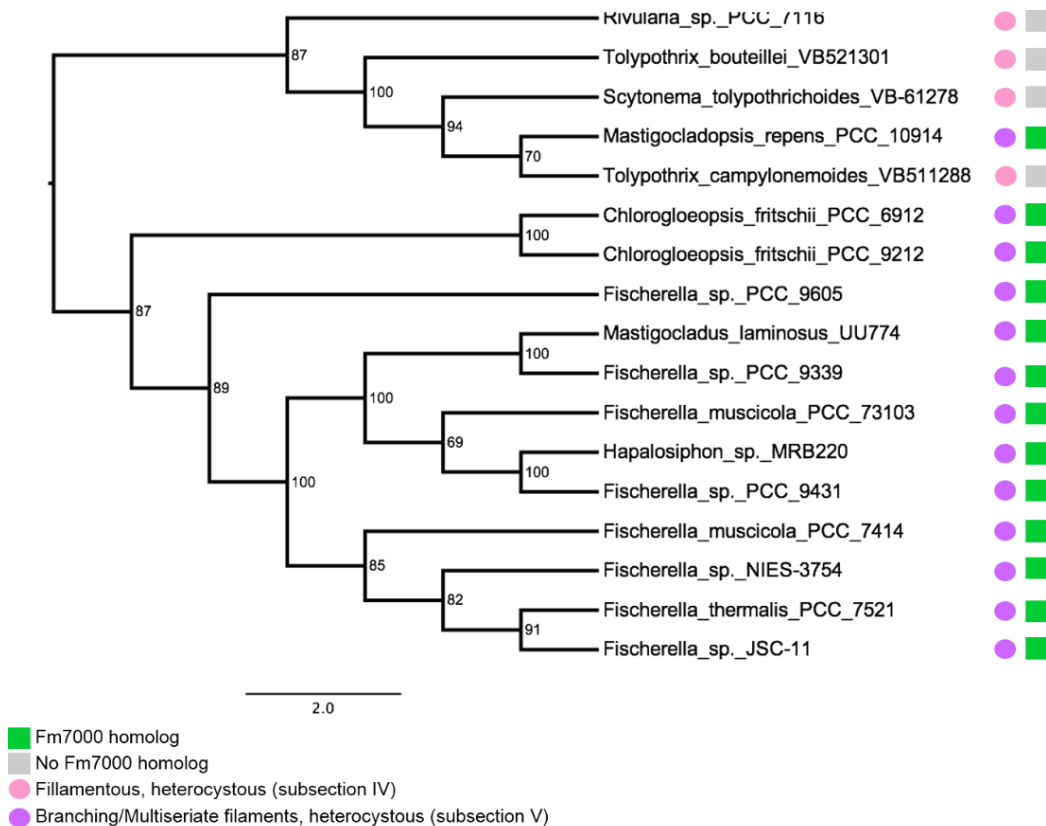


Fig. S1: Phylogenetic tree of Fm7001 and its homologous proteins

Fm7001 homologs are restricted to subsection IV and V cyanobacteria. Species possessing Fm7000 homologs are marked by a green rectangle and those organisms where no Fm7000 homolog was identified are marked by a grey rectangle.

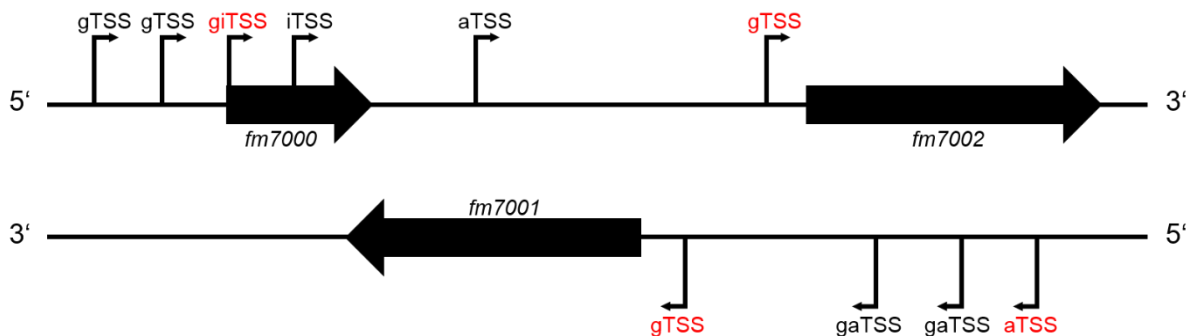


Fig. S2: Genomic environment of *fm7001*

fm7001 resides on the plus strand and is enclosed by *fm7000* and *fm7002*, located on the minus strand. The 3' end of *fm7001* possesses a 9 bp overlap to the 3' end of *fm7000*. *fm7000* exhibits two genomic transcriptional start sites (gTSS), one genomic or internal TSS (giTSS) and one iTSS. *fm7001* possesses one gTSS and one antisense TSS (aTSS). *fm7002* contains one gTSS and three aTSSs while two are also identified as gTSSs for *fm7001* (gaTSS). giTSS of *fm7000* and aTSS as well as gTSS of *fm7002* marked in red are differentially expressed in the treatment condition applied by Koch et al., 2017. gTSS of *fm7001* highlighted in red is highly expressed under control and treatment conditions.

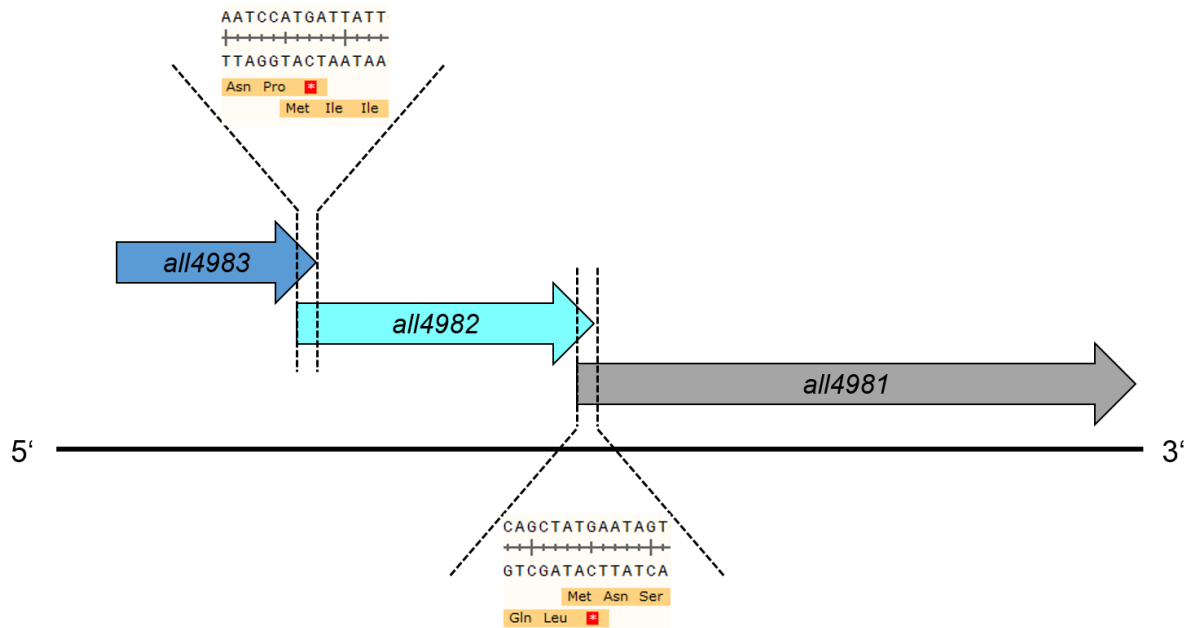


Fig. S3: Genomic environment of *all4981*

The 3' end of *all4983* displays a 4 bp overlap to the 5' region of *all4982*, which in turn has an overlap of 4 bp at its 3' end with the 5' end of *all4981*. In both cases, the overlapping sequence is comprised of the same nucleotides (ATGA).

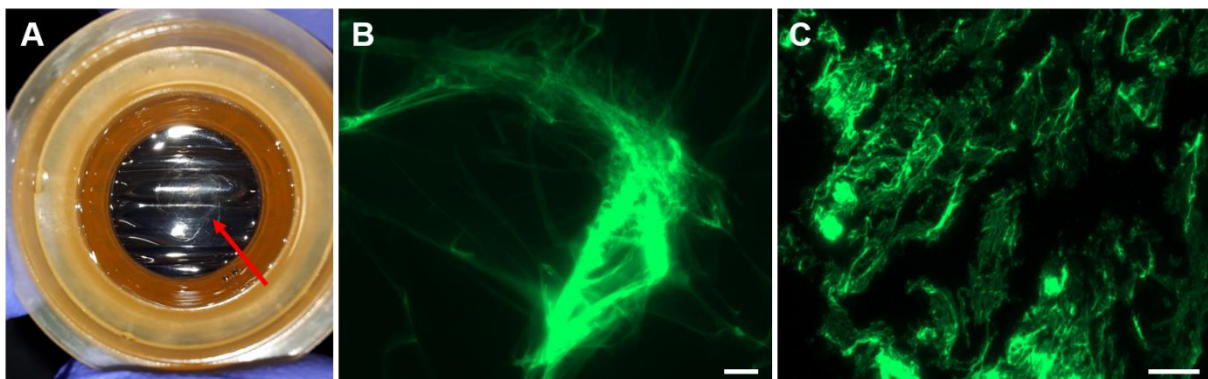


Fig. S4: *In vitro* polymerization of Fm7001 into filamentous sheets

(A) Bright field micrograph of a sheet-like flat object floating on top of the dialysate (red arrow) formed upon dialysis of Fm7001 (0.7 mg ml^{-1}) into 2 mM Tris-HCl, 4.5 M urea, pH7.5. (B,C) Epifluorescence micrographs of filamentous structures formed by (B) whole cell extract of *E. coli* BL21 (DE3) expressing Fm7001-GFP (0.7 mg ml^{-1} whole protein) in 2 mM Tris-HCl, 3 M urea, pH 7.5 and by (C) natively purified MBP-Fm7001-His (0.8 mg ml^{-1}) dialyzed into HLB. Scale bars: (B) 20 μ m and (C) 10 μ m.

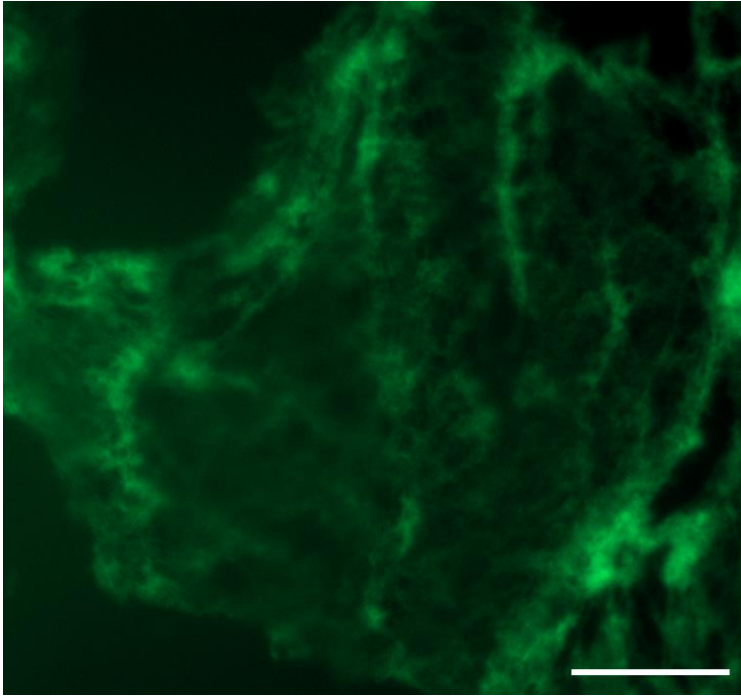


Fig. S5: CreS forms aggregate-like filaments without monovalent ions

Epifluorescence micrograph of filamentous aggregates formed by purified and renatured CreS (0.5 mg ml^{-1}) in 25 mM HEPES, pH 7.4. Proteins were dialyzed in a step-wise urea-decreasing manner and stained with an excess of NHS-Fluorescein. Scale bar: 50 μm .

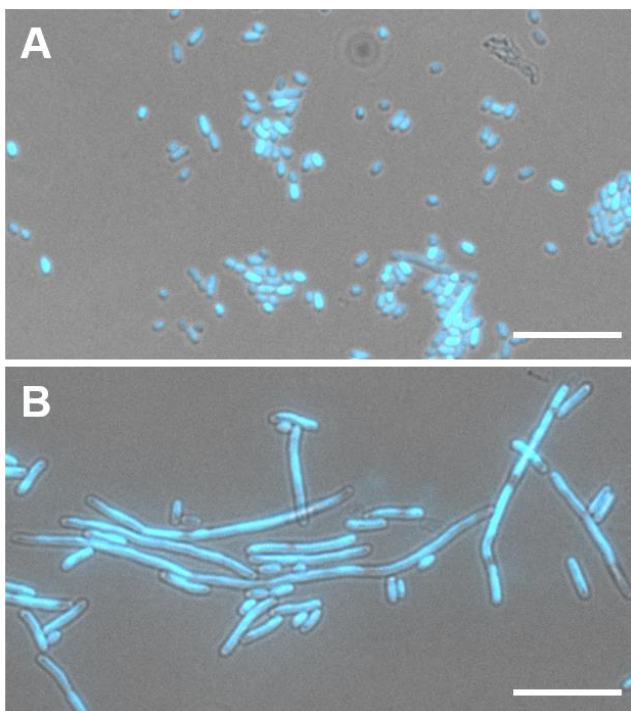


Fig. S6: Heterologously expressed MBP-Fm7001-His induces a filamentous phenotype in *E. coli*

Merged bright field and DAPI fluorescence micrographs of *E. coli* BL21 (DE3) cells expressing (A) MBP or (B) MBP-Fm7001-His. Protein expression was induced with 0.05 mM IPTG and cells were grown for 48 hours at 20 °C and subsequently stained with $10 \mu\text{g ml}^{-1}$ DAPI and then immobilized on an agarose pad. Scale bars: 10 μm .

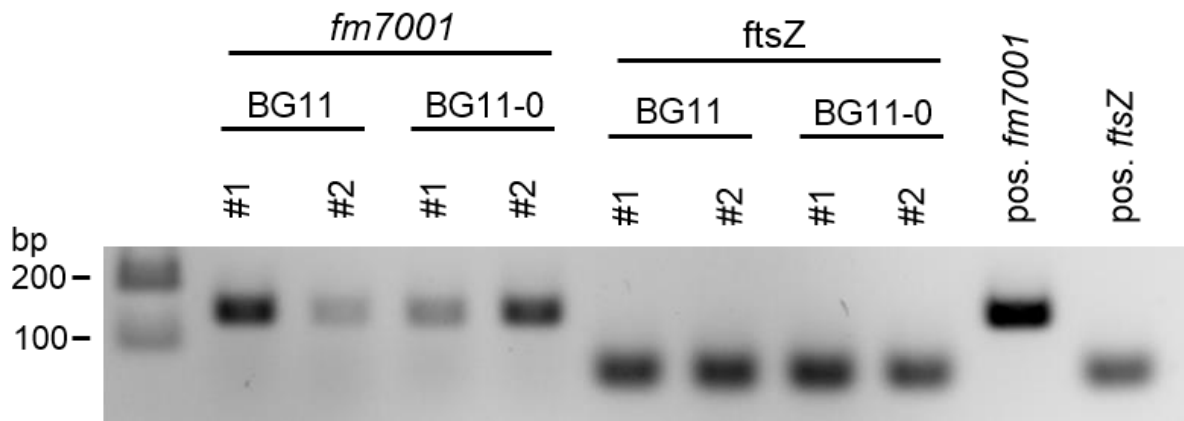


Fig. S7: *fm7001* is expressed in early growth stages

RT-PCR of reverse transcribed whole RNA from young *Fischerella* wt cultures grown in BG11 or BG11-0 at standard growth conditions from two independent biological replicates. Gene transcripts were verified using internal *fm7001* gene primers or internal *ftsZ* gene primers, as a control. *Fischerella* genomic DNA was included as positive control. PCR fragments were resolved on a 1% agarose gel in TAE buffer.

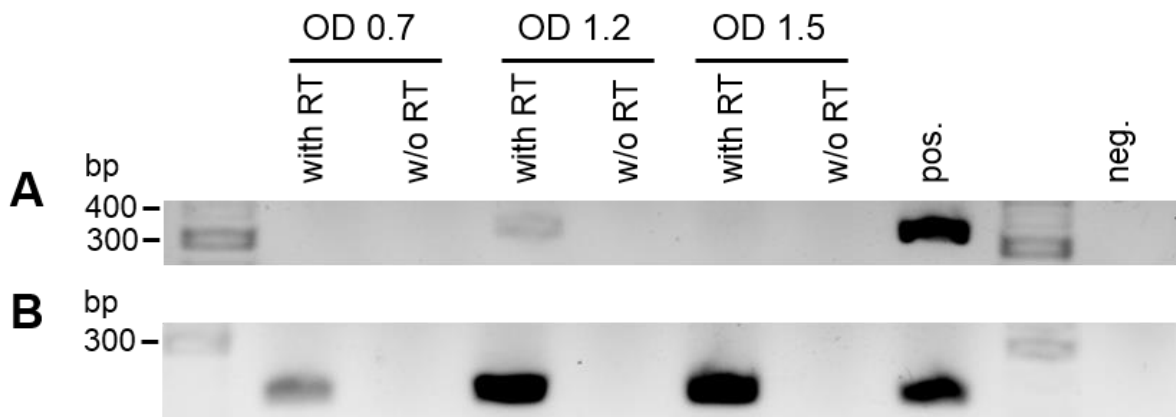


Fig. S8: *slr7083* expression occurs at later growth stages

RT-PCR of reverse transcribed whole RNA from *Synechocystis* wt (OD₇₅₀ 0.7, 1.2 or 1.5) grown in BG11 at standard growth conditions using (A) internal *slr7083* gene primers or (B) internal *rnpB* gene primers as control. RNA was either reverse transcribed in reaction buffer containing reverse transcriptase (with RT) or without reverse transcriptase (w/o RT) as a control for residual genomic DNA contamination. *Synechocystis* genomic DNA was included as positive control. PCR fragments were resolved on a 2% agarose gel in TAE buffer.

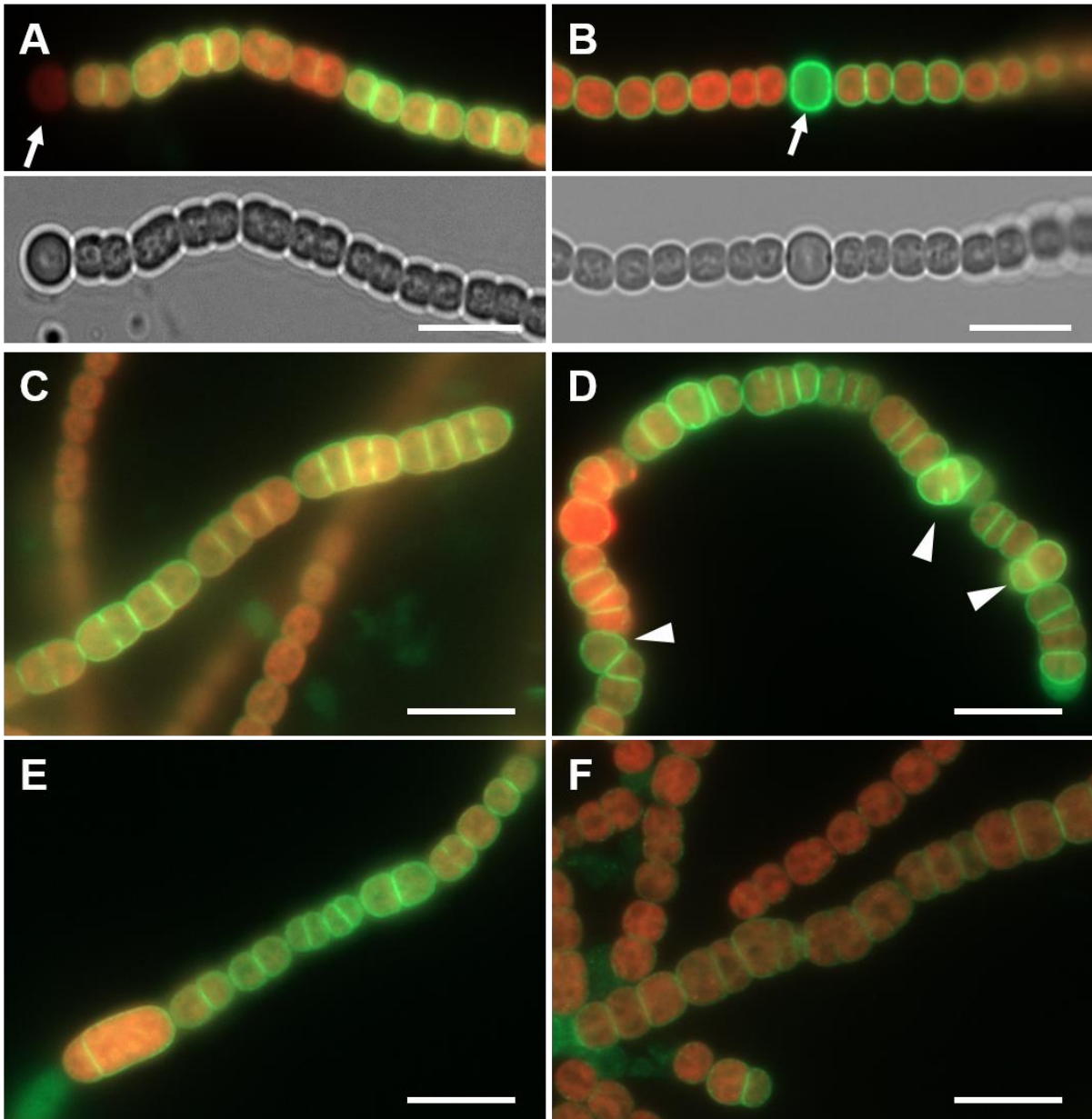


Fig. S9: Tag-orientation dependency of Slr7083 in *Anabaena*

Merged GFP fluorescence and chlorophyll auto-fluorescence and bright field micrographs of *Anabaena* cells expressing (A) Slr7083-GFP or (B,C,D,E,F) YFP-Slr7083. (A,B) Cells were either grown in (A) BG11-0 supplemented with $0.5 \mu\text{M}$ CuSO_4 for 28 hours or (B) in BG11-0. (C,D) Growth of *Anabaena* expressing YFP-Slr7083 in BG11 for (C) 2 days or (D) 9 days. (E,F) *Anabaena* cells expressing YFP-Slr7083 were grown in BG11 without copper with subsequent induction of protein expression by $5 \mu\text{M}$ CuSO_4 for (E) 2 or (F) 9 days. White arrows indicate heterocysts. White triangles point to multiserial *Anabaena* trichome growth. Scale bars: $10 \mu\text{m}$.

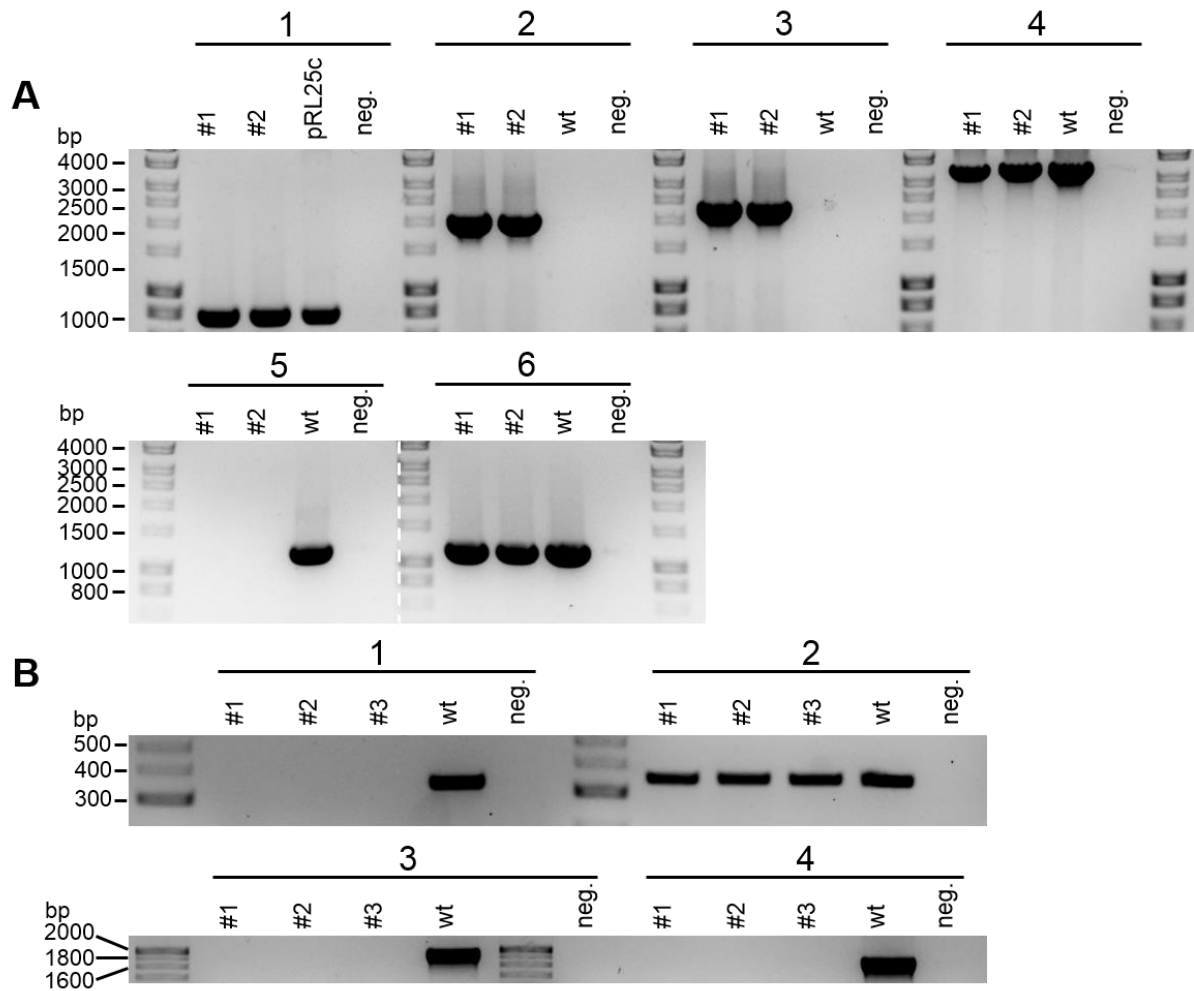


Fig. S10: Verification of $\Delta slr7083$

(A) PCR of isolated genomic DNA from two $\Delta slr7083$ GT-Kazusa clones. As a control pRL25c plasmid DNA or *Synechocystis* wt genomic DNA was used. The following primers were used for the corresponding PCR reaction using DreamTaq Green PCR Master Mix: (1) P56+P57; (2) P56+P131; (3) P130+P57; (4) P130+P131; (5) P115+P116; (6) P132+P133. (B) Colony PCR of three $\Delta slr7083$ PCC-M clones. As a control *Synechocystis* wt genomic DNA was used. The following primers were used for the corresponding PCR reaction using DreamTaq Green PCR Master Mix: (1) P134+P135; (2) P280+P281; (3) P134+P131; (4) P130+P135. DNA products were subjected to (A) 1% or (B) 2% agarose gel electrophoresis in TAE buffer. Neg. control contained H₂O instead of any template.

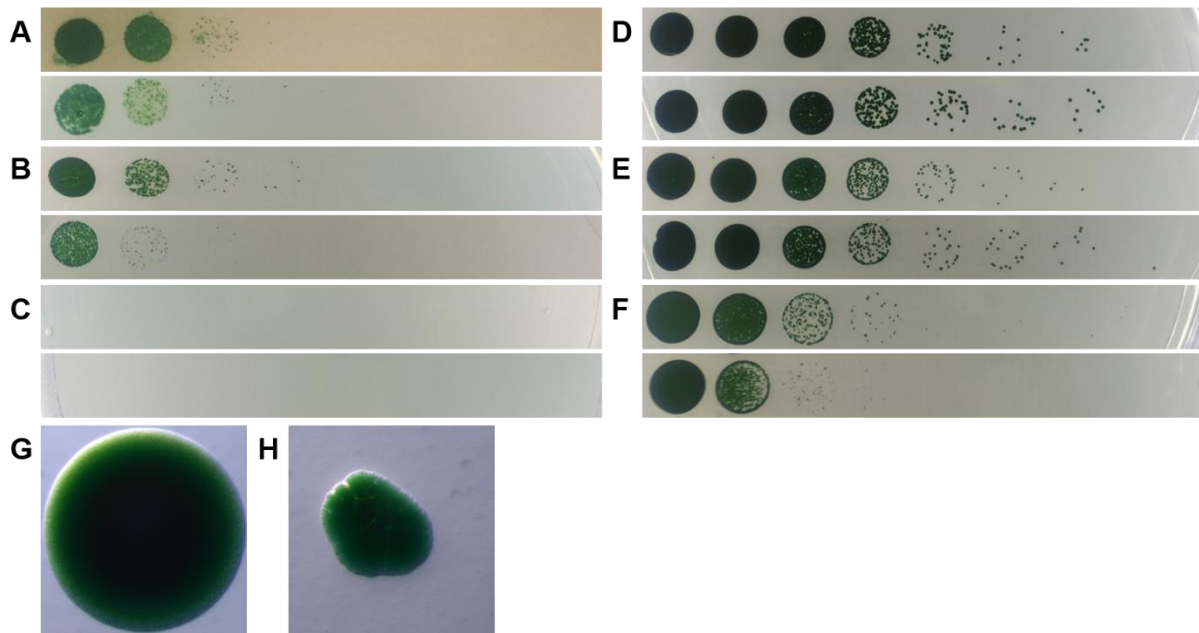


Fig. S11: Slr7083 affects cell viability and colony formation

(A-C) Motile PCC-M substrain wt (upper lane) and $\Delta slr7083$ PCC-M (lower lane) or (D-F) non-motile GT-Kauzusa substrain wt (upper lane) and $\Delta slr7083$ GT-Kauzusa (lower lane) were grown in liquid culture at growth conditions until an OD_{750} of about 2.0, diluted to an OD_{750} of 0.4 in BG11 and spotted on (A,D) BG11 plates, (B,E) BG11 plates supplemented with $100 \mu\text{g ml}^{-1}$ Lysozyme or (C,F) BG11 plates supplemented with $30 \mu\text{g ml}^{-1}$ Proteinase K in triplicates of serial dilutions of factor 1/10. Cells were grown until no further colonies arose in the highest dilution. (G,H) Bright field micrographs of non-motile *Synechocystis* GT-Kauzusa (G) wt or (H) Slr7083-GFP expressing strain grown on BG11 plates. No PCC-M strain expressing Slr7083-GFP could be obtained.

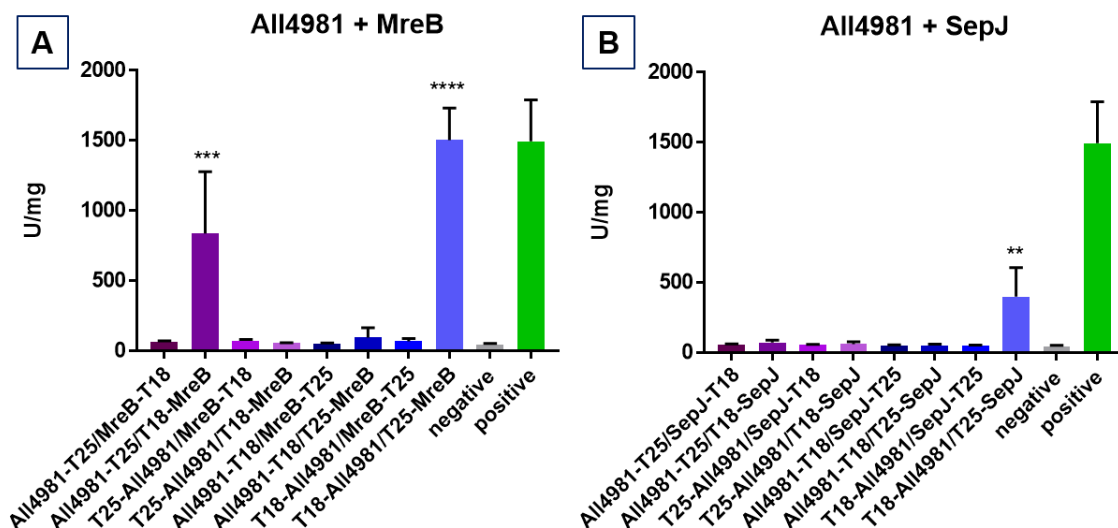


Fig. S12: All4981 interacts with MreB and SepJ in a bacterial two-hybrid assay

Beta-galactosidase assays of *E. coli* cells co-expressing indicated translational fusion constructs of all possible pairwise combinations of (A) All4981+MreB or (B) All4981+SepJ. Cells were grown for 2 days at 20 °C. Quantity values are given in Miller Units per milligram LacZ of the mean results from three independent colonies. Error bars indicate standard deviations. Neg: pKNT25 plasmid carrying the respective gene insert co-transformed with empty pUT18C. Pos: Zip/Zip control. *: $P < 0.05$, **: $P < 0.01$, ***: $P < 0.001$, ****: $P < 0.0001$ (Dunnett's multiple comparison test and one-way ANOVA).

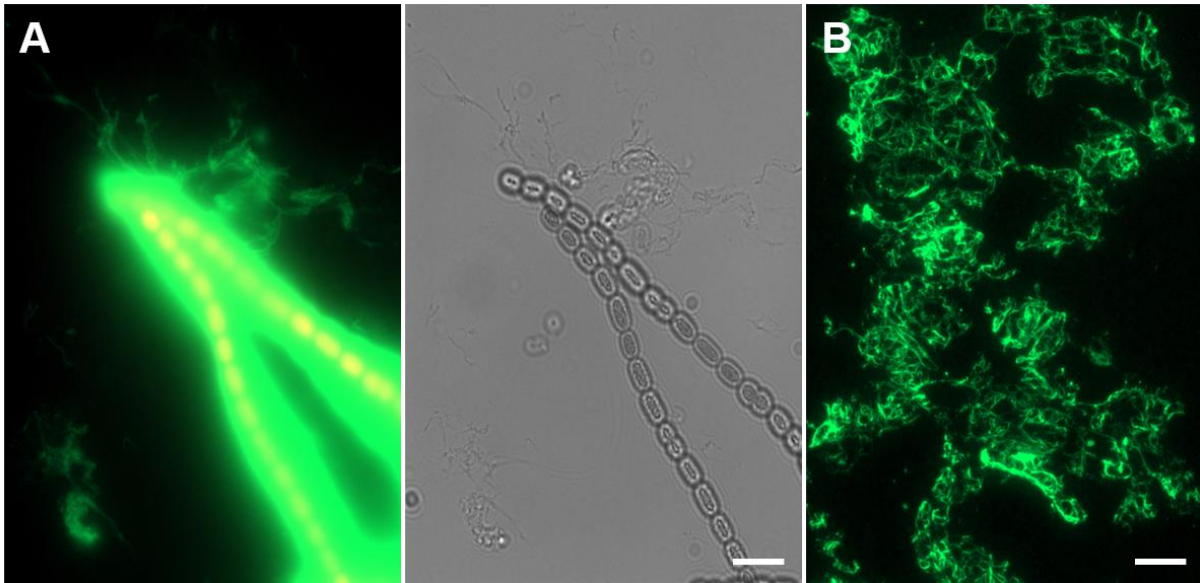


Fig. S13: All4981-GFP forms extracellular filaments upon cell lysis

GFP fluorescence and bright field micrographs of (A) *Anabaena* expressing All4981-GFP grown in BG11 supplemented with 0.5 μM CuSO_4 for 1 day or (B) extracellular filaments formed from upon cell lysis of All4981-GFP expressing *Anabaena* cells grown in BG11-0 supplemented with 0.25 μM CuSO_4 for 40 hours. Scale bars: (A) 10 μm or (B) 20 μm .

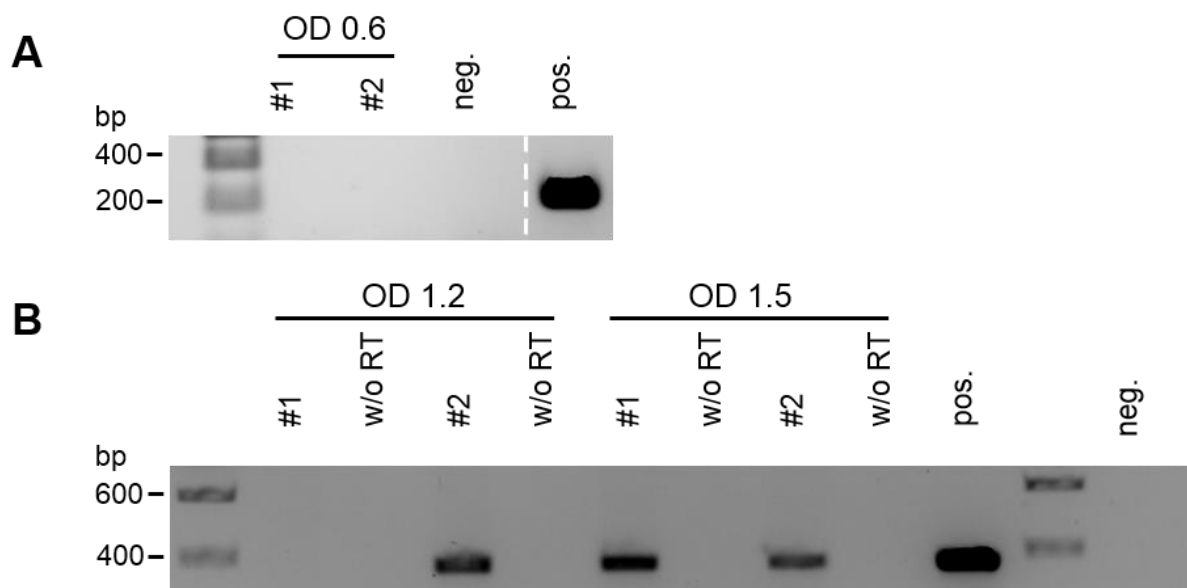


Fig. S14: *synpcc7942_2039* is expressed in stationary phase cultures

RT-PCR of reverse transcribed whole RNA from *Synechococcus* wt (OD₇₅₀ 1.2 or 1.5) grown in BG11 at standard growth conditions from two independent biological replicates. Gene transcripts were verified using (A) internal *synpcc7942_2039* gene primers. RNA was either reverse transcribed in reaction buffer containing reverse transcriptase (#1 and #2) or without reverse transcriptase (w/o RT) as a control for residual genomic DNA contamination. *Synechococcus* genomic DNA was included as positive control. PCR fragments were resolved on a 1% agarose gel in TAE buffer.

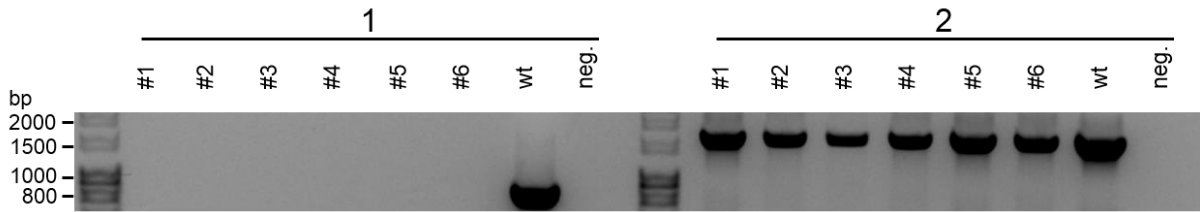


Fig. S15: Verification of Δ *synpcc7942_2039*

Colony PCRs of six Δ *synpcc7942_2039* clones using (1) *synpcc7942_2039* gene primers (P136+P137) or (2) *synpcc7942_1139* gene primers (P311+P312) as a control. As a positive control, *Synechococcus* genomic DNA was included.

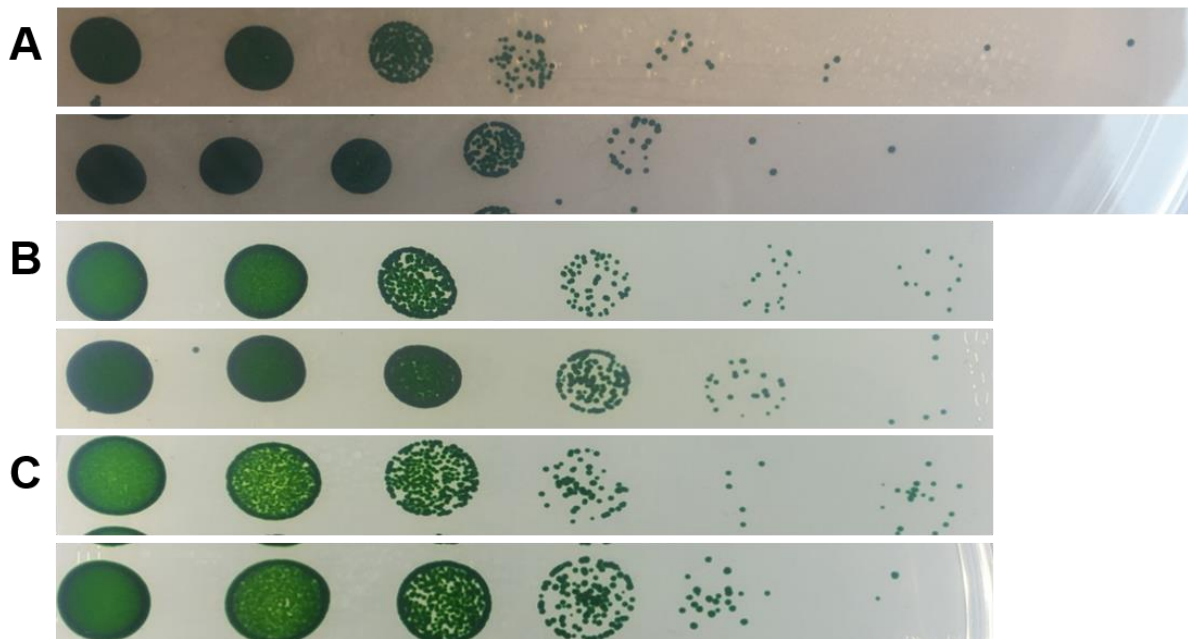


Fig. S16: Δ *synpcc7942_2039* does not affect cell viability

Synechococcus wt (upper lane) and Δ *synpcc7942_2039* (lower lane) were grown in liquid culture at growth conditions until an OD_{750} of about 2.0, diluted to an OD_{750} of 0.4 in BG11 and spotted on (A) BG11 plates or BG11 plates supplemented either with (B) $30 \mu\text{g ml}^{-1}$ Lysozyme or (C) $30 \mu\text{g ml}^{-1}$ Proteinase K in triplicates of serial dilutions of factor 1/10. Cells were grown until no further colonies arose in the highest dilution.

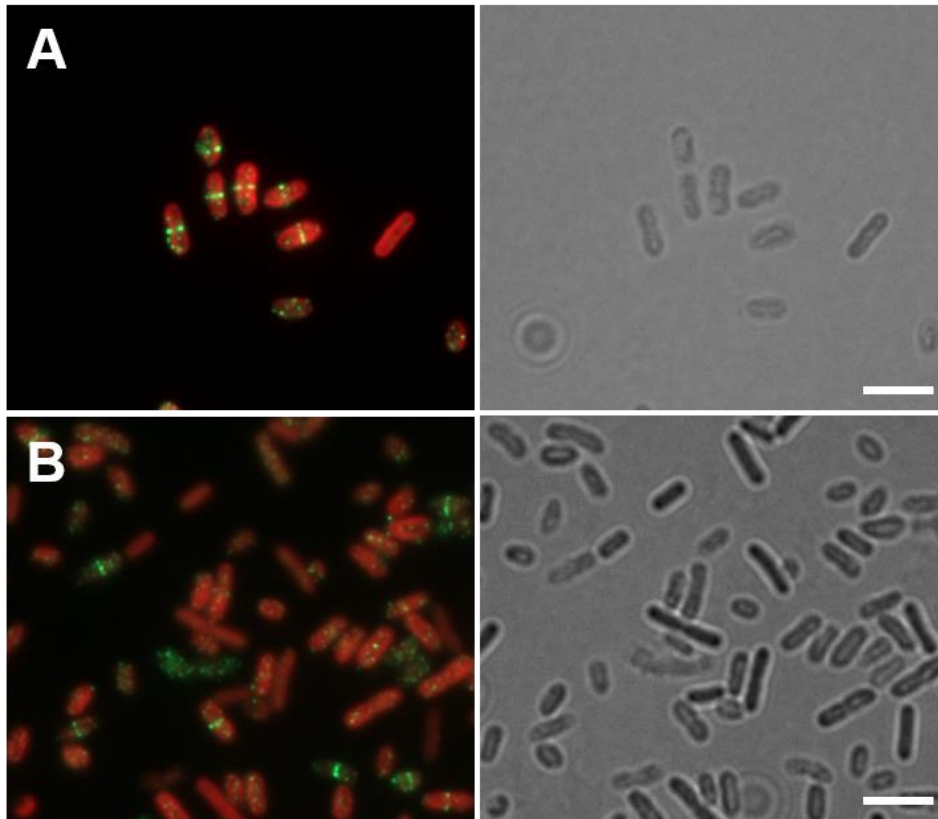


Fig. S17: Δ synpcc7942_2039 does not affect FtsZ localization

Merged Alexa Fluor-488 fluorescence and chlorophyll autofluorescence and bright field micrographs of (A) *Synechococcus* wt and (B) Δ synpcc7942_2039 grown on BG11 plates. Cells were resuspended in BG11 liquid medium and subjected to immunofluorescence staining using an anti-FtsZ primary antibody (raised against *Anabaena* FtsZ) and an Alexa Fluor-488 coated secondary antibody. Cells were mounted in Prolong Diamond antifade mountant (Thermo Fischer Scientific). Scale bars: 5 μ m.

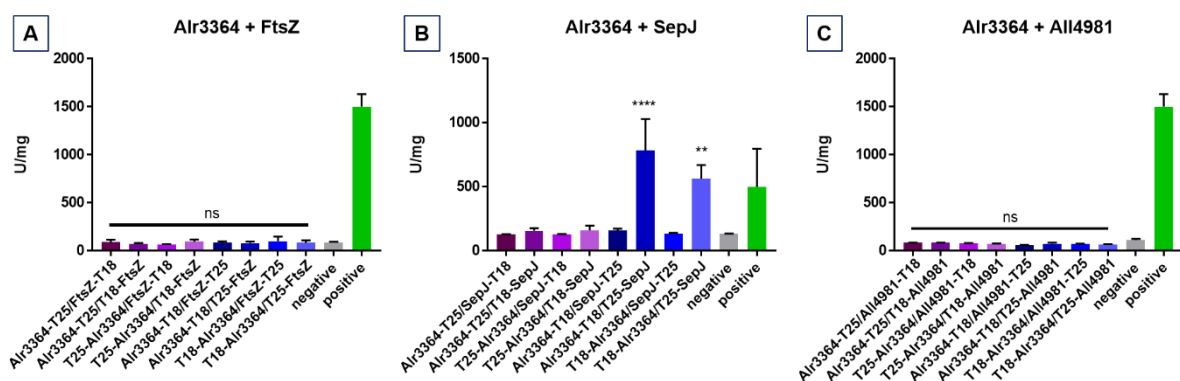


Fig. S18: Alr3364 interacts with SepJ in a bacterial two-hybrid assay

Beta-galactosidase assays of *E. coli* cells co-expressing indicated translational fusion constructs of all possible pairwise combinations of (A) Alr3364+FtsZ, (B) Alr3364+SepJ and (C) Alr3364+All4981. Cells were grown for 2 days at 20 °C. Quantity values are given in Miller Units per milligram LacZ of the mean results from three independent colonies. Error bars indicate standard deviations. Neg: pKNT25 plasmid carrying the respective gene insert co-transformed with empty pUT18C. Pos: Zip/Zip control. *: P < 0.05, **: P < 0.01, ***: P < 0.001, ****: P < 0.0001 (Dunnett's multiple comparison test and one-way ANOVA)

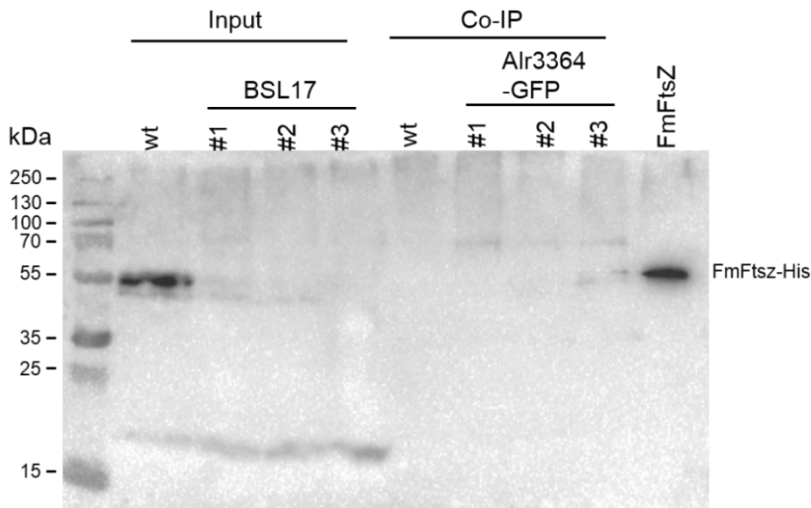


Fig. S19: Western blot analysis of anti-GFP co-IP from Alr3364-GFP expressing *Anabaena* cells

Anabaena wt and Alr3364-GFP expressing cells were grown in BG11 liquid culture, fixed in 0.7% formaldehyde, lysed in CLB and Alr3364-GFP interacting proteins were co-precipitated using anti-GFP μ Beads (Miltenyi Biotec). Co-precipitation of FtsZ was assessed by western blot analysis using a specific anti-FtsZ antibody. As a positive control, 0.5 μ g purified FtsZ from *Fischerella* (FmFtsZ-His) and as an input control 5% of the total cell-free protein extract from lysed *Anabaena* wt and Alr3364-GFP expressing *Anabaena* cells was also included in the analysis.

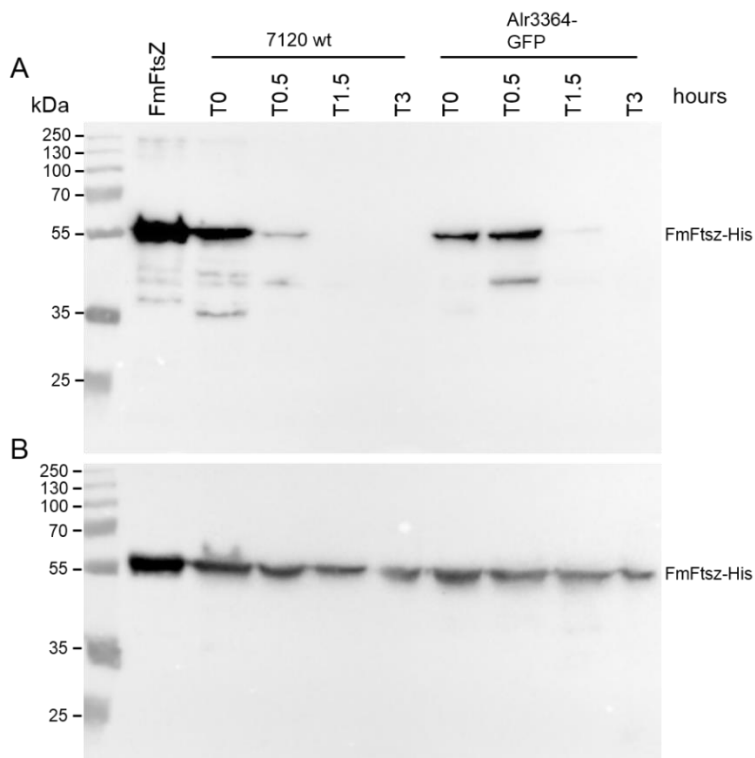


Fig. S20: Western blot analysis of FtsZ-His degradation assay

One microgram of purified FmFtsZ-His was incubated for 3 h at 30°C with 50 μ g of total protein extracts from *Anabaena* wt or Alr3364-GFP expressing *Anabaena* cells lysed in (A) CLB or (B) CLB supplemented with protease inhibitor cocktail (EDTA-free; hereafter: PIC, Roche). Samples corresponding to 51 μ g total protein were taken at indicated time points. FmFtsZ-His degradation was assessed by western blot analysis using a specific anti-His antibody. As a control, 1 μ g FmFtsZ-His was also included in the analysis.

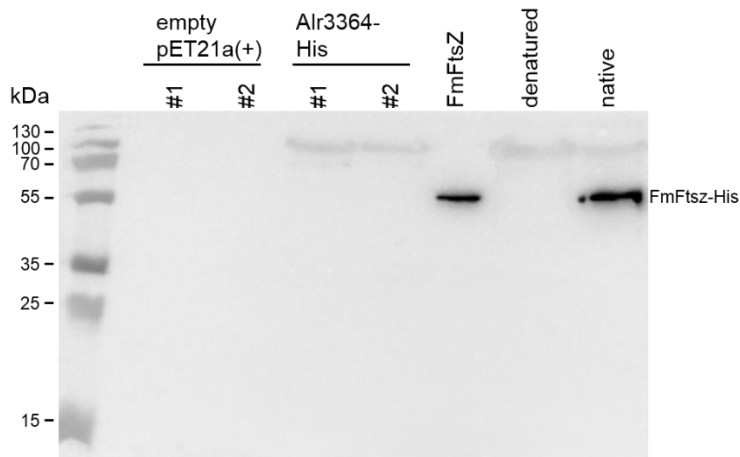


Fig. S21: Western blot analysis of indirect co-IP of Alr3364-His with *Anabaena* extract

E. coli BL21 (DE) cells expressing empty pET21a(+) or Alr3364-His were lysed and His-tag proteins were purified by Ni-NTA under denaturing conditions. Immobilized proteins were incubated with *Anabaena* wt cell-free whole protein extract lysed in CLB supplemented with PIC followed by western blot analysis of co-precipitated proteins using a specific anti-FtsZ antibody. As a positive control, 0.5 μ g FmFtsZ-His was included. Furthermore, 40 μ g elution fractions of Alr3364-His purified under native or denaturing conditions were also applied.

14 Supplementary figures Chapter II

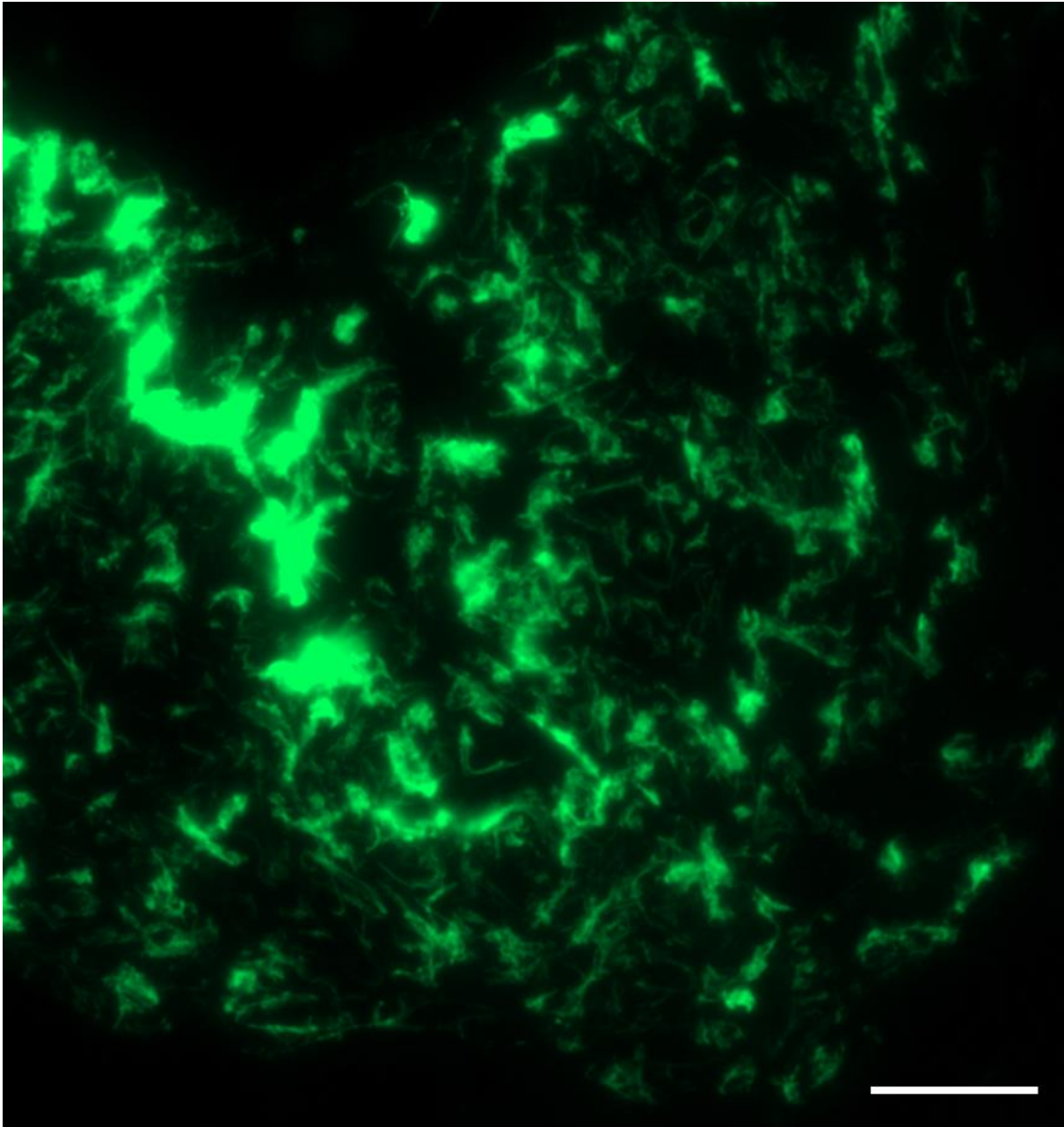


Fig. S22: Alr0931 assembles into a filamentous network

Epifluorescence micrograph of filaments formed by purified and renatured Alr0931 (1 mg ml^{-1}) in HLB. Proteins were dialyzed in a step-wise urea-decreasing manner and stained with an excess of NHS-Fluorescein. Scale bar: $20 \mu\text{m}$.

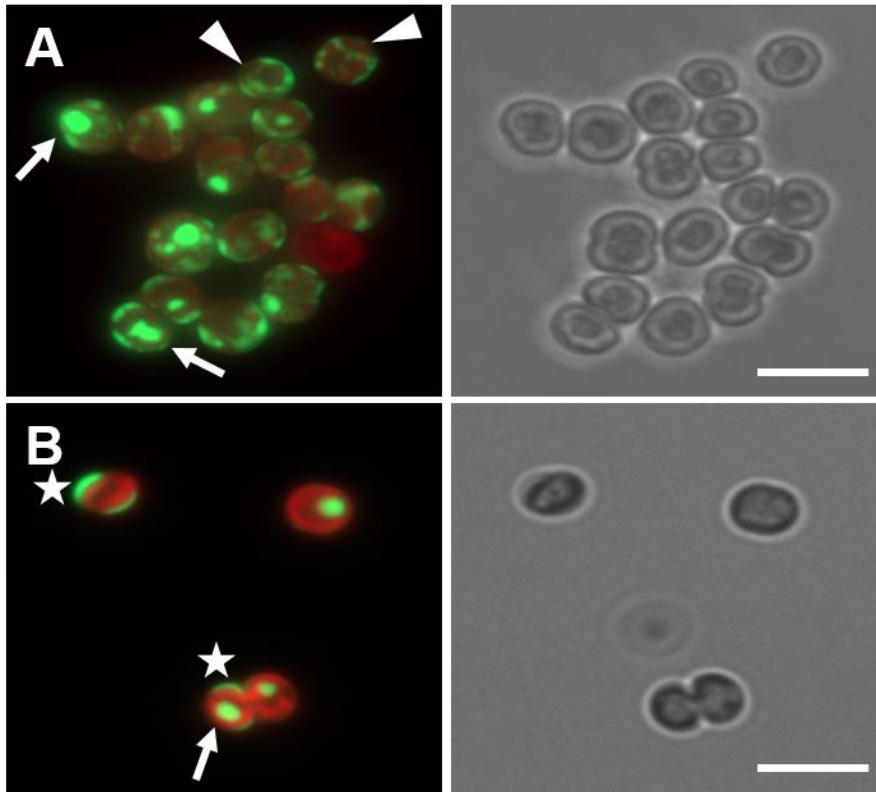


Fig. S23: Slr1301-YFP forms filaments in the motile PCC-M substrain

Merged GFP fluorescence and chlorophyll auto-fluorescence and bright field micrographs of PCC-M expressing Slr1301-YFP. Cells were grown under standard growth conditions in liquid culture and immobilized on an agarose pad. (A) Maximum intensity projection of a Z-stack. White arrows indicate focal accumulations. White triangles mark *in vivo* filaments. White stars show crescent-like localization. Scale bar: 5 μ m.

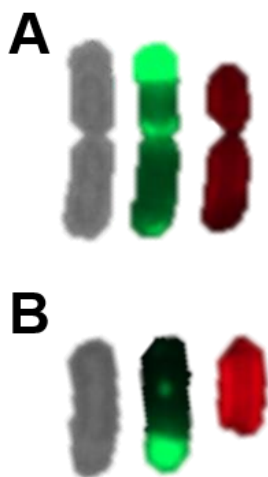


Fig. S24: Displacement of thylakoid membranes by Alr0931-GFP and Slr1301-GFP in *Synechococcus*

Cropped and aligned bright field, GFP fluorescence and chlorophyll auto-fluorescence micrographs of *Synechococcus* cells expressing (A) Alr0931-GFP or (B) Slr1301-GFP. Cells were either grown on BG11 plates supplemented with (A) 0.5 mM or (B) 0.05 mM IPTG and immobilized on an agarose pad. (A,B) Maximum intensity projection of a Z-stack.

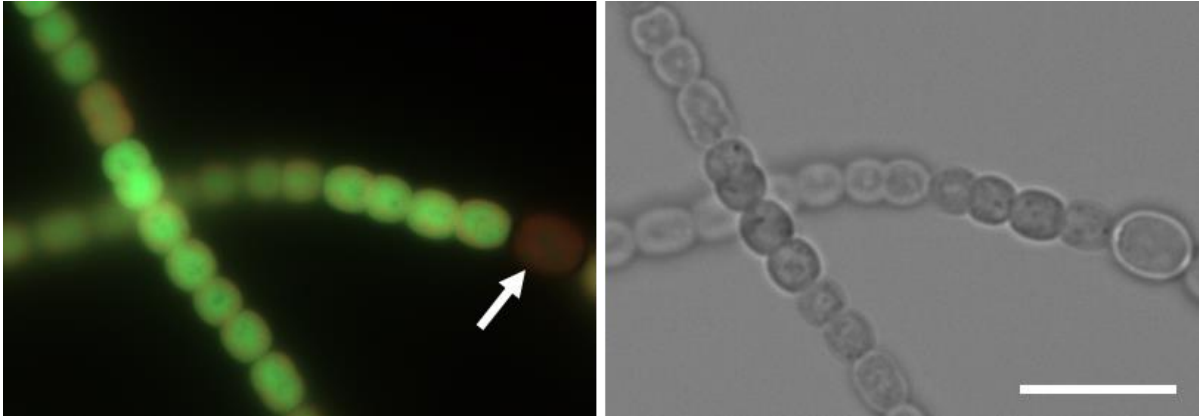


Fig. S25: Diffuse localization of Alr0931-GFP in *Anabaena*

Merged GFP fluorescence and chlorophyll auto-fluorescence and bright field micrographs of *Anabaena* cells expressing Alr0931-GFP grown in BG11-0 without copper supplemented for 1 day with 1 μM CuSO_4 . White arrow marks a heterocyst. Scale: 10 μm .

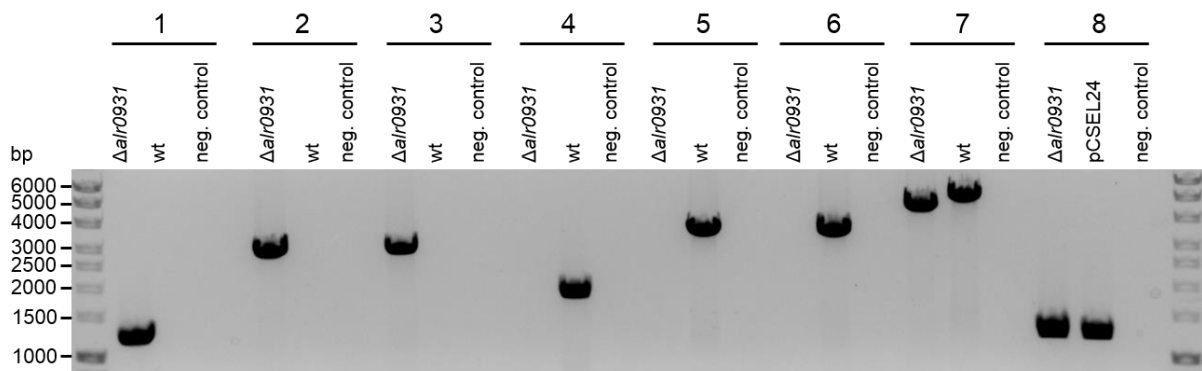


Fig. S26: Verification of $\Delta alr0931$

Colony PCR of $\Delta alr0931$ grown on a BG11 plate supplemented with 2.5 $\mu\text{g ml}^{-1}$ Sm and Sp. Cells were resuspended in 10 μl sterile H_2O and 1 μl of this suspension was added to the respective PCR reaction. As a control *Anabaena* wt genomic DNA or purified pCSEL24 plasmid was used. Neg. control contained H_2O instead of any template. The following primers were used for the corresponding PCR reaction using DreamTaq Green PCR Master Mix: (1) P264+P265; (2) P264+P353; (3) P352+P265; (4) P292+P293; (5) P292+P353; (6) P352+P293; (7) P352+P353; (8) P485+P486. DNA products were subjected to 0.7% agarose gel electrophoresis in TAE buffer.

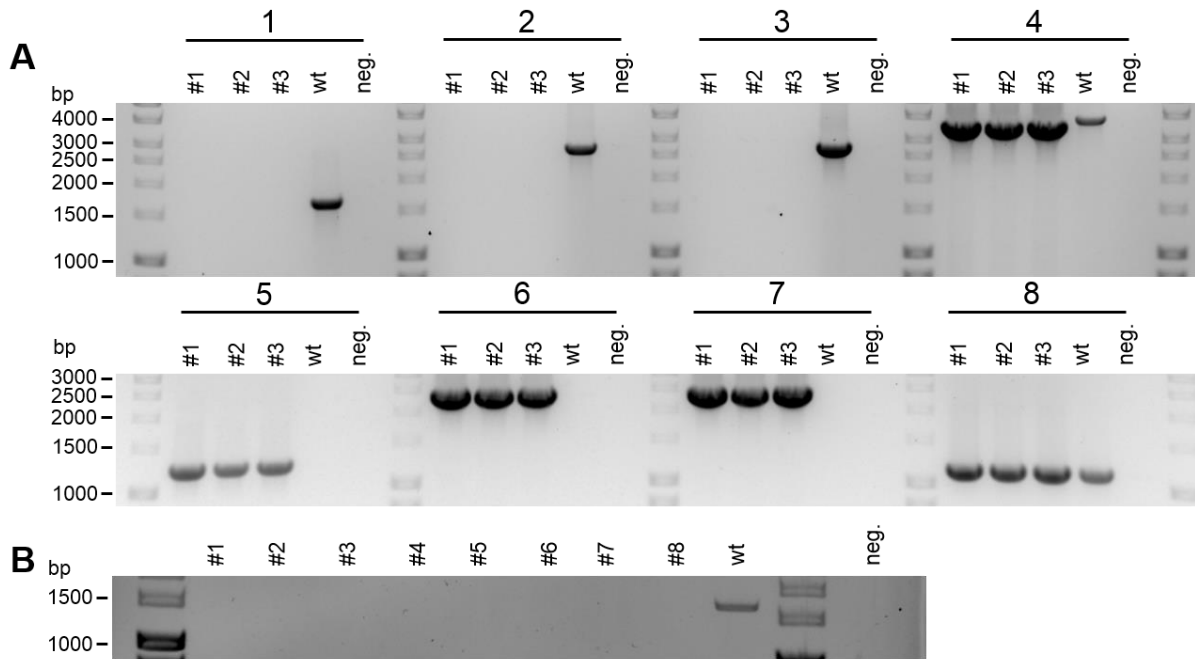


Fig. S27: Verification of $\Delta slr1301$

(A) PCR of isolated $\Delta slr1301$ PCC-M genomic DNA from three fully segregated clones. The following primers were used for the corresponding PCR reaction using DreamTaq Green PCR Master Mix: (1) P270+P271; (2) P270+P349; (3) P348+P271; (4) P348+P349; (5) P264+P265; (6) P264+P349; (7) P348+P265; (8) P115+P116. (B): Colony PCR of eight fully segregated $\Delta slr1301$ GT-Kazusa clones using *slr1301* gene primers (P270+P271). DNA products were subjected to 1% agarose gel electrophoresis in TAE buffer. Neg. control contained H₂O instead of any template. As a control *Synechocystis* wt genomic DNA was used.

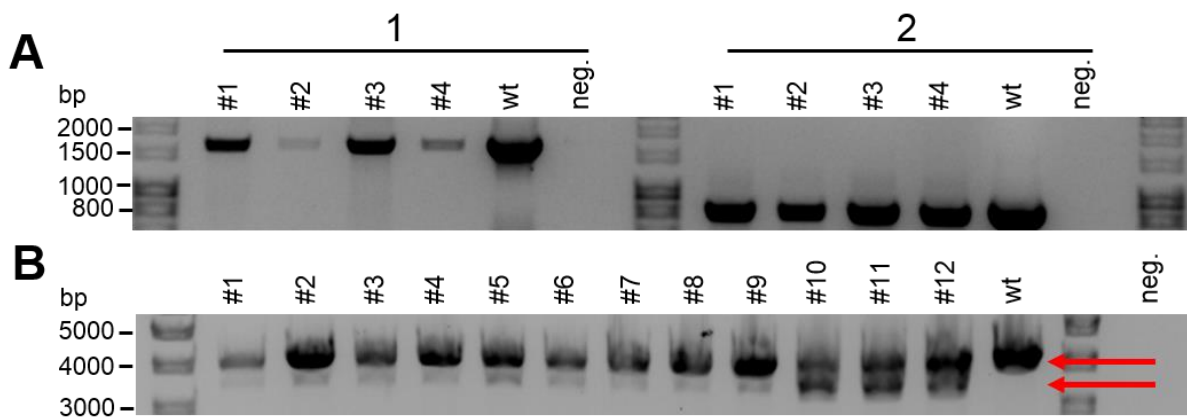


Fig. S28: Colony PCRs of non-segregated $\Delta synpcc7942_1139$

(A) Colony PCRs of four non-segregated $\Delta synpcc7942_1139$ clones using (1) *synpcc7942_1139* gene primers (P311+P312) or (2) *synpcc7942_2039* gene primers (P136+P137) as a control. (B) Colony PCRs of twelve non-segregated $\Delta synpcc7942_1139$ clones using primers encompassing the homologous flanking regions used for homologous recombination (P350+P351). Upper red arrow indicates wt allele PCR product. Lower red arrow indicates $\Delta synpcc7942_1139$ PCR product. As a positive control, *Synechococcus* genomic DNA was included.

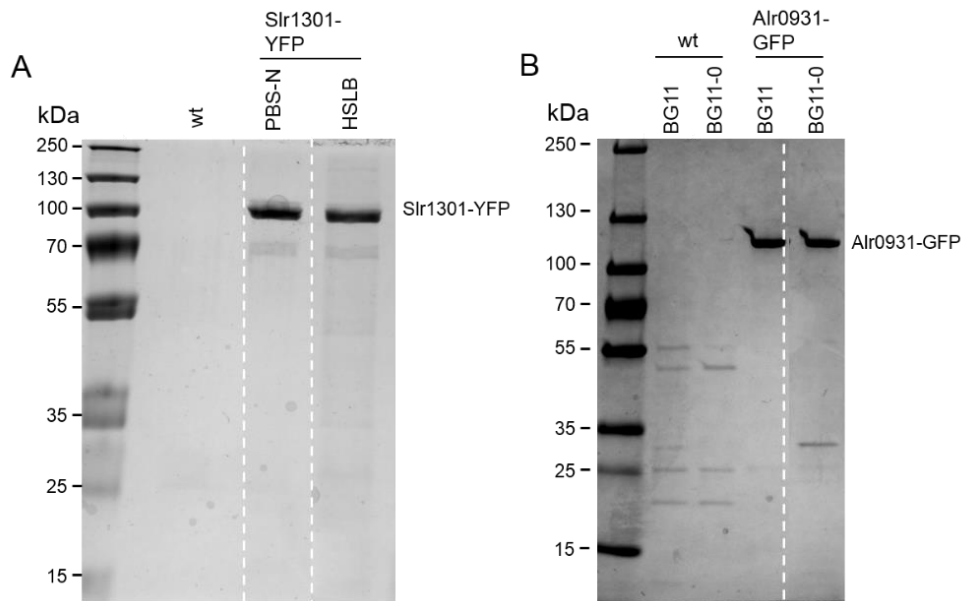


Fig. S29: Interactor proteins of Slr1301-YFP and Alr0931-GFP

(A) Cell-free extracts of *Synechocystis* wt and *Synechocystis* expressing Slr1301-YFP grown in liquid culture were subjected to co-immunoprecipitation using anti-GFP magnetic beads. Cells were lysed in PBS supplemented with 1% NP-40 (PBS-N) or in a high salt lysis buffer (HSLB). (B) Cell-free extracts of *Anabaena* wt cells grown in BG11 and BG11-0 or Alr0931-GFP expressing *Anabaena* cells grown in BG11 and BG11-0 without copper supplemented with 0.5 μM CuSO_4 for 1 day were subjected to co-immunoprecipitation using anti-GFP magnetic beads. Cells were lysed in PBS-N. (A,B) Pooled duplicates of precipitated proteins of two independent experiments were analyzed by mass spectrometry and 25 μl of the precipitate were resolved in a (A) 10% SDS-polyacrylamide gel or in a (B) 4-15% TGX precast gel (Bio-Rad) and detected by Quick Coomassie stain (Serva).

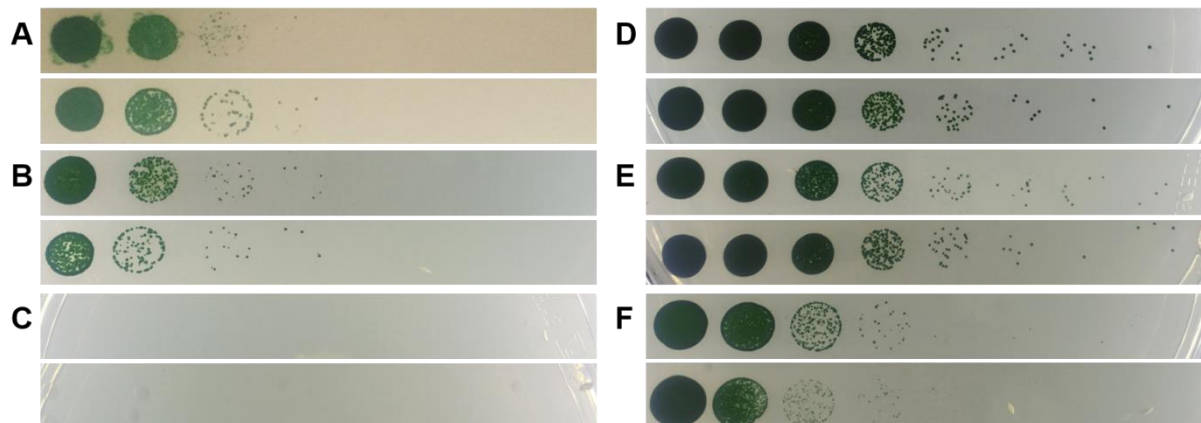


Fig. S30: Viability tests of $\Delta slr1301$ GT-Kazusa and $\Delta slr1301$ PCC-M

(A-C) Motile *Synechocystis* substrain PCC-M wt (upper lane) and $\Delta slr1301$ PCC-M (lower lane) or (D-F) non-motile GT-Kazusa wt (upper lane) and $\Delta slr1301$ GT-Kazusa (lower lane) were grown in liquid culture at growth conditions until an OD_{750} of about 2.0, diluted to an OD_{750} of 0.4 in BG11 and spotted on (A,D) BG11 plates, BG11 plates supplemented with (B,E) 100 $\mu\text{g ml}^{-1}$ Lysozyme or (C,F) 30 $\mu\text{g ml}^{-1}$ Proteinase K in triplicates of serial dilutions of factor 1/10. Cells were grown until no further colonies arose in the highest dilution.

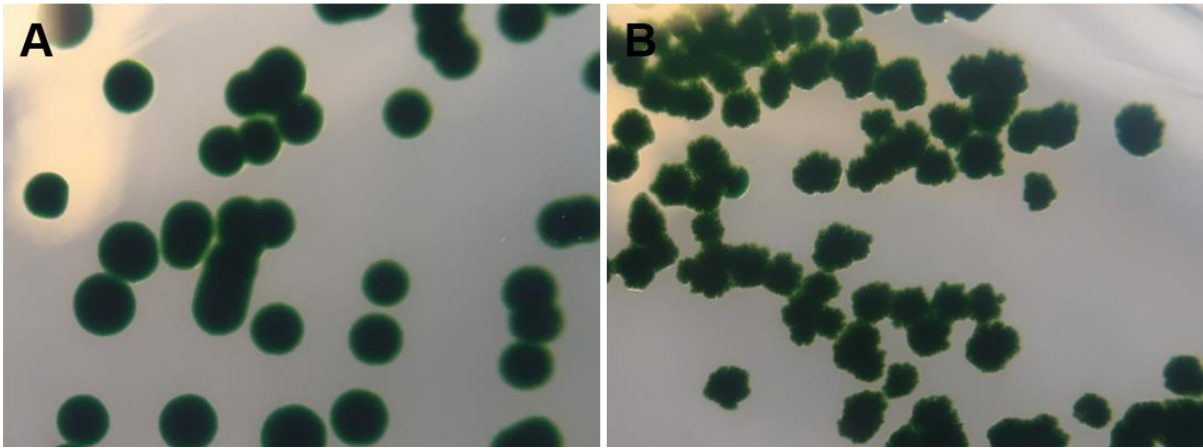


Fig. S31: Non-segregated Δ synpcc7942_1139 alters *Synechococcus* colony morphology

Bright field micrographs of (A) *Synechococcus* wt and (B) non-segregated Δ synpcc7942_1139 grown on (A) BG11 growth plates or (B) BG11 growth plates supplemented with kanamycin ($50 \mu\text{g ml}^{-1}$).

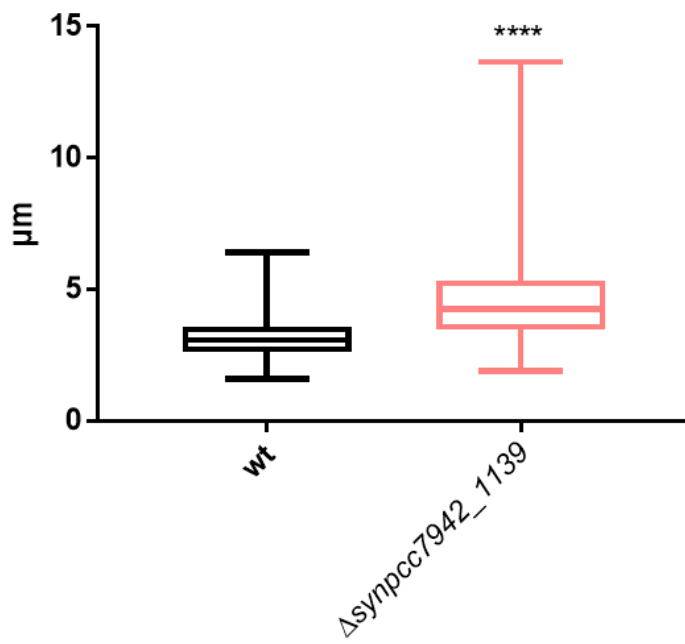


Fig. S32: Cell length of non-segregated Δ synpcc7942_1139 is increased

Cell length of *Synechococcus* wt ($n = 648$) and non-segregated Δ synpcc7942_1139 ($n = 417$) cells was measured using the software ImageJ. Mean wt cell length was $3.156 \mu\text{m} \pm 0.74$ and mean non-segregated Δ synpcc7942_1139 cell length was $4.665 \mu\text{m} \pm 1.762$. unpaired t-test: $P < 0.0001$.

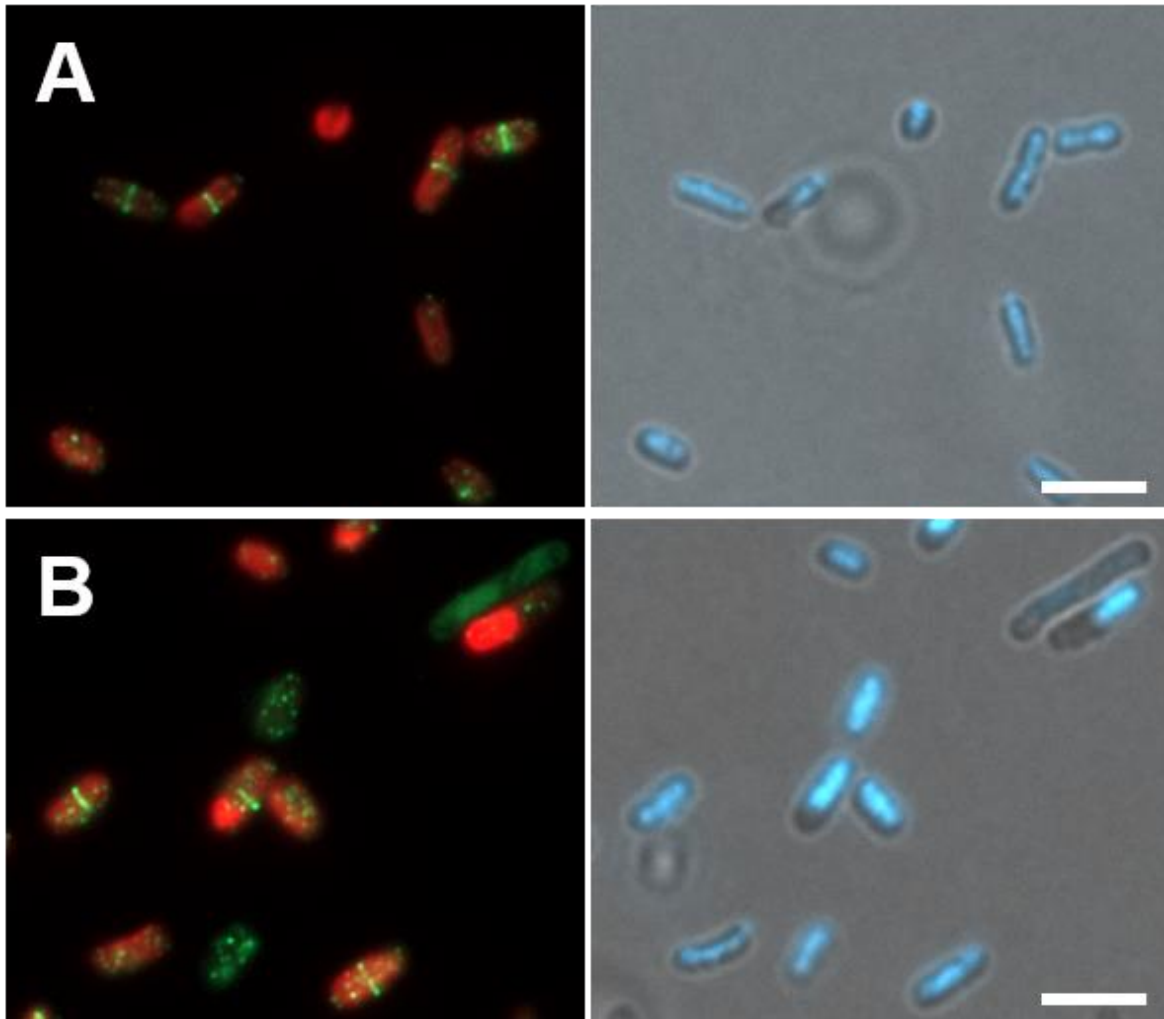


Fig. S33: Non-segregated Δ synpcc7942_1139 has no effect on FtsZ localization

Merged Alexa Fluor-488 fluorescence and chlorophyll autofluorescence or merged bright field and DAPI fluorescence micrographs of (A) *Synechococcus* wt or (B) non-segregated Δ synpcc7942_1139 grown on (A) BG11 plates or (B) BG11 plates supplemented with 50 $\mu\text{g ml}^{-1}$ Km. Cells were resuspended in BG11 liquid medium and subjected to immunofluorescence staining using an anti-FtsZ primary antibody (raised against *Anabaena* FtsZ) and an Alexa Fluor-488 coated secondary antibody. Cells were mounted in Prolong Diamond antifade mountant with DAPI (Thermo Fischer Scientific). Scale bars: 5 μm

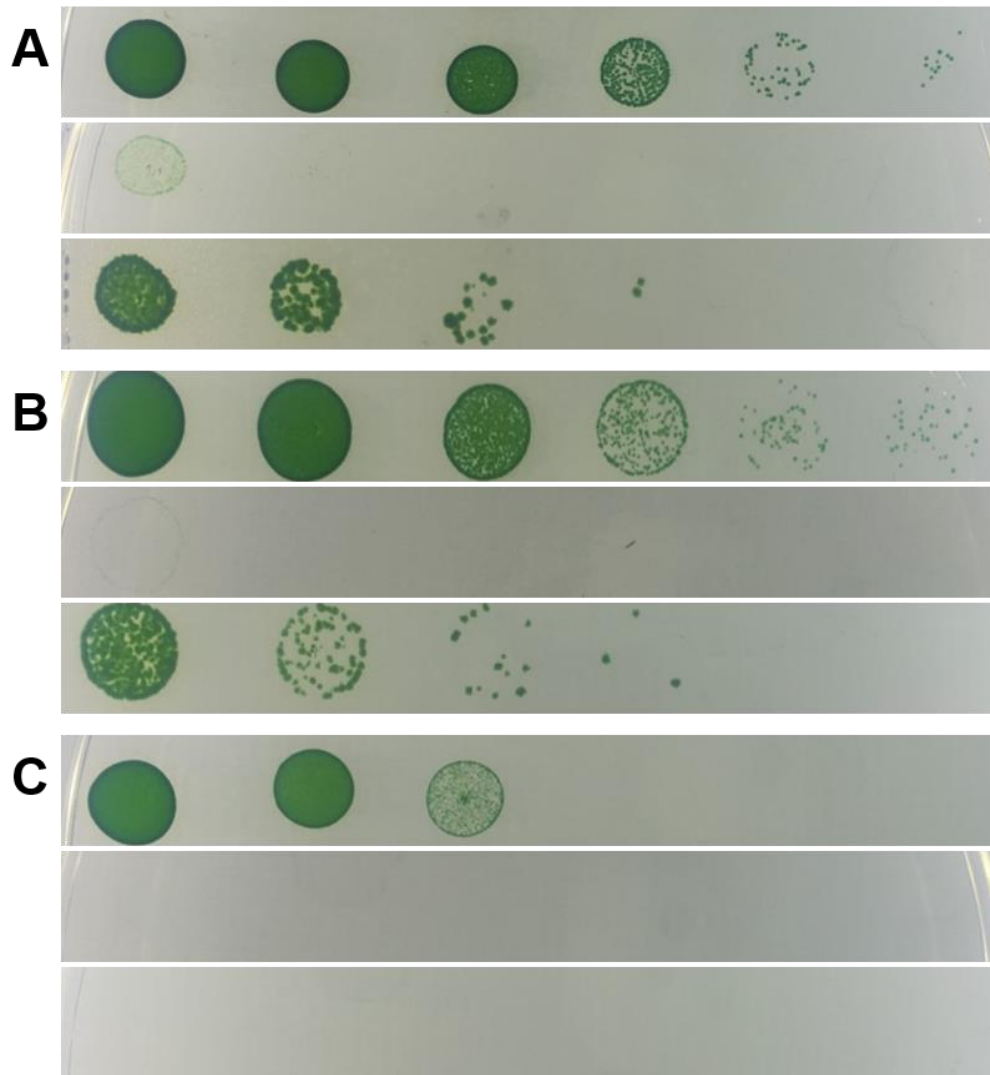


Fig. S34: Non-segregated Δ *synpcc7942_1139* displays decreased viability in a spot assay

Synechococcus wt (upper lane, after 6 days) and Δ *synpcc7942_1139 strain (middle lane: after 6 days and lower lane after 16 days) were grown on BG11 plates or BG11 plates supplemented with 50 μ g ml⁻¹ Km, resuspended in BG11, adjusted to an OD₇₅₀ of 0.4 and spotted on (A) BG11 plates or BG11 plates supplemented either with (B) 50 μ g ml⁻¹ Proteinase K or (C) 100 μ g ml⁻¹ Lysozyme in triplicates of serial dilutions of factor 1/10. Cells were grown until no further colonies arose in the highest dilution. Growth plates for non-segregated Δ *synpcc7942_1139* were always supplemented with 50 μ g ml⁻¹ Km.*

15 Supplementary figures Chapter III

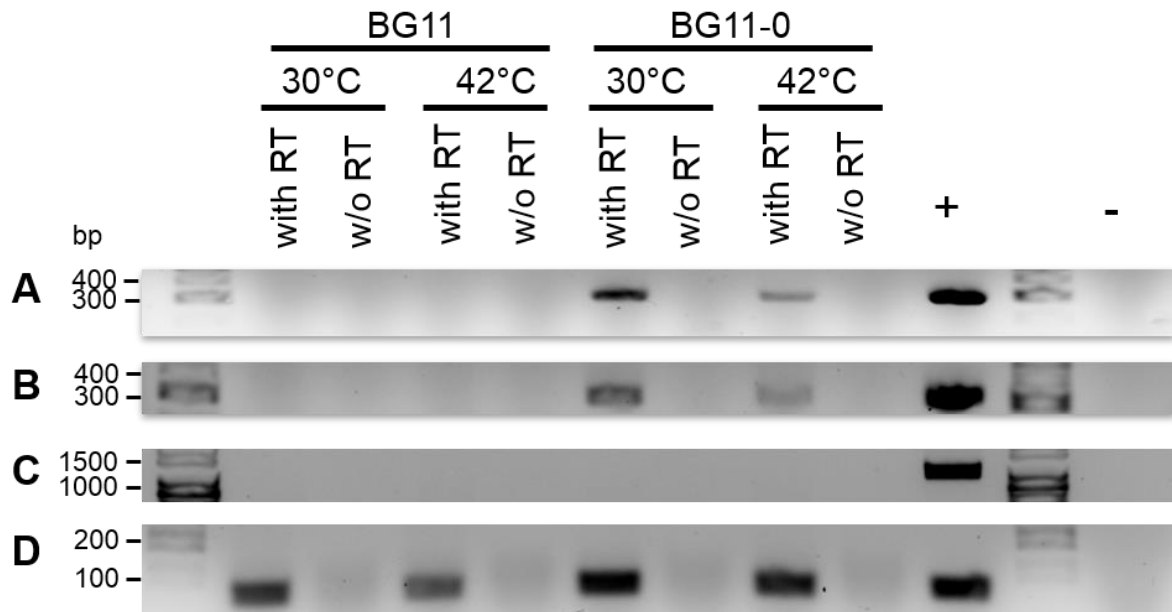


Fig. S35: *alr4504* and *alr4505* share no common transcript

RT-PCR of reverse transcribed whole RNA from *Anabaena* wt (OD₇₅₀ 0.6) grown in BG11 or BG11-0 at standard growth conditions with or without a 15 minutes heat shock at 42 °C using (A) internal *alr4504* gene primers, (B) internal *alr4505* gene primers, (C) primers encompassing *alr4504* and *alr4505* or (D) internal *ftsZ* primers as control. RNA was either reverse transcribed in reaction buffer containing reverse transcriptase (with RT) or without reverse transcriptase (w/o RT) as a control for residual genomic DNA contamination. *Anabaena* genomic DNA was included as positive control. PCR fragments were resolved on a (A,B) 2% or (C,D) 1% agarose gel in TAE buffer.

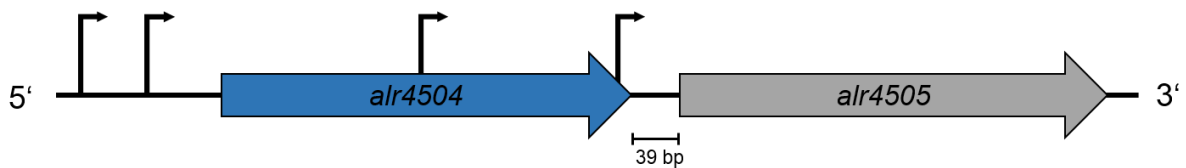


Fig. S36: Genomic region of *alr4504* and *alr4505* in *Anabaena* genome

Depiction of the genomic structure of *alr4504* (blue) and *alr4505* (grey) within the *Anabaena* genome and their respective promoters depicted by black arrows (promoters predicted by BPPROM; Softberry; Solovyev and Salamov (2011)). Promoters of *alr4504* are 204 bp and 543 bp upstream and promoters of *alr4505* are located 22 bp and 450 bp upstream, residing within the *alr4504* open reading frame.

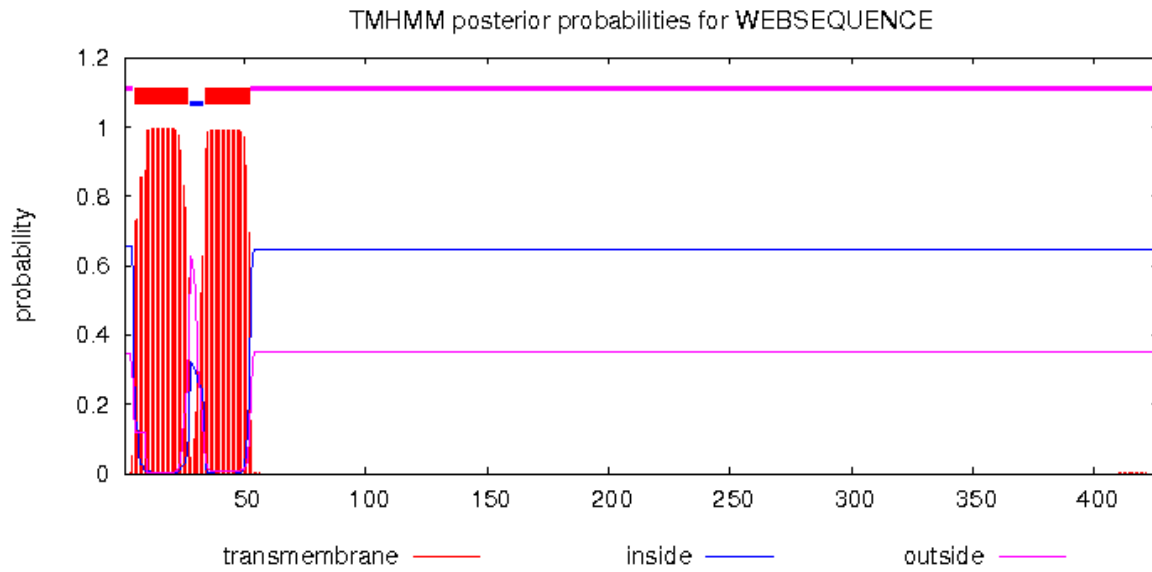


Fig. S37: Prediction of AlI2460 transmembrane domains

Graphical depiction of transmembrane helix domains from AlI2460 amino acid sequence using TMHMM (Server v. 2.0). Transmembrane helices are predicted to span amino acids 5 - 27 and 34 - 52. In contrast to TMHMM, PSORTb (version 3.0.2) predicts the non-membrane part to be localized inside of the cytosol (Data not shown).

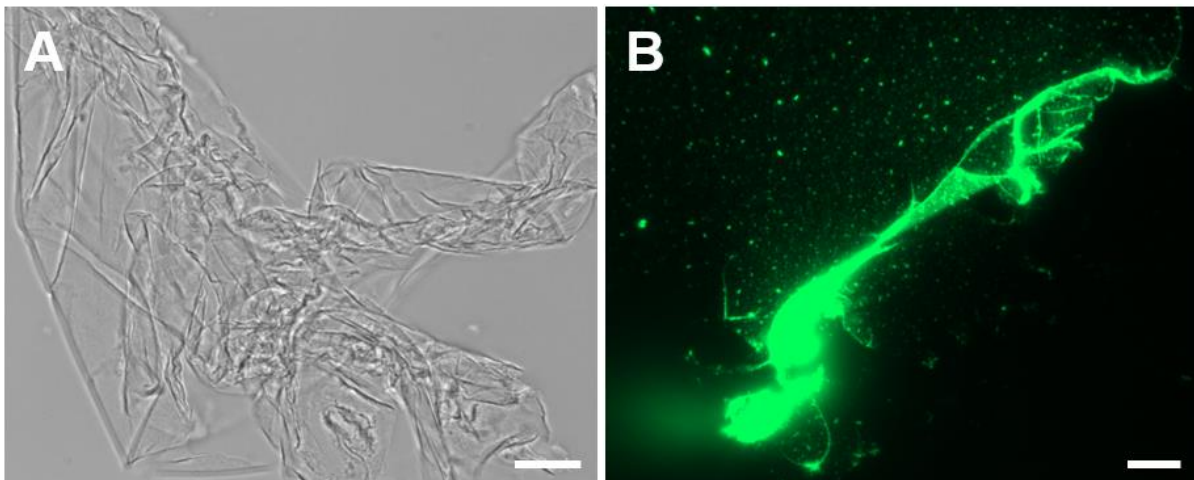


Fig. S38: *In vitro* filamentation of Alr4505

(A) Bright field and (B) epifluorescence micrographs of sheath-like filaments formed upon (A) step wise dialyzed and purified Alr4505 (0.5 mg ml^{-1}) into 25 mM HEPES pH 7.4 or (B) Alr4505 direct dialysis into HLB followed by subsequent NHS-Fluorescein labeling. Scale bars: (A) $20 \mu\text{m}$ or (B) $10 \mu\text{m}$.

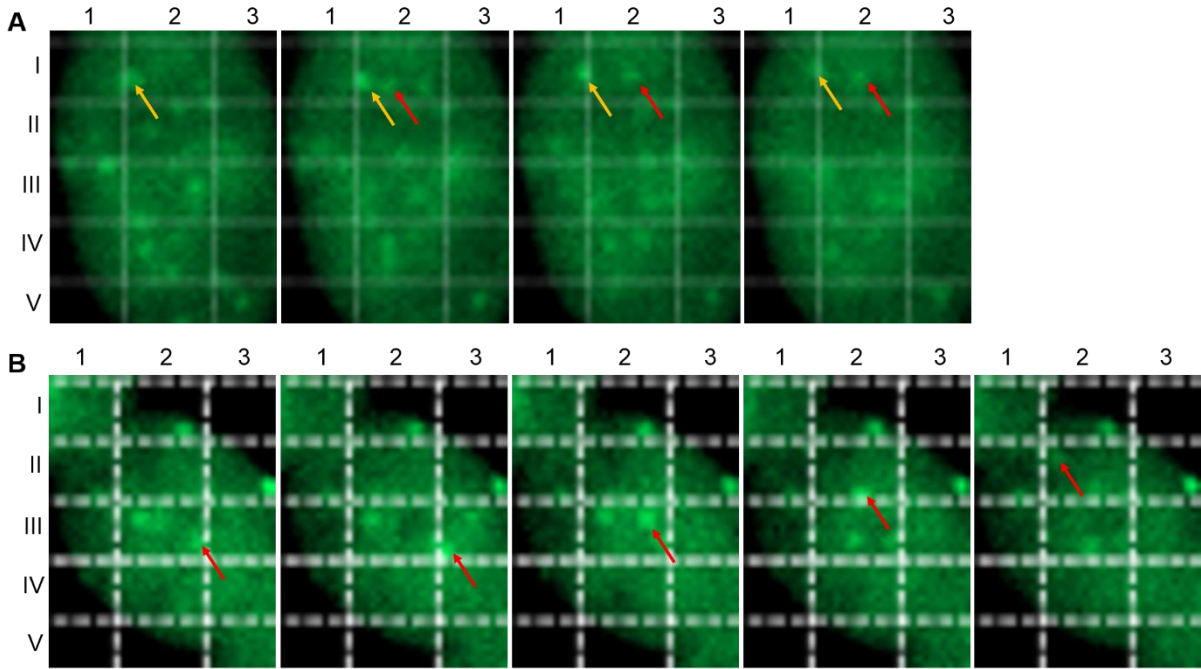


Fig. S39: Alr4504-GFP and Alr4505-GFP show motile properties upon ectopic expression in *Anabaena*

GFP fluorescence micrographs of *Anabaena* cells expressing (A) Alr4504-GFP or (B) Alr4505-GFP grown in (A) BG11 supplemented with 0.5 μM CuSO₄ for 2 days or (B) BG11. Orange and/or red arrows point to single (A) Alr4504-GFP and (B) Alr4505-GFP spots moving through the cells.

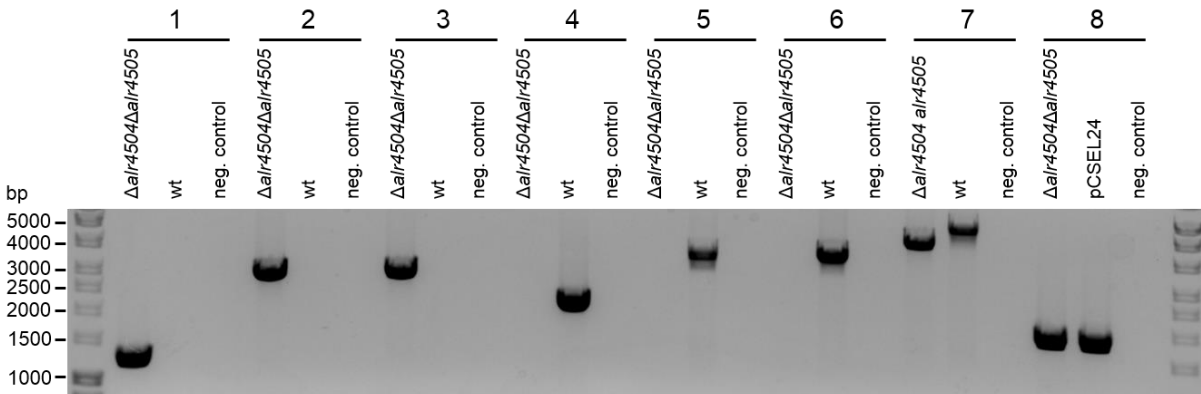


Fig. S40: Verification of $\Delta alr4504\Delta alr4505$

Colony PCR of $\Delta alr4504\Delta alr4505$ grown on BG11. Cells were resuspended in 10 μl sterile H₂O and 1 μl of this suspension was added to the respective PCR reaction. As a control *Anabaena* wt genomic DNA or purified pCSEL24 plasmid was used. Neg. control contained H₂O instead of any template. The following primers were used for the corresponding PCR reaction using DreamTaq Green PCR Master Mix: (1) P413+P414; (2) P413+P355; (3) P354+P414; (4) P424+P461; (5) P424+P355; (6) P354+P461; (7) P354+P355; (8) P292+P293. DNA products were subjected to 0.7% agarose gel electrophoresis in TAE buffer.

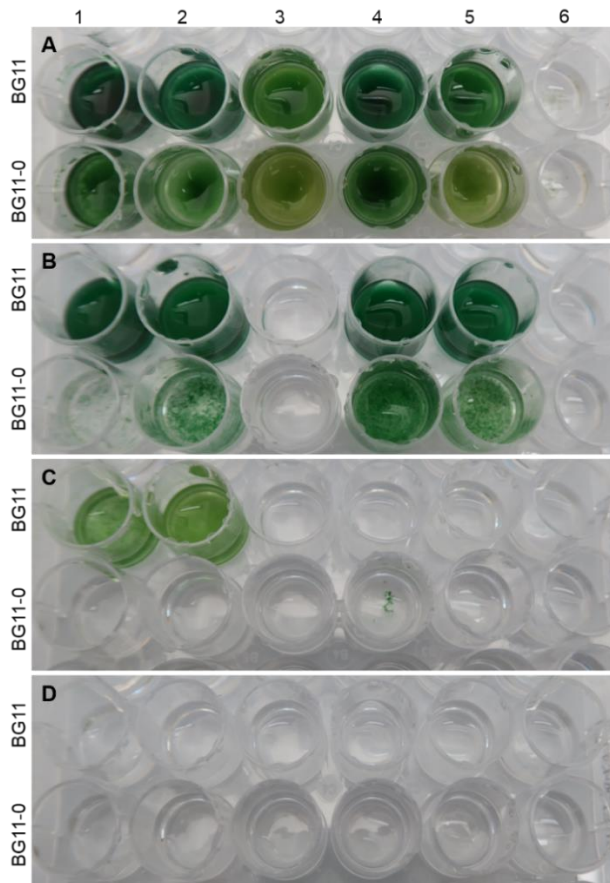


Fig. S41: Growth of *Anabaena* deletion strains in liquid media with osmotic stress factors

(A) *Anabaena* wt as well as *Anabaena* deletion strains (B) $\Delta all2460$, (C) $\Delta alr4504\Delta alr4505$ and (D) $\Delta alr0931$ were transferred from BG11 agar plates to (column 1) BG11 and BG11-0 or BG11 and BG11-0 supplemented with (column 2) 5 mM glucose, (column 3) 200 mM glucose, (column 4) 2 mM NH_4Cl , (column 5) 200 mM maltose or (column 6) 500 mM NaCl.

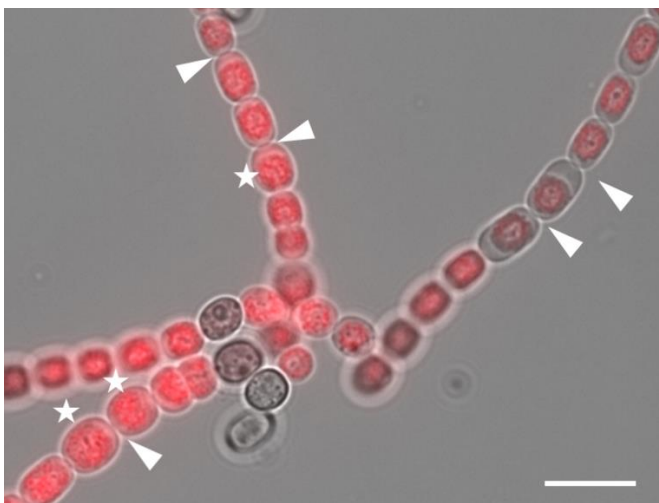


Fig. S42: Overexpression of Alr0931-His alters cell shape and chlorophyll distribution in *Anabaena*

Merged bright field and chlorophyll auto-fluorescence micrograph of *Anabaena* cells expressing Alr0931-His grown in BG11 supplemented with 2.5 μM $CuSO_4$ for 2 days. White triangles indicate selected cell septa with decreased chlorophyll content. White stars mark enlarged cells. Scale bar: 10 μm .

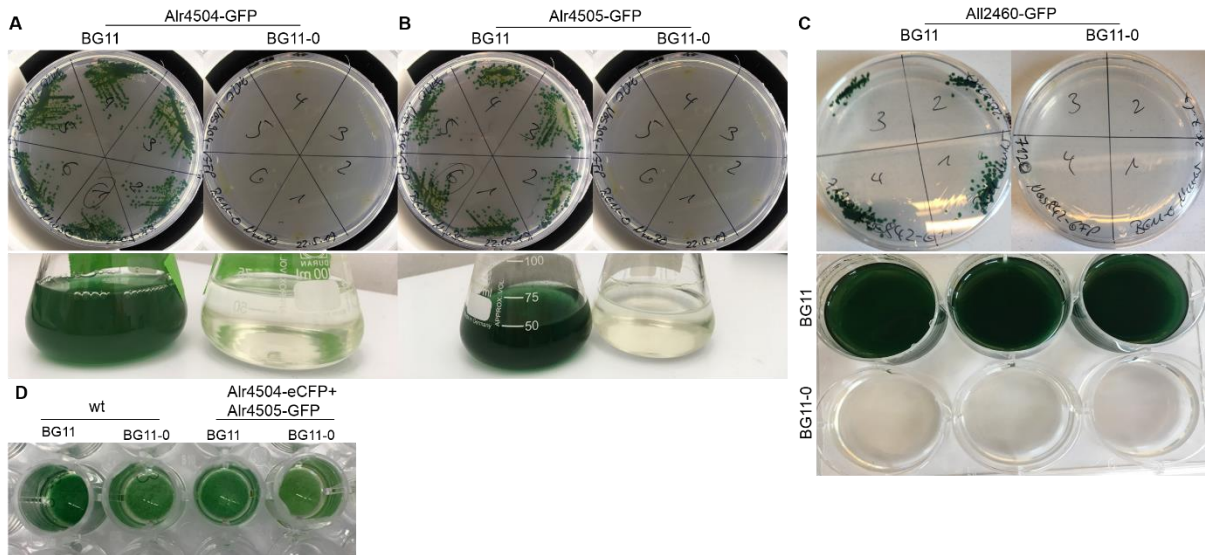


Fig. S43: Growth of *Anabaena* strains expressing fluorescently tagged CCRPs

Anabaena strains expressing (A) Alr4504-GFP, (B) Alr4505-GFP or (C) All2460-GFP grown on BG11 or BG11-0 plates and in BG11 and BG11-0 liquid medium in culture flasks. (C) Growth of *Anabaena* wt and *Anabaena* co-expressing Alr4504-eCFP and Alr4505-GFP in BG11 and BG11-0 liquid medium in a 96-well plate.

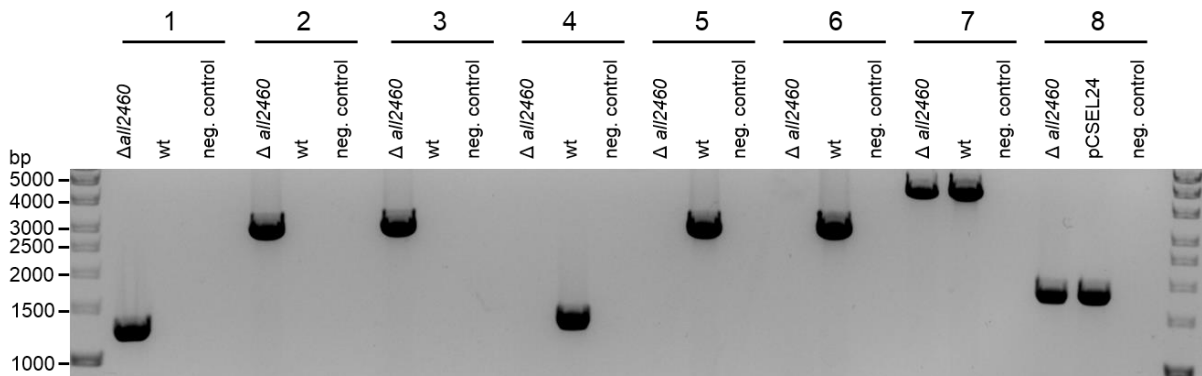


Fig. S44: Verification of $\Delta all2460$

Colony PCR of $\Delta all2460$ grown on BG11 plates. Cells were resuspended in 10 μ l sterile H₂O and 1 μ l of this suspension was added to the respective PCR reaction. As a control *Anabaena* wt genomic DNA or purified pCSEL24 plasmid was used. Neg. control contained H₂O instead of any template. The following primers were used for the corresponding PCR reaction using DreamTaq Green PCR Master Mix: (1) P413+P414; (2) P413+P357 (3) P356+P414; (4) P485+P486; (5) P485+P357; (6) P356+P486; (7) P356+P357; (8) P292+P293. DNA products were subjected to 0.7% agarose gel electrophoresis in TAE buffer.

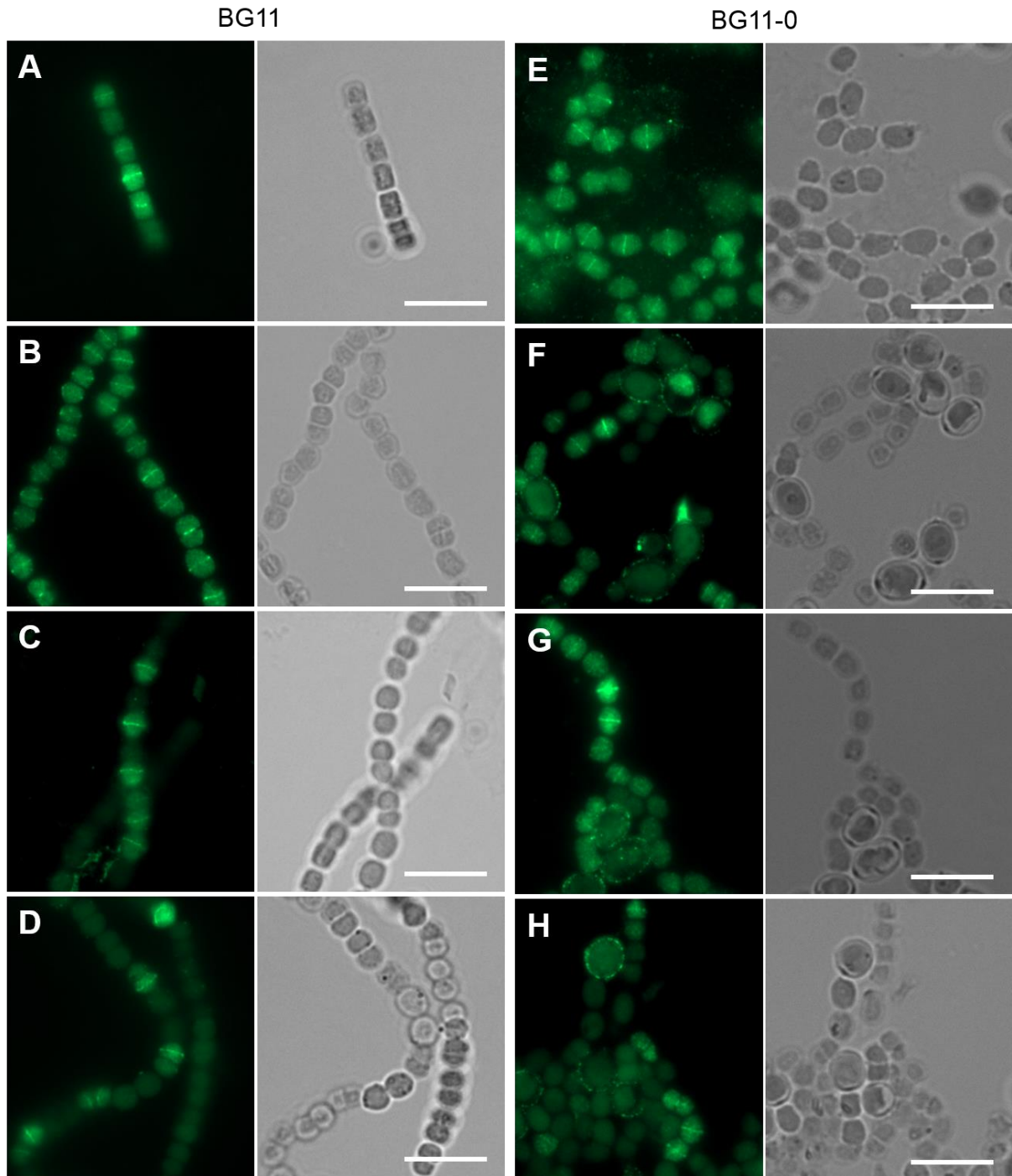


Fig. S45: Immunolocalization of FtsZ in *Anabaena* deletion strains

Alexa Fluor-488 fluorescence and bright field micrographs of (A,E) *Anabaena* wt and *Anabaena* mutant strains (B,F) $\Delta all2460$, (C,G) $\Delta alr4504\Delta alr4505$ and (D,H) $\Delta alr0931$ grown on (A,B,C,D) BG11 or (E,F,G,H) BG11-0 plates. Cells were resuspended in BG11 or BG11-0 liquid medium and subjected to immunofluorescence staining using anti-FtsZ primary antibody and Alexa Fluor-488 coated secondary antibody essentially as described by Ramos-León *et al.* (2015). Cells were mounted in Prolong Diamond antifade mountant (Thermo Fischer Scientific). Scale bars: 10 μ m.

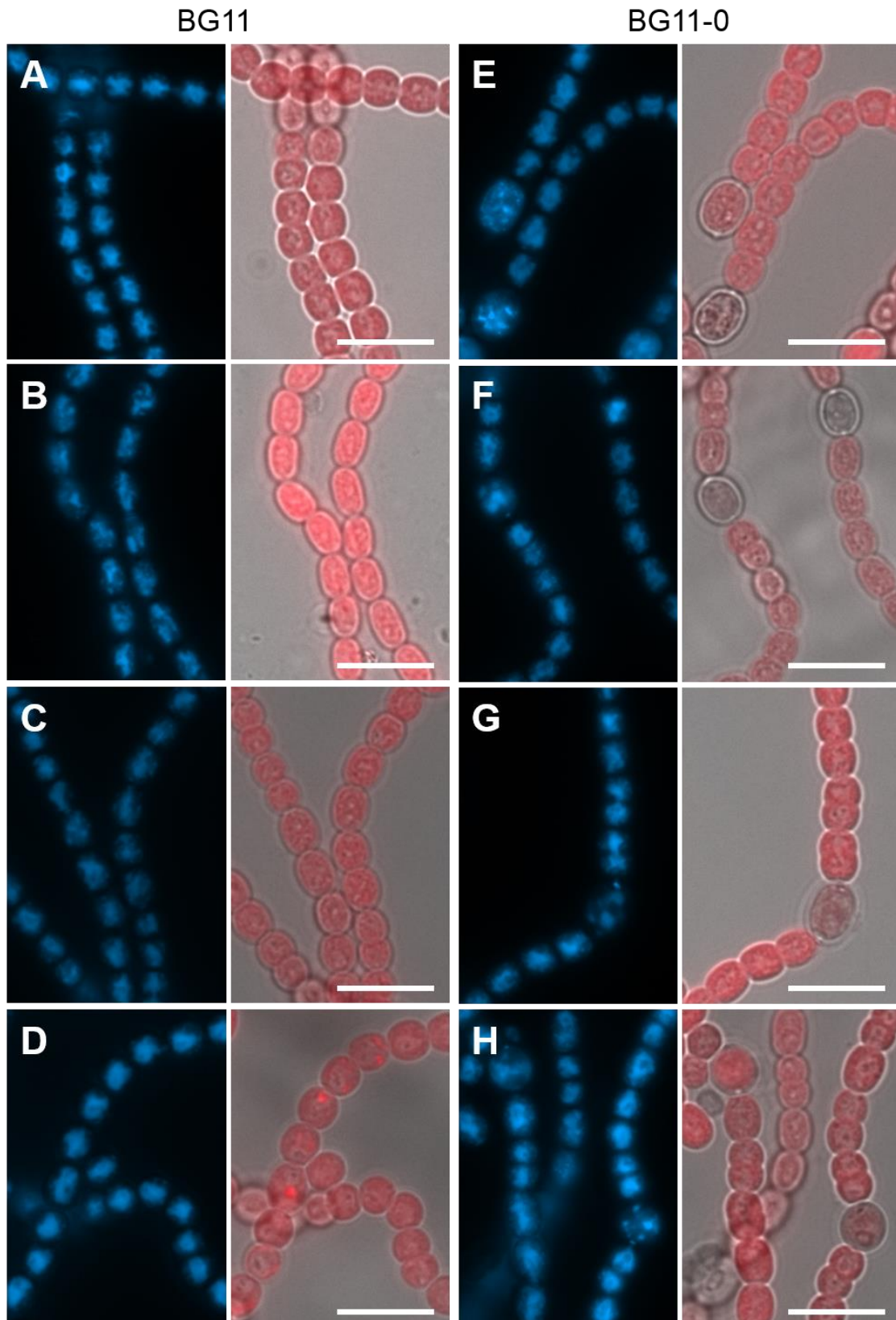


Fig. S46: DAPI-staining of *Anabaena* gene mutant strains

DAPI fluorescence and merged bright field and chlorophyll auto-fluorescence micrographs of (A,E) *Anabaena* wt and *Anabaena* mutant strains (B,F) $\Delta all2460$, (C,G) $\Delta alr4504\Delta alr4505$ and (D,H) $\Delta alr0931$ grown on (A,B,C,D) BG11 or (E,F,G,H) BG11-0 agar plates. Cells were resuspended in BG11 or BG11-0 liquid medium and incubated with $20 \mu\text{g ml}^{-1}$ DAPI and then immobilized on agarose pads. Scale bars: $10 \mu\text{m}$.

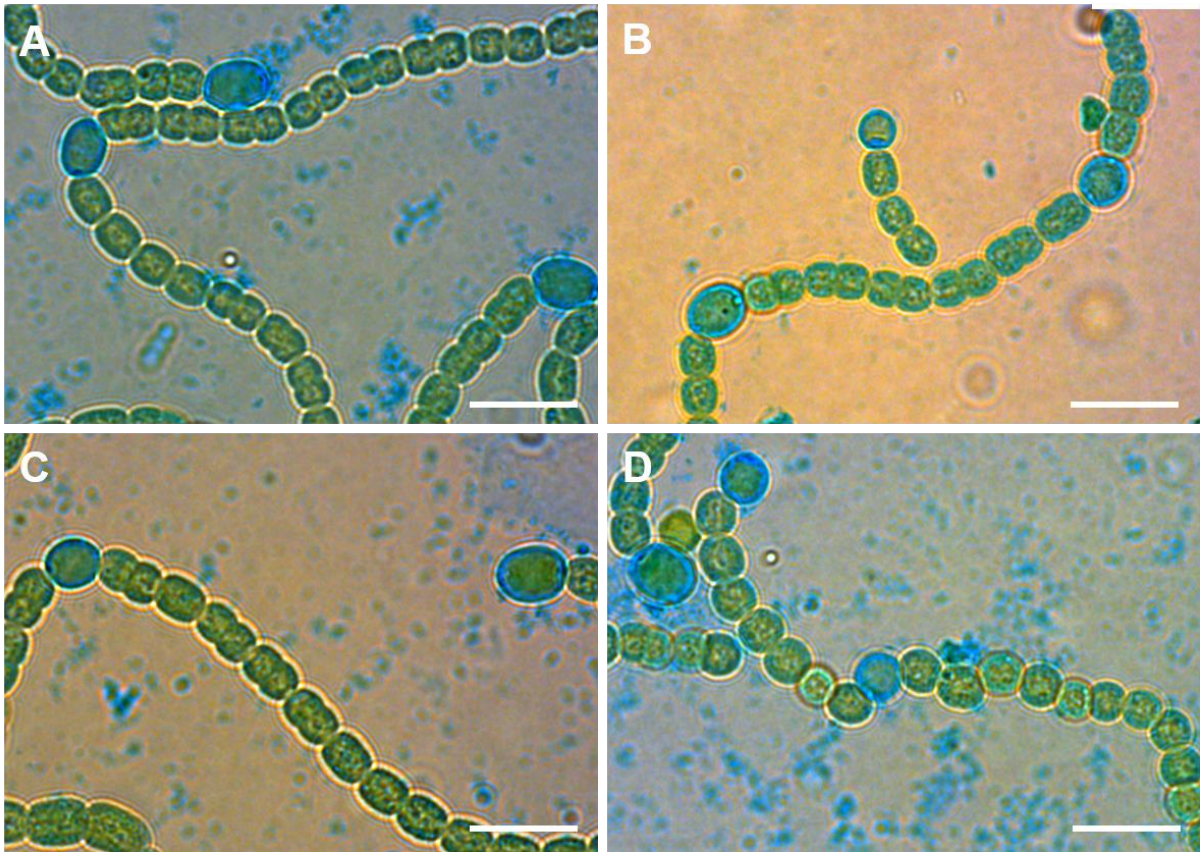


Fig. S47: Alcian blue staining of *Anabaena* deletion strains

Bright field micrographs of (A) *Anabaena* wt and *Anabaena* mutant strains (B) $\Delta alI2460$, (C) $\Delta alr4504\Delta alr4505$ and (D) $\Delta alr0931$ grown on BG11-0 plates, resuspended in BG11-0 and stained with 0.5% alcian blue. Scale bars: 10 μ m.

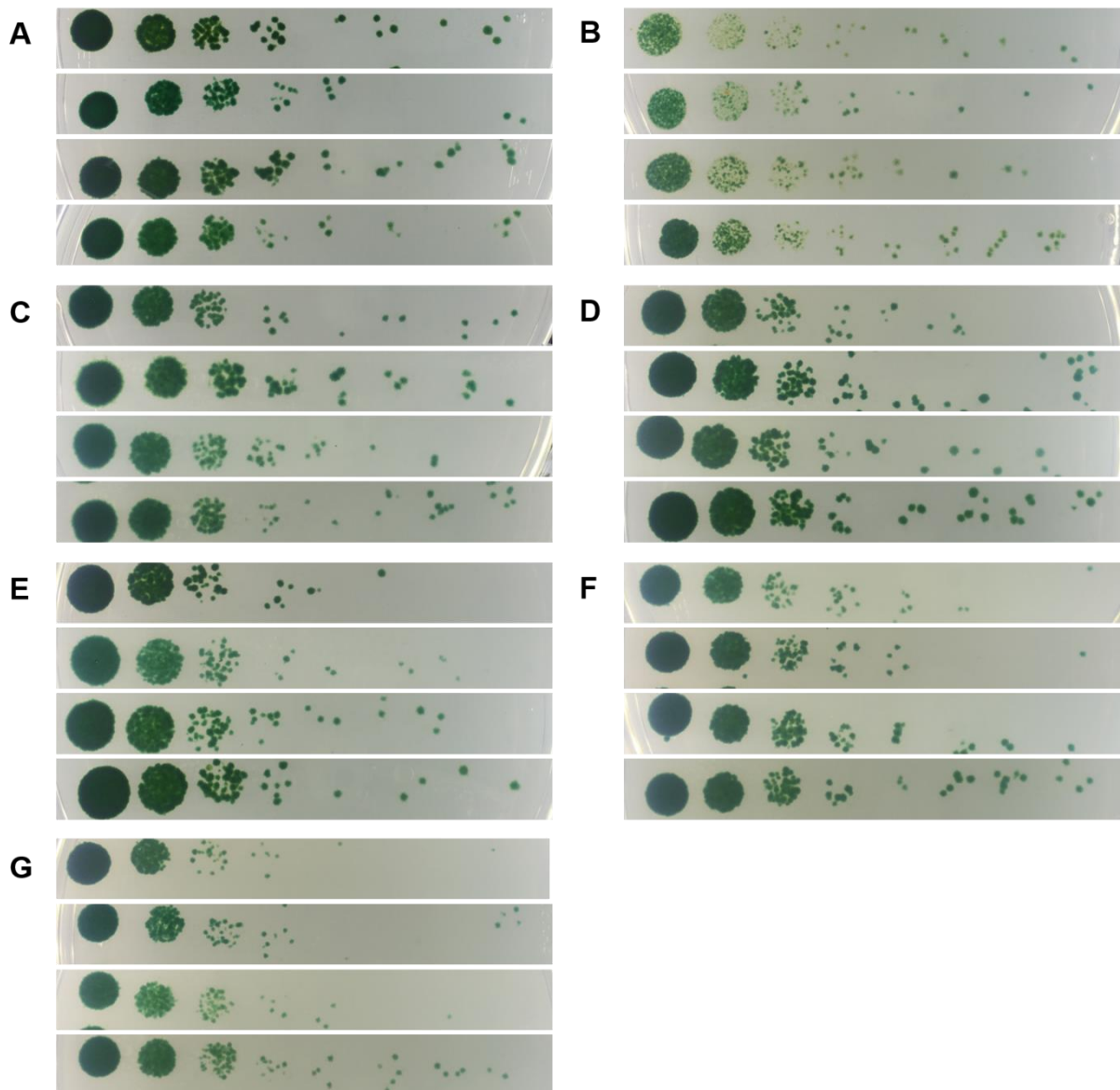


Fig. S48: Spot assay of *Anabaena* deletion strains

Anabaena wt (always 1st row), $\Delta all2460$ (always 2nd row), $\Delta alr4504\Delta alr4505$ (always 3rd row) and $\Delta alr0931$ (always 4th row) cells were grown on BG11 plates, resuspended in BG11 liquid medium and adjusted to OD₇₅₀ of 0.4. Cells were spotted onto (A) BG11, (B) BG11-0, (C) BG11-0 supplemented with 2 mM NH₄Cl or BG11 plates supplemented with (D) 5 µg ml⁻¹ Proteinase K, (E) 30 µg ml⁻¹ Proteinase K, (F) 30 µg ml⁻¹ Lysozyme or (G) 100 µg ml⁻¹ Lysozyme in triplicates of serial dilutions of factor 1/10 and grown until no further colonies arose in the highest dilution.

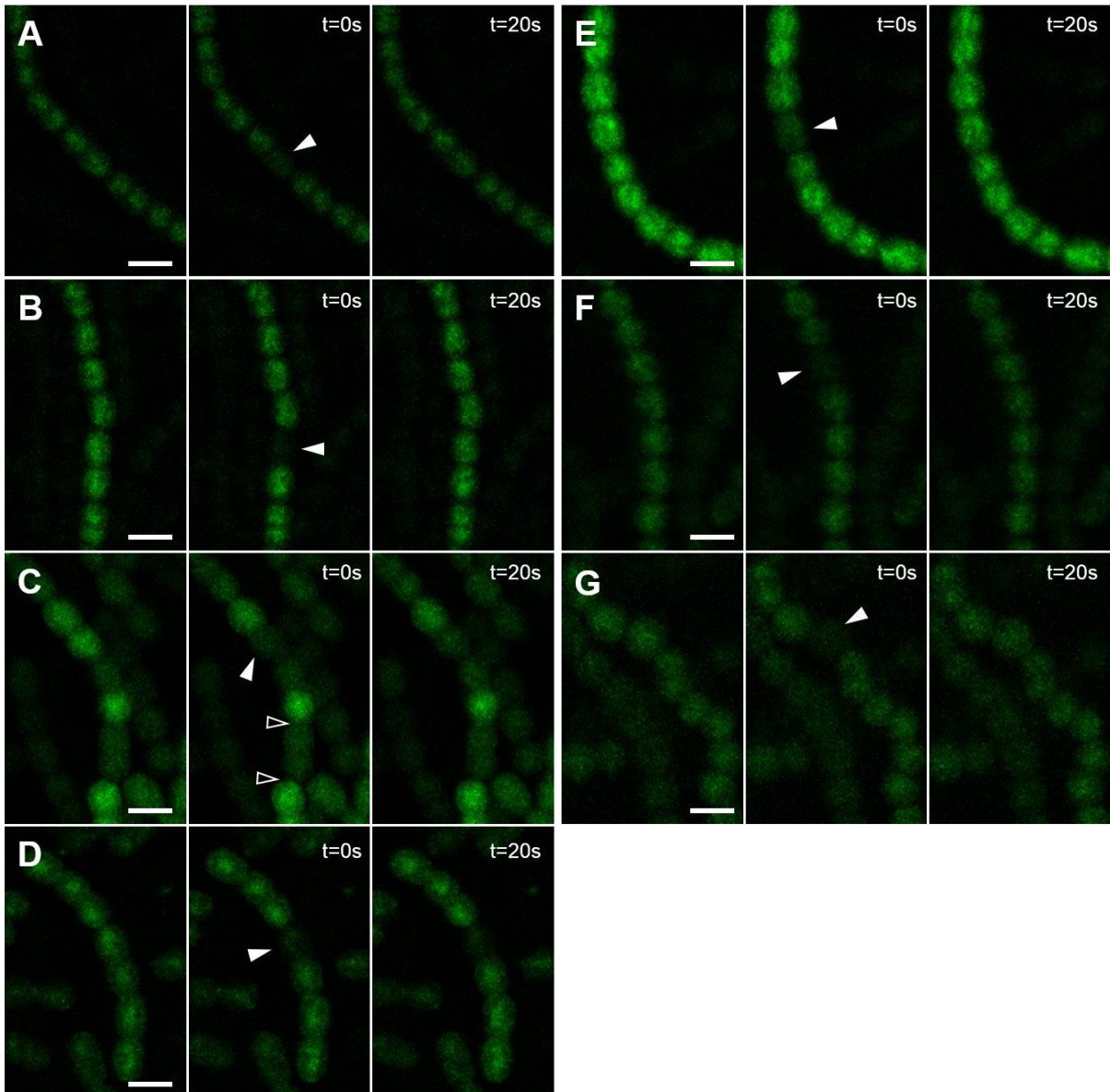


Fig. S49: Fluorescence recovery of bleached cells from *Anabaena* mutant strains

Exemplary calcein fluorescence micrographs depicting intercellular molecular exchange following laser-based bleaching of calcein fluorescence in *Anabaena* wt grown in (A) liquid BG11, (B) liquid BG11-0 or on (E) BG11 plate and $\Delta all2460$ grown in (C) liquid BG11 or (D) liquid BG11-0 as well as (F) $\Delta alr4504alr4505$ and (G) $\Delta alr0931$ grown on BG11 plates. White triangles indicated bleached cells. Translucent triangles show diffusion barriers. Fluorescence images show respective cells prior bleaching, immediately after bleaching (t=0) and at a later stage (t=20s). Scale bars: 5 μ m.

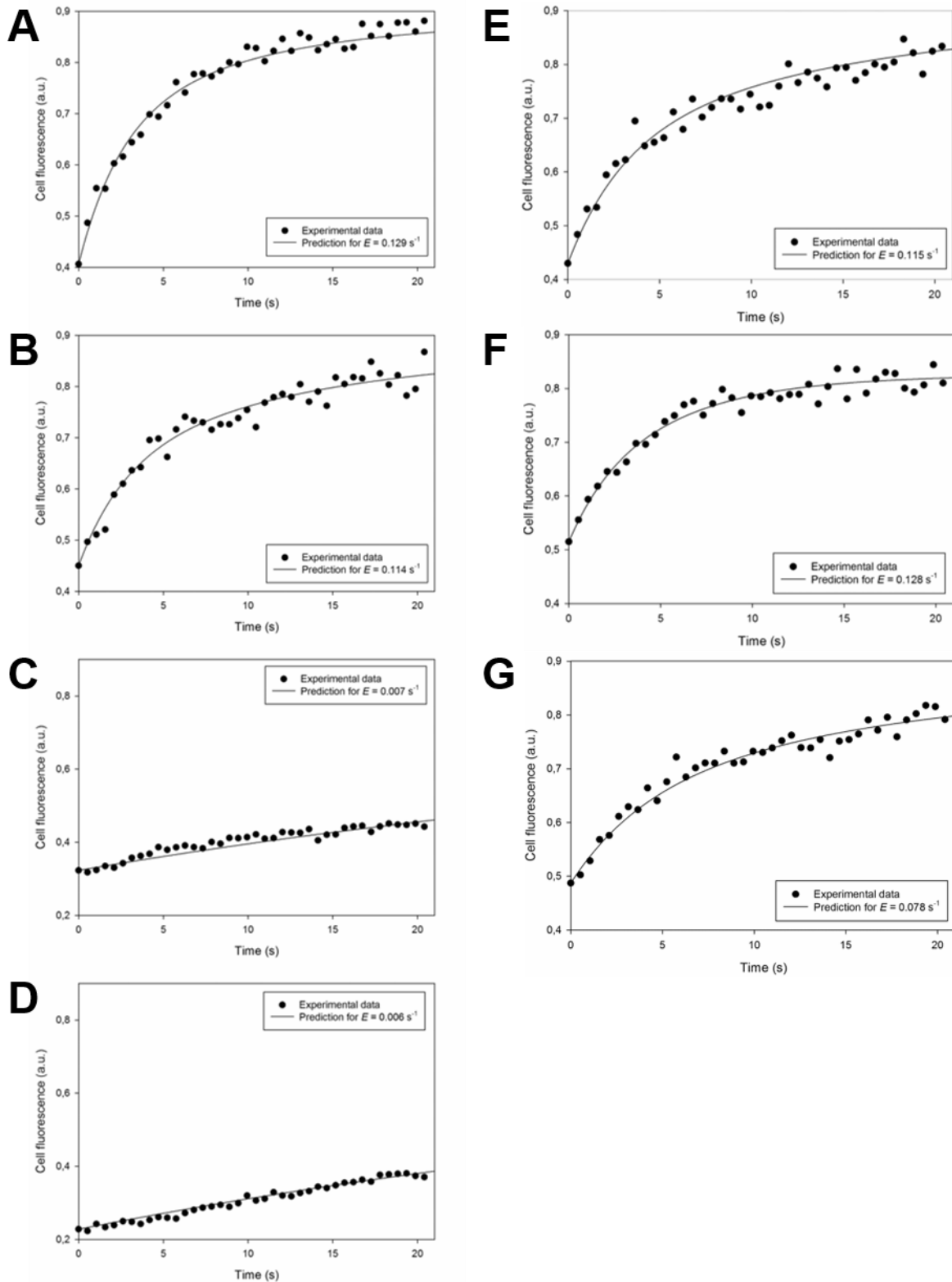


Fig. S50: Fluorescence recovery for representative bleached cells

Fluorescence recovery curves for selected bleached cells of *Anabaena* wt grown in (A) liquid BG11, (B) liquid BG11-0 or on (E) BG11 plate and $\Delta all2460$ grown in (C) liquid BG11 or (D) liquid BG11-0 as well as (F) $\Delta alr4504\Delta alr4505$ and (G) $\Delta alr0931$ grown on BG11 plates. Fluorescence values are given in arbitrary units (a.u.) over a time course of 20 s post bleaching.

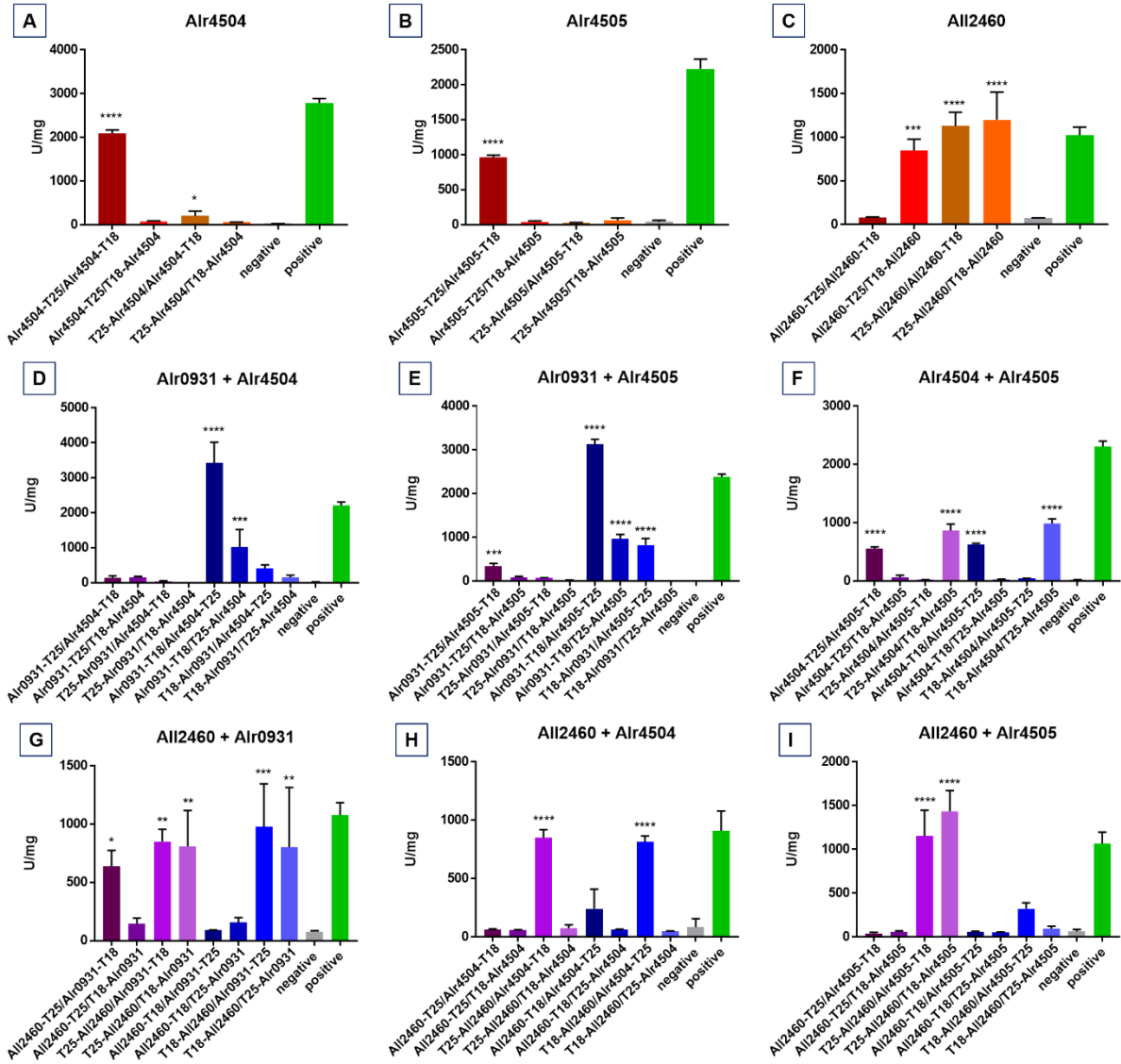


Fig. S51: Network-forming CCRPs self-interact and cross-interact

Beta-galactosidase assays of *E. coli* cells co-expressing indicated translational fusion constructs of all possible pairwise combinations of (A) A1r4504, (B) A1r4505, (C) A1l2460, (D) A1r0931+A1r4504, (E) A1r0931+A1r4505, (F) A1r4504+A1r4505, (G) A1l2460+A1r0931, (H) A1l2460+A1r4504 and (I) A1l2460+A1r4505. Cells were grown for 2 days at 20 °C. Quantity values are given in Miller Units per milligram LacZ of the mean results from three independent colonies. Error bars indicate standard deviations. Neg: pKNT25 plasmid carrying the respective gene insert co-transformed with empty pUT18C. Pos: Zip/Zip control. *: P < 0.05, **: P < 0.01, ***: P < 0.001, ****: P < 0.0001 (Dunnett's multiple comparison test and one-way ANOVA).

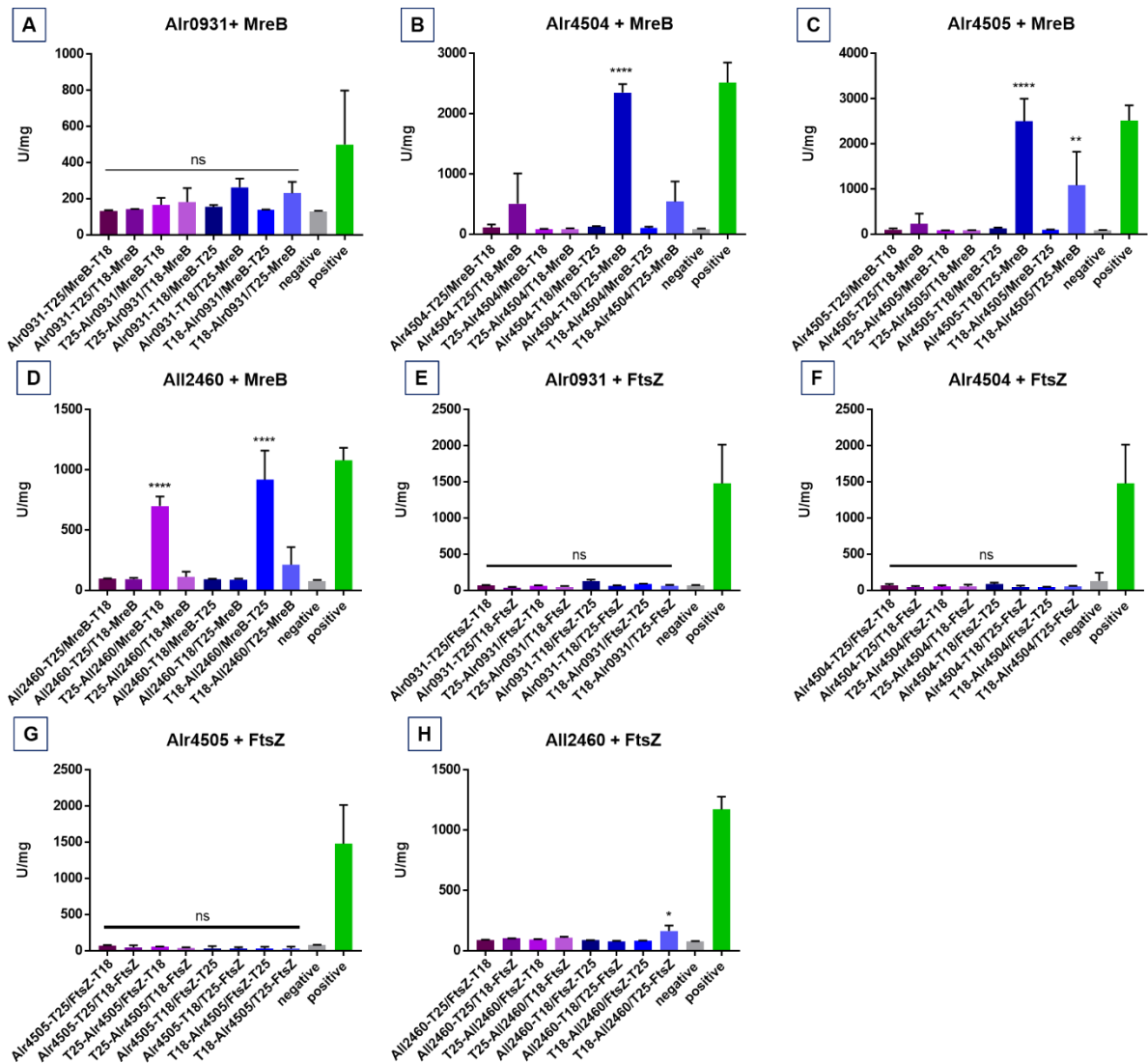


Fig. S52: Network-forming CCRPs interact with the MreB cytoskeleton

Beta-galactosidase assays of *E. coli* cells co-expressing indicated translational fusion constructs of all possible pairwise combinations of (A) Alr0931+FtsZ, (B) Alr4504+FtsZ, (C) Alr4505+FtsZ, (D) All2460+FtsZ, (E) Alr0931+MreB, (F) Alr4504+MreB, (G) Alr4505+MreB and (H) All2460+MreB. Cells were grown for 2 days at 20 °C. Quantity values are given in Miller Units per milligram LacZ of the mean results from three independent colonies. Error bars indicate standard deviations. Neg: pKNT25 plasmid carrying the respective gene insert co-transformed with empty pUT18C. Pos: Zip/Zip control. *: $P < 0.05$, **: $P < 0.01$, ***: $P < 0.001$, ****: $P < 0.0001$ (Dunnett's multiple comparison test and one-way ANOVA).

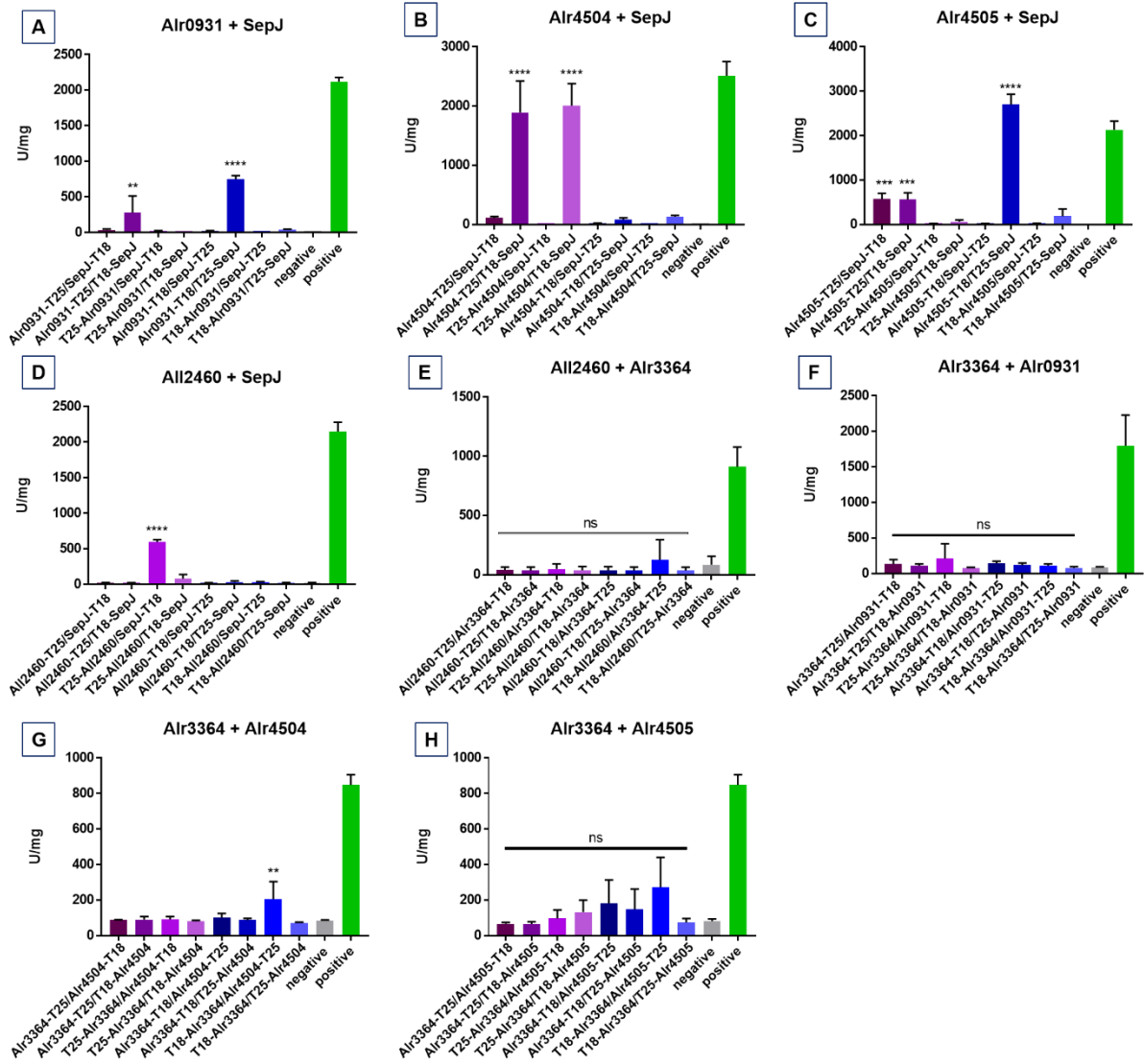


Fig. S53: Interactions of network-forming CCRPs with SepJ and Alr3364

Beta-galactosidase assays of *E. coli* cells co-expressing indicated translational fusion constructs of all possible pairwise combinations of (A) Alr0931+SepJ, (B) Alr4504+SepJ, (C) Alr4505+SepJ, (D) All2460+SepJ, (E) All2460+Alr3364, (F) Alr3364+Alr0931, (G) Alr3364+Alr4504 and (H) Alr3364+Alr4505. Cells were grown for 2 days at 20 °C. Quantity values are given in Miller Units per milligram LacZ of the mean results from three independent colonies. Error bars indicate standard deviations. Neg: pKNT25 plasmid carrying the respective gene insert co-transformed with empty pUT18C. Pos: Zip/Zip control. *: P < 0.05, **: P < 0.01, ***: P < 0.001, ****: P < 0.0001 (Dunnett's multiple comparison test and one-way ANOVA).

16 Supplementary tables – Oligonucleotides, plasmids and strains

Table 9: Chapter I oligonucleotides

Primer	Description	Sequence 5'-3'
P1	pET19bmod-Fwd	GGAATTGTGAGCGGATAACAATT
P2	T7R	CTAATACGACTCACTATAGGGA
P3	pAM2991_Seq_A	GCGCCGACATCATAACGGTTC
P4	pAM2991_Seq_B	GCTGAAAATCTTCTCTCATCCGCC
P5	pJET1.2 forward sequencing primer	CGACTCACTATAGGGAGAGCGGC
P6	pJET1.2 reverse sequencing primer	AAGAACATCGATTTTCCATGGCAG
P7	pKO_Seq_Fwd	GCCTTTTTACGGTTCCTGGC
P8	pKO_Seq_Rev	TCTTTTCTACGGGGTCTGACG
P9	pIGA_Seq_Fwd	TGCGCATAGAAATTGCATCA
P10	pIGA_Seq_Rev	GTCAGCAACACCTTCTTCA
P11	pRL271_Seq_Fwd	GCCTGGTGCTACGCCTGAATA
P12	pRL271_Seq_Rev	CCAGTTAATAGTTTGCGCAACGTTG
P13	pRL278_Seq_Fwd	GGGGCGTAATTTTTTTAAGGCAGTTATTG
P14	pSL2680_Seq_A	CAAGAGGGCAA AAAACTCAATTTG
P15	cpf1_1A	TTGGTCATGAGATTATCAAAAAGGATCCTGGAAAAC GTTCTTCGGGGC
P16	pRL25c_CRISPR_2 B	AGGCCCTTTTCGTCTTCAAGAATTCTTTACACTGATGA ATGTTCCGTTGCG
P17	cpf1-1	CTCCAGAAGCTATAAACTATGAAC
P18	cpf1-2	CTACTTCAAGCTAGTGCGGAA
P19	cpf1-3	GTTGAAAATCAAGGCTACAAACTAAC
P20	cpf1-4	CGTTTCAAGGTAGAGAAGCAGG
P21	pRL25c_Seq_Fwd	CTTTGATCTTTTCTACGGGGTCT
P22	pRL25c_Seq_Rev	TTGAGGTGAGGGATGAGCG
P23	pMAL_Seq_Fwd	AGAAAGGTGAAATCATGCCG
P24	pMAL_Seq_Rev	CTGCAAGGCGATTAAGTTGG
P25	MB_Seq_A	GGCTCGTATGTTGTGTGG
P26	MB_Seq_B	GGCTTAACTATGCGGCATC
P27	MB_Seq_C	TAACGCCAGGGTTTTCCA
P28	pKNT25_Seq_Rev	CGTTTGCGTAACCAGCC
P29	pKT25_Seq_Fwd	GATTCGGTGACCGATTACCTG
P30	pUT18_Seq_Rev	GATGCGTTCGCGATCCAG
P31	pUT18C_Seq_Fwd	TCGCCGGATGTA CTGGAAAAC
P32	N-term_1A	GAGGATCCCCGGGTACC
P33	N-term_1B	TAGAGTCGACCTGCAGGCA
P34	pKT25_1A	CCCCGGGTACCTAAGTAAGTAAG
P35	pKT25_1B	ATCCTCTAGAGTCGACCCTGC
P36	pUT18C_1A	CCGAGCTCGAATTCATCGAT
P37	pUT18C_1B	TACCCGGGGATCCTCTAGAGT
P38	pET21a_1A	CACCACCACCACCACCAC
P39	pET21a_1B	ATGTATATCTCCTTCTTAAAGTTAAACAAAATTATTTCTAGAGG
P40	pRL271_Fwd	GAGCTCGCGAAAGCTTG CATG
P41	pRL271_Rev	CTCGAGATCTAGATATCGAATTTCTGCCAT
P42	pRL278_Rev	CCGCTTATTATCACTTATTCAGGCG

Supplementary tables – Oligonucleotides, plasmids and strains

P77	Fragment 4.REV	CCCTGCAGGTCGAGGAATTCGCTGTCTCGAAGTTGAAC ATCAGTAAGC
P78	7001_TrbcL_2B	CCGACAATCCAAACACCGGTTTCAGACTAAGGCAGTC ATTAATAGTGAAG
P79	pRL25c-903_V_F	TGGATGAACTATACAAATAAAGAATTCTTGAAGACGA AAGGGCC
P80	pRL25c-903_V_R	GCAAAAAATTCTGAGTACTGGGATCCTTTTTGATAAT CTCATGACCAAAATCC
P81	petE_903_Fwd	GAGATTATCAAAAAGGATCCCAGTACTCAGAATTTTT TGCTGAGGACT
P82	petE_903_Rev	TTGAGTGCAACTGTCGTCATGGCGTTCTCCTAACCT GTAGTTTTATTTTT
P83	pRL25-Nos903_Fwd	CTACAGGTTAGGAGAACGCCATGACGACAGTTGCAC TCAAAGATAG
P84	pRL25-Nos903_Rev	GCACTAGCAGATGCACTAGCTTTAGCCGTAGAACTA TCAAAGCTCTCATTGC
P85	GFP_903_Fwd	TTGATAGTTCTACGGCTAAAGCTAGTGCATCTGCTA GTGCTAGT
P86	GFP_903_Rev	CTTTCGTCTTCAAGAATTCTTTATTTGTATAGTTCATC CATGCCATGTGTAATCC
P87	7001F_BamHI	ACTGGATCCAGGGAAAATACGAAAACATTGGA
P88	7001R_NotI	AGCGGCCGCTCAGACTAAGGCAGTCATTAATAGTG
P89	7001F_KpnI_C	ACTGGTACCATGAGGGAAAATACGAAAAC
P90	7001F_KpnI_N	ACTGGTACCAGGGAAAATACGAAAACAT
P91	7001R_EcoRI_N	AGCGAATTCTCAGACTAAGGCAGTCAT
P92	7001F_NheI	AACTGCTAGCAGGGAAAATACGAAAAC
P93	7001_3A	CTCTGGATCGGGTTCAGGAATGAGGGAAAATACGAA AAACATTGG
P94	7001_3B	CTTTTCGTCTTCAAGAATTCTTCAGACTAAGGCAGTC ATTAATAGTG
P95	7001_intern_A	AGCGGGAAGATGGCTACTATC
P96	7001_northern	TCTGCGGCTTGACTTGATAC
P97	pRL271_7up_F	AGAAATTCGATATCTAGATCTCGAGAGCAATGTGAG TGAGTTCGTGAGC
P98	pRL271_7down_R	CAGGCATGCAAGCTTTCGCGAGCTCTGCTACCAAGA CGATGCGTTTCATGTC
P99	7001KO_1A	CCCCTGATTCTGTGGATAACCGTAAGCAATGTGAGT GAGTTCGTGAG
P100	7001KO_1B	GTGCTTGCGGCAGCGTGAAGCTTGGGGTTATCCTTA ATAGAAGAAGAGTGC
P101	7001KO_2A	CGCCTTCTTGACGAGTTCTTCTGAATCAAGAGCATT TTGATTTCTGTCTCA
P102	7001KO_2B	GATTATCAAAAAGGATCTTCACCTTGCTACCAAGACG ATGCGTTTC
P103	7001KO_2A2	AATTCGATATCTAGATCTCGAGTTGCGTTTCAAACA CTACAAATTAGTACAAAC
P104	7001KO_2B2	AAGGTGCTGTGCACGGATCGGGTATCCTTAATAG AAGAAGAGTGC
P105	7001KO_4A2	CAAGGTAGTCGGCAAATAAATCAAGAGCATTCTTGA TTTCTGTCTC
P106	7001KO_4B2	TGCAAGCTTTCGCGAGCTCCTGAAGACAAAGATGAA GTTTCGATATTACC
P107	trunc7001_2A	CTGAATAAGTGATAATAAGCGGTTGCGTTTCAAACA CTACAAATTAGTACAAA

Supplementary tables – Oligonucleotides, plasmids and strains

P139	Syc484_2A2	TACAGGTTAGGAGAACGCCATGAACTACGCTCTTAC CCAAG
P140	Syc484_2B2	CACTAGCAGATGCACTAGCAGACCCTAACCAGCGG C
P141	Syc484_pAM2991_2 A	CACACAGGAAACAGACCATGAACTACGCTCTTACCC AAGC
P142	Syc484_KO_2A	TGTAGGAGATCTTCTAGAAAGATGTAGGCATCAAAG GCAGGC
P143	Syc484_KO_2B	CTTGCGGCAGCGTGAAGCTTAGCAAAGCAAAGAAG CGATCG
P144	Syc484_KO_4A	TTCTTGACGAGTTCTTCTGATTCTGCTGCGATGCGTT AGG
P145	Syc484_KO_4B	CTCGAGTTTTTCAGCAAGATCAAGTAAGACTGGCTG CCATG
P146	Syc484_Seq_A	GATGCCACCGAGCAGAATTAG
P147	Syc484_Seq_B	GGCAGATCAATCAGCAGCTC
P148	Syc484_intern_A	CTACCATTCTTGGTGTGGCGG
P149	Syc484_intern_B	GAAATCCTGCGATCGCTGTTG
P150	Nos389_pET_2A	GTTTAACTTTAAGAAGGAGATATACATATGAATAGTG AGTTGTTCCAGAAGC
P151	Nos389_NdeI_F	GCTACATATGAATAGTGAGTTGTTCCAGAAG
P152	Nos389_XhoI_wo_R	GCTACTCGAGGATGTTACTATCACTACTTTGAATTTT T
P153	Nos389_2A	CTACAGGTTAGGAGAACGCCATGAATAGTGAGTTGT TCCAGAAGCTAGC
P154	Nos389_2B	GCACTAGCAGATGCACTAGCGATGTTACTATCACTA CTTTGAATTTTTTTGAGTTTGCC
P155	Nos389_3A	CTCTGGATCGGGTTCAGGAATGAATAGTGAGTTGTT CCAGAAGC
P156	Nos389_3B	CCTTTCGTCTTCAAGAATTCTTTAGATGTTACTATCA CTACTTTGAATTTTTTTGAG
P157	Nos389_pIGA_2A	TAAAGTCAAGTAGGAGATTAATTCAATGAATAGTGAG TTGTTCCAGAAGC
P158	Nos389_TrbcL_2B	CCGACAATCCAAACACCGGTTTAGATGTTACTATCAC TACTTTGAATTTTTTTGAGTTTG
P159	389KO_2A	ATTCGATATCTAGATCTCGAGTGTCAGATTTAGTACT TTAAATACAAGACTTACACAC
P160	389KO_2B	CAAGGTGCTGTGCACGGATCAGCTGTTTCGCTCTTGA GGG
P161	389KO_4A	CCAAGGTAGTCGGCAAATAAAGTAACGCGATGTGCG ACT
P162	389KO_4B	ATGCAAGCTTTTCGCGAGCTCGATTAATACCTTTGGT GTTTCATGACACTGG
P163	trunc389_2A	CTGAATAAGTGATAATAAGCGGAAGCCATTTTAGATC GAGAGGCG
P164	trunc389_2B	TGCAAGCTTTTCGCGAGCTCGCTAAATTCCAAAACCTC ACTGCCTT
P165	Nos389_gRNA-A	AGATCAGAAGCTAGCAAAGCACA
P166	Nos389_gRNA-B	AGACTGTGCTTTTGCTAGCTTCTG
P167	Nos389_HL1A	TTTGTCTAGCTTTAATGCGGTAGTTGGTACCGTGTG GGGTAATTTGCGGG
P168	Nos389_HL1B	ATAAGTCGCACATCGCGTTACTTCATAGCTGTTTCGCT CTTGAGG

Supplementary tables – Oligonucleotides, plasmids and strains

P169	Nos389_HR2A	CCTCAAGAGCGAACAGCTATGAAGTAACGCGATGTG CGACTTATTC
P170	Nos389_HR2B	GGATTACAGATCCTCTAGAGTCGACGGTACCGGACA CCACCAGCCATTTTC
P171	Nos389_intern_A	ATCACCTGAATTAGCTGCGG
P172	Nos389_intern_B	CTAATAATGCCGCAATCAGCG
P173	Nos752_NdeI_F	GCTACATATGGGTGGTTCAAGAGTGAT
P174	Nos752_XhoI_wo_R	GCTACTCGAGTTGACCATTAGGCTTGTGAAAATT
P175	Nos752_pET_2A	TGTTTAACTTTAAGAAGGAGATATACATATGGGTGGT TCAAGAGTGATGAATG
P176	Nos752_GFP_2B	ACTAGCACTAGCAGATGCACTAGCTTGACCATTAGG CTTGTGAAAATTTCG
P177	Nos752_2A	TAAAACACTACAGGTTAGGAGAACGCCGTGGGTGGTTC AAGAGTGATGAATG
P178	Nos752_intern_A	ATGGCGAAAAGCAAGCACAG
P179	Nos752_intern_B	GTCGTTTGGACGGCAGTTTC
P180	7001F_BamHI	GGATCCTATGAGGGAAAATACGAAAAAC
P181	7001R_EcoRI	AGCGAATTCTCAGACTAAGGCAGTCAT
P182	7001R_SacI	GAGCTCCTGACTAAGGCAGTCATTA
P183	MB_1A	TGCCTGCAGGTGCGACTCTAATGAATAGTGAGTTGTT CCAGAAGC
P184	MB_1B	TCGGTACCCGGGGATCCTCGATGTTACTATCACTAC TTTGAATTTTTTTGAGT
P185	MB_2A	AGGGTGCAGTCTAGAGGATATGAATAGTGAGTTGTT CCAGAAGC
P186	MB_2B	CTTACTTAGGTACCCGGGGGATGTTACTATCACTAC TTTGAATTTTTTTGAGT
P187	MB_4A	TCTAGAGGATCCCCGGGTAATGAATAGTGAGTTGTT CCAGAAGC
P188	MB_4B	TCGATGAATTGAGCTCGGGATGTTACTATCACTACT TTGAATTTTTTTGAGT
P189	MB_13A	TGCCTGCAGGTGCGACTCTAATGACAAGTCAAATTTT GTTTCTGATCAAG
P190	MB_13B	TCGGTACCCGGGGATCCTCTGGTAAATAAGGGGGA GTGGGAC
P191	MB_14A	AGGGTGCAGTCTAGAGGATATGACAAGTCAAATTT TGTTTCTGATCAAG
P192	MB_14B	CTTACTTAGGTACCCGGGGTGGTAAATAAGGGGGA GTGGGAC
P193	MB_16A	TCTAGAGGATCCCCGGGTAATGACAAGTCAAATTT TGTTTCTGATCAAG
P194	MB_16B	TCGATGAATTGAGCTCGGTGGTAAATAAGGGGGAG TGGGAC
P195	MB_45A	TGCCTGCAGGTGCGACTCTAATGAACTACGCTCTTAC CCAAG
P196	MB_45B	TCGGTACCCGGGGATCCTCAGACCCTAACCAGCGG C
P197	MB_46A	AGGGTGCAGTCTAGAGGATATGAACTACGCTCTTAC CCAAG
P198	MB_46B	CTTACTTAGGTACCCGGGGAGACCCTAACCAGCGG C
P199	MB_48A	TCTAGAGGATCCCCGGGTAATGAACTACGCTCTTAC CCAAG

P200	MB_48B	TCGATGAATTCGAGCTCGGAGACCCTAACCCAGCGG C
P201	MB_49A	ATGCCTGCAGGTCGACTCTAATGACACTTGATAATAA CCAAGAGCTTACC
P202	MB_49B	CTCGGTACCCGGGGATCCTCATTITTTGGGTGGTTCG CGTC
P203	MB_50A	CAGGGTCGACTCTAGAGGATATGACACTTGATAATA ACCAAGAGCTTACC
P204	MB_50B	TACTTACTTAGGTACCCGGGGATTITTTGGGTGGTTCG CCGTC
P205	MB_52A	CTCTAGAGGATCCCCGGGTAATGACACTTGATAATA ACCAAGAGCTTACC
P206	MB_52B	TATATCGATGAATTCGAGCTCGGATTITTTGGGTGGT CGCCGTC
P207	MB_53A	ATGCCTGCAGGTCGACTCTAATGGGGCTITTTAGGA ACTTTTCG
P208	MB_53B	CTCGGTACCCGGGGATCCTCCATITTTGAGATCGT CCGCTAAAAAC
P209	MB_54A	CAGGGTCGACTCTAGAGGATATGGGGCTITTTAGGA ACTTTTCG
P210	MB_54B	TACTTACTTAGGTACCCGGGGCATITTTGAGATCG TCCGCTAAAAAC
P211	MB_56A	CTCTAGAGGATCCCCGGGTAATGGGGCTITTTAGGA ACTTTTCG
P212	MB_56B	TATATCGATGAATTCGAGCTCGGCATITTTGAGATC GTCCGCTAAAAAC
P213	MB_65A	GCTTGCATGCCTGCAGGTCGACTCTAATGGGTGGTT CAAGAGTGATG
P214	MB_65B	GAGCTCGGTACCCGGGGATCCTCTTGACCATTAGG CTTGTGAAAATTTCG
P215	MB_66A	GCTGCAGGGTCGACTCTAGAGGATATGGGTGGTTC AAGAGTGATGA
P216	MB_66B	TTACTTACTTAGGTACCCGGGGTTGACCATTAGGCT TGTGAAAATTTCG
P217	MB_68A	GTCGACTCTAGAGGATCCCCGGGTAATGGGTGGTT CAAGAGTGATGAA
P218	MB_68B	TATATCGATGAATTCGAGCTCGGTTGACCATTAGGC TTGTGAAAATTTCG

Table 10: Chapter I bacterial strains and plasmids

Strain	Description	Reference
<i>Fischerella muscicola</i> PCC 7414	wt	Pasteur culture collection of cyanobacteria (PCC), France
BLS1	<i>PpetE-fm7001-gfp</i> , wt harboring pTHS19, Km ^R , Nm ^R	This study
BLS2	<i>PpetE-yfp-fm7001</i> , wt harboring pTHS20, Km ^R , Nm ^R	This study
<i>Synechocystis</i> sp. PCC 6803	Glucose tolerant Kazusa substrain wt	PCC, France

Supplementary tables – Oligonucleotides, plasmids and strains

BLS3	$\Omega_{pta}::P_{cpc560-yfp^1}-fm7001$, Km ^R	This study
BLS4	$\Omega_{pta}::P_{cpc560-fm7001-gfp^2}$, Km ^R	This study
BLS5	$\Omega_{pta}::P_{cpc560-sl7083-gfp}$, Km ^R	This study
BLS6	$\Omega_{pta}::P_{cpc560-synpcc7942_2039-gfp-his}$, Km ^R	This study
BLS7	$\Omega_{pta}::P_{cpc560-all4981-gfp}$, Km ^R	This study
BLS8	$\Delta_{slr7083}::Km^R$	This study
<i>Synechocystis</i> sp. PCC-M 6803	Glucose tolerant and motile Moscow PCC-M substrain wt	A gift from Annegret Wilde (University of Freiburg)
BLS9	$\Delta_{slr7083}::Km^R$	This study
<i>Synechococcus</i> <i>elongatus</i> PCC 7942	wt	A gift from Martin Hagemann (Uni Rostock)
BLS10	$\Delta_{synpcc7942_2039}::Km^R$	This study
BLS11	$\Omega_{synpcc7942_2498(NS1)}::lacI-$ $synpcc7942_2039-gfp$, Sm ^R , Sp ^R	This study
<i>Anabaena</i> sp. PCC 7120	WT	PCC, France
BLS12	$P_{petE-fm7001-gfp}$, wt harboring pTHS19, Km ^R , Nm ^R	This study
BLS13	$P_{petE-yfp-fm7001}$, wt harboring pTHS20, Km ^R , Nm ^R	This study
BLS14	$P_{petE-yfp-sl7083}$, wt harboring pTHS21, Km ^R , Nm ^R	This study
BLS15	$P_{petE-sl7083-gfp}$, wt harboring pTHS22, Km ^R , Nm ^R	This study
BLS16	$P_{petE-synpcc7942_2039-gfp}$, wt harboring pTHS23, Km ^R , Nm ^R	This study
BLS17	$P_{petE-yfp-all4981}$, wt harboring pTHS24, Km ^R , Nm ^R	This study
BLS18	$P_{petE-all4981-gfp}$, wt harboring pTHS25, Km ^R , Nm ^R	This study
BLS19	$P_{petE-als3364-gfp}$, wt harboring pTHS26, Km ^R , Nm ^R	This study
<i>E. coli</i> DH5 α	Cloning and expression strain	Meselson and Yuan (1968)
<i>E. coli</i> DH5 α MCR + pRL623	Methylation and Conjugation strain	Elhai <i>et al.</i> , 1997
<i>E. coli</i> XL1-blue	Cloning strain	Stratagene
<i>E. coli</i> BTH101	Expression strain for bacterial two-hybrid assay	Euromedex
<i>E. coli</i> BL21 (DE3)	Expression strain	Studier and Moffatt (1986)
Plasmids	Description	Reference
pJET1.2/blunt	<i>E. coli</i> subcloning vector, Amp ^R	Thermo Scientific
pETM-22	Bacterial vector for expressing N-terminal <i>trxA</i> (<i>E. coli</i>) and/or C/N-terminal His6-tagged translational fusion proteins in <i>E. coli</i> with a HRV 3C site, Km ^R	A gift from Axel Scheidig (Uni Kiel), created by Arie Geerlof
pMAL-c2x	Bacterial vector for expressing N-terminal MBP- tagged proteins in <i>E. coli</i> with a Factor Xa cleavage site, Amp ^R	A gift from Axel Scheidig (Uni Kiel); NEB

Supplementary tables – Oligonucleotides, plasmids and strains

pet21a(+)	Bacterial vector for expressing C-terminal His6-tagged proteins in <i>E. coli</i> , Amp ^R	Novagen
pRL25C	Shuttle cosmid vector for cyanobacteria and <i>E. coli</i> , Km ^R , Nm ^R	Wolk <i>et al.</i> , 1988
pRL623	Methylation plasmid, Cm ^R	Wolk <i>et al.</i> , 1988
pRL443	Conjugation plasmid, Amp ^R	Wolk <i>et al.</i> , 1988
pRL271	<i>sacB</i> containing plasmid to select for double homologous recombination in <i>Anabaena</i> ; Cm ^R	Wolk <i>et al.</i> , 1990
pRL278	<i>sacB</i> containing plasmid to select for double homologous recombination in <i>Anabaena</i> ; Km ^R	Wolk <i>et al.</i> , 1990
pSL2680	Cpf1-mediated CRISPR editing plasmid, Km ^R , Nm ^R	Ungerer and Pakrasi, 2016
pRL25c-CRISPR	Functional CRISPR cassette from pSL2680 transferred into EcoRI and BamHI digested pRL25c by GIBSON assembly, Km ^R , Nm ^R	This work
pSM2-Pcpc560ter	pMD18-T derivate for insertion into <i>pta</i> open reading frame containing <i>Pcpc560-ter-Trbcl</i> expression cassette, Amp ^R , Km ^R	A gift from Yin Li (Chinese Academy of Science). Zhou <i>et al.</i> 2014
pIGA	Cyanobacterial vector for insertion into neutral locus (RS1 and RS2) of <i>slr0168</i> in <i>Synechocystis</i> , Amp ^R	A gift from Martin Hagemann (Uni Rostock), Kunert <i>et al.</i> 2000
pKNT25	Bacterial vector for expressing chimeric translational fusion proteins with the N-terminal T25 subunit of the <i>B. pertussis</i> adenylate cyclase under the control of the lac promoter, Nm ^R , Km ^R	Euromedex
pKT25	Bacterial vector for expressing chimeric translational fusion proteins with the C-terminal T25 subunit of the <i>B. pertussis</i> adenylate cyclase under the control of the lac promoter, Nm ^R , Km ^R	Euromedex
pUT18	Bacterial vector for expressing chimeric translational fusion proteins with the N-terminal T18 subunit of the <i>B. pertussis</i> adenylate cyclase under the control of the lac promoter, Amp ^R	Euromedex
pUT18C	Bacterial vector for expressing chimeric translational fusion proteins with the C-terminal T18 subunit of the <i>B. pertussis</i> adenylate cyclase under the control of the lac promoter, Amp ^R	Euromedex
pKT25-zip	pKT25 with the leucine zipper of GCN4 inserted into the KpnI site, Nm ^R , Km ^R	Euromedex
pUT18C-zip	pUT18C with the leucine zipper of GCN4 inserted into the KpnI and EcoRI site, Amp ^R	Euromedex
pAM2991	Cyanobacterial vector for expressing proteins under the control of the <i>trc</i> promoter that inserts into the NS1 site of <i>Synechococcus</i> , Sm ^R , Sp ^R	A gift from Susan Golden (Addgene plasmid # 40248)
pTHS1	pIGA carrying <i>Pcpc560-fm7001-gfp-Trbcl</i> created by GIBSON assembly, Amp ^R , Km ^R	This study
pTHS2	pRL25C-based vector carrying <i>PpetE-als4504-gfp</i> created by GIBSON assembly, Nm ^R , Km ^R	This study

Supplementary tables – Oligonucleotides, plasmids and strains

pTHS3	pET21a(+) with <i>slr7083</i> inserted between the NdeI and XhoI sites, Amp ^R	This study
pTHS4	pET21a(+) with <i>synpcc7942_2039</i> inserted by GIBSON assembly, Amp ^R	This study
pTHS5	pET21a(+) with <i>fm7001</i> inserted between the BamHI and NotI sites, Amp ^R	This study
pTHS6	pET21a(+) with <i>all4981</i> inserted between the NdeI and XhoI sites, Amp ^R	This study
pTHS7	pET21a(+) with <i>alr3364</i> inserted between the NdeI and XhoI sites, Amp ^R	This study
pTHS8	pET21a(+) with <i>slr7083-gfp</i> inserted by GIBSON assembly, Amp ^R	This study
pTHS9	pET21a(+) with <i>fm7001-gfp</i> inserted between the BamHI and EcoRI sites, Amp ^R	This study
pTHS10	pET21a(+) with <i>synpcc7942_2039-gfp</i> inserted by GIBSON assembly, Amp ^R	This study
pTHS11	pET21a(+) with <i>all4981-gfp</i> inserted by GIBSON assembly, Amp ^R	This study
pTHS12	pET21a(+) with <i>alr3364-gfp</i> inserted by GIBSON assembly, Amp ^R	This study
pTHS13	pMAL-c2x with <i>fm7001-6His</i> inserted between the EcoRI and PstI sites, Amp ^R	This study
pTHS14	pTSH1 with <i>fm7001-gfp</i> replaced with <i>yfp-fm7001</i> by GIBSON assembly, Amp ^R , Km ^R	This study
pTHS15	pTSH1 with <i>fm7001</i> replaced with <i>slr708</i> by GIBSON assembly, Amp ^R , Km ^R	This study
pTHS16	pTSH1 with <i>fm7001-gfp</i> replaced with <i>yfp-all4981</i> by GIBSON assembly, Amp ^R , Km ^R	This study
pTHS17	pTSH1 with <i>fm7001</i> replaced with <i>all4981</i> by GIBSON assembly, Amp ^R , Km ^R	This study
pTHS18	pTSH1 with <i>fm7001</i> replaced with <i>synpcc7942_2039</i> by GIBSON assembly, Amp ^R , Km ^R	This study
pTHS19	pRL25C with P <i>petE-fm7001-gfp</i> inserted between the BamHI and EcoRI sites, Nm ^R , Km ^R	This study
pTHS20	pTHS2 with <i>alr4504-gfp</i> replaced with <i>yfp-fm7001</i> by GIBSON assembly, Nm ^R , Km ^R	This study
pTHS21	pTHS2 with <i>alr4504-gfp</i> replaced with <i>yfp-slr7083</i> by GIBSON assembly, Nm ^R , Km ^R	This study
pTHS22	pTHS2 with <i>alr4504</i> replaced with <i>slr7083</i> by GIBSON assembly, Nm ^R , Km ^R	This study
pTHS23	pTHS2 with <i>alr4504</i> replaced with <i>synpcc7942_2039</i> by GIBSON assembly, Nm ^R , Km ^R	This study
pTHS24	pTHS2 with <i>alr4504-gfp</i> replaced with <i>yfp-all4981</i> by GIBSON assembly, Nm ^R , Km ^R	This study
pTHS25	pTHS2 with <i>alr4504</i> replaced with <i>all4981</i> by GIBSON assembly, Nm ^R , Km ^R	This study
pTHS26	pTHS2 with <i>alr4504</i> replaced with <i>alr3364</i> by GIBSON assembly, Nm ^R , Km ^R	This study
pTHS27	pETM-22 with <i>synpcc7942_2039</i> inserted by GIBSON assembly, Km ^R	This study
pTHS28	pRL25C with P <i>petE-creS-gfp</i> inserted between the BamHI and EcoRI sites, Nm ^R , Km ^R	This study

Supplementary tables – Oligonucleotides, plasmids and strains

pTHS29	pKNT25 with <i>fm7001</i> inserted between BamHI and SacI sites, Nm ^R , Km ^R	This study
pTHS30	pKT25 with <i>fm7001</i> inserted between BamHI and EcoRI sites, Nm ^R , Km ^R	This study
pTHS31	pUT18 with <i>fm7001</i> inserted between BamHI and SacI sites, Amp ^R	This study
pTHS32	pUT18C with <i>fm7001</i> inserted between BamHI and EcoRI sites, Amp ^R	This study
pTHS33	pKNT25 with <i>slr7083</i> inserted by GIBSON assembly, Nm ^R , Km ^R	This study
pTHS34	pKT25 with <i>slr7083</i> inserted by GIBSON assembly, Nm ^R , Km ^R	This study
pTHS35	pUT18 with <i>slr7083</i> inserted by GIBSON assembly, Amp ^R	This study
pTHS36	pUT18C with <i>slr7083</i> inserted by GIBSON assembly, Amp ^R	This study
pTHS37	pKNT25 with <i>synpcc7942_2039</i> inserted by GIBSON assembly, Nm ^R , Km ^R	This study
pTHS38	pKT25 with <i>synpcc7942_2039</i> inserted by GIBSON assembly, Nm ^R , Km ^R	This study
pTHS39	pUT18 with <i>synpcc7942_2039</i> inserted by GIBSON assembly, Amp ^R	This study
pTHS40	pUT18C with <i>synpcc7942_2039</i> inserted by GIBSON assembly, Amp ^R	This study
pTHS41	pKNT25 with <i>all4981</i> inserted by GIBSON assembly, Nm ^R , Km ^R	This study
pTHS42	pKT25 with <i>all4981</i> inserted by GIBSON assembly, Nm ^R , Km ^R	This study
pTHS43	pUT18 with <i>all4981</i> inserted by GIBSON assembly, Amp ^R	This study
pTHS44	pUT18C with <i>all4981</i> inserted by GIBSON assembly, Amp ^R	This study
pTHS45	pKNT25 with <i>alr3364</i> inserted by GIBSON assembly, Nm ^R , Km ^R	This study
pTHS46	pKT25 with <i>alr3364</i> inserted by GIBSON assembly, Nm ^R , Km ^R	This study
pTHS47	pUT18 with <i>alr3364</i> inserted by GIBSON assembly, Amp ^R	This study
pTHS48	pUT18C with <i>alr3364</i> inserted by GIBSON assembly, Amp ^R	This study
pTHS49	pKNT25 with <i>alr3858</i> inserted by GIBSON assembly, Nm ^R , Km ^R	This study
pTHS50	pKT25 with <i>alr3858</i> inserted by GIBSON assembly, Nm ^R , Km ^R	This study
pTHS51	pUT18 with <i>alr3858</i> inserted by GIBSON assembly, Amp ^R	This study
pTHS52	pUT18C with <i>alr3858</i> inserted by GIBSON assembly, Amp ^R	This study
pTHS53	pKNT25 with <i>all0087</i> inserted by GIBSON assembly, Nm ^R , Km ^R	This study
pTHS54	pKT25 with <i>all0087</i> inserted by GIBSON assembly, Nm ^R , Km ^R	This study
pTHS55	pUT18 with <i>all0087</i> inserted by GIBSON assembly, Amp ^R	This study

pTHS56	pUT18C with <i>all0087</i> inserted by GIBSON assembly, Amp ^R	This study
pTHS57	pAM2991 with <i>synpcc7942_2039-gfp</i> inserted by GIBSON assembly, Sm ^R , Sp ^R	This study
pTHS58	pJET1.2/blunt with ~1000 bp upstream and downstream of <i>synpcc7942_2039</i> flanking <i>nptII</i> inserted by GIBSON assembly, Amp ^R , Km ^R	This study
pTHS59	Circularized puC ori with 1000 bp upstream and downstream of <i>slr7083</i> flanking <i>nptII</i> assembled by GIBSON assembly, Nm ^R , Km ^R	This study
pTHS60	pSL2680 with <i>fm7001</i> gRNA and homologous repair templates 1000 bp upstream and downstream of <i>fm7001</i> , Nm ^R , Km ^R	This study
pTHS61	pRL25c-CRISPR with <i>fm7001</i> gRNA and homologous repair templates 1000 bp upstream and downstream of <i>fm7001</i> , Nm ^R , Km ^R	This study
pTHS62	pSL2680 with <i>all4981</i> gRNA and homologous repair templates 1000 bp upstream and downstream of <i>all4981</i> , Nm ^R , Km ^R	This study
pTHS63	pRL25c-CRISPR with <i>all4981</i> gRNA and homologous repair templates 1000 bp upstream and downstream of <i>all4981</i> , Nm ^R , Km ^R	This study
pTHS64	pRL271 containing 2000 bp upstream and downstream of <i>fm7001</i> flanking <i>nptII</i> assembled by GIBSON assembly, Nm ^R , Km ^R , Cm ^R	This study
pTHS65	pRL278 containing 2000 bp upstream and downstream of <i>fm7001</i> flanking <i>aadA</i> assembled by GIBSON assembly, Nm ^R , Km ^R , Sm ^R , Sp ^R	This study
pTHS66	pRL278 containing 2000 bp upstream of <i>fm7001</i> and the first 398 bp of <i>fm7001</i> , Nm ^R , Km ^R	This study
pTHS67	pRL278 containing 1000 bp upstream and downstream of <i>all4981</i> flanking <i>aadA</i> assembled by GIBSON assembly, Nm ^R , Km ^R , Sm ^R , Sp ^R	This study
pTHS68	pRL278 containing 151 bp upstream of <i>all4981</i> and the first 449 bp of <i>all4981</i> , Nm ^R , Km ^R	This study

Table 11: Chapter II oligonucleotides

Primer	Description	Sequence 5'-3'
P219	pET19bmod-Fwd	GGAATTGTGAGCGGATAACAATT
P220	T7R	CTAATACGACTCACTATAGGGA
P221	pRL25c_Seq_Fwd	CTTTGATCTTTTCTACGGGGTCT
P222	pRL25c_Seq_Rev	TTGAGGTGAGGGATGAGCG
P223	pRL153_Seq_Rev	AGGAGATTAACCCGCCCAAG
P224	pAM2991_Seq_A	GCGCCGACATCATAACGGTTC
P225	pAM2991_Seq_B	GCTGAAAATCTTCTCTCATCCGCC
P226	pRL271_Seq_Fwd	GCCTGGTGCTACGCCTGAATA
P227	pRL271_Seq_Rev	CCAGTTAATAGTTTGCGCAACGTTG
P228	CS3_Seq_Fwd	CGCGCAGATCAGTTGGAAG
P229	CS3_Seq_Rev	AACGTCGGTTCGAGATGGC
P230	GFP_Seq_Rev	TTGTGCCCATTAACATCACCATC

Supplementary tables – Oligonucleotides, plasmids and strains

P272	Syn708_pET_2A	GTTTAACTTTAAGAAGGAGATATACATATGCTCTATC TGGCTGAAATTAAGAAAC
P273	Syn708_pRL25c_Fw d	TAAACTACAGGTTAGGAGAACGCCATGCTCTATCT GGCTGAAATTAAGAAACAAAC
P274	Syn708_pRL25c_Re v	CACTAGCACTAGCAGATGCACTAGCACCGCCAAACA ATAGGGTCT
P275	Syn708_3A	CTCTGGATCGGGTTCAGGAGTGCTCTATCTGGCTGA AATTAAG
P276	Syn708_3B	CCTTTCGTCTTCAAGAATTCTCTAACCGCCAAACAAT AGGGTC
P277	153Syn708_2A	AGAATTAAGAGGAGAAATTAAGCATGCTCTATCTG GCTGAAATTAAGAAAC
P278	153Syn708_2B	TCAGAGATGAGTTTCTGCTCACCGCCAAACAATAGG GTC
P279	Syn708_pAM2991_ 2A	CACACAGGAAACAGACCATGCTCTATCTGGCTGAAA TTAAGAAAC
P280	Syn708_intern_A	TGGAGTGCCCTGCCTAACG
P281	Syn708_intern_B	CCCTTCTAACCTTTGTCTGGGC
P282	pJET708_2A	TGTAGGAGATCTTCTAGAAAGATAATAGACTGCAATG TCAAAAAACTCAG
P283	708KO_CS3_2B	CAAGGTGCTGTGCACGGATCAAGTCGTTGTCCTGAG CAG
P284	708KO_CS3_4A	CCAAGGTAGTCGGCAAATAATTGGGTTGGTTGCCGA C
P285	pJET708_4B	CTCGAGTTTTTCAGCAAGATTTAGCAAGGTGGGGGG AATG
P286	708KO_1Aa	CCTGATTCTGTGGATAACCGTACGTCAAATCGAATT CCCGGTC
P287	708KO_1B	TGCTTGCGGCAGCGTGAAGCTTAAGTCGTTGTCCTG AGCAGTG
P289	708KO_2A	CGCCTTCTTGACGAGTTCTTCTGATTGGGTTGGTTG CCGACTTC
P290	708KO_2B	GATTATCAAAAAGGATCTTCACCTTTAGCAAGGTGG GGGAATGC
P291	708GFP_Fwd	CCTCTGCAGGATCAGTTGGATG
P292	Nos295_NdeI_Fwd	GCTACATATGCTGTATTTAGCAGAAGTACAAA
P293	Nos295_XhoI_wo_R ev	GCTACTCGAGAGATGCCAACAACCTCAGG
P294	Nos295_SacI_wo_R	GCTAGAGCTCAGATGCCAACAACCTCAGG
P295	Nos295_3A	CTCTGGATCGGGTTCAGGAATGCTGTATTTAGCAGA AGTACAAAAGC
P296	Nos295_3B	CCTTTCGTCTTCAAGAATTCTTTAAGATGCCAACAAC TCAGGCT
P297	Nos295_pAM2991_ 2A	CACACAGGAAACAGACCATGCTGTATTTAGCAGAAG TACAAAAGC
P298	pIGA_V_295_F	AGCCTGAGTTGTTGGCATCTGCTAGTGCATCTGCTA GTGCT
P299	pIGA_V_295_R	ACTTCTGCTAAATACAGCATTGAATTAATCTCCTACT TGACTTTATGAGT
P300	pIGA_Nos295_F	TCAAGTAGGAGATTAATTCAATGCTGTATTTAGCAGA AGTACAAAAGC
P301	pIGA_Nos295_R	GCACTAGCAGATGCACTAGCAGATGCCAACAACCTCA GGC
P302	Nos295_intern_A	CAAAGTCAGGCGATGAGTGA

Supplementary tables – Oligonucleotides, plasmids and strains

P303	Nos295_intern_B	GGAACCGCATTACCAGAAGT
P304	295KO_2A	ATTCGATATCTAGATCTCGAGACTCAACATAATCATC GGTATATACCGAAAT
P305	295KO_2B	CAAGGTGCTGTGCACGGATCACCGTTCTTCCTCTTG TGTACTIONGA
P306	295KO_4A	CCAAGGTAGTCGGCAAATAACAATTCAAATTCAAAA TTCAAATATTTAGGACTTACG
P307	295KO_4B	ATGCAAGCTTTTCGCGAGCTCTGTAAATTTCTCACTAA GTGATGGATCAACACT
P308	Syc879_pET_2A	GTTTAACTTTAAGAAGGAGATATACATATGCTCTATC TGGCTGAAGTCG
P309	Syc879_pET_2B	CAGTGGTGGTGGTGGTGGTGGGCTGCAATCAGTTG ATGACT
P310	Syc879_pIGA_2A	TAAAGTCAAGTAGGAGATTAATTCAAGTGCTCTATCTG GCTGAAGTCGG
P311	Syc879_2A	TACAGGTTAGGAGAACGCCATGCTCTATCTGGCTGA AGTCG
P312	Syc879_2B	CACTAGCAGATGCACTAGCGGCTGCAATCAGTTGAT GACTG
P313	Syc879_pAM2991_2 A	CACACAGGAAACAGACCATGCTCTATCTGGCTGAAG TCGG
P314	Syc879_KO_2A	TGTAGGAGATCTTCTAGAAAGATCTGGAGCGATCGC TATGG
P315	Syc879_KO_2B	CTTGCGGCAGCGTGAAGCTTTATCGATGCCTCGCCT TAATCAATC
P316	Syc879_KO_4A	CCTTCTTGACGAGTTCTTCTGAGCCAGTCCCCCGCG ACTA
P317	Syc879_KO_4B	CTCGAGTTTTTCAGCAAGATGGCAAGCGCAACTGAA TTCTTAC
P318	MB_5A	TGCCTGCAGGTCGACTCTAATGCTGTATTTAGCAGA AGTACAAAAG
P319	MB_5B	TCGGTACCCGGGGATCCTCAGATGCCAACAACTCAG GC
P320	MB_6A	AGGGTTCGACTCTAGAGGATATGCTGTATTTAGCAGA AGTACAAAAGC
P321	MB_6B	CTTACTTAGGTACCCGGGGAGATGCCAACAACTCAG GC
P322	MB_8A	TCTAGAGGATCCCCGGGTAATGCTGTATTTAGCAGA AGTACAAAAG
P323	MB_8B	TCGATGAATTCGAGCTCGGAGATGCCAACAACTCAG GC
P324	MB_9A	TGCCTGCAGGTCGACTCTAATGCTCTATCTGGCTGA AATTAAGAAAC
P325	MB_9B	TCGGTACCCGGGGATCCTCACCGCCAAACAATAGG GT
P326	MB_10A	AGGGTTCGACTCTAGAGGATATGCTCTATCTGGCTGA AATTAAGAAAC
P327	MB_10B	CTTACTTAGGTACCCGGGGACCGCCAAACAATAGGG TC
P328	MB_12A	TCTAGAGGATCCCCGGGTAATGCTCTATCTGGCTGA AATTAAGAAAC
P329	MB_12B	TCGATGAATTCGAGCTCGGACCGCCAAACAATAGGG TC

P330	MB_13A	TGCCTGCAGGTCGACTCTAATGACAAGTCAAATTTT GTTTCTGATCAAG
P331	MB_13B	TCGGTACCCGGGGATCCTCTGGTAAATAAGGGGGA GTGGGAC
P332	MB_14A	AGGGTTCGACTCTAGAGGATATGACAAGTCAAATTT TGTTTCTGATCAAG
P333	MB_14B	CTTACTTAGGTACCCGGGGTGGTAAATAAGGGGGA GTGGGAC
P334	MB_16A	TCTAGAGGATCCCCGGGTAATGACAAGTCAAATTT TGTTTCTGATCAAG
P335	MB_16B	TCGATGAATTCGAGCTCGGTGGTAAATAAGGGGGAG TGGGAC
P336	MB_33A	TGCCTGCAGGTCGACTCTAATGCTCTATCTGGCTGA AGTCG
P337	MB_33B	TCGGTACCCGGGGATCCTCGGCTGCAATCAGTTGAT GACT
P338	MB_34A	AGGGTTCGACTCTAGAGGATATGCTCTATCTGGCTGA AGTCG
P339	MB_34B	CTTACTTAGGTACCCGGGGGGCTGCAATCAGTTGAT GACT
P340	MB_36A	TCTAGAGGATCCCCGGGTAATGCTCTATCTGGCTGA AGTCG
P341	MB_36B	TCGATGAATTCGAGCTCGGGGCTGCAATCAGTTGAT GACT
P342	MB_45A	TGCCTGCAGGTCGACTCTAATGAACTACGCTCTTAC CCAAG
P343	MB_45B	TCGGTACCCGGGGATCCTCAGACCCTAACCAGCGG C
P344	MB_46A	AGGGTTCGACTCTAGAGGATATGAACTACGCTCTTAC CCAAG
P345	MB_46B	CTTACTTAGGTACCCGGGGAGACCCTAACCAGCGG C
P346	MB_48A	TCTAGAGGATCCCCGGGTAATGAACTACGCTCTTAC CCAAG
P347	MB_48B	TCGATGAATTCGAGCTCGGAGACCCTAACCAGCGG C
P348	708_Seq_A	CCAACAACTACCTACCACCAGTC
P349	708_Seq_B	CCGTAGGGATGCCTGATAAACC
P350	Syc879_Seq_A	CATCAGGAATGGATGCAGGAGG
P351	Syc879_Seq_B	GGCCGCTAATCACTTTTCAGTG
P352	295KO_Seq_A	GCCATCCTAGCTCTGATTTGATC
P353	295KO_Seq_B	CAGGGTTATCGGTAAGGAATCG

Table 12: Chapter II bacterial strains and plasmids

Strain	Description	Reference
<i>Synechocystis</i> sp. PCC 6803	Glucose tolerant Kazusa substrain wt	PCC, France
BLS20	Ω pta::Pcpc560- <i>alr0931-gfp</i> , Km ^R	This study
BLS21	Ω pta::Pcpc560- <i>slr1301-gfp</i> , Km ^R	This study
BLS22	Ω pta::Pcpc560- <i>synpcc7942_1139-gfp</i> , Km ^R	This study
BLS23	<i>Ptrc-slr1301-yfp</i> , wt harboring pTHS84	This study

Supplementary tables – Oligonucleotides, plasmids and strains

BLS24	Δ slr1301::Km ^R	This study
<i>Synechocystis</i> sp. PCC-M 6803	Glucose tolerant and motile Moscow PCC-M substrain wt	A gift from Annegret Wilde (Uni Freiburg)
BSL25	Δ slr1301::Sm ^R , Sp ^R	This study
<i>Synechococcus elongatus</i> PCC 7942	wt	A gift from from Martin Hagemann (Uni Rostock)
BLS26	Non-segregated Δ synpcc7942_2039::Km ^R	This study
BLS27	Ω synpcc7942_2498(NS1)::lacI- <i>alr0931-gfp</i> , Sm ^R , Sp ^R	This study
BLS28	Ω synpcc7942_2498(NS1)::lacI- <i>slr1301-gfp</i> , Sm ^R , Sp ^R	This study
BLS29	Ω synpcc7942_2498(NS1)::lacI- <i>synpcc7942_1139-gfp</i> , Sm ^R , Sp ^R	This study
<i>Anabaena</i> sp. PCC 7120	wt	Pasteur culture collection of cyanobacteria (PCC), France
BLS30	<i>PpetE-alr0931-gfp</i> , wt harboring pTHS78, Km ^R , Nm ^R	This study
BLS31	<i>PpetE-yfp-al0931</i> , wt harboring pTHS79, Km ^R , Nm ^R	This study
BLS32	<i>PpetE-slr1301-gfp</i> , wt harboring pTHS80, Km ^R , Nm ^R	This study
BLS33	<i>PpetE-yfp-slr1301</i> , wt harboring pTHS81, Km ^R , Nm ^R	This study
BLS34	<i>PpetE-synpcc7942_1139-gfp</i> , WT harboring pTHS82, Km ^R , Nm ^R	This study
BLS35	<i>Ptrc-slr1301-yfp</i> , wt harboring pTHS84	This study
BLS36	Δ alr0931::Sm ^R /Sp ^R	This study
<i>E. coli</i> DH5 α	Cloning strain	Meselson and Yuan (1968)
<i>E. coli</i> DH5 α MCR + pRL623	Methylation and Conjugation strain	Elhai <i>et al.</i> , 1997
<i>E. coli</i> XL1-blue	Cloning strain	Stratagene
<i>E. coli</i> BTH101	Expression strain for bacterial two-hybrid assay	Euromedex
<i>E. coli</i> BL21 (DE3)	Expression strain	Studier and Moffatt (1986)
Plasmids	Description	Reference
pJET1.2/blunt	<i>E. coli</i> subcloning vector, Amp ^R	Thermo Scientific
pet21a(+)	Bacterial vector for expressing C-terminal His6-tagged proteins in <i>E. coli</i> , Amp ^R	Novagen
pRL25C	Shuttle cosmid vector for cyanobacteria and <i>E. coli</i> , Km ^R , Nm ^R	Wolk <i>et al.</i> , 1988
pRL623	Methylation plasmid, Cm ^R	Wolk <i>et al.</i> , 1988
pRL443	Conjugation plasmid, Amp ^R	Wolk <i>et al.</i> , 1988
pRL278	<i>sacB</i> containing plasmid to select for double homologous recombination in <i>Anabaena</i> ; Km ^R	Wolk <i>et al.</i> , 1990
pRL153-GFP	Mobilizable broad host range vector containing <i>Ptrc-gfp</i> , Km ^R	Tolonen <i>et al.</i> , 2006

Supplementary tables – Oligonucleotides, plasmids and strains

pSM2-Pcpc560ter	pMD18-T derivate for insertion into <i>pta</i> open reading frame containing <i>Pcpc560-ter-TrbcL</i> expression cassette, Amp ^R , Km ^R	A gift from Yin Li (Chinese Academy of Science). Zhou <i>et al.</i> , 2014
pIGA	Cyanobacterial vector for insertion into neutral locus (RS1 and RS2) of <i>slr0168</i> in <i>Synechocystis</i> , Amp ^R	A gift from Martin Hagemann (Uni Rostock), Kunert <i>et al.</i> , 2000
pKNT25	Bacterial vector for expressing chimeric translational fusion proteins with the N-terminal T25 subunit of the <i>B. pertussis</i> adenylate cyclase under the control of the lac promoter, Nm ^R , Km ^R	Euromedex
pKT25	Bacterial vector for expressing chimeric translational fusion proteins with the C-terminal T25 subunit of the <i>B. pertussis</i> adenylate cyclase under the control of the lac promoter, Nm ^R , Km ^R	Euromedex
pUT18	Bacterial vector for expressing chimeric translational fusion proteins with the N-terminal T18 subunit of the <i>B. pertussis</i> adenylate cyclase under the control of the lac promoter, Amp ^R	Euromedex
pUT18C	Bacterial vector for expressing chimeric translational fusion proteins with the C-terminal T18 subunit of the <i>B. pertussis</i> adenylate cyclase under the control of the lac promoter, Amp ^R	Euromedex
pKT25- <i>zip</i>	pKT25 with the leucine zipper of GCN4 inserted into the KpnI site, Nm ^R , Km ^R	Euromedex
pUT18C- <i>zip</i>	pUT18C with the leucine zipper of GCN4 inserted into the KpnI and EcoRI site, Amp ^R	Euromedex
pAM2991	Cyanobacterial vector for expressing proteins under the control of the <i>trc</i> promoter that inserts into the NS1 site of <i>Synechococcus</i> , Sm ^R , Sp ^R	A gift from Susan Golden (Addgene plasmid # 40248)
pTHS1	pIGA carrying <i>Pcpc560-fm7001-gfp-TrbcL</i> created by GIBSON assembly, Amp ^R , Km ^R	This study
pTHS2	pRL25C-based vector carrying <i>PpetE-alr4504-gfp</i> , Nm ^R , Km ^R	This study
pTHS69	pET21a(+) with <i>alr0931</i> inserted between the NdeI and XhoI sites, Amp ^R	This study
pTHS70	pET21a(+) with <i>slr1301</i> inserted between the BamHI and XhoI sites, Amp ^R	This study
pTHS71	pET21a(+) with <i>synpcc7942_1139</i> inserted by GIBSON assembly, Amp ^R	This study
pTHS72	pET21a(+) with <i>alr0931-gfp</i> inserted between the NdeI and EcoRI sites, Amp ^R	This study
pTHS73	pET21a(+) with <i>slr1301-gfp</i> inserted by GIBSON assembly, Amp ^R	This study
pTHS74	pET21a(+) with <i>synpcc7942_1139-gfp</i> inserted by GIBSON assembly, Amp ^R	This study
pTHS75	pTHS1 with <i>fm7001</i> replaced with <i>alr0931</i> by GIBSON assembly, Amp ^R , Km ^R	This study
pTHS76	pTHS1 with <i>fm7001</i> replaced with <i>slr1301</i> by GIBSON assembly, Amp ^R , Km ^R	This study

Supplementary tables – Oligonucleotides, plasmids and strains

pTHS77	pTHS1 with <i>fm7001</i> replaced with <i>synpcc7942_1139</i> by GIBSON assembly, Amp ^R , Km ^R	This study
pTHS78	pRL25C with <i>PpetE-alr0931-gfp</i> inserted between the BamHI and EcoRI sites, Nm ^R , Km ^R	This study
pTHS79	pTHS2 with <i>alr4504-gfp</i> replaced with <i>yfp-alr0931</i> by GIBSON assembly, Nm ^R , Km ^R	This study
pTHS80	pTHS2 with <i>alr4504</i> replaced with <i>slr1303</i> by GIBSON assembly, Nm ^R , Km ^R	This study
pTHS81	pTHS2 with <i>alr4504-gfp</i> replaced with <i>yfp-slr1303</i> by GIBSON assembly, Nm ^R , Km ^R	This study
pTHS82	pTHS2 with <i>alr4504</i> replaced with <i>synpcc7942_1139</i> by GIBSON assembly, Nm ^R , Km ^R	This study
pTHS83	pTHS2 with <i>alr4504</i> replaced with <i>yfp-synpcc7942_1139</i> by GIBSON assembly, Nm ^R , Km ^R	This study
pTHS84	pRL153 with <i>gfp</i> replaced by <i>slr1301-yfp</i> , Km ^R	This study
pTHS33	pKNT25 with <i>slr7083</i> inserted by GIBSON assembly, Nm ^R , Km ^R	This study
pTHS34	pKT25 with <i>slr7083</i> inserted by GIBSON assembly, Nm ^R , Km ^R	This study
pTHS35	pUT18 with <i>slr7083</i> inserted by GIBSON assembly, Amp ^R	This study
pTHS36	pUT18C with <i>slr7083</i> inserted by GIBSON assembly, Amp ^R	This study
pTHS37	pKNT25 with <i>synpcc7942_2039</i> inserted by GIBSON assembly, Nm ^R , Km ^R	This study
pTHS38	pKT25 with <i>synpcc7942_2039</i> inserted by GIBSON assembly, Nm ^R , Km ^R	This study
pTHS39	pUT18 with <i>synpcc7942_2039</i> inserted by GIBSON assembly, Amp ^R	This study
pTHS40	pUT18C with <i>synpcc7942_2039</i> inserted by GIBSON assembly, Amp ^R	This study
pTHS85	pKNT25 with <i>alr0931</i> inserted by GIBSON assembly, Nm ^R , Km ^R	This study
pTHS86	pKT25 with <i>alr0931</i> inserted by GIBSON assembly, Nm ^R , Km ^R	This study
pTHS87	pUT18 with <i>alr0931</i> inserted by GIBSON assembly, Amp ^R	This study
pTHS88	pUT18C with <i>alr0931</i> inserted by GIBSON assembly, Amp ^R	This study
pTHS89	pKNT25 with <i>slr1301</i> inserted by GIBSON assembly, Nm ^R , Km ^R	This study
pTHS90	pKT25 with <i>slr1301</i> inserted by GIBSON assembly, Nm ^R , Km ^R	This study
pTHS91	pUT18 with <i>slr1301</i> inserted by GIBSON assembly, Amp ^R	This study
pTHS92	pUT18C with <i>slr1301</i> inserted by GIBSON assembly, Amp ^R	This study
pTHS93	pKNT25 with <i>synpcc7942_1139</i> inserted by GIBSON assembly, Nm ^R , Km ^R	This study
pTHS94	pKT25 with <i>synpcc7942_1139</i> inserted by GIBSON assembly, Nm ^R , Km ^R	This study

pTHS95	pUT18 with <i>synpcc7942_1139</i> inserted by GIBSON assembly, Amp ^R	This study
pTHS96	pUT18C with <i>synpcc7942_1139</i> inserted by GIBSON assembly, Amp ^R	This study
pTHS97	pAM2991 with <i>alr0931-gfp</i> inserted by GIBSON assembly, Sm ^R , Sp ^R	This study
pTHS98	pAM2991 with <i>slr1301-gfp</i> inserted by GIBSON assembly, Sm ^R , Sp ^R	This study
pTHS99	pAM2991 with <i>synpcc7942_1139-gfp</i> inserted by GIBSON assembly, Sm ^R , Sp ^R	This study
pTHS100	pRL278 containing 1000 bp upstream and downstream of <i>alr0391</i> flanking <i>aadA</i> assembled by GIBSON assembly, Nm ^R , Km ^R , Sm ^R , Sp ^R	This study
pTHS101	pJET1.2/blunt with ~1000 bp upstream and downstream of <i>slr1303</i> flanking <i>aadA</i> inserted by GIBSON assembly, Amp ^R , Km ^R	This study
pTHS102	Circularized puC ori with 1000 bp upstream and downstream of <i>slr1301</i> flanking <i>nptII</i> assembled by GIBSON assembly, Nm ^R , Km ^R	This study
pTHS103	pJET1.2/blunt with ~1000 bp upstream and downstream of <i>synpcc7942_1139</i> flanking <i>nptII</i> inserted by GIBSON assembly, Amp ^R , Km ^R	This study

Table 13: Chapter III oligonucleotides

Primer	Description	Sequence 5'-3'
P354	903KO_Seq_A	TGCGAATTCCAGTAGGTCTTGGTAA
P355	904KO_Seq_B	GGTGGCGCAGAAGTATTTTTG
P356	842KO_Seq_A	TCAACAGTCAACAGTCAATAGTGAAGG
P357	842KO_Seq_B	TTCATCTACACCGATATCTTGACCC
P358	pET19bmod-Fwd	GGAATTGTGAGCGGATAACAATT
P359	T7R	CTAATACGACTCACTATAGGGA
P360	pRL25c_Seq_Fwd	CTTTGATCTTTTCTACGGGGTCT
P361	pRL25c_Seq_Rev	TTGAGGTGAGGGATGAGCG
P362	pRL271_Seq_Fwd	GCCTGGTGCTACGCCTGAATA
P363	pRL271_Seq_Rev	CCAGTTAATAGTTTGCGCAACGTTG
P364	CS3_Seq_Fwd	CGCGCAGATCAGTTGGAAG
P365	CS3_Seq_Rev	AACGTCGGTTCGAGATGGC
P366	GFP_Seq_Rev	TTGTGCCCATTAACATCACCATC
P367	904GFP_Fwd	GCGGTAAAAGCTATTGAAGGTACTGC
P368	pIGA_Seq_Fwd2	CAAAGCCCGAAAGGAAGCTG
P369	pETM22_Seq_Fwd	GGTCAGTTGAAAGAGTTCCTC
P370	pETM22_Seq_F2	ATCTTCCCCATCGGTGATGTC
P371	MB_Seq_A	GGCTCGTATGTTGTGTGG
P372	MB_Seq_B	GGCTTAACTATGCGGCATC
P373	MB_Seq_C	TAACGCCAGGGTTTTCCCA
P374	pKNT25_Seq_Rev	CGTTTGCGTAACCAGCC
P375	pKT25_Seq_Fwd	GATTCGGTGACCGATTACCTG
P376	pUT18_Seq_Rev	GATGCGTTCGCGATCCAG
P377	pUT18C_Seq_Fwd	TCGCCGGATGTACTGGAAAC
P378	N-term_1A	GAGGATCCCCGGGTACC

Supplementary tables – Oligonucleotides, plasmids and strains

P418	cpf1-1	CTCCAGAAGCTATAAACTATGAAC
P419	cpf1-2	CTACTTCAAGCTAGTGCGGAA
P420	cpf1-3	GTTGAAAATCAAGGCTACAACTAAC
P421	cpf1-4	CGTTTCAAGGTAGAGAAGCAGG
P422	Nos295His_2A	TACAGGTTAGGAGAACGCCATGCTGTATTTAGCAGA AGTACAAAAG
P423	Nos295His_2B	CCTTTCGTCTTCAAGAATTCTTCAGTGGTGGTGGTG GTG
P424	Nos903_NdeI_F	GCTACATATGACGACAGTTGCACTCA
P425	Nos903_XhoI_R_w/ o	GCTACTCGAGTTTAGCCGTAGAACTATCAAAGC
P426	Nos903_pET_2A	GTTTAACTTTAAGAAGGAGATATACATATGACGACAG TTGCACTCAAAG
P427	pRL25-Nos903_Fwd	CTACAGGTTAGGAGAACGCCATGACGACAGTTGCAC TCAAAGATAG
P428	pRL25-Nos903_Rev	GCACTAGCAGATGCACTAGCTTTAGCCGTAGAACTA TCAAAGCTCTCATTGC
P429	pRL25c-903_V_F	TGGATGAACTATACAAATAAAGAATTCTTGAAGACGA AAGGGCC
P430	pRL25c-903_V_R	GCAAAAATTCTGAGTACTGGGATCCTTTTTGATAAT CTCATGACCAAAATCC
P431	petE_903_Fwd	GAGATTATCAAAAAGGATCCCAGTACTCAGAATTTTT TGCTGAGGTA
P432	petE_903_Rev	TTGAGTGCAACTGTCTCATGGCGTTCTCCTAACCT GTAGTTTTATTTTT
P433	GFP_903_Fwd	TTGATAGTTCTACGGCTAAAGCTAGTGCATCTGCTA GTGCTAGT
P434	GFP_903_Rev	CCTTTCGTCTTCAAGAATTCTTTATTTGTATAGTTCATC CATGCCATGTGTAATCC
P435	Nos903_2B	TTCGCTGATAAGCTTCTGTTCTTTAGCCGTAGAACTA TCAAAGCTCTC
P436	Nos903_3A	CTCTGGATCGGGTTCAGGAATGACGACAGTTGCACT CAAAG
P437	Nos903_3B	CCTTTCGTCTTCAAGAATTCTTTATTTAGCCGTAGAA CTATCAAAGCTC
P438	Nos903_pIGA_2A	TAAAGTCAAGTAGGAGATTAATTCAATGACGACAGTT GCACTCAAAG
P439	Nos903_Pcpc560_A	AGATTAATTCAATGACGACAGTTGCACTCAAAG
P440	CFP_pIGA_B	ACCACACCCGTCCTGTGGATTTACTTGTACAGCTCG TCCATGCC
P441	petE_BamHI_2A	TTGGTCATGAGATTATCAAAAAGCAGTACTCAGAATT TTTTGCTGAGG
P442	GFP_BamHI_2B	ATTGATTTAAACTTTCATTTTTAATTTAAAAGTTATTTG TATAGTTCATCCATGCCATGTG
P443	Nos903CFP_3A	GGTTCAGGAATGACGACAGTTGCACTCAAAGA
P444	Nos903CFP_3B	CCTTTCGTCTTCAAGAATTCTTTATTTAGCCGTAGAA CTATCAAAGCTCTCA
P445	Nos903_intern_A	TCAGCTAGACGTAAGAGTGGC
P446	Nos903_intern_B	TAATTCTGCTGGGAATGCAGC
P447	903KO_2A	ATTCGATATCTAGATCTCGAGAAGCAACGGCAACGC C
P448	903KO_2B	AAGGTGCTGTGCACGGATCATTCAACTCCCTTGAT TAGATAATGATTAATCGAG

Supplementary tables – Oligonucleotides, plasmids and strains

P449	903KO_4A	CAAGGTAGTCGGCAAATAAATATTAATTTTGGGAAAT TTGCAATAAATAGAGGTTTTTATG
P450	903KO_4B2	TGCAAGCTTTTCGCGAGCTCTTATTTATTTTCACTTG ACTTTTTGCCTGTTCT
P451	trunc903_2A	CTGAATAAGTGATAATAAGCGGTTCTACAGGATTTTG GATTGAGCCT
P452	trunc903_2B	TGCAAGCTTTTCGCGAGCTCTAGCCGTATCTTGCTCT AGAGTT
P453	Nos903_gRNA-A	AGATCACTCAAAGATAGTAAGCAG
P454	Nos903_gRNA-B	AGACCTGCTTACTATCTTTGAGTG
P455	Nos903_HL1A	TTTGTCTAGCTTTAATGCGGTAGTTGGTACGTGATGA GACGCTGACGACG
P456	Nos903_HL1B	CCAAAATTAATATATTTCAACTCCCTTGATTAGATAAT GATTAATCG
P457	Nos903_HR2A	AGGGAGTTGAAATATATTAATTTTGGGAAATTTGCAA TAAATAGAGGTTT
P458	Nos903_HR2B	TTACAGATCCTCTAGAGTCGACGGTACAGTTTTGTA GTCGCGTCTCTTGA
P459	Nos904_pET_2A	GTTTAACTTTAAGAAGGAGATATACATATGGCAGTCA AAAAGTTAACAGAC
P460	Nos904_2A	CTACAGGTTAGGAGAACGCCATGGCAGTCAAAAAGT TAACAGACAAAAAC
P461	Nos904_2B	GCACTAGCAGATGCACTAGCTTTATTTTCACTTGAC TTTTTGCCTGTTCTAAAGC
P462	Nos904_3A	CTCTGGATCGGGTTCAGGAATGGCAGTCAAAAAGTT AACAGACA
P463	Nos904_3B	CCTTTCGTCTTCAAGAATTCTTTATTTATTTTCACTT GACTTTTTGCCTGT
P464	Nos904_piGA_2A	TAAAGTCAAGTAGGAGATTAATTCAATGGCAGTCAAA AAGTTAACAGACA
P465	Nos904_intern_A	TGGAATTAGCGAAGGGGTGG
P466	Nos904_intern_B	TGTTTCATAGCCATCTGTTGCCA
P467	904KO_2A	ATTCGATATCTAGATCTCGAGTTCACTACATTCACAC TTTGGCGAT
P468	904KO_2B	AAGGTGCTGTGCACGGATCAAAAACCTCTATTTATTG CAAATTTCCCAAAT
P469	904KO_4A	CAAGGTAGTCGGCAAATAAATACAAATAATAAAAAT AAATAAAAAGACGTAACGAAAATTACG
P470	904KO_4B	TGCAAGCTTTTCGCGAGCTCGTAGTGGGTTTCGCACA AGCTATC
P471	trunc904_2A	CTGAATAAGTGATAATAAGCGGGCAGAATTAGAAGA AGCAGTGAAAAAATC
P472	trunc904_2B	TGCAAGCTTTTCGCGAGCTCCTTCATAAGTAGTAATAA GTGTATCTAATGTATTTTCAG
P473	Nos904_HL1A	TCTAGCTTTAATGCGGTAGTTGGTACGACGACAGTT GCACTCAAAGATAG
P474	Nos904_HL1B	ATTTTTATTATTTGTATTAACCTCTATTTATTGCAA ATTTCCAAAA
P475	Nos904_HR2A	AATAAATAGAGGTTTTTAATACAAATAATAAAAATAAA TAAAAGACGTAACGAAAATTACG
P476	Nos904_HR2B	TTACAGATCCTCTAGAGTCGACGGTACACGGACTAG TAGCTACTCGTG
P477	Nos904_gRNA-A	AGATACAGACAAAAACACCAAAGC
P478	Nos904_gRNA-B	AGACGCTTTGGTGTTTTTGTCTGT

Supplementary tables – Oligonucleotides, plasmids and strains

P479	903_split_A	AAGGTGGCTCTGGCTCTGGCTCGAGCATGACGACA GTTGCACTCAAAG
P480	903_split_B	CGGGCTTTGTTAGCAGCCGTTATTTAGCCGTAGAAC TATCAAAAGCTCTC
P481	904_split_A	TTAACTTTAAGAAGGAGATATACCATGGCAGTCAAA AAGTTAACAGACA
P482	904_split_B	TTACCGCTTCCACCCGACGTTTTATTTTCACTTGAC TTTTTGCTGTTC
P483	903_split_A2	TTAACTTTAAGAAGGAGATATACATATGACGACAGTT GCACTCAAAG
P484	903_split_B2	CCATGGTGATGGTGGTGATGAGATGCACTAGCTTTA GCCGTAGAACTATCAAAAGCTCT
P485	Nos842_NdeI_F	GCTACATATGCAACAAGTCATAGTAAGTAATCG
P486	Nos842_XhoI_wo_R	GCTACTCGAGGGATGCGTATCTAGCTATTAGATG
P487	Nos842_pETM22_A	AAGTTCTGTTCCAGGGGCCCATGCAACAAGTCATAG TAAGTAATCG
P488	Nos842_pETM22_B	CCGGTACCTCATTAGTCCATTCAGGATGCGTATCTA GCTATTAGATG
P489	Nos842_pET_2A	GTTTAACTTTAAGAAGGAGATATACATATGCAACAAG TCATAGTAAGTAATCG
P490	Nos842_pETM22_B 2	ATATGGCCAGAACCAGAACCGGATGCGTATCTAGCT ATTAGATGTTC
P491	Nos842_pIGA_2A	AAAGTCAAGTAGGAGATTAATTCAATGCAACAAGTCA TAGTAAGTAATCG
P492	Nos842_2A	TACAGGTTAGGAGAACGCCATGCAACAAGTCATAGT AAGTAATCGATT
P493	Nos842_2B	CACTAGCAGATGCACTAGCGGATGCGTATCTAGCTA TTAGATGTTC
P494	Nos842_3A	CTCTGGATCGGGTTCAGGAATGCAACAAGTCATAGT AAGTAATCGATT
P495	Nos842_3B	CCTTCGTCTTCAAGAATTCTTCAGGATGCGTATCTA GCTATTAGATG
P496	Nos842_intern_A	TCGGGCAGAAATTACCCAGT
P497	Nos842_intern_B	TGCCATTCTTCAGGCAAAGC
P498	842KO_2A	ATTCGATATCTAGATCTCGAGATGGATAATCCAGCAA TGTCGGC
P499	842KO_2B	AAGGTGCTGTGCACGGATCATTGCTGATTTTAGCG TAGTTAAGCTTT
P500	842KO_4A	CAAGGTAGTCGGCAAATAAAATTTAATATCCCTAGCT CATCGTAAAATTTTATAAAAATATG
P501	842KO_4B	ATGCAAGCTTTTCGCGAGCTCTTTAAACTAGAACTAT GAACTAGCTCGCTAAAC
P502	MB_5A	TGCCTGCAGGTCGACTCTAATGCTGTATTTAGCAGA AGTACAAAAG
P503	MB_5B	TCGGTACCCGGGGATCCTCAGATGCCAACAACTCAG GC
P504	MB_6A	AGGGTCGACTCTAGAGGATATGCTGTATTTAGCAGA AGTACAAAAGC
P505	MB_6B	CTTACTTAGGTACCCGGGGAGATGCCAACAACTCAG GC
P506	MB_8A	TCTAGAGGATCCCCGGGTAATGCTGTATTTAGCAGA AGTACAAAAG
P507	MB_8B	TCGATGAATTCGAGCTCGGAGATGCCAACAACTCAG GC

Supplementary tables – Oligonucleotides, plasmids and strains

P508	MB_17A	TGCCTGCAGGTCGACTCTAATGACGACAGTTGCACT CAAAG
P509	MB_17B	TCGGTACCCGGGGATCCTCTTTAGCCGTAGAACTAT CAAAGCTCTC
P510	MB_18A	AGGGTCGACTCTAGAGGATATGACGACAGTTGCACT CAAAG
P511	MB_18B	CTTACTTAGGTACCCGGGGTTTATAGCCGTAGAACTAT CAAAGCTCTC
P512	MB_20A	TCTAGAGGATCCCCGGGTAATGACGACAGTTGCACT CAAAG
P513	MB_20B	TCGATGAATTCGAGCTCGGTTTATAGCCGTAGAACTAT CAAAGCTCTC
P514	MB_21A	TGCCTGCAGGTCGACTCTAATGGCAGTCAAAAAGTT AACAGACAA
P515	MB_21B	TCGGTACCCGGGGATCCTCTTTATTTTTCACTTGACT TTTTGCCTGTTC
P516	MB_22A	AGGGTCGACTCTAGAGGATATGGCAGTCAAAAAGTT AACAGACAA
P517	MB_22B	CTTACTTAGGTACCCGGGGTTTATTTTTCACTTGACT TTTTGCCTGTTC
P518	MB_24A	TCTAGAGGATCCCCGGGTAATGGCAGTCAAAAAGTT AACAGACAA
P519	MB_24B	TCGATGAATTCGAGCTCGGTTTATTTTTCACTTGACT TTTTGCCTGTTC
P520	MB_25A	TGCCTGCAGGTCGACTCTAATGCAACAAGTCATAGT AAGTAATCGAT
P521	MB_25B	TCGGTACCCGGGGATCCTCGGATGCGTATCTAGCTA TTAGATGTTC
P522	MB_26A	AGGGTCGACTCTAGAGGATATGCAACAAGTCATAGT AAGTAATCGAT
P523	MB_26B	CTTACTTAGGTACCCGGGGGATGCGTATCTAGCTA TTAGATGTTC
P524	MB_28A	TCTAGAGGATCCCCGGGTAATGCAACAAGTCATAGT AAGTAATCGAT
P525	MB_28B	TCGATGAATTCGAGCTCGGGGATGCGTATCTAGCTA TTAGATGTTC
P526	MB_41A	TGCCTGCAGGTCGACTCTAATGGGGCGATTTGAGAA GC
P527	MB_41B	TCGGTACCCGGGGATCCTCACCTTCTGCATTGGCAG G
P528	MB_42A	AGGGTCGACTCTAGAGGATATGGGGCGATTTGAGAA GC
P529	MB_42B	CTTACTTAGGTACCCGGGGACCTTCTGCATTGGCAG G
P530	MB_44A	TCTAGAGGATCCCCGGGTAATGGGGCGATTTGAGAA GC
P531	MB_44B	TCGATGAATTCGAGCTCGGACCTTCTGCATTGGCAG G
P532	MB_49A	ATGCCTGCAGGTCGACTCTAATGACACTTGATAATAA CCAAGAGCTTACC
P533	MB_49B	CTCGGTACCCGGGGATCCTCATTTTTGGGTGGTTCG CGTC
P534	MB_50A	CAGGGTCGACTCTAGAGGATATGACACTTGATAATA ACCAAGAGCTTACC

P535	MB_50B	TACTTACTTAGGTACCCGGGGATTTTTGGGTGGTCCG CCGTC
P536	MB_52A	CTCTAGAGGATCCCCGGGTAATGACACTTGATAATA ACCAAGAGCTTACC
P537	MB_52B	TATATCGATGAATTCGAGCTCGGATTTTTGGGTGGT CGCCGTC
P538	MB_53A	ATGCCTGCAGGTCGACTCTAATGGGGCTTTTTAGGA ACTTTTCG
P539	MB_53B	CTCGGTACCCGGGGATCCTCCATATTCGAGATCGT CCGCTAAAAAC
P540	MB_54A	CAGGGTCGACTCTAGAGGATATGGGGCTTTTTAGGA ACTTTTCG
P541	MB_54B	TACTTACTTAGGTACCCGGGGCATATTCGAGATCG TCCGCTAAAAAC
P542	MB_56A	CTCTAGAGGATCCCCGGGTAATGGGGCTTTTTAGGA ACTTTTCG
P543	MB_56B	TATATCGATGAATTCGAGCTCGGCATATTCGAGATC GTCCGCTAAAAAC

Table 14: Chapter III bacterial strains and plasmids

Strains	Description	Reference
<i>Synechocystis</i> sp. PCC 6803	Glucose tolerant Kazusa substrain wt	PCC, France
BLS37	Ω pta::Pcpc560- <i>alr4504-gfp</i> , Km ^R	This study
BLS38	Ω pta::Pcpc560- <i>alr4505-gfp</i> , Km ^R	This study
BLS39	Ω pta::Pcpc560- <i>all2460-gfp</i> , Km ^R	This study
<i>Anabaena</i> sp. PCC 7120	wt	PCC, France
BLS40	<i>PpetE-alr0931-his</i> , wt harboring pTHS115, Km ^R , Nm ^R	This study
BLS41	<i>PpetE-alr4504-gfp</i> , wt harboring pTHS2, Km ^R , Nm ^R	This study
BLS42	<i>PpetE-yfp-alr4504</i> , wt harboring pTHS116, Km ^R , Nm ^R	This study
BLS43	<i>PpetE-alr4505-gfp</i> , wt harboring pTHS117, Km ^R , Nm ^R	This study
BLS44	<i>PpetE-yfp-alr4505</i> , wt harboring pTHS118, Km ^R , Nm ^R	This study
BLS45	<i>PpetE-all2460-gfp</i> , wt harboring pTHS119, Km ^R , Nm ^R	This study
BLS46	<i>PpetE-yfp-all2460</i> , wt harboring pTHS120, Km ^R , Nm ^R	This study
BLS47	<i>PpetE-alr4504-ecfp</i> and <i>PpetE-alr4505-gfp</i> ; WT harboring pTHS150	This study
BLS48	(Δ <i>alr4504</i> Δ <i>alr4505</i>)::Sm ^R /Sp ^R	This study
BLS49	Δ <i>all2460</i> ::Sm ^R /Sp ^R	This study
<i>E. coli</i> DH5 α	Cloning strain	Meselson and Yuan (1968)
<i>E. coli</i> DH5 α MCR + pRL623	Methylation and Conjugation strain	Elhai <i>et al.</i> 1997

<i>E. coli</i> XL1-blue	Cloning strain	Stratagene
<i>E. coli</i> BTH101	Expression strain for bacterial two-hybrid assay	Euromedex
<i>E. coli</i> BL21 (DE3)	Expression strain	Studier and Moffatt (1986)
Plasmids	Description	Reference
pet21a(+)	Bacterial vector for expressing C-terminal His6-tagged proteins in <i>E. coli</i> , Amp ^R	Novagen
pRL25C	Shuttle cosmid vector for cyanobacteria and <i>E. coli</i> , Km ^R , Nm ^R	Wolk <i>et al.</i> , 1988
pETM-22	Bacterial vector for expressing N-terminal <i>trxA</i> (<i>E. coli</i>) and/or C/N-terminal His6-tagged translational fusion proteins in <i>E. coli</i> with a HRV 3C site, Km ^R	A gift from Axel Scheidg (Uni Kiel), created by Arie Geerlof
pRL623	Methylation plasmid, Cm ^R	Wolk <i>et al.</i> , 1988
pRL443	Conjugation plasmid, Amp ^R	Wolk <i>et al.</i> , 1988
pRL278	<i>sacB</i> containing plasmid to select for double homologous recombinations in <i>Anabaena</i> ; Km ^R	Wolk <i>et al.</i> , 1990
pSL2680	Cpf1-mediated CRISPR editing plasmid, Km ^R , Nm ^R	Ungerer and Pakrasi, 2016
pRL25c-CRISPR	Functional CRISPR cassette from pSL2680 transferred into EcoRI and BamHI digested pRL25c by GIBSON assembly, Km ^R , Nm ^R	This work
pSM2-Pcpc560ter	pMD18-T derivate for insertion into <i>pta</i> open reading frame containing <i>Pcpc560-ter-TrbcL</i> expression cassette, Amp ^R , Km ^R	A gift from Yin Li (Chinese Academy of Science). Zhou <i>et al.</i> , 2014
pIGA	Cyanobacterial vector for insertion into neutral locus (RS1 and RS2) of <i>slr0168</i> in <i>Synechocystis</i> , Amp ^R	A gift from Martin Hagemann (Uni Rostock), Kunert <i>et al.</i> , 2000
pET11a-link-NGFP	IPTG-inducible expression vector for translational fusion of target gene with a N-terminal <i>gfp</i> fragment in <i>E. coli</i> , Amp ^R	A gift from Lynne Regan (Yale University), Magliery <i>et al.</i> , 2004
pMRBAD-link-CGFP	L-arabinose-inducible expression vector for translational fusion of target gene with a C-terminal <i>gfp</i> fragment in <i>E. coli</i> , Km ^R	A gift from Lynne Regan (Yale University), Magliery <i>et al.</i> , 2004
pKNT25	Bacterial vector for expressing chimeric translational fusion proteins with the N-terminal T25 subunit of the <i>B. pertussis</i> adenylate cyclase under the control of the <i>lac</i> promoter, Nm ^R , Km ^R	Euromedex
pKT25	Bacterial vector for expressing chimeric translational fusion proteins with the C-terminal T25 subunit of the <i>B. pertussis</i> adenylate cyclase under the control of the <i>lac</i> promoter, Nm ^R , Km ^R	Euromedex
pUT18	Bacterial vector for expressing chimeric translational fusion proteins with the N-terminal T18 subunit of the <i>B. pertussis</i> adenylate	Euromedex

Supplementary tables – Oligonucleotides, plasmids and strains

	cyclase under the control of the <i>lac</i> promoter, Amp ^R	
pUT18C	Bacterial vector for expressing chimeric translational fusion proteins with the C-terminal T18 subunit of the <i>B. pertussis</i> adenylate cyclase under the control of the <i>lac</i> promoter, Amp ^R	Euromedex
pKT25-zip	pKT25 with the leucine zipper of GCN4 inserted into the KpnI site, Nm ^R , Km ^R	Euromedex
pUT18C-zip	pUT18C with the leucine zipper of GCN4 inserted into the KpnI and EcoRI site, Amp ^R	Euromedex
pAM5084	Bacterial vector for expression of <i>P_{trc}-ecfp-kaiC</i> in <i>E. coli</i> , Amp ^R	A gift from Susan Golden (Addgene plasmid # 85105), Cohen et al., 2014
pTHS1	pIGA carrying <i>P_{cpc560-fm7001-gfp-TrbcL}</i> created by GIBSON assembly, Amp ^R , Km ^R	This study
pTHS2	pRL25C-based vector carrying <i>P_{petE-alr4504-gfp}</i> created by GIBSON assembly, Nm ^R , Km ^R	This study
pTHS104	pET21a(+) with <i>alr4504</i> inserted between the NdeI and XhoI sites, Amp ^R	This study
pTHS105	pET21a(+) with <i>alr4505</i> inserted by GIBSON assembly, Amp ^R	This study
pTHS106	pET21a(+) with <i>all2460</i> inserted between the NdeI and XhoI sites, Amp ^R	This study
pTHS107	pET21a(+) with <i>alr4504-gfp</i> inserted by GIBSON assembly, Amp ^R	This study
pTHS108	pET21a(+) with <i>alr4505-gfp</i> inserted by GIBSON assembly, Amp ^R	This study
pTHS109	pET21a(+) with <i>all2460-gfp</i> inserted by GIBSON assembly, Amp ^R	This study
pTHS110	pETM-22 with <i>trxA (E. coli)</i> inserted by GIBSON assembly, Km ^R	This study
pTHS111	pTHS102 with <i>all2460</i> replacing the second <i>trxA</i> by GIBSON assembly, Km ^R	This study
pTHS112	pTHS1 with <i>fm7001</i> replaced with <i>alr4504</i> by GIBSON assembly. Amp ^R , Km ^R	This study
pTHS113	pTHS1 with <i>fm7001</i> replaced with <i>alr4505</i> by GIBSON assembly. Amp ^R , Km ^R	This study
pTHS114	pTHS1 with <i>fm7001</i> replaced with <i>all2460</i> by GIBSON assembly. Amp ^R , Km ^R	This study
pTHS115	pTHS2 with <i>alr4504-gfp</i> replaced with <i>alr0931-his</i> by GIBSON assembly. Nm ^R , Km ^R	This study
pTHS116	pTHS2 with <i>alr4504-gfp</i> replaced with <i>yfp-alr4504</i> by GIBSON assembly. Nm ^R , Km ^R	This study
pTHS117	pTHS2 with <i>alr4504</i> replaced with <i>alr4505</i> by GIBSON assembly. Nm ^R , Km ^R	This study
pTHS118	pTHS2 with <i>alr4504-gfp</i> replaced with <i>yfp-alr4505</i> by GIBSON assembly. Nm ^R , Km ^R	This study
pTHS119	pTHS2 with <i>alr4504</i> replaced with <i>all2460</i> by GIBSON assembly. Nm ^R , Km ^R	This study
pTHS120	pTHS2 with <i>alr4504-gfp</i> replaced with <i>yfp-all2460</i> by GIBSON assembly. Nm ^R , Km ^R	This study
pTHS49	pKNT25 with <i>alr3858</i> inserted by GIBSON assembly, Nm ^R , Km ^R	This study

Supplementary tables – Oligonucleotides, plasmids and strains

pTHS50	pKT25 with <i>alr3858</i> inserted by GIBSON assembly, Nm ^R , Km ^R	This study
pTHS51	pUT18 with <i>alr3858</i> inserted by GIBSON assembly, Amp ^R	This study
pTHS52	pUT18C with <i>alr3858</i> inserted by GIBSON assembly, Amp ^R	This study
pTHS53	pKNT25 with <i>all0087</i> inserted by GIBSON assembly, Nm ^R , Km ^R	This study
pTHS54	pKT25 with <i>all0087</i> inserted by GIBSON assembly, Nm ^R , Km ^R	This study
pTHS55	pUT18 with <i>all0087</i> inserted by GIBSON assembly, Amp ^R	This study
pTHS56	pUT18C with <i>all0087</i> inserted by GIBSON assembly, Amp ^R	This study
pTHS85	pKNT25 with <i>alr0931</i> inserted by GIBSON assembly, Nm ^R , Km ^R	This study
pTHS86	pKT25 with <i>alr0931</i> inserted by GIBSON assembly, Nm ^R , Km ^R	This study
pTHS87	pUT18 with <i>alr0931</i> inserted by GIBSON assembly, Amp ^R	This study
pTHS88	pUT18C with <i>alr0931</i> inserted by GIBSON assembly, Amp ^R	This study
pTHS121	pKNT25 with <i>alr4504</i> inserted by GIBSON assembly. Nm ^R , Km ^R	This study
pTHS122	pKT25 with <i>alr4504</i> inserted by GIBSON assembly. Nm ^R , Km ^R	This study
pTHS123	pUT18 with <i>alr4504</i> inserted by GIBSON assembly. Amp ^R	This study
pTHS124	pUT18C with <i>alr4504</i> inserted by GIBSON assembly. Amp ^R	This study
pTHS125	pKNT25 with <i>alr4505</i> inserted by GIBSON assembly. Nm ^R , Km ^R	This study
pTHS126	pKT25 with <i>alr4505</i> inserted by GIBSON assembly. Nm ^R , Km ^R	This study
pTHS127	pUT18 with <i>alr4505</i> inserted by GIBSON assembly. Amp ^R	This study
pTHS128	pUT18C with <i>alr4505</i> inserted by GIBSON assembly. Amp ^R	This study
pTHS129	pKNT25 with <i>all2460</i> inserted by GIBSON assembly. Nm ^R , Km ^R	This study
pTHS130	pKT25 with <i>all2460</i> inserted by GIBSON assembly. Nm ^R , Km ^R	This study
pTHS131	pUT18 with <i>all2460</i> inserted by GIBSON assembly. Amp ^R	This study
pTHS132	pUT18C with <i>all2460</i> inserted by GIBSON assembly. Amp ^R	This study
pTHS133	pKNT25 with <i>alr2338</i> inserted by GIBSON assembly. Nm ^R , Km ^R	This study
pTHS134	pKT25 with <i>alr2338</i> inserted by GIBSON assembly. Nm ^R , Km ^R	This study
pTHS135	pUT18 with <i>alr2338</i> inserted by GIBSON assembly. Amp ^R	This study
pTHS136	pUT18C with <i>alr2338</i> inserted by GIBSON assembly. Amp ^R	This study

Supplementary tables – Oligonucleotides, plasmids and strains

pTHS137	pRL278 containing 1000 bp upstream and downstream of <i>alr4504</i> flanking <i>aadA</i> assembled by GIBSON assembly, Nm ^R , Km ^R , Sm ^R , Sp ^R	This study
pTHS138	pRL278 containing 1000 bp upstream and downstream of <i>alr4505</i> flanking <i>aadA</i> assembled by GIBSON assembly, Nm ^R , Km ^R , Sm ^R , Sp ^R	This study
pTHS139	pRL278 containing 1000 bp upstream and downstream of <i>alr4504/alr4505</i> flanking <i>aadA</i> assembled by GIBSON assembly, Nm ^R , Km ^R , Sm ^R , Sp ^R	This study
pTHS140	pRL278 containing 1000 bp upstream and downstream of <i>all2460</i> flanking <i>aadA</i> assembled by GIBSON assembly, Nm ^R , Km ^R , Sm ^R , Sp ^R	This study
pTHS141	pSL2680 with <i>alr4504</i> gRNA and homologous repair templates 1000 bp upstream and downstream of <i>alr4504</i> , Nm ^R , Km ^R	This study
pTHS142	pRL25c-CRISPR with <i>alr4504</i> gRNA and homologous repair templates 1000 bp upstream and downstream of <i>alr4504</i> , Nm ^R , Km ^R	This study
pTHS143	pSL2680 with <i>alr4505</i> gRNA and homologous repair templates 1000 bp upstream and downstream of <i>alr4505</i> , Nm ^R , Km ^R	This study
pTHS144	pRL25c-CRISPR with <i>alr4505</i> gRNA and homologous repair templates 1000 bp upstream and downstream of <i>alr4505</i> , Nm ^R , Km ^R	This study
pTHS145	pET11a-link-NGFP with <i>alr4504</i> inserted by GIBSON assembly between the XhoI and BamHI sites, Amp ^R	This study
pTHS146	pMRBAD-link-CGFP with <i>alr4505</i> inserted by GIBSON assembly between the NcoI and AatII sites, Km ^R	This study
pTHS147	pET11a-link-NGFP with <i>alr4504</i> inserted by GIBSON assembly into the NheI site, Amp ^R	This study
pTHS148	pTHS112 with <i>Pcpc560-ecfp-alr4504</i> inserted by GIBSON assembly into the EcoRV site, Amp ^R , Km ^R	This study
pTHS149	pRL25C with <i>PpetE-alr4504-ecfp</i> inserted into ClaI site by Gibson assembly. Nm ^R , Km ^R	This study
pTHS150	pTHS149 with <i>PpetE-alr4505-gfp</i> inserted into the BamHI site by Gibson assembly, Nm ^R , Km ^R	This study

Restriction sites are underlined. Sm^R: streptomycin resistance; Sp^R: spectinomycin resistance; Amp^R: ampicillin resistance, Km^R: kanamycin resistance, Nm^R: neomycin resistance; Cm^R: chloramphenicol resistance.

- 1) The eYFP is C-terminally followed by a myc-tag, which is then followed by a heptapeptide of glycine and serine. Abbreviated: *yfp*.
- 2) Modified *gfpmut3.1* in which the internal NdeI site was removed by replacing CAT by the synonymous CAC codon. The GFP is N-terminally preceded by 12 alanine and serine residues. Abbreviated: *gfp* (Stucken *et al.*, 2012).

17 Acknowledgements

First of all, I would like to thank Tal for giving me the opportunity to perform my thesis in her group and for providing me with scientific support wherever it was possible. She enabled me to explore my research topic freely and unrestrictedly. And specifically this scientific freedom that she gave me allowed me to adopt this project as my own and motivated me to explore more and more of it every day.

Dear Karina, although we've been separated by a few thousand kilometers, you still provided me with every conceivable support, be it scientifically or motivationally in distressing moments. You were always so understanding and provided me with so many helpful suggestions to shape this thesis properly. I am thankful for your guidance and support and I hope that we will proceed to cooperate beyond the framework of this thesis.

During my thesis I got the opportunity to meet so many different and friendly people from different scientific backgrounds and different continents. It was a pleasure to be at the Gordons conference in Andover (USA) where I could meet the leading minds of cytoskeletal research. I very much appreciate the openness of Martin Thanbichler for inviting me to visit his group in Marburg and for supporting me with mass spectrometry analyses. Similarly, Iris Maldener did not hesitate to cooperate and offer her support with my project and supplied me with valuable electron microscopy data. I am also thankful for the support of Andreas Tholey and Andreas Helbig for their help with the mass spectrometry-based identification of interaction partners of my protein candidates. With the support of the FAZIT-Stiftung, I was able to visit the Imperial College in London where I met Dennis Nürnberg, an amazingly friendly scientist who taught me how to perform FRAP experiments. All those connections and travels broadened not only my scientific horizon, but they also allowed me to discover the world a little bit more.

I am so grateful to my father, Helmut, and my deceased grandmother, Traute, for their sheer never ending mental support, the magnificent advices and their financial support. I was always able to rely on you no matter what kind of situation arose. Moreover, I am extremely thankful to have Sarah, my love, in my life. Her love, her understanding and her wonderful support guided me not only through this thesis but also through all other aspects of life. This is even more significant in the light of her own ongoing PhD thesis, which she has to carry out under the most adverse conditions. Without any of you three, this would not have been possible! Thank you so much!

Also, I am indescribably happy that I can call Tjorben, Hannes, Kröger, Marcel, Jonas, Lena, Simon, Paddy, Caro, Henning, Nils, Brice, Alex, Melli and many others my friends, as these have been by my side for more than a decade and never ceased to encourage me to proceed

with my educational pathway and have always been open for advice and, most important, fooleries.

Last but not least, I would like to thank all other members of the group of Tal - specifically Tana, Ryszard, Katrin, Sophie and Samer - not only for their scientific support but also for their social support and the nice company with amusing and sometimes quite unusual conversation topics.